CCCF
CHINESE CRITICAL CARE CONGRESS 2026
中国危重病医学大会

第17届中国医师协会重症医学医师分会年会暨危重病医学大会-2026

Chinese Critical Care Congress 2026, Chinese Medical Doctor Association

济南 中国 2026年9月3日-6日
September 3 – 6, 2026

Oral论文汇编

塑造重症未来
Shape the Future of Critical Care

目录

Early immune phenotypes and dynamic transitions in elderly patients with sepsis: a multicenter cohort study 03

Early Physiological Trajectories Are Associated With ICU Mortality in VV-ECMO Patients With Pulmonary Infection-Related Respiratory Failure 04

Efficacy and safety of oxycodone hydrochloride for long-term analgesia in mechanical ventilated ICU patients: A Pilot study 05

Intraoperative Tissue Perfusion Pressure as Predictors of Postoperative Acute Kidney Injury: A Retrospective Cohort Study 09

IRF1 基因 rs2057656 位点多态性对 IRF1-AS1 转录与 ARDS 免疫功能失衡的分子机制 10

Machine Learning and Untargeted Metabolomics Identify Serum Biomarkers for Diagnosis and Prognosis Prediction of Sepsis 30

MRAB 协同恢复线粒体补充与自噬重建线粒体稳态改善脓毒症心肌功能障碍 39

Neurogenic Pulmonary Edema in Acute Cerebral Infarction: A Case Report and Review of the Literature 44

Physiological comparison of high-flow oxygen via endotracheal tube and T-piece strategies during spontaneous breathing trials: a randomized crossover study 47

"Physiological effects of combining awake prone positioning with different oxygen therapies on regional ventilation assessed by electrical impedance tomography: a randomized crossover trial" 48

Predictive Value of the Murray Lung Injury Score for Ventilator-Associated Pneumonia and Mortality in Mechanically Ventilated ICU Patients: A Mediation Analysis 65

Urinary [TIMP-2]×[IGFBP7] for biomarker-enhanced AKI staging and short-term prognosis in ICU patients 84

改良时间加权平均动脉压对心脏术后患者急性肾损伤预测价值：一项前瞻性、观察性研究 93

基于边际结构模型的充分营养干预生理阈值窗口识别及外部验证 94

基于单细胞转录组学细胞间通讯分析机械通气相关肺纤维化中成纤维细胞与肺泡上皮细胞的时空交互 106

脓毒症患者淋巴细胞数目与出院后健康相关生活质量相关：一项多中心研究 108

脓毒症患者入 ICU 24 h 内的糖皮质激素使用与 28 d 死亡率的队列研究 109

脓毒症凝血动态轨迹识别及基于组学的分子内型特征研究 112

下呼吸道感染中抗菌药物耐药性的全球负担：基于 2021 年全球疾病负担研究的系统分析 119

组织灌注压与心脏手术相关急性肾损伤发生的相关性研究 125

Early immune phenotypes and dynamic transitions in elderly patients with sepsis: a multicenter cohort study

姓名：王先文，张丽娜，钱招昕
单位：中南大学湘雅医院

Purpose: To identify early immune phenotypes in older adults with sepsis, characterize their transitions, and examine associations of baseline phenotype and immune recovery with clinical outcomes.

Methods: This secondary analysis of a multicentre prospective cohort included 816 patients aged ⩾ 60 years with Sepsis-3. Data-driven immune phenotypes were defined from day-1 immune-inflammatory profiles and reassessed on days 3 and 7 when available. Associations with in-hospital mortality and mechanical ventilation were evaluated using multivariable logistic regression. Among baseline-IS1 patients, transition-associated factors and outcomes were assessed, including a propensity-score-matched cohort with exact matching on hospital.

Results: Day-1 phenotyping identified IS1 in 693 patients (84.9%) and IS2 in 123 (15.1%). IS1 showed greater organ dysfunction and inflammation, with lower lymphocyte, T-cell, CD8+ T-cell, and natural killer-cell counts. Mortality was 30.9% in IS1 versus 8.9% in IS2. After adjustment, IS2 was associated with lower odds of mortality (adjusted odds ratio 0.36, 95% confidence interval 0.18–0.71) and mechanical ventilation (0.57, 0.33–0.96). Among 405 baseline-IS1 patients with repeat phenotyping, 69 transitioned to IS2 by day 3 or 7. In 67 matched pairs, mortality was lower with transition to IS2 than with persistent IS1 (11.9% vs 38.8%; P = 0.002). Higher day-1 CD8+ T-cell count was associated with transition in the matched analysis (odds ratio 1.45 per 100 cells/μL, 1.02–2.05).

Conclusion: Older adults with sepsis exhibited clinically distinct, dynamic immune phenotypes. Transition from a lymphopenic-inflammatory to an immune-preserved phenotype was associated with lower in-hospital mortality, supporting repeated immunophenotyping for biological stratification and hypothesis generation.

Early Physiological Trajectories Are Associated With ICU Mortality in VV-ECMO Patients With Pulmonary Infection-Related Respiratory Failure

姓名：田静，闫德超，韩艺
单位：哈尔滨医科大学附属第二医院

Background: Early prognostic assessment in patients receiving venovenous extracorporeal membrane oxygenation (VV-ECMO) is commonly based on variables measured at ECMO initiation. This study evaluated whether early dynamic laboratory and blood gas changes were associated with ICU mortality in patients receiving VV-ECMO for respiratory failure secondary to pulmonary infection.

Background: Early prognostic assessment in patients receiving venovenous extracorporeal membrane oxygenation (VV-ECMO) is commonly based on variables measured at ECMO initiation. This study evaluated whether early dynamic laboratory and blood gas changes were associated with ICU mortality in patients receiving VV-ECMO for respiratory failure secondary to pulmonary infection.

Methods: This single-center retrospective cohort study included patients treated with VV-ECMO in the ICU of the Second Affiliated Hospital of Harbin Medical University between January 2023 and May 2026. Patients were grouped as ICU survivors or non-survivors. Laboratory parameters were assessed at ECMO initiation and on Days 1-3, and blood gas parameters at 0, 6, and 24 h. Between-group comparisons, repeated-measures analysis, logistic regression, and ROC analysis were performed.

Results: Among 141 included patients, 39 were ICU non-survivors and 102 were ICU survivors. At ECMO initiation, non-survivors had higher total bilirubin and lactate levels. Significant group × time interactions were observed for white blood cell count, D-dimer, pH, and lactate. Higher white blood cell count, D-dimer, and lactate were associated with increased odds of ICU mortality, whereas higher albumin, total protein, and prothrombin activity were associated with lower odds. The dynamic combined model showed better discrimination than the initial combined model.

Conclusions: In patients receiving VV-ECMO for pulmonary infection-related respiratory failure, ICU mortality was associated with baseline metabolic and hepatic dysfunction and early dynamic changes in inflammatory, coagulation-fibrinolytic, acid-base, lactate, and protein-status parameters.

Results:

Among 141 included patients, 39 were ICU non-survivors and 102 were ICU survivors. At ECMO initiation, non-survivors had higher total bilirubin and lactate levels. Significant group × time interactions were observed for white blood cell count, D-dimer, pH, and lactate. Higher white blood cell count, D-dimer, and lactate were associated with increased odds of ICU mortality, whereas higher albumin, total protein, and prothrombin activity were associated with lower odds. The dynamic combined model showed better discrimination than the initial combined model.

Conclusions:

In patients receiving VV-ECMO for pulmonary infection-related respiratory failure, ICU mortality was associated with baseline metabolic and hepatic dysfunction and early dynamic changes in inflammatory, coagulation-fibrinolytic, acid-base, lactate, and protein-status parameters.

Efficacy and safety of oxycodone hydrochloride for long-term analgesia in mechanical ventilated ICU patients: A Pilot study

姓名：Yunhang Zhang, Jieqiong Song, Ming Zhong
单位：Zhongshan Hospital, Fudan University

Objective:

The aim of this study was to evaluate the efficacy and safety of oxycodone hydrochloride compared with remifentanil for long-term analgesia in mechanically ventilated ICU patients.

Methods:

In this single-centered randomized pilot study, adult postoperative patients requiring invasive mechanical ventilation for longer than 24 h were randomized to receive continuous intravenous oxycodone hydrochloride or remifentanil.Analgesia was titrated to maintain a Critical-Care Pain Observation Tool(CPOT) score <3, while sedation was maintained at a Richmond Agitation-Sedation Scale (RASS) score between − 2 and 1. The primary outcome was the percentage of time with CPOT <3 without rescue analgesia during the first 7 days of mechanical ventilation. The secondary outcomes included ventilatorfree days at day 28, successful extubation rate, length of ICU stay, gastrointestinal function changes, incidence of ventilator-associated pneumonia(VAP), delirium, and adverse events.

Results:

A total of 60 patients were randomized, with 30 patients assigned to the oxycodone and the remifentanil group, respectively. No difference was identified between the oxycodone group and remifentanil group in median age [69 (IQR, 64–72) years vs. 62 (IQR, 42–72) years, respectively, p=0.070] or the median duration of study drug infusion [48 (IQR, 28–144) hours vs. 42 (IQR,24–75) hours, respectively, p=0.236]. Target CPOT was reached at a median of 100% in the two groups during the study drug infusion time. No differences were identified between the two groups in terms of ventilator-free days at day 7,length of ICU stay, 28-day mortality or adverse events.

Conclusion:

This pilot study suggested that oxycodone hydrochloride was comparable to remifentanil in providing effective analgesia for mechanically ventilated ICU patients, with a favorable safety profile. Further large-scale randomized studies are warranted to confirm these findings.

Characteristics	Oxycodone (n=29)	Remifentanil (n=30)	p
Age, yr	69 (64,72)	62 (42.2,72)	0.070
Male	16 (55.2%)	26 (86.7%)	0.008
BMI	22.2±4.3	22.4±3.7	0.784
APACHE II	19.2±7.5	19.2±6.2	0.997
SOFA	5.8±3.2	5.9±3.3	0.899
RASS	-2 (-3,-1)	-2 (-2,-1)	0.308
CPOT	1 (0,2)	1.5 (1,2)	0.214
sepsis	13 (44.8%)	11 (36.7%)	0.524
Respiratory failure	8 (27.6%)	7 (23.3%)	0.708
Causes of mechanical ventilation			
Respiratory failure	8 (27.6%)	8 (26.7%)	0.937
Airway protection	6 (20.7%)	10 (33.3%)	0.275
Delayed extubation after surgery	16 (55.2%)	14 (46.7%)	0.514
Ventilation mode at trial initiation			
SIMV pressure	15 (51.7%)	12 (40%)	0.366
SIMV volume	13 (44.8%)	18 (60%)	0.243
Time from ICU admission to drug initiation, h	18 (8,32)	15 (8.5,21.5)	0.457
P/F ratio	247.5 (179,351)	264.4 (198.6,380)	0.409
Vasopressors	15 (51.7%)	19 (65.5%)	0.286
Platelets, 10^9/L	125 (90,180)	150 (107.8,243.5)	0.100
Bilirubin, μmol/L	13.6 (9.8,30)	14.6 (8,29.2)	0.838
Creatinine, μmol/L	70 (53,110)	73 (57.8,107.2)	0.814

Table 1: Demographic and clinical characteristics of the patients at baseline

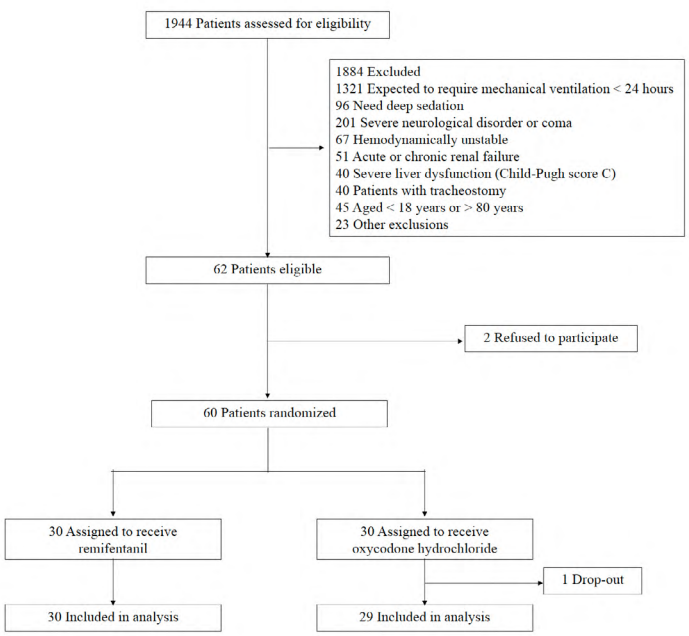


Fig 1: Flow diagram of patient enrollment.

Characteristics	Oxycodone (n=29)	Remifentanil (n=30)	p
Primary outcome			
Percentage of time with a CPOT score less than 3 without rescue, %	100 (97.6,100)	100 (66.7,100)	0.043
Secondary outcomes			
Ventilator-free hours within 7 days, h	96 (0,135)	115 (50,141.8)	0.394
Successful extubation	18 (62.1%)	23 (76.7%)	0.223
ICU length (h)	204 (93,384)	134 (86,252)	0.252
Hospital length (day)	22 (15,26)	17 (11.2,29.2)	0.476
Mortality day 28	4 (13.8%)	5 (16.7%)	1.000
Adverse events			
VAP	2 (6.9%)	3 (10%)	1.000
Hypotension	1 (3.4%)	0 (0%)	0.492
Hypotension with intervention	1 (3.4%)	0 (0%)	0.492
Delirium	1 (3.4%)	3 (10%)	0.629
Bradycardia	0 (0%)	0 (0%)	-

Table 2: Primary outcomes, secondary outcomes and adverse events

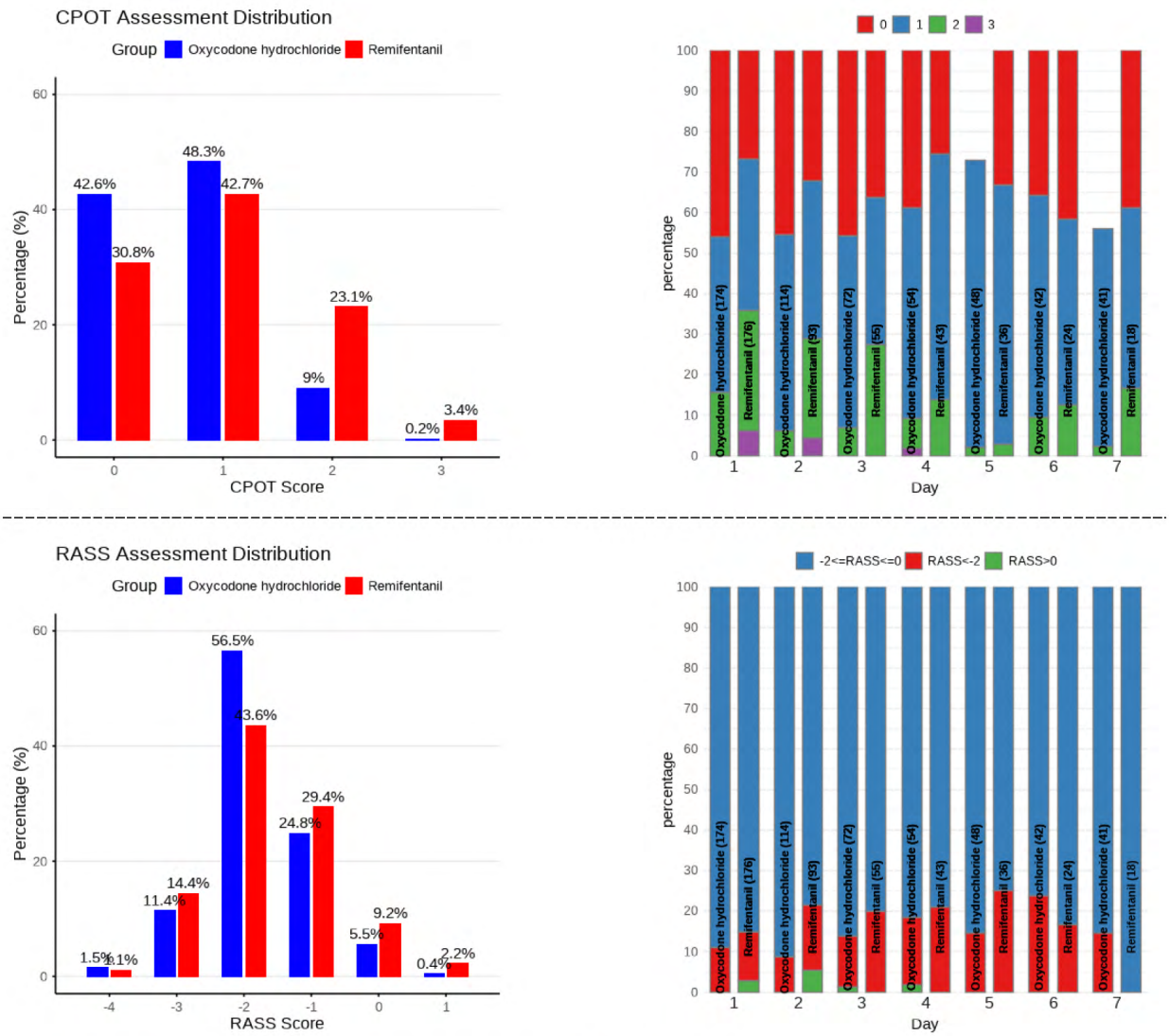


Fig 2: CPOT and RASS assessment distribution

Efficacy and safety of oxycodone hydrochloride for long-term analgesia in mechanical ventilated ICU patients: A Pilot study

姓名：孙亚丽，翁利，彭劲民，杜斌
单位：北京协和医院

Mean arterial pressure (MAP) remains the dominant target in intraoperative hemodynamic management, yet it incompletely reflects tissue perfusion. Tissue perfusion pressure (TPP), defined as MAP minus critical closing pressure (Pcc), represents the effective driving pressure for arterial blood flow. Whether intraoperative TPP and Pcc independently predict postoperative acute kidney injury (AKI) beyond MAP remains unknown.

We conducted a retrospective cohort study of adult surgical patients with intraoperative invasive arterial pressure monitoring and admitted to the ICU postoperatively at Peking Union Medical College Hospital between January 2021 and December 2025. Pcc was estimated via linear regression of intraoperative arterial pressure against the product of heart rate and pulse pressure, and TPP was calculated as MAP minus Pcc. AKI was defined by 48-hour postoperative serum creatinine criteria per KDIGO criterion.

Among 4,992 eligible patients, 681 (13.6%) developed postoperative AKI. The distribution of TPP is not always consistent with that of MAP (Figure A).The correlation between MAP and TPP was modest (r = 0.39, Figure B), indicating that MAP alone does not adequately capture tissue perfusion pressure.When patients were stratified by TPP quartiles, AKI incidence decreased progressively from Q1 to Q4 (17.3%, 13.8%, 12.9%, and 10.6%, respectively; P for trend = 0.001, Figure C). Forest Plot analysis confirmed this dose-response relationship: compared with the highest TPP quartile (Q4, reference), odds ratios for AKI were 1.77 (Q1), 1.35 (Q2), and 1.25 (Q3), with a consistent gradient across quartiles (Figure D). Multivariable-adjusted restricted cubic spline analysis further revealed a significant nonlinear association between intraoperative TPP and postoperative AKI risk (overall $P < 0.001$; non-linearity $P < 0.001$, Figure E). Two clinically meaningful thresholds were identified: AKI risk increased markedly when TPP fell below 32 mmHg, and risk approached a plateau above 40 mmHg. To evaluate the independent value of TPP beyond MAP, patients were stratified by four MAP ranges (<65, 65–75, 75–85, and >85 mmHg). Within each stratum, intraoperative TPP remained significantly lower in patients who developed AKI compared with those who did not (Figure F), demonstrating that TPP provides prognostic information independent of MAP level.

Intraoperative TPP was independently associated with postoperative AKI risk in a nonlinear fashion. These findings suggest that TPP may be a new indicator for reflecting tissue perfusion.

IRF1 基因 rs2057656 位点多态性对 IRF1-AS1 转录与 ARDS 免疫功能失衡的分子机制

姓名：张媛媛，邱海波，张实，王关嵩

单位：山东大学附属第三医院，东南大学附属中大医院，山东大学附属第三医院，陆军军医大学第二附属医院

论文题目：IRF1 基因 rs2057656 位点多态性对 IRF1-AS1 转录与 ARDS 免疫功能失衡的分子机制

背景 / 目的：基因多态性是 ARDS 个体差异的重要分子机制。探索基因多态性在 ARDS 发病机制中的作用可为 ARDS 个体化治疗提供分子靶标。

方法及结果：

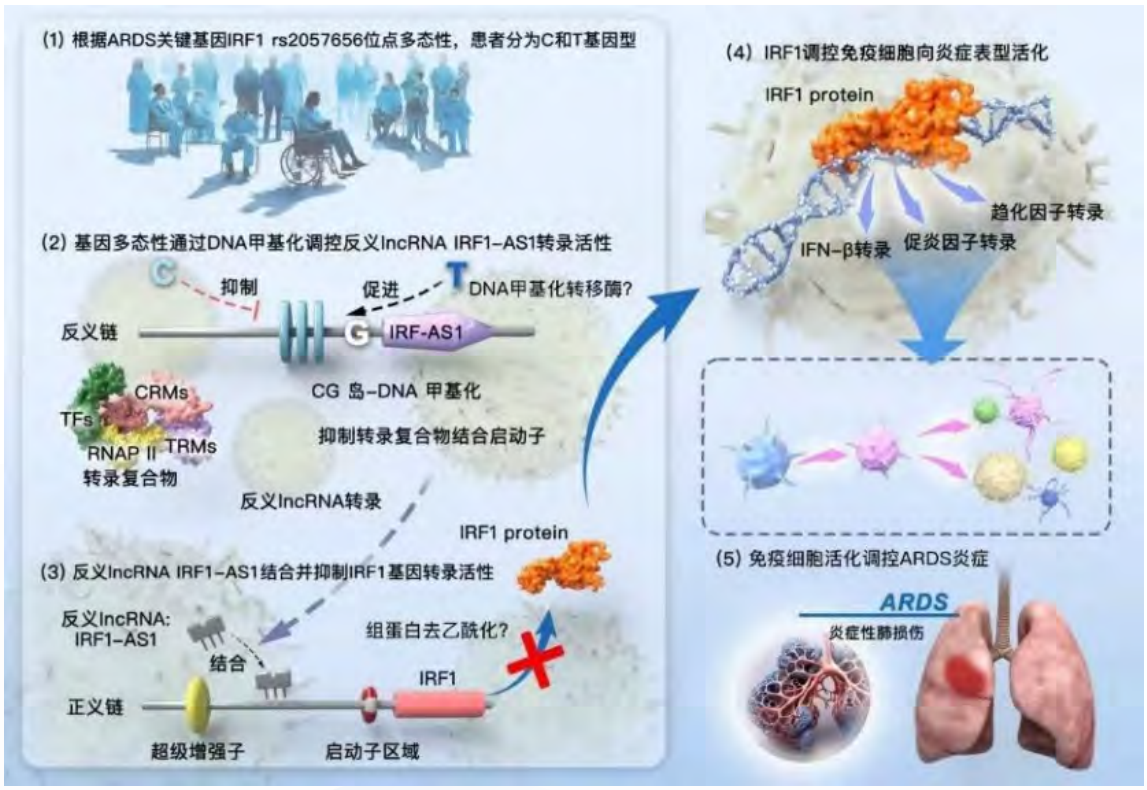
（1）通过 991 例 ARDS 患者外周血基因组和转录组分析，发现 IRF1 基因 rs2057656 位点多态性与 ARDS 易感性密切相关，该位点分为 C 和 T 两种基因型，C 基因型 ARDS 发病风险是 T 基因型的 1.63 倍。

（2）野生小鼠为 C 基因型，构建基因编辑小鼠（将 C 转为 T 基因型），构建气道注射克雷伯杆菌（KP）和盲肠结扎穿孔（CLP）ARDS 动物模型。结果显示，与 C 基因型小鼠相比，T 基因型小鼠肺损伤较轻；肺内 M1 型巨噬细胞、Th1 和 Th17 型 T 细胞以及成熟中性粒细胞数量显著减少；炎症因子表达水平降低。外源性给予 IRF1-AS1 可治疗 C 基因型小鼠的 ARDS 炎症性肺损伤。

（3）体外实验进一步验证，C 基因型来源的原代巨噬细胞更容易向 M1 型极化，T 细胞更易向 Th1 和 Th17 表型分化，中性粒细胞成熟程度更高。

（4）机制研究表明，rs2057656 位点多态性通过调控 DNA 甲基化抑制 IRF1-AS1 表达，IRF1-AS1 通过调控组蛋白去乙酰化降低 IRF1 的转录活性。分子互作实验进一步揭示，DNA 甲基化转移酶 DNMT3a 结合 rs2057656 位点，诱导其甲基化；去乙酰化酶 HDAC2 在 IRF1-AS1 介导下富集于 IRF1 编码区域，从而抑制 IRF1 转录活性。

结论：本研究揭示 IRF1 基因 rs2057656 位点多态性与 ARDS 易感性以及疾病严重程度显著相关。C 基因型患者表现为 IRF1-AS1 低表达和 IRF1 高表达特征，这种分子特征导致更严重的炎症性肺损伤。针对 C 基因型患者，外源性输注 IRF1-AS1 可能成为潜在的治疗策略。



本研究总结

三、研究内容

研究背景和现状、目的：

急性呼吸窘迫综合征（ARDS）是一种临床常见危重症，严重危害人民健康，目前尚缺乏针对其发病机制的特异性治疗手段。近年来，GEN-SEP Network 团队和 ARDS-net 团队分别发现 FLT1 基因的多态性与 ARDS 易感性相关，IFNAR2 基因多态性与患者对激素治疗的反应密切相关。邱海波教授团队进一步发现 PI3 基因的多态性可能是导致 ARDS 患者个体差异的重要内在因素。上述研究提示，**基因多态性可能是 ARDS 患者个体差异的重要分子机制。**

在肿瘤学领域，基因测序已广泛应用于指导个体化的分子靶向治疗。以非小细胞肺癌为例，通过检测 EGFR、ALK、KRAS 等基因变异，可为患者制定针对性的治疗方案。这种基于基因多态性的精准医疗模式显著延长了生存期，提升了生活质量。然而，ARDS 领域的基因多态性研究和分子靶向治疗进展尚不充分。因此，**探索基因多态性与 ARDS 发病机制的关系，可为 ARDS 个体化精准治疗提供分子靶标。**

为探索基因多态性与 ARDS 发病机制的关系，本项目通过 991 例患者外周血多组学测序和生信分析筛选，以及进一步的动物、细胞和分子机制实验，**发现 rs2057656 位点多态性通过调控 IRF1 和 IRF1-AS1 表达影响 ARDS 内免疫细胞功能，外源性输注 IRF1-AS1 可治疗 ARDS 炎症性肺损伤，为 ARDS 分子靶向治疗提供分子靶标。**

设计及方法：

1. 多组学联合分析筛选与 ARDS 发病机制相关的基因多态性位点

本研究纳入两个临床 队列，训练队列为我院 96 例 ARDS 患者，均在入院 48H 内采集外周血样本，进行全基因组测序（WGS）和转录组测序（RNA-seq）；验证队列选自 ARDS-net 公共数据库，包含 895 例患者和全基因组测序数据。通过全基因组关联分析（GWAS）和表达数量性状基因座（e-QTL），筛选与 ARDS 易感性相关的基因多态性位点。

2. 基因编辑小鼠验证 rs2057656 位点多态性通过 IRF1 调控 ARDS 的发生

野生型小鼠 rs2057656 位点碱基为 C（即 C 基因型）。本研究委托集萃药康生物技术有限公司将碱基 C 编辑为 T（即 T 基因型）。构建 ARDS 小鼠模型：盲肠结扎穿孔（CLP）和气道内注射肺炎克雷伯菌（KP）。采用 HE 染色、肺干湿重比评估 rs2057656 位点多态性对 ARDS 肺损伤的影响；采用流式细胞术分析 rs2057656 位点多态性对 ARDS 小鼠肺组织中巨噬细胞、中性粒细胞和 T 细胞表型的影响；采用 qPCR 检测 rs2057656 位点多态性对 ARDS 相关炎症因子的影响。

3. 原代细胞证明 rs2057656 位点多态性通过 IRF1 调控免疫细胞向炎症表型活化

与 T 基因型相比，C 基因型患者体内 IRF1 表达水平显著升高，且 C 基因型单核细胞更易向炎症表型巨噬细胞分化。拟通过 CRISPR/Cas9 基因编辑技术构建 C/T 基因型小鼠模型，并分离培养不同基因型原代细胞。采用 qPCR 和 Western blot 检测 C/T 基因型原代免疫细胞中 IRF1-AS1 和 IRF1 表达；采用 qPCR、Western blot、流式细胞术检测 C/T 基因型免疫细胞中共刺激分子、促炎分子和趋化因子的表达；采用流式细胞术、免疫细胞吞噬实验，评估 C/T 基因型淋巴细胞向炎症表型分化。

4. 分子互作实验探索 rs2057656 位点多态性调控 IRF1 表达的分子机制

采用 CHIP、DNA pull-down 等 DNA- 蛋白质互作实验和外源性表达等挽救实验验证 DNA 甲基化分子机制；采用 CHIRP 技术、RIP、EMSA 等分子互作实验、特异性蛋白质抑制剂处理及功能挽救实验阐明局部组蛋白去乙酰化分子机制。

5. 探索外源性输注 IRF1-AS1 治疗 C 基因型 ARDS 的可能性

本研究构建 IRF1-AS1 过表达的 RAW264.7 细胞来源外泌体（IRF1-AS1-EVs），采用活体成像验证 IRF1-AS1-EVs 能成功到达小鼠肺部；采用病理切片 HE 染色、免疫组化、肺损伤评分、伊文思蓝实验和湿干重比实验评估外源性输注 IRF1-AS1-EVs 对 ARDS 肺损伤的改善；采用流式细胞术和 qPCR 实验评估外源性输注 IRF1-AS1-EVs 对 ARDS 免疫细胞向炎症表型活化的改善。

结果及结论：

1 rs2057656 位点多态性与 ARDS 易感性显著相关

本研究共纳入训练和验证两个队列，共 991 例患者，其中训练队列 96 例 CAP 患者（53 例 ARDS）；验证队列 895 例 CAP 患者（661 例 ARDS）。

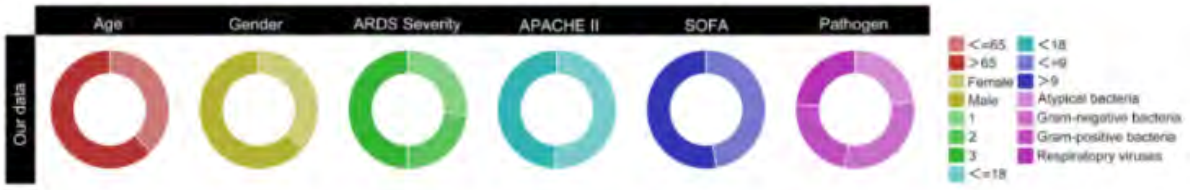


图 1：训练队列信息



图 2：验证队列信息

在训练队列中，通过全基因组测序数据分析，筛选出 10 个与 ARDS 易感性显著相关的单核苷酸多态性（SNP）位点（P <0.05）。

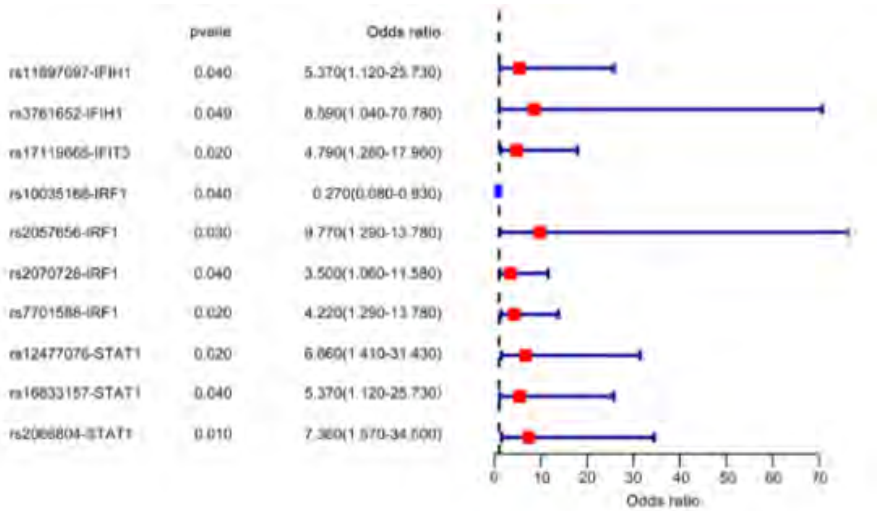


图 3：训练队列全基因组测序数据

在验证队列中，通过全基因组测序数据分析，筛选出 15 个与 ARDS 易感性显著相关的 SNP 位点（P<0.05）。

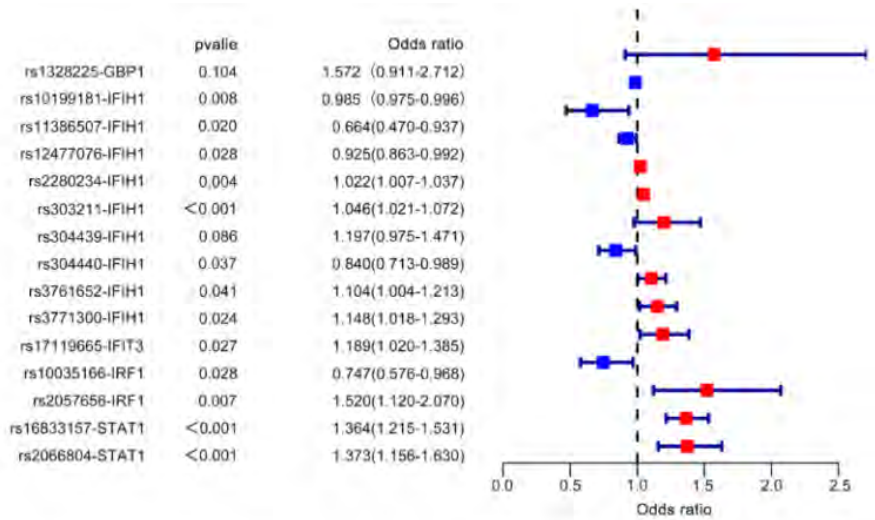


图 4：验证队列全基因组测序数据

通过交集分析，整合训练队列 10 个位点和验证队列 15 个位点两组数据分析，最终确定 6 个 SNP 位点与 CAP 进展为 ARDS 密切相关。



图 5：两队列交集分析

对 6 个候选 SNP 位点进行 eQTL 分析，发现 IRF1 基因 rs2057656 位点与 IRF1 mRNA 表达水平显著相关（P<0.001）。rs2057656 位点存在两种基因型：参考基因型 C 和突变基因型 T。其中，C 基因型表达高于 T 基因型，提示该位点可能在 ARDS 发病过程中具有调控作用。

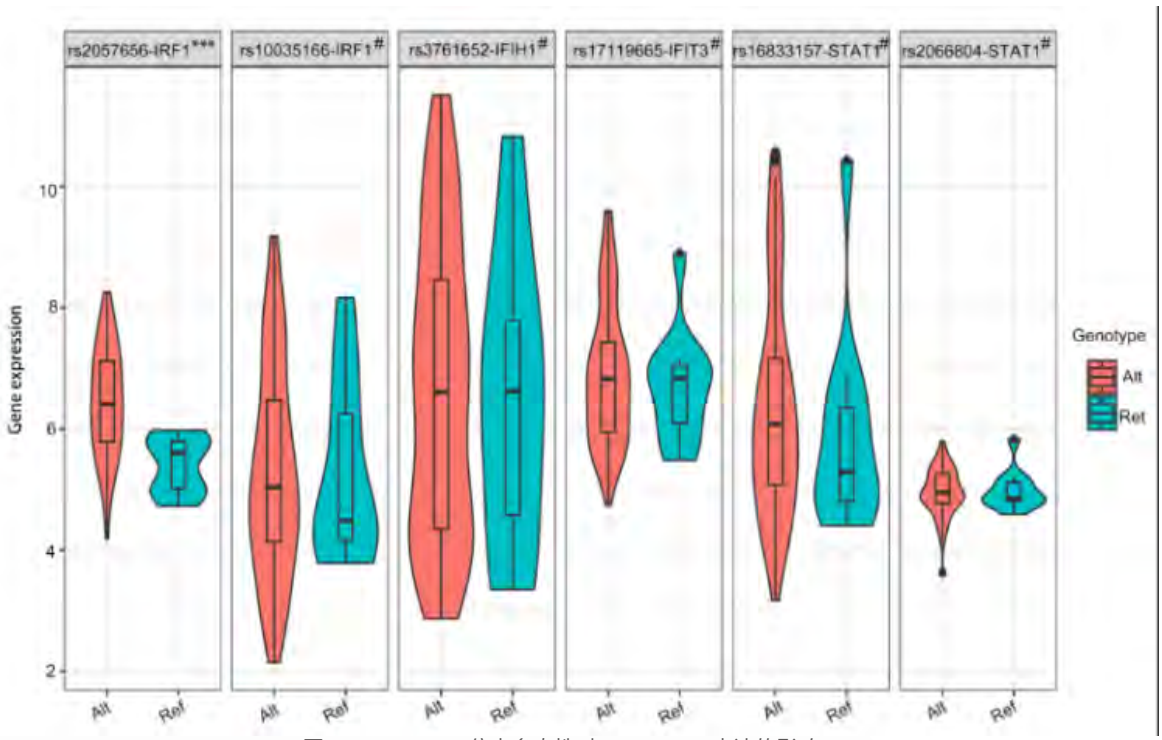


图 6：rs2057656 位点多态性对 IRF1mRNA 表达的影响

rs2057656 位于 IRF1 的反义 lncRNA（IRF1-AS1）的启动子区域（Chr5:132473613）。

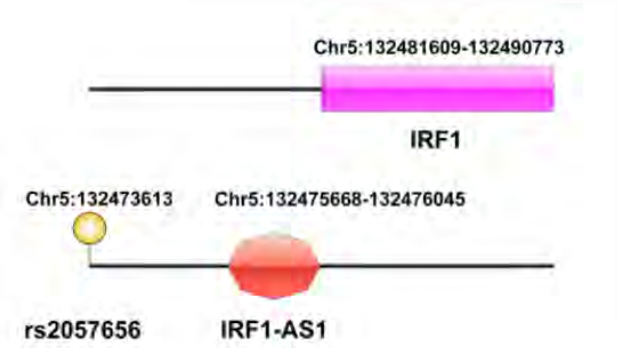


图 7：rs2057656 位于 IRF1-AS1 启动子区域

国家生物技术信息中心（NCBI）数据显示，C 基因型主要见于欧美和非洲人群（频率 40%-60%），而 T 基因型在亚洲人群多见（92%）。在本研究中，国内 CAP 患者，C 基因型占比 11%，T 基因型 89%。

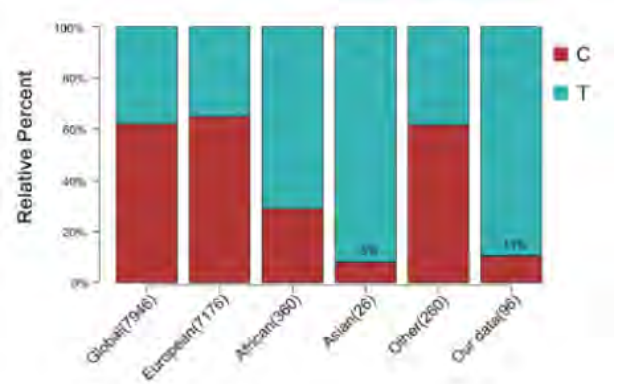


图 8：rs2057656 位点多态性在不同人群中的分布频率

卡方检验提示，rs2057656 位点多态性与 ARDS 易感性相关，P<0.05。

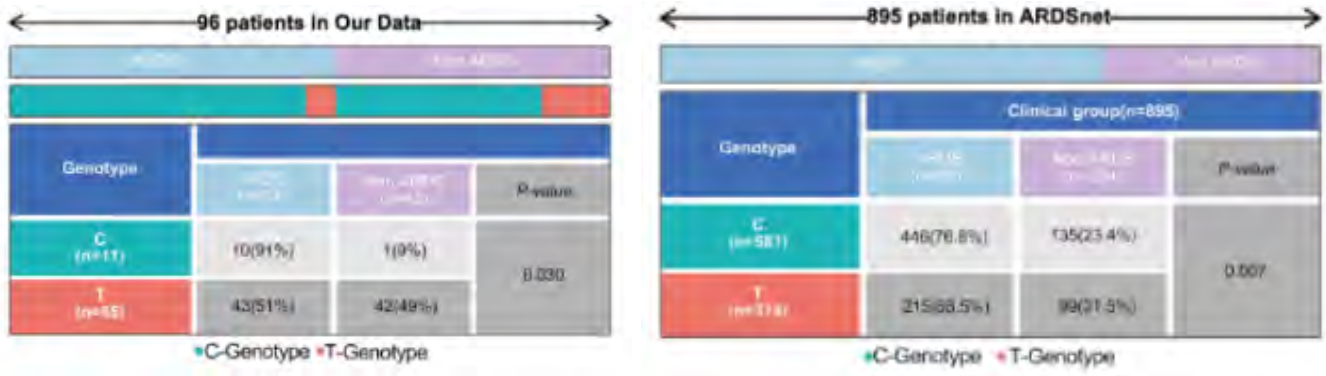


图 9：rs2057656 位点多态性与 ARDS 易感性相关

纳入我国 96 例 CAP 患者以及美国 895 例 CAP 患者，进行 SNP meta 分析显示，rs2057656 位点 C 基因型显著增加 CAP 进展为 ARDS 的风险（OR[95%CI]: 1.63[1.21,2.20]）。

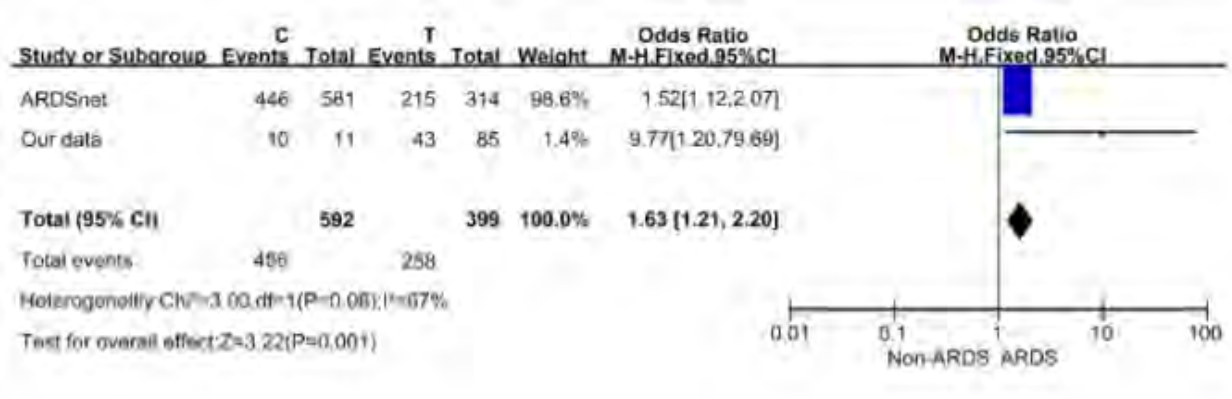


图 10：rs2057656 位点多态性与 CAP 进展 ARDS 风险的 meta 分析

rs2057656位点多态性与ARDS严重程度显著相关，T基因型患者重症ARDS发生率显著低于C基因型（P<0.001）。

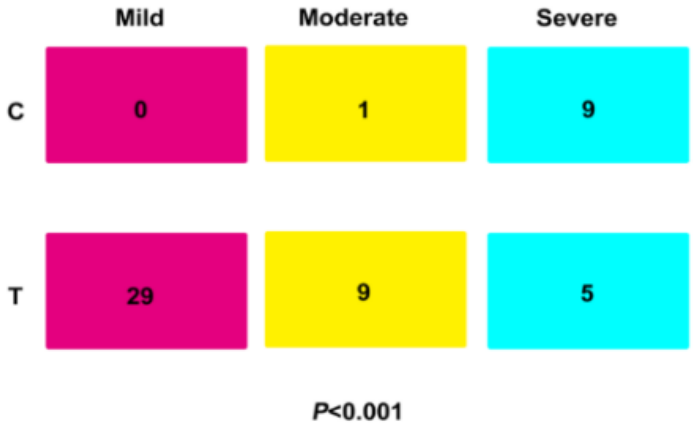


图 11：rs2057656 位点多态性与 ARDS 严重程度的关联分析

eQTL 分析发现，与 C 基因型患者相比，T 基因型患者的 IRF1-AS1 表达水平显著增加（P<0.001）。

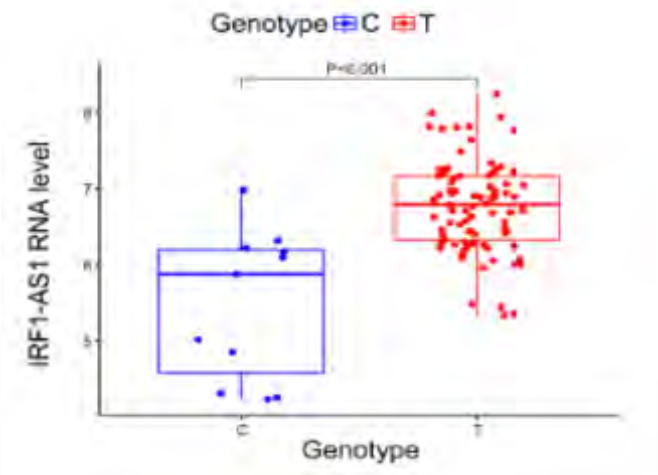


图 12：rs2057656 位点多态性对 IRF1-AS1 RNA 表达的影响

目前关于反义 lncRNA（IRF1-AS1）的研究提示，IRF1-AS1 主要通过表观遗传机制抑制所在基因转录。本研究散点图进一步表明，IRF1-AS1 表达与 IRF1 表达显著负相关，（P <0.001, 皮尔森相关系数 -0.61）。

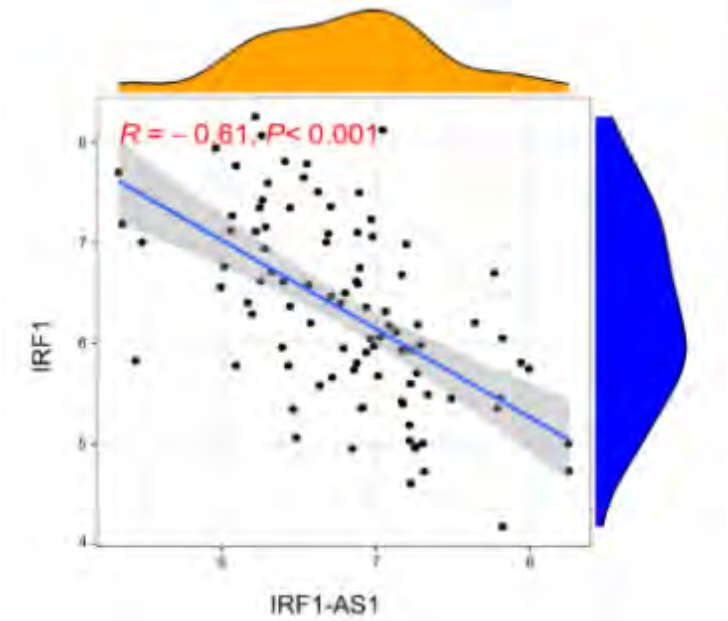


图 13：IRF1-AS1 与 IRF1 表达的负相关性

将 IRF1-AS1 与 IRF1 的表达水平分别用 ARDS 严重程度进行关联分析，结果显示：IRF1-AS1 在重度 ARDS 中显著低表达，两者呈显著负相关 (P<0.001)。IRF1 在重度 ARDS 中显著高表达，两者呈显著正相关（P<0.001）。

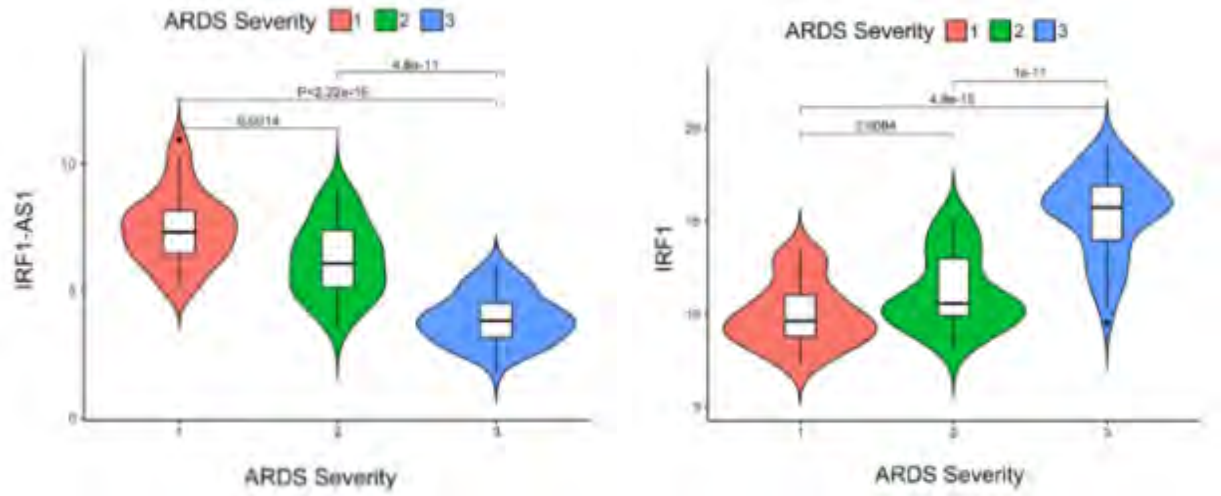


图 14：IRF1-AS1 与 IRF1 表达水平在 ARDS 严重程度中的关联分析

通过多组学分析，筛选出与 ARDS 严重程度显著相关的关键分子。结果显示：IRF1 是与 ARDS 严重程度正相关最显著的分子，IRF1-AS1 是与 ARDS 严重程度负相关最显著的分子。

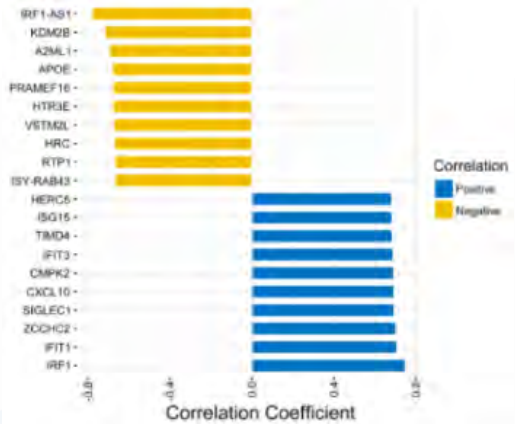


图 15：与 ARDS 严重程度相关分子

2.rs2057656 位点多态性调控 ARDS 发展

委托集萃药康生物技术有限公司构建 rs2057656 位点基因编辑小鼠：野生型小鼠（WT）为 C 基因型，基因编辑小鼠为 T 基因型。采用一代测序和 BSP-seq 验证小鼠基因型。

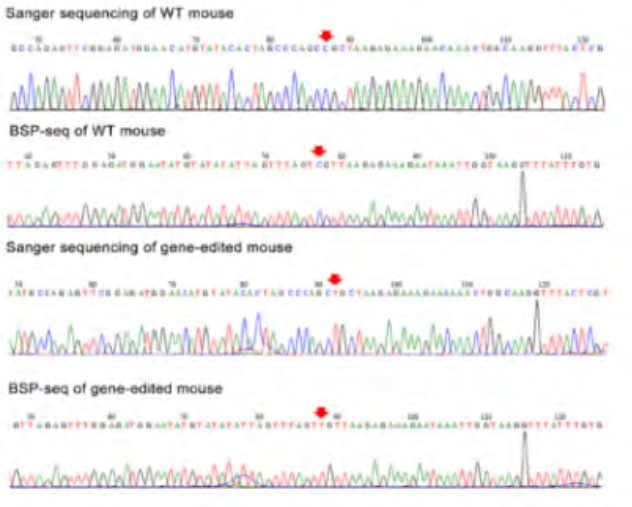


图 16：rs2057656 位点基因编辑小鼠的构建与基因型验证

为验证 rs2057656 位点多态性调控 ARDS 肺损伤，对 C 型和 T 型小鼠构建 ARDS 模型，进行 HE 染色和免疫组化分析。结果表明，T 基因型小鼠肺损伤程度明显轻于 C 基因型（P<0.05），T 基因型 IRF1 表达显著低于 C 基因型。

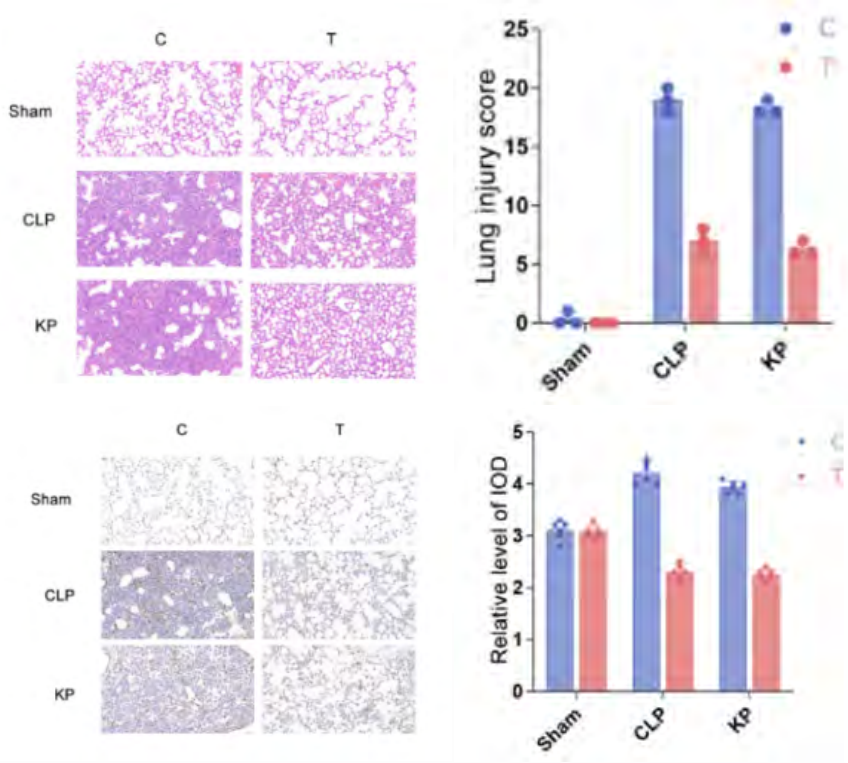


图 17：rs2057656 位点多态性对 ARDS 肺损伤影响

进一步采用湿干重比评估小鼠肺组织水肿程度。结果显示 T 基因型肺水肿程度明显低于 C 基因型（P<0.001）。

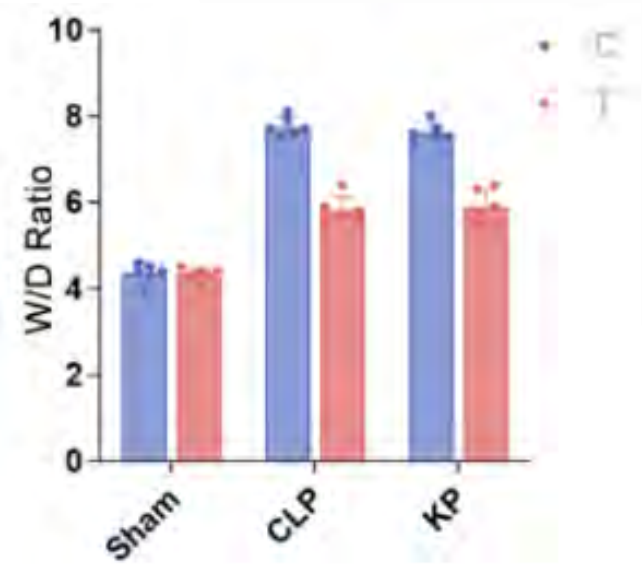


图 18：rs2057656 位点多态性对肺组织湿干重比的影响

为了探讨 rs2057656 位点多态性对小鼠肺内 IRF1 表达的影响，采用 Western blot 和 qPCR 分析。结果表明，T 基因型小鼠 IRF1-AS1 表达显著升高，IRF1 蛋白及 iNOS 表达明显降低（P <0.001）。提示该多态性可能通过调控 IRF1 通路影响 ARDS 炎症反应。

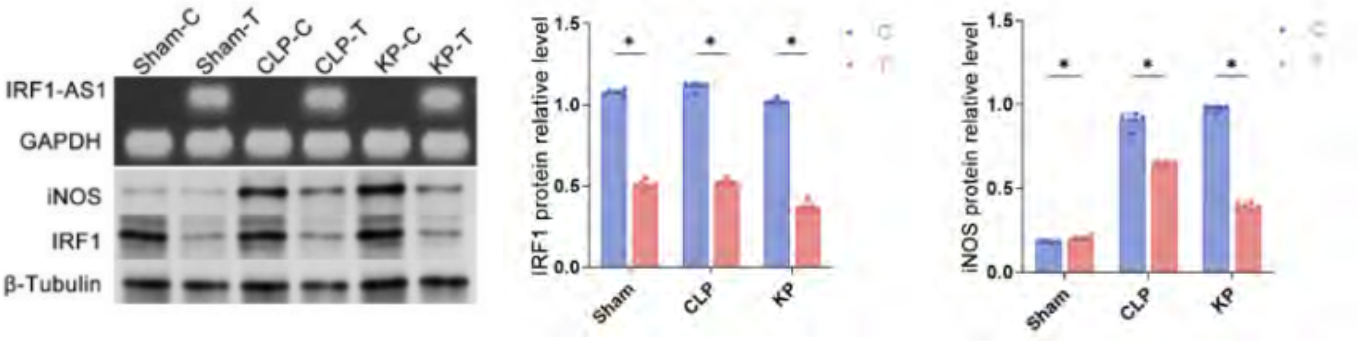


图 19：rs2057656 位点多态性对 IRF1 与 iNOS 表达的影响

为探究 rs2057656 位点多态性对 ARDS 肺内免疫细胞表型的调控，采用流式细胞术检测不同基因型小鼠肺内巨噬细胞、T 细胞及成熟中性粒细胞的活化状态。结果表明：T 基因型显著抑制巨噬细胞向 M1 型活化，降低 Th1 和 Th17 细胞分化，并减少成熟中性粒细胞活化水平，提示该多态性可能通过调控多种免疫细胞炎症表型缓解 ARDS 病理损伤。

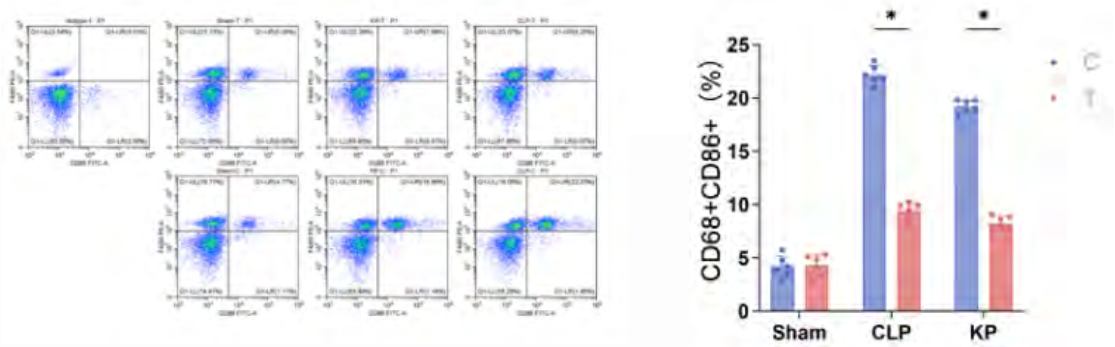


图 20：rs2057656 位点多态性对巨噬细胞炎性活化的影响

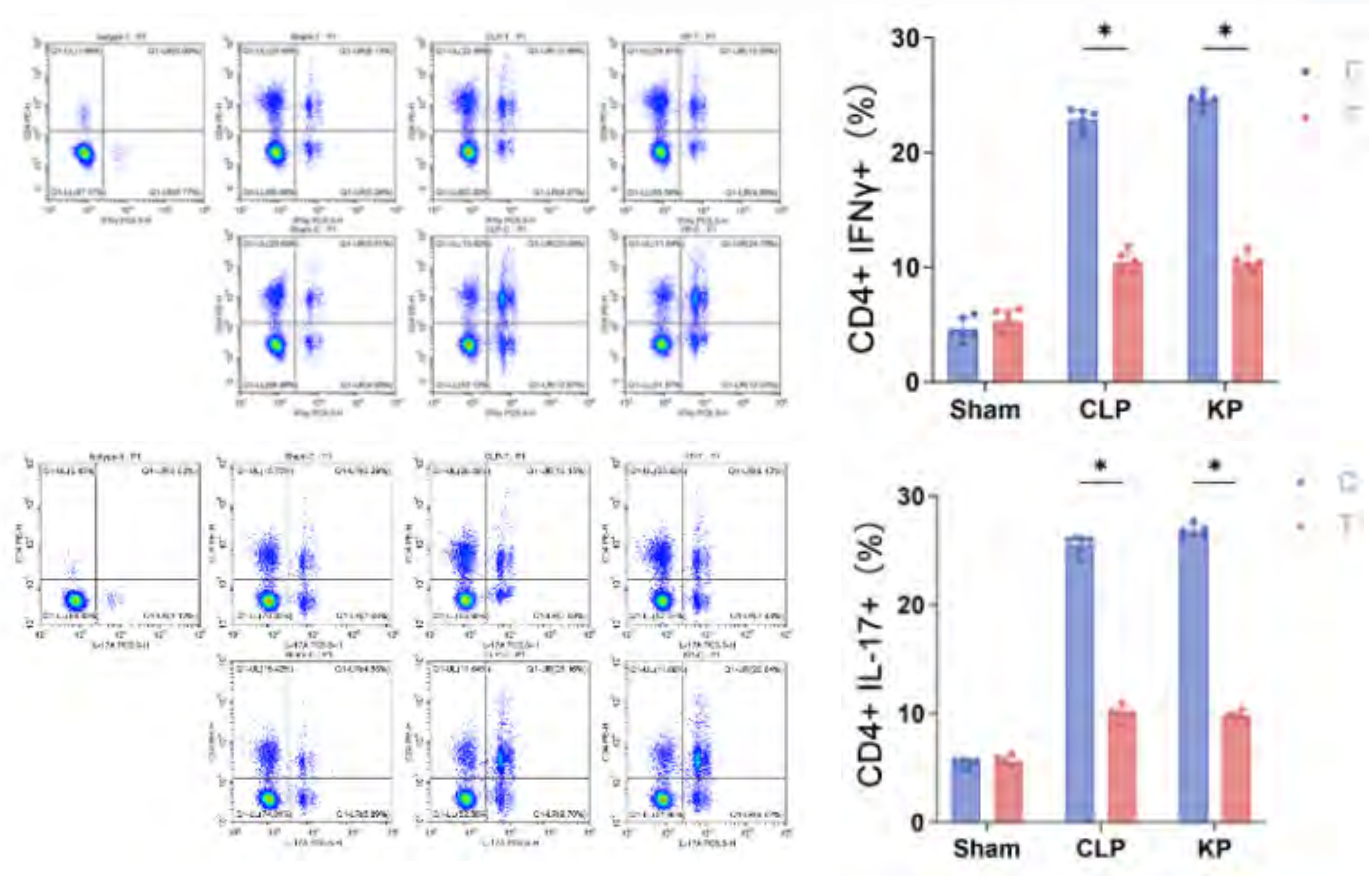


图 21：rs2057656 位点多态性对 T 细胞活化的影响

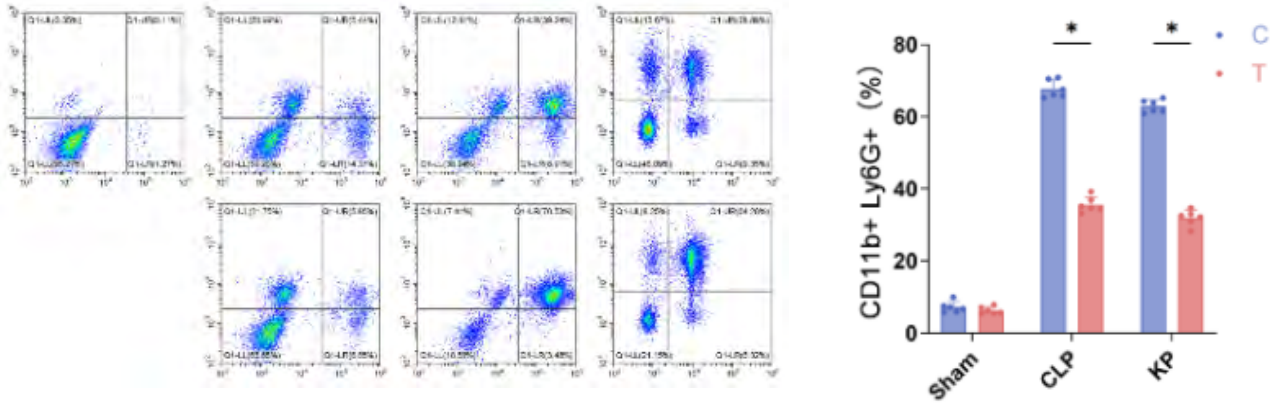


图 22：rs2057656 位点多态性对成熟中性粒细胞活化的影响

为探究 rs2057656 位点多态性对 ARDS 肺内炎症因子表达的调控，采用 qPCR 实验。结果表明，T 基因型 IL1B、IL6、TNF 和 CCL2 等炎症因子的 mRNA 表达水平均显著低于 C 基因组。

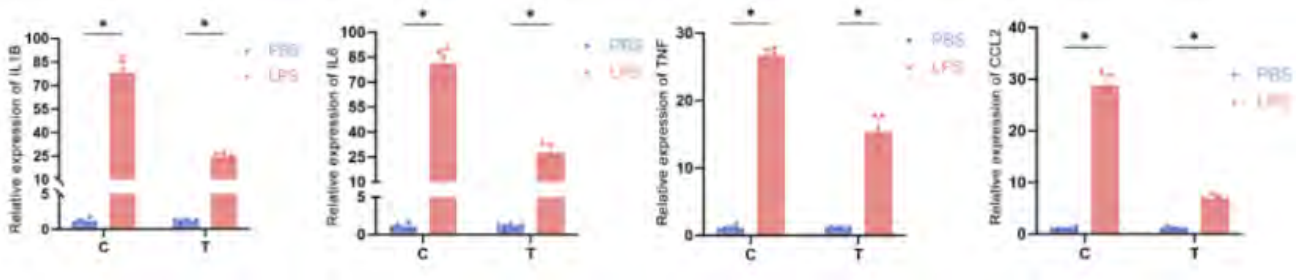


图 23：rs2057656 位点多态性对炎症因子的影响

3.rs2057656 位点多态性通过 IRF1-AS1 和 IRF1 调控免疫细胞向炎症表型活化

IRF1-AS1 in Human Chr5:132473579-132473648
IRF1-AS1 in Mouse Chr11: 53659803-53659838

从我院 ARDS 患者生物样本库中筛选 C 型和 T 型基因型外周血，通 Ficoll 法提取 PBMC 后进行 Western blot、PCR 检测 IRF1-AS1 和 IRF1 的表达；流式检测免疫细胞炎症表型数目；qPCR 检测炎症因子。

Western blot 和 PCR 结果提示，相较于 C 基因型，T 基因型中 IRF1 蛋白和 iNOS 表达显著降低（P <0.05），而 IRF1-AS1 表达显著升高。

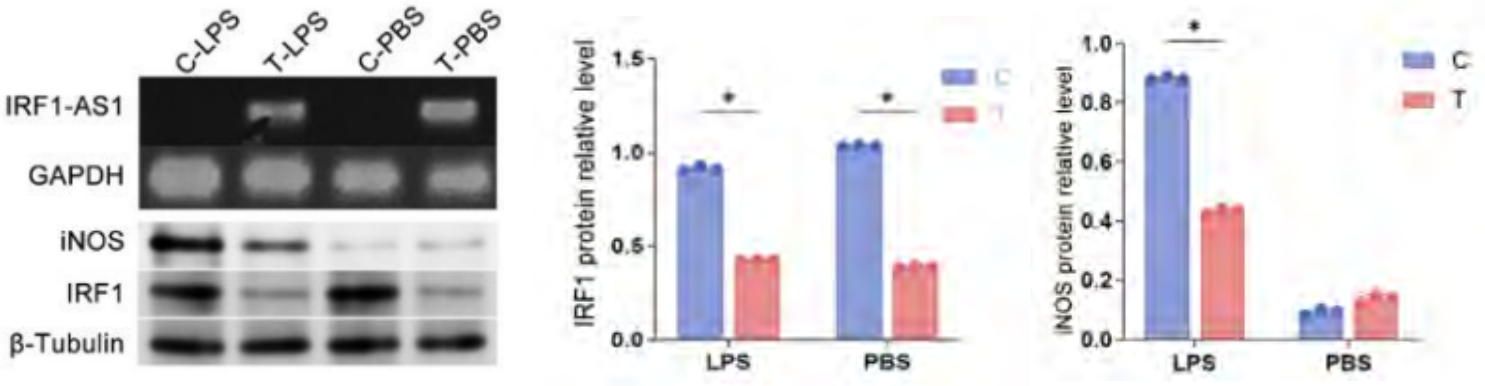


图 24：rs2057656 位点多态性对 IRF1 和 iNOS 表达的影响

流式细胞术结果提示，相较于 C 基因型，T 基因型显著抑制巨噬细胞向 M1 型活化（P<0.05），T 细胞炎症表型（Th1、Th17）活化比例降低（P<0.05），成熟中性粒细胞占比降低（P<0.05），提示 T 基因型抑制免疫细胞炎症性活化。

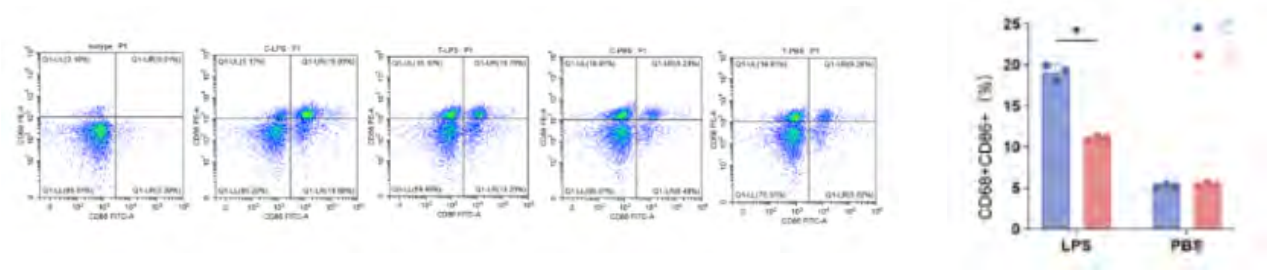


图 25：rs2057656 位点多态性对巨噬细胞极化的影响

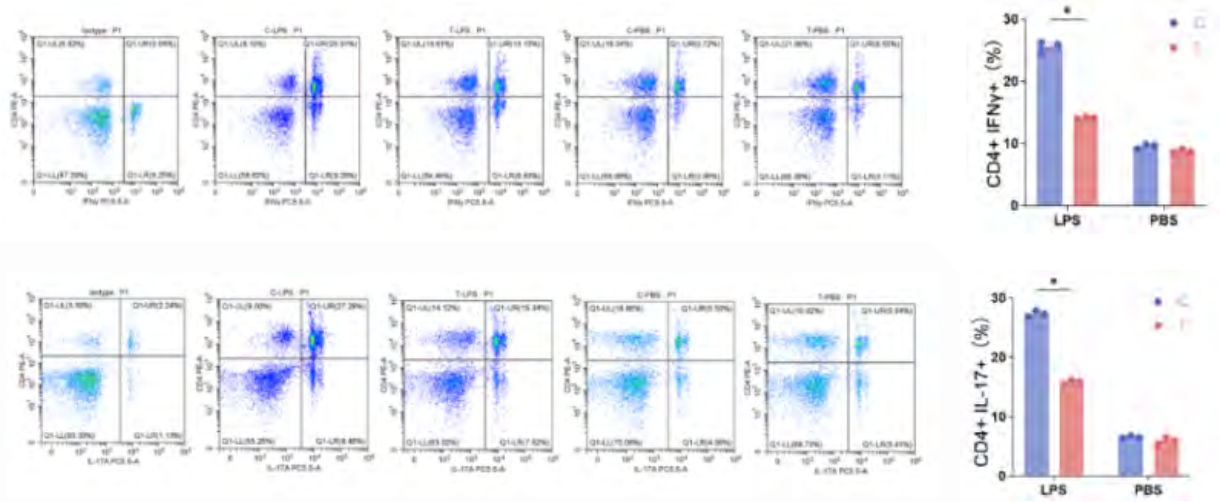


图 26:rs2057656 位点多态性对 T 细胞向炎症表型活化的影响

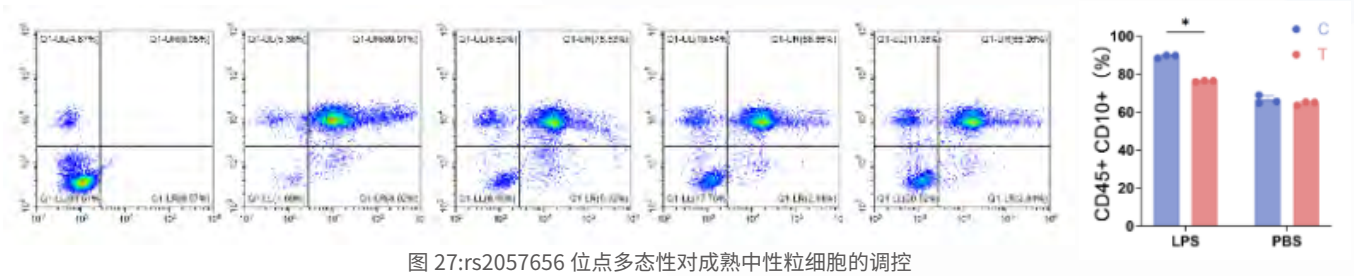


图 27:rs2057656 位点多态性对成熟中性粒细胞的调控

qPCR 结果显示，T 基因型组中，IL1B、IL6、TNF 和 CCL2 的 mRNA 表达水平均显著下降（P<0.05），提示较 C 基因型，T 基因型促炎反应明显减弱。

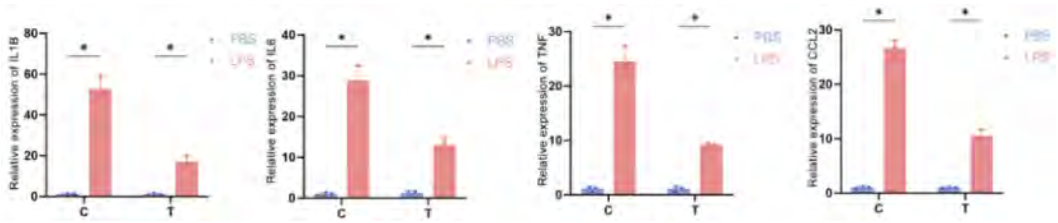


图 28:rs2057656 位点多态性对炎症因子的影响

为了探讨 rs2057656 位点多态性对小鼠巨噬细胞的影响。通过 Western blot、PCR 检测 IRF1-AS1 和 IRF1 的表达；流式细胞术对 BMDMsMFI 进行检测；qPCR 检测炎症因子。

Western blot 和 PCR 结果提示，相较于 C 基因型，T 基因型中 IRF1 蛋白和 iNOS 表达显著降低（P <0.05），而 IRF1-AS1 表达显著升高。

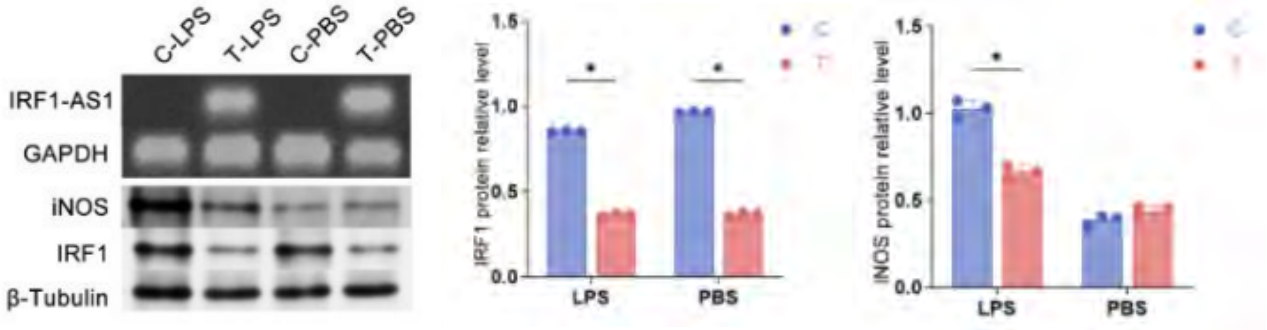


图 29：rs2057656 位点多态性对 IRF1-AS1 和 IRF1 表达水平的影响

流式结果提示，T 基因型显著抑制巨噬细胞向 M1 型炎症表型活化。

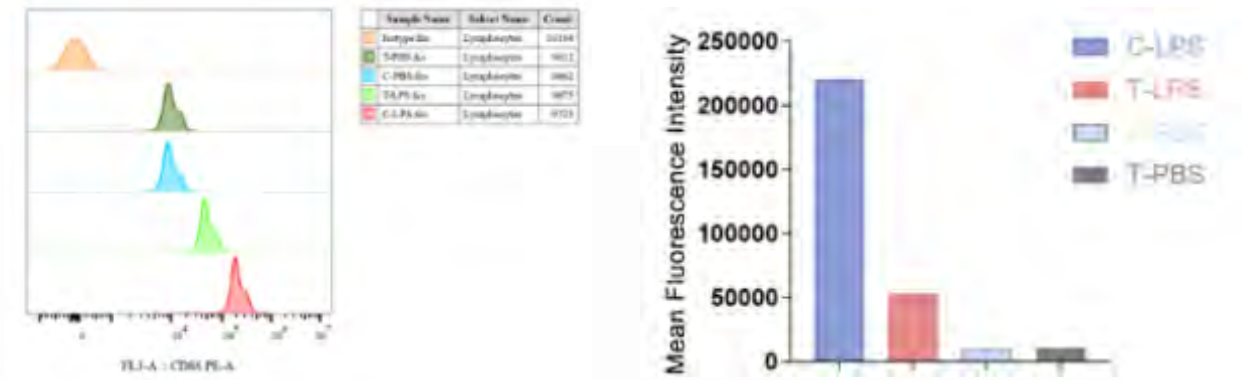


图 30:rs2057656 位点多态性对巨噬细胞活化的影响

qPCR 结果显示，较 C 基因型，T 基因型 IL1B、IL6、TNF 和 CCL2 的 mRNA 表达水平均显著下降（P<0.05）。

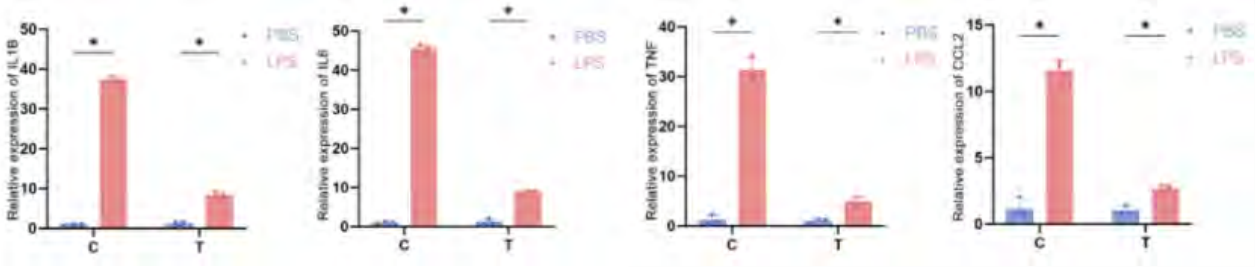


图 31: rs2057656 位点多态性对炎症因子的影响

进行挽救实验验证，采用 PCR 和 Wb 检测结果显示，CD14+ 中过表达 IRF1-AS1-T 显著增加了 IRF1-AS1 的 RNA 表达，显著减少 IRF1 的表达（P<0.05）。

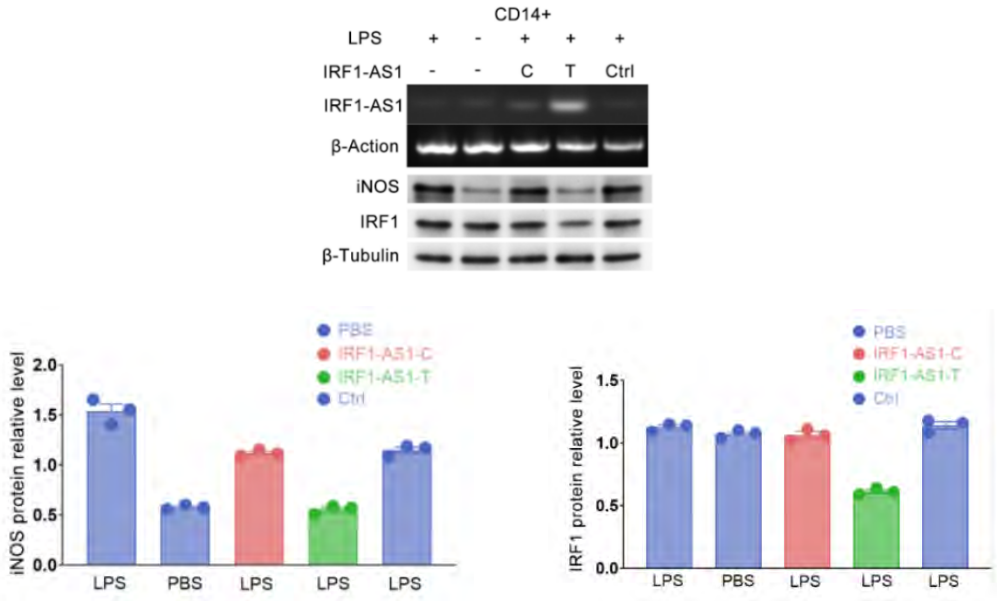


图 32：过表达 IRF1-AS1 对 IRF1 表达的影响

采用 PCR 和 Wb 检测，结果显示 BMDMs 中过表达 IRF1-AS1-T 显著增加 IRF1-AS1 的表达，显著减少 IRF1 和 iNOS 蛋白表达（P<0.05）。

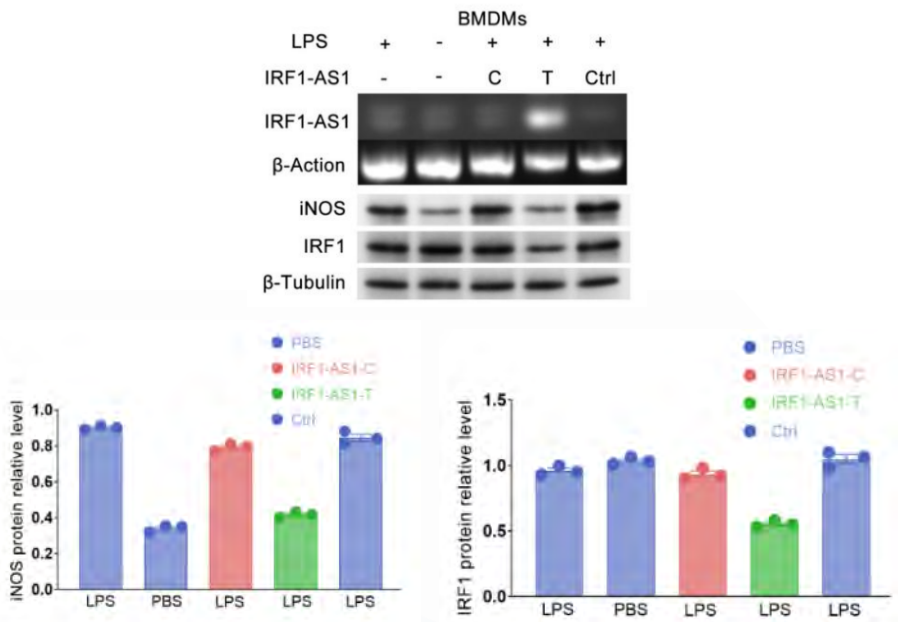


图 33：过表达 IRF1-AS1 对 IRF1 表达的影响

4.rs2057656 位点多态性通过 DNA 甲基化抑制 IRF1-AS1 表达

为评估 rs2057656 位点是否通过发生甲基化调控 IRF1-AS1，首先通过 BSP-seq 检测 IRF1-AS1-C 质粒，结果提示该位点未发生甲基化。将 IRF1-AS1-C 质粒转染入 CD14+ 后，再次用 BSP-seq 检测发现 rs2057656 位点出现甲基化。提示 rs2057656 位点需在细胞环境中才能发生 DNA 甲基化。

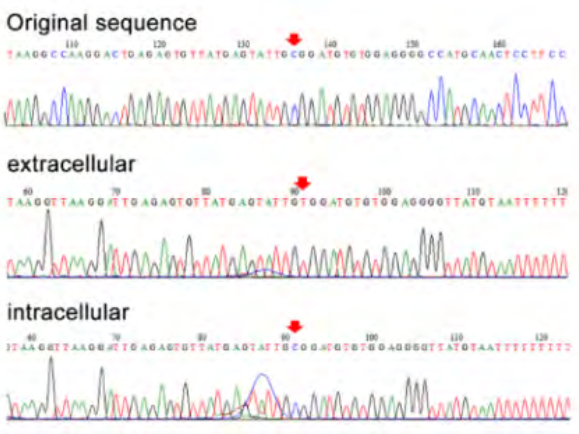


图 34：rs2057656 位点甲基化依赖细胞环境

为探索 rs2057656 位点在细胞中发生甲基化的机制，使用 DNA 甲基化转移酶抑制剂 RG108 处理 C 基因型 PBMCs，甲基化特异性 PCR 分析提示，在 RG108 处理后，rs2057656 位点的甲基化消失，提示 **rs2057656 位点甲基化依赖于细胞中 DNA 甲基化转移酶。**

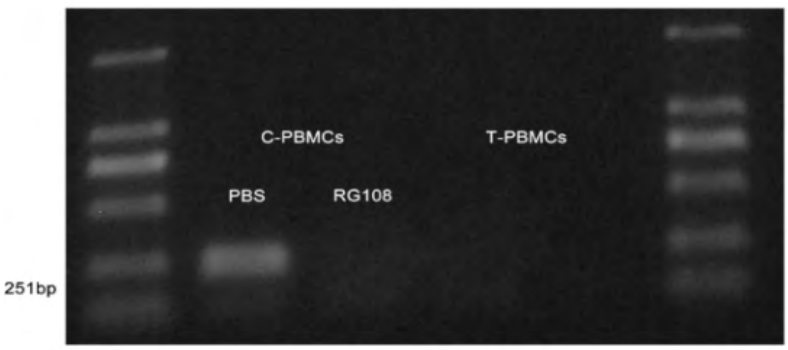


图 35：RG108 抑制 rs2057656 位点甲基化

为明确介导 rs2057656 位点甲基化的 DNA 甲基转移酶，通过 EMSA 实验进行筛选。购买 DNMT1、DNMT3a 及 DNMT3b 重组蛋白，通过 T7 转录合成并生物素标记 IRF1-AS1 启动子。结果显示，DNMT3a 能与 IRF1-AS1 启动子特异性结合，而 DNMT1 和 DNMT3b 未显示出结合能力，提示 DNMT3a 可能介导该位点甲基化。

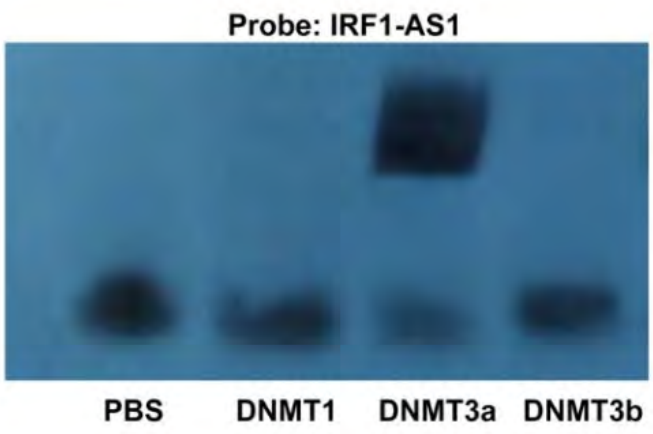


图 36：EMSA 筛选结合 IRF1-AS1 启动子的 DNA 甲基转移酶

使用 DNMT3a 进行 CHIP-seq 和 Motif 分析，结果显示 DNMT3a 特异性结合于 IRF1 基因 rs2057656 区域，进一步确认 DNMT3a 是介导该位点甲基化的关键酶。

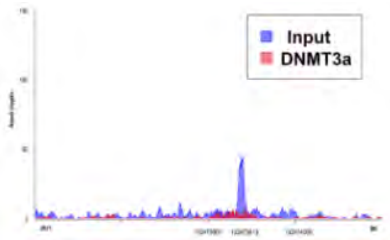


图 37：CHIP-seq 发现结合位点是 rs2057656 区域碱基



图 38：Motif 分析发现结合位点是 rs2057656 区域碱基

为探究 DNA 甲基化抑制 IRF1-AS1 转录的机制，采用 DNA pull down 和 EMSA 实验评估 RNA 聚合酶 II 与 IRF1-AS1 DNA 结合情况。结果表明，RNA 聚合酶 II 可结合 T 基因型 DNA，而无法结合 C 基因型 DNA，提示甲基化阻断其转录起始。

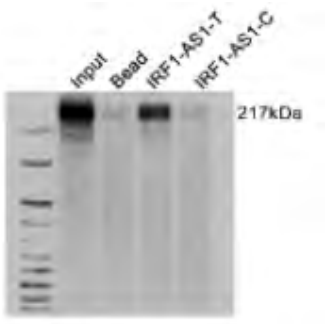


图 39:RNA 聚合酶 II 未结合 C 基因型 IRF1-AS1 DNA

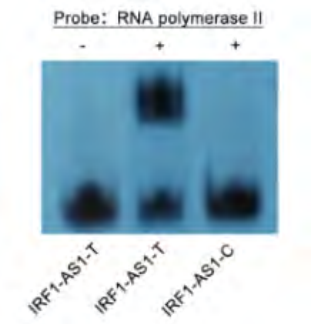


图 40:RNA 聚合酶 II 结合 T 基因型 IRF1-AS1 DNA

5. IRF1-AS1 通过组蛋白去乙酰化抑制 IRF1 转录

通过 ATAC-seq 和 PCR 实验评估 IRF1-AS1 对 IRF1 转录活性的调控。结果表明，相较于 C 基因型，T 基因型在 IRF1 转录起始位点附近 2kb 区域的染色质开放性明显受限，提示 T 基因型表达的 IRF1-AS1 可抑制 IRF1。

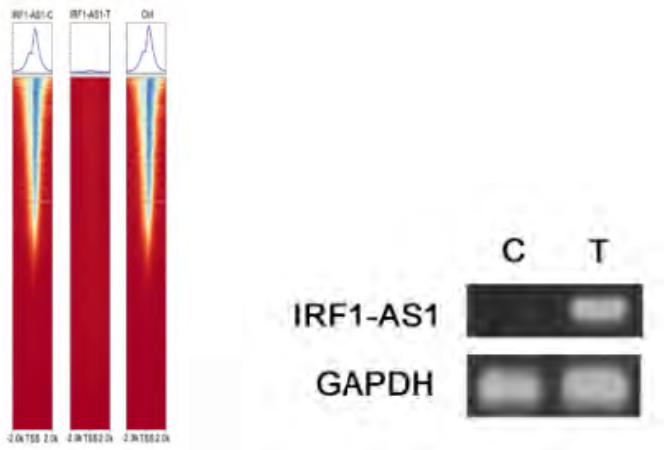


图 41：rs2057656 基因多态性对 IRF1 转录活性的影响

进一步探索 IRF1-AS1 抑制 IRF1 染色质孔径开放的原因，采用 CHIP-seq 实验分析组蛋白乙酰化标志物，结果表明，T 基因型启动子和超级增强子区域的组蛋白 H3K4me1 和 H3K4me3 去乙酰化，这证明 IRF1 的启动子和超级增强子未活化，这也是 T 基因型染色质孔径开放性关闭的原因。

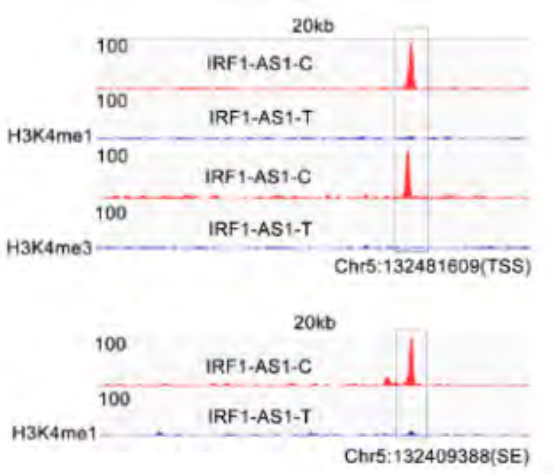


图 42：T 基因型抑制 IRF1 启动子和增强子活性

为探究 IRF1-AS1 抑制 IRF1 转录的分子机制，采用 CHIRP 实验评估 IRF1-AS1 与 IRF1 基因的结合能力。测序和 PCR 分析结果发现，IRF1-AS1 可特异性结合 IRF1 基因的 DNA 区域（chr5:132410929）。提示其可能通过直接结合靶基因 DNA 抑制 IRF1 的转录活性。

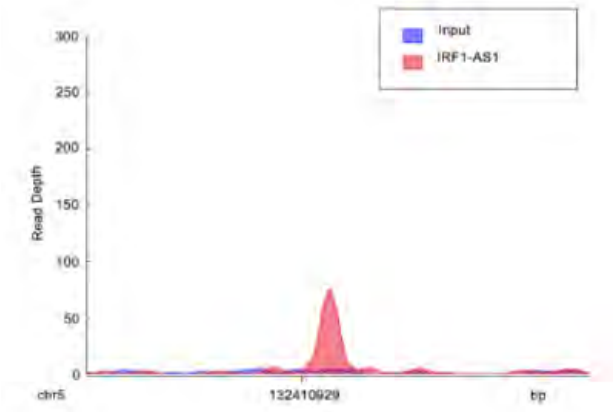


图 43:CHIRP-seq 验证 IRF1-AS1 结合 IRF1 DNA

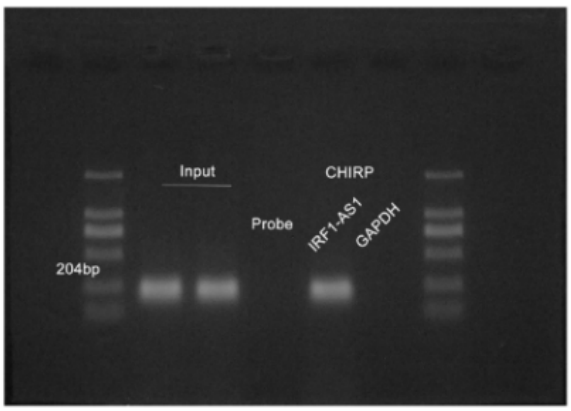


图 44:CHIRP-PCR 验证 IRF1-AS1 结合 IRF1 DNA

去乙酰化蛋白酶局部蓄积是导致组蛋白去乙酰化的原因。故采用 RNA-EMSA 结合 CHIRP 筛选与 IRF1-AS1 相互作用的组蛋白去乙酰化酶。结果显示，在常见的组蛋白去乙酰化酶（HDAC1、HDAC2、HDAC3）中， HDAC2 能与 IRF1-AS1 互相结合，这可能是 IRF1-AS1 导致 IRF1 组蛋白去乙酰化以及转录抑制的机制。

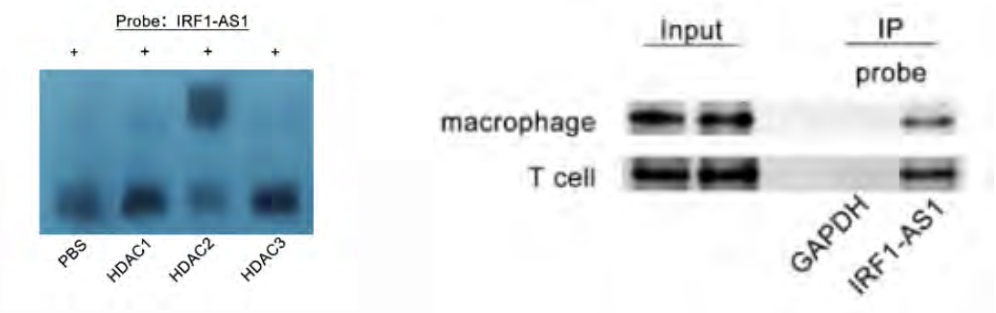


图 45:HDAC2 与 IRF1-AS1 特异性结合

为了探讨 HDAC2 在 IRF1 转录调控中的作用，采用去乙酰化酶抑制剂（CAY10863）处理细胞。PCR 和 Western blot 检测显示，抑制 HDAC2 后 IRF1-AS1 表达无明显变化，而 IRF1 和 iNOS 蛋白表达水平显著上调（$P<0.05$），提示去乙酰化酶抑制剂能解除 IRF1-AS1 介导的 IRF1 转录抑制作用。

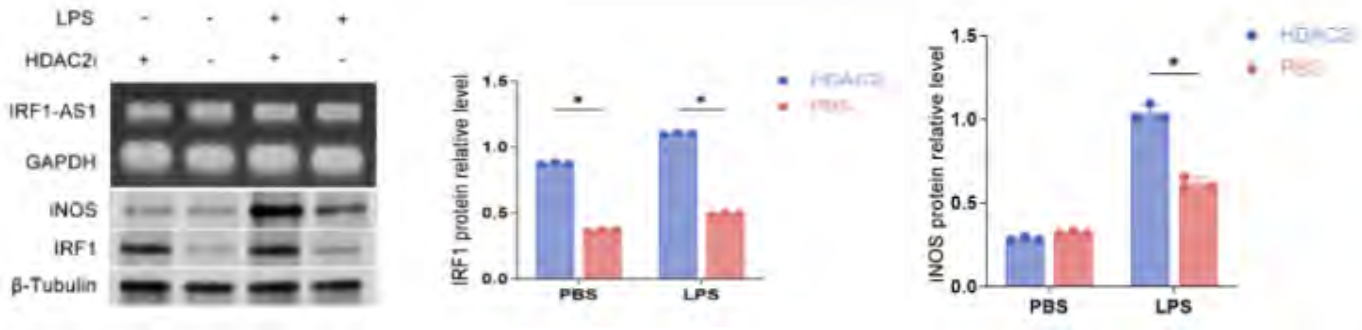


图 46:HDAC2 对 IRF1 的调控作用

CAY10863 对 PBMCs 表现出剂量依赖性，抑制 HDAC 酶活性同时引起细胞活力下降。采用 CCK-8 与酶活性检测，在 2uM 浓度下，细胞活性水平高，而酶抑制率达 80%，提示 CAY10863 在 2uM 可能是较合适的药效毒性平衡浓度。

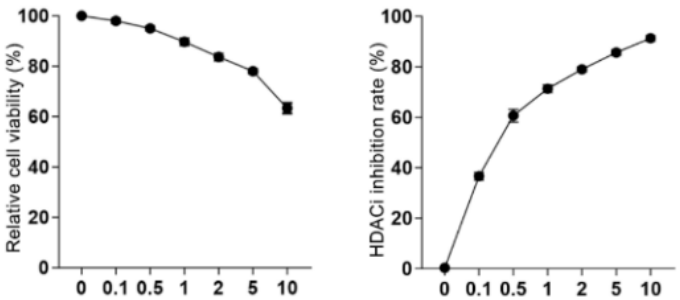


图 47：CAY10863 浓度依赖性影响细胞活力与 HDAC 酶活性

6．IRF1-AS1-EVs 治疗 C 基因型 ARDS

为了研究 IRF1-AS1 是否可以通过调控 IRF1 表达改善 ARDS，构建 IRF1-AS1 过表达的 RAW264.7 细胞外泌体（IRF1-AS1-EVs），空白质粒为对照（Ctrl-EVs）。结果提示，IRF1-AS1 成功转运至外泌体中。

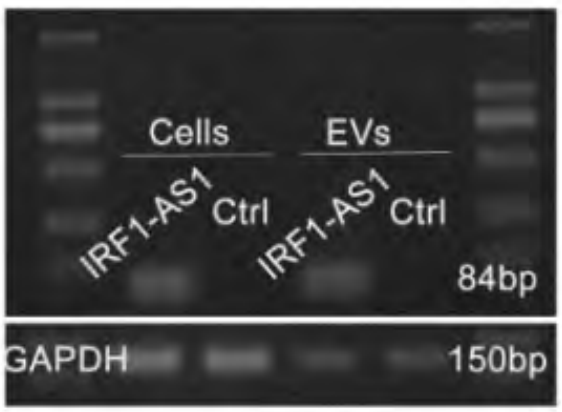


图 48:IRF1-AS1 成功转运至外泌体

构建 KP-ARDS 小鼠，假手术作为对照。将 IRF1-AS1-EVs 和 Ctrl-EVs 经鼠尾静脉输注，治疗 KP-ARDS。为明确 IRF1-AS1 能否入细胞核，注射 EVs 24 小时后提取外周血单核细胞，荧光显微镜显示 IRF1-AS1 分布于细胞质及细胞核。进一步活体成像提示，IRF1-AS1-EVs 成功到达小鼠肺部。

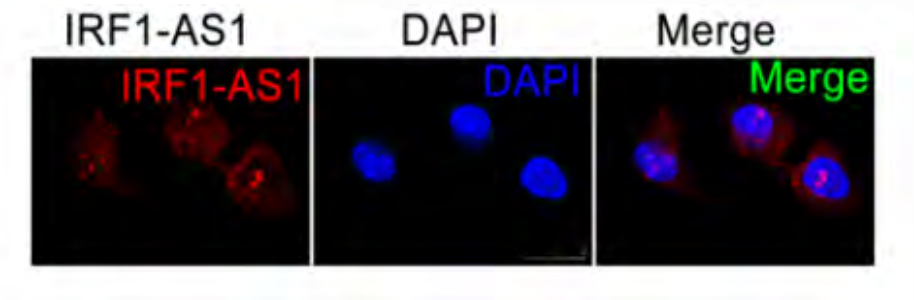


图 49:IRF1-AS1 分布于细胞质及细胞核

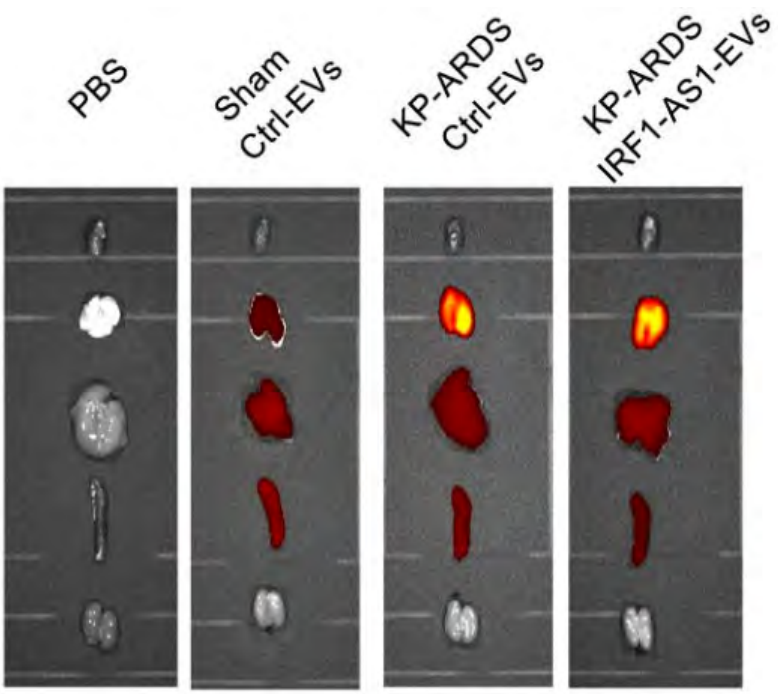


图 50:IRF1-AS1-EVs 在小鼠体内分布

采用免疫组化评估 IRF1 表达。结果提示，与空白对照组相比，IRF1-AS1-EVs 显著下调 IRF1 表达水平（P<0.001）。

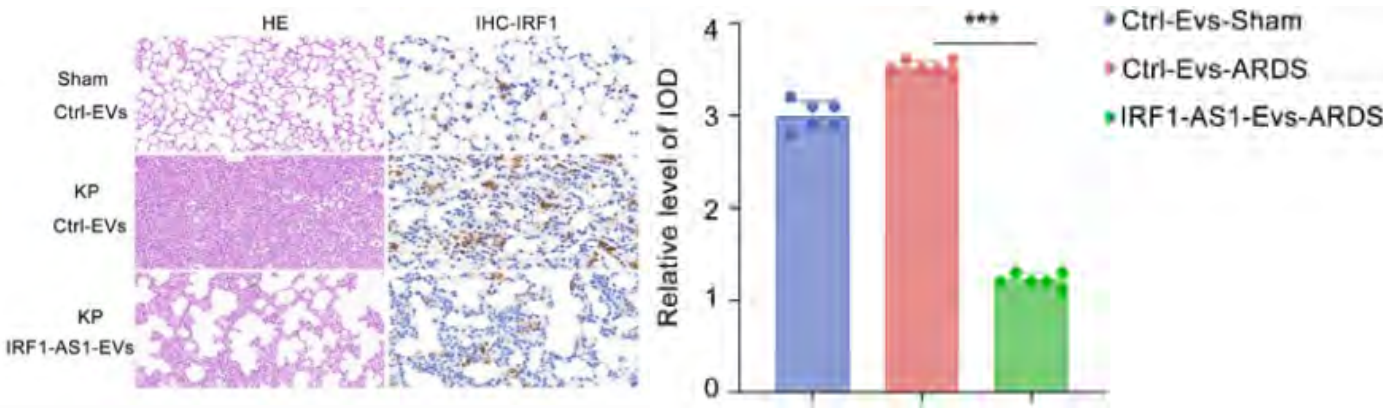


图 51: 免疫组化评估 IRF1 表达

采用伊文思蓝实验评估 IRF1-AS1-EVs 改善肺血管通透性。结果提示：与 Ctrl-EVs 相比，IRF1-AS1-EVs 显著改善肺通透性 (P <0.001)。

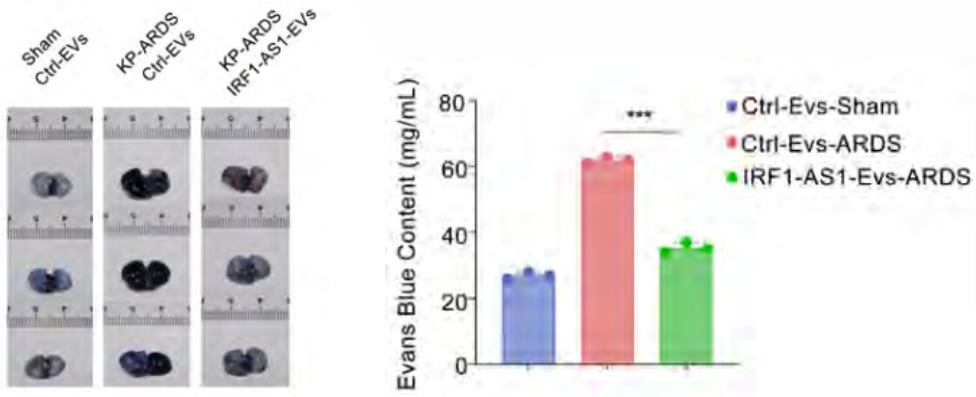


图 52:IRF1-AS1-EVs 改善 ARDS 肺血管通透性

采用肺组织 HE 染色切片评估肺损伤。结果提示：与 Ctrl-EVs 相比，IRF1-AS1-EVs 显著降低肺损伤评分 (P<0.001)。

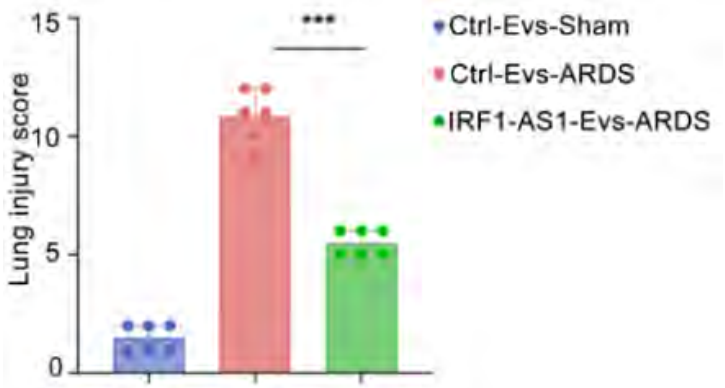


图 53:IRF1-AS1-EVs 改善肺损伤评分

采用湿干重比评估肺组织水肿改善程度。结果表明，与 Ctrl-EVs 相比，IRF1-AS1-EVs 显著改善肺组织水肿 (P<0.001)。

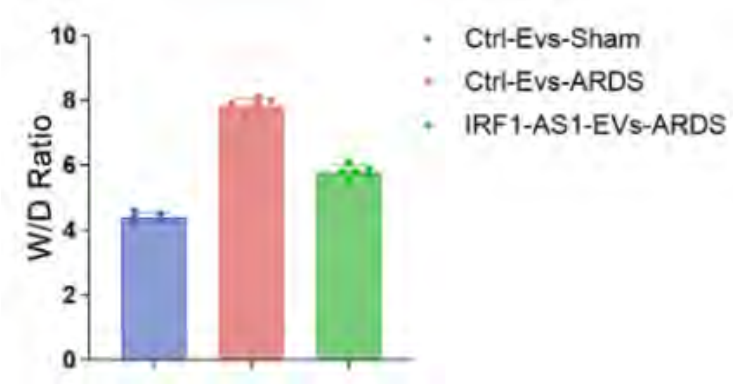


图 54:IRF1-AS1-EVs 对肺湿干重比的改善

采用流式细胞术评估小鼠免疫细胞表型，结果提示，与空白对照组相比，IRF1-AS1-EVs 组显著减少 KP-ARDS 小鼠肺部的 M1 巨噬细胞比例；同时显著抑制 Th1 和 Th17 的活化。

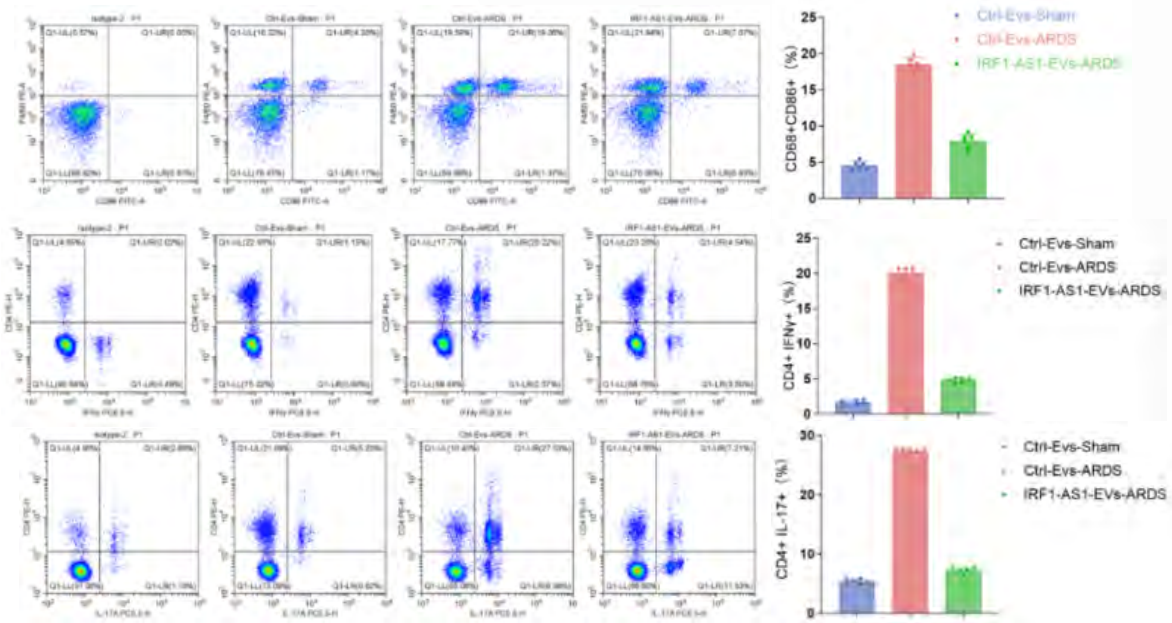


图 55:IRF1-AS1-EVs 对免疫细胞活化的影响

采用 qPCR 检测炎症因子，结果显示较空白治疗组，IRF1-AS1-EVs 显著减少炎症因子 IL1B、IL6、TNF、CCL2 数量。

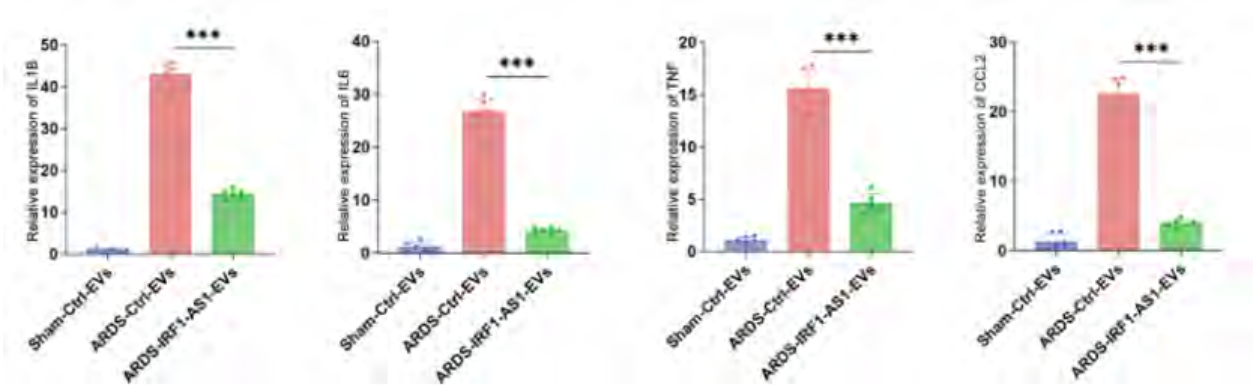


图 56:IRF1-AS1-EVs 对炎症因子表达的影响

Machine Learning and Untargeted Metabolomics Identify Serum Biomarkers for Diagnosis and Prognosis Prediction of Sepsis

姓名：杨雨欣，董琼兰
单位：四川大学华西医院，绵阳市第三人民医院

Abstract:

Objective: Efficient biomarkers for early diagnosis and mortality risk prediction in sepsis are currently lacking, while traditional clinical indicators (e.g., SOFA score) exhibit limitations.This study, leveraging serum untargeted metabolomics technology and machine learning, aims to screen sepsis-specific metabolites for assisting diagnosis and constructing diagnostic and mortality risk prediction models.

Methods: Sepsis patients (SEP,n=89) were enrolled as the experimental group, while non-sepsis critically ill patients (NSEP,n=30) and healthy individuals (HC,n=30) served as control groups. Serum metabolites were analyzed using liquid chromatography-tandem mass spectrometry (LC-MS/MS). Multivariate statistics (PLS-DA) were applied to identify differential metabolites. Key metabolites were screened using Least Absolute Shrinkage and Selection Operator (LASSO) regression, Random Forest Recursive Feature Elimination (RF-RFE), and Support Vector Machine Recursive Feature Elimination (SVM-RFE) algorithms were employed. Three machine learning approaches (Logistic Regression, Random Forest, and Support Vector Machine) were used to develop diagnostic and prediction models.

Results: Metabolic profiles significantly differed between the sepsis group and control groups. Machine learning identified six key metabolites for distinguishing sepsis patients from non-sepsis patients or healthy individuals. The diagnostic efficacy of the metabolite combination was significantly higher than that of traditional clinical indicators (AUC 0.97,95%CI (0.943- 0.997)). In the sepsis mortality group versus the non-mortality group, two critical metabolites were selected, and the combined metabolite-based risk prediction model outperformed traditional single indicators (AUC 0.859,95%CI(0.784-0.934)), with statistically significant differences (P<0.05). In the septic shock group versus non-septic shock group, seven key metabolites were selected. Although the composite risk prediction model with combined metabolites was superior to traditional single indicators (AUC 0.878,95%CI(0.808-0.947)), the difference was not statistically significant.

Conclusion: This study delineates the metabolic landscape of sepsis, demonstrating that metabolomics-based models surpass traditional scoring systems in diagnosis and mortality risk prediction, thereby offering novel tools for personalized clinical intervention.

Key words:sepsis；metabolomics；machine learning.

1.Introduction

Sepsis is a life-threatening organ dysfunction resulting from a dysregulated host response to infection [1]. Its pathophysiology involves a complex process characterized by aberrant activation and regulatory imbalance of the immune system. Currently, the global incidence of sepsis has reached 37%, with sepsis-related deaths accounting for 19.7% of total mortality worldwide [2]. For patients with sepsis, early and accurate identification and clinical assessment are of paramount importance. However, the early diagnosis of sepsis remains challenging. Pathogen detection is often unavailable, and host responses frequently present with non-specific manifestations. Traditional biomarkers, such as C-reactive protein (CRP), procalcitonin (PCT), and white blood cell count, lack sufficient discriminative power [3]. Although numerous novel sepsis biomarkers have emerged over the years, none have consistently outperformed existing standards or achieved widespread clinical application [4, 5]. In recent years, advancements in omics technologies have propelled research at the molecular level—encompassing genomic, transcriptomic, proteomic, and metabolomic analyses—deepening our understanding of the mechanisms underlying host dysregulation, facilitating the development of diagnostic approaches, and enabling the identification of novel clinical subtypes of sepsis [6].

Metabolomics research effectively captures alterations in biosynthesis and consumption within organisms under disease conditions [7], reflecting the integrated outcomes of interactions among genetic, environmental, pathological, and therapeutic factors. Untargeted metabolomics, utilizing LC-MS/MS, facilitates comprehensive and in-depth analyses of metabolites that are highly polar, easily ionized, and challenging to volatilize. By incorporating bioinformatic approaches, researchers can unveil the physiological mechanisms underlying these metabolic changes, thereby enhancing the understanding of their functions and impacts within biological systems. This line of investigation provides critical insights and guidance for the development of disease biomarkers, elucidation of pathogenic mechanisms, and exploration of drug therapeutic actions.

Current studies have revealed significant differential expression of key metabolites in sepsis patients, including hydroxybutyrate, lactate, phenylalanine, glutamate, choline, phosphatidylcholine, creatinine, and tryptophan [8-10]. These markers provide considerable clinical utility due to their detectability, aiding clinicians in the early identification and intervention of septic patients. However, existing research remains limited, characterized by variations in control group selection and specimen collection timing. Therefore, further extensive studies are essential to develop metabolomic models of sepsis, which will offer robust support for the early recognition of sepsis, assessment of disease severity, and prognosis evaluation.To address the over-reliance on clinical experience and the uneven distribution of medical resources in traditional disease diagnosis, machine learning algorithms have been introduced for early disease detection [11,12]. Machine learning-based diagnostic frameworks typically encompass data preprocessing (extracting features conducive to model training) and machine learning algorithms (including feature dimension reduction, model construction, and model evaluation). The application of machine learning facilitates more accurate clinical diagnoses, reduces instances of misdiagnosis and missed diagnoses, and promotes the advancement of precision medicine. Consequently, it has become an indispensable discipline in the field of early disease diagnosis [13].

In this context, the present study conducted untargeted metabolomic analysis on serum samples from sepsis patients, incorporating machine learning algorithms. Our aim was to identify novel biomarkers associated with diagnosis or prognosis and to explore metabolic pathway alterations in sepsis. This research may provide effective support for early identification, clinical intervention, and prognostic assessment of sepsis, thereby laying a foundation for precision medicine in sepsis management.

2.Materials and methods

2.1Collections and preparation of clinical specimen

This study was approved by the Ethics Committee of The Third Hospital of Mianyang (Ethics Approval No: 2024.13) and carried out in accordance with relevant guidelines and regulations.Informed consent was obtained from all subjects and/or their legal guardian(s) prior to their participation in the study. Septic patients (SEP group) hospitalized in the Intensive Care Unit (ICU) of our tertiary Grade A hospital between February 2024 and June 2025 were recruited as the experimental group. Concurrently, non-septic patients (NSEP group) admitted to the ICU during the same period, along with healthy individuals (HC group) undergoing physical examinations at our hospital, were selected as the control group. The NSEP group and HC group collectively constituted the control group for the septic cohort. The septic cohort was further subdivided into a mortality group (SEPS group) and a survival group (SEPNS group) based on whether death occurred within 28 days of enrollment. Additionally, patients were categorized into a shock group (SS group) and a non-shock group (NSS group) based on the presence or absence of shock at enrollment or during the follow-up period.

SEP Group inclusion Criteria: (1) Age $\geqslant$ 18 years;(2) Meeting the Sepsis-3.0 diagnostic criteria, fulfilling both of the following conditions: i.Confirmed or suspected infection, and ii. An increase in sequential organ failure assessment (SOFA) score $\geqslant$ 2 points. Exclusion Criteria: (1) Pregnancy;(2) ICU length of stay $\leqslant$ 24 hours;(3) Missing data > 50%; (4) Advanced malignant tumor; (5) Severe immunodeficiency; (6) History of antibiotic or antiviral medication use within one month prior to admission.NSEP group inclusion Criteria: (1) Age $\geqslant$ 18 years; (2) Diagnosed with a non-infectious disease.Exclusion Criteria: (1) Pregnancy; (2) ICU length of stay $\leqslant$ 24 hours; (3) Missing data > 50%; (4) Advanced malignant tumor; (5) Severe immunodeficiency; (6) History of antibiotic or antiviral medication use within one month prior to admission.

Baseline information from patients was gathered, which included factors such as age, sex, reasons for ICU admission, and existing comorbidities (evaluated using the Charlson Comorbidity Index, aCCI). Clinical parameters recorded included the acute physiology and chronic health evaluation II (APACHE-II) score, SOFA score, lactate concentration, interleukin-6 (IL-6) levels, procalcitonin (PCT)

levels, the use of invasive mechanical ventilation, the incidence of septic shock, and mortality rates over 28 days. For patients classified in the sepsis cohort, fresh blood samples were obtained using blood collection or sterile centrifuge tubes (without anticoagulants or coagulants) within 6 hours following hospital admission and diagnosis, and before the initiation of antibiotic therapy. The samples were maintained at 4° C for one hour, followed by centrifugation at 4° C at 600 g for 10 minutes. Once blood cells had fully settled, the upper serum layer was drawn off and divided into 2-mL centrifuge tubes. These serum aliquots were labeled, quickly frozen in liquid nitrogen for 15 minutes, and then stored at -80° C. Similarly, peripheral blood serum samples from the control group were collected and processed using the same technique.

2.2 Metabolomics Sequencing and Data Preprocessing

Untargeted metabolomics was conducted LC-MS/MS technology. Data were captured in both positive ion (pos) and negative ion (neg) modes to effectively and comprehensively identify and analyze unknown metabolites present in the samples.Initially, 100 µL from each original sample was taken, followed by the addition of 500 µL of pre-chilled (− 80 ° C) mass spectrometry-grade methanol containing internal standards. This solution was vortexed for 1 minute, incubated at 4° C for a duration of 10 minutes, and then centrifuged at 4 ° C at 14,000 rpm for 20 minutes. Post-centrifugation, 200 µL of supernatant was collected, lyophilized at low temperatures, and subsequently stored at − 20 ° C.Subsequently, equal volumes from each experimental sample were combined and thoroughly mixed to create quality control (QC) samples. Furthermore, blank samples were prepared using a solution of 20% methanol in water, processed according to the same protocols and data acquisition methods used for the actual samples.

Before the injection of samples, QC samples were evaluated to oversee the performance of the instrument. Simultaneously, the LC-MS system was stabilized to ensure its consistent functionality. During the course of the experiment, QC samples were intermittently included among experimental samples to evaluate the stability of the platform and support future data quality control. (Comprehensive details regarding instruments and reagents can be found in Table S1 and Table S2; conditions for chromatography and mass spectrometry are presented in Table S3.)The raw data files in .raw format were loaded into the Compound Discoverer (CD) software for initial filtering, utilizing criteria such as retention time and mass-to-charge ratio (m/z). Peak alignment was executed with a tolerance of 0.2 minutes for deviations in retention time and 5 ppm for mass deviations, in order to improve identification precision. The extraction of peaks was executed based on the following standards: mass deviation $\leqslant$ 5 ppm, signal intensity deviation $\leqslant$ 30%, signal-to-noise ratio $\geqslant$ 3, and a minimum signal intensity of $\geqslant$ 100,000, in addition to the information on adduct ions. The areas of peaks were measured, and target ions were integrated. Molecular formula predictions were conducted based on the peaks of molecular ions and fragment ions, followed by a comparison with the mzCloud, MZvault, and Chemspider databases. To eliminate background ions, blank samples were utilized, resulting in the generation of identified and quantified outcomes.

2.3Statistical Analysis

Multivariate statistical analysis was conducted with the R package Ropls, specifically utilizing Partial Least Squares Discrimination Analysis (PLS-DA). A Variable Importance in Projection (VIP) threshold of greater than 1.0 was established, along with a fold change (FC) criterion exceeding 2 or falling below 0.5, and a P-value threshold of less than 0.05. The primary differential metabolites identified were further confirmed by cross-referencing spectral databases such as Human Metabolome Database (HMDB,https://hmdb.ca/metabolites), LIPID MAPS Structure Database (LM,http://www.lipidmaps.org/), and Kyoto Encyclopedia of Genes and Genomes (KEGG,https://www.genome.jp/kegg/pathway.html) for secondary qualitative annotation. Metabolic pathway analysis was performed using functional enrichment and the pathway analysis tool of the free web-based software MetaboAnalyst 6.0 (https://www.metaboanalyst.ca/MetaboAnalyst/). Metabolic pathways that showed significant impact ($P < 0.05$) were recognized as pertinent pathways.Key metabolites were identified through the application of LASSO, RF-RFE, and SVM-RFE. Various models, including logistic regression (LR), random forest (RF), and support vector machine (SVM), were built, and the most effective model was chosen utilizing 5-fold cross-validation to serve as the scoring tool for the metabolite combinations.In the diagnostic evaluation for sepsis (comparing SEP to NSEP + HC groups), the chosen metabolite combination was analyzed against the SOFA score, PCT, and IL-6 through ROC curve analysis. The area under the curve (AUC) was assessed, alongside diagnostic performance metrics—such as sensitivity, specificity, positive predictive value, negative predictive value, and accuracy—with their respective 95% confidence intervals calculated at the optimal threshold. Additionally, the quantification of diagnostic enhancement was

evaluated using Integrated Discrimination Improvement (IDI) and Net Reclassification Improvement (NRI) metrics.For assessing sepsis prognosis and stratifying risk, a composite model was created by merging the selected metabolite combination with clinical factors, including the SOFA score, APACHE II score, and lactate levels. This composite model was then compared to individual clinical factors through ROC curve analysis, and the AUC values were juxtaposed.Continuous variables that followed a normal distribution were assessed using the independent samples t-test, whereas non-normally distributed continuous variables were evaluated using the non-parametric Wilcoxon rank-sum test. Categorical variables were reported as frequencies (n %), and group comparisons were conducted using the chi-square test. A P-value of less than 0.05 was deemed statistically significant.All statistical analyses were performed using R software (version 4.3.0). The comprehensive workflow of this research is depicted in Figure 1.

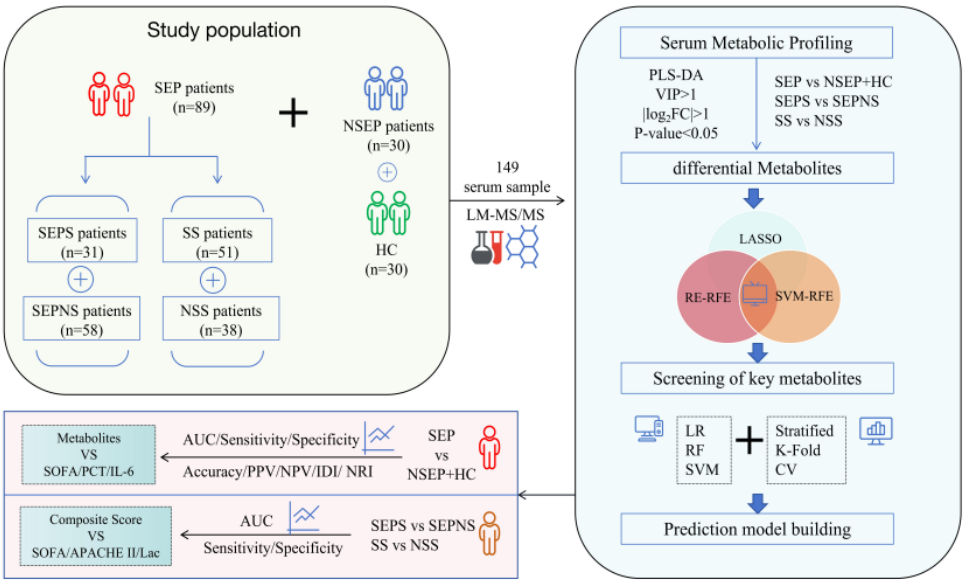


Figure 1. The overall process of the study. SEP, sepsis; NSEP, non-sepsis; HC, heath controls; SEPS, septic shock; SEPNS, non-septic shock; SS, sepsis survival; NSS, sepsis non-survival; LC-MS/MS, liquid chromatography-tandem mass spectrometry; PLS-DA, partial least squares discrimination analysis; VIP, variable important projection; FC, fold change; LASSO, least absolute shrinkage and selection operator; RF, random forest; RFE, recursive feature elimination; SVM, support vector machine; LR, logistic regression; CV, cross-validation; AUC, area under the receiver operating characteristic curve; PPV, positive predictive value; NPV, negative predictive value; IDI, integrated discriminant improvement index; NRI, net weight classification improvement index; SOFA, sequential organ failure assessment; PCT, procalcitonin; IL-6, interleukin-6; APACHE II, acute physiology and chronic health evaluation II; Lac, lactic acid.

3.Results

3.1Comparison of Baseline Characteristics of Enrolled Subjects

This study included a total of 89 patients diagnosed with sepsis, comprising 51 individuals with septic shock and 38 without shock. Among these, 31 were non-survivors and 58 were survivors. Additionally, the study involved 30 critically ill patients in the ICU who were not diagnosed with sepsis and 30 healthy controls. The median age of the healthy controls was 64.5 years, with a demographic breakdown of 16 males and 14 females. The clinical characteristics of both the sepsis and non-sepsis groups are detailed in Table 1. No significant differences were observed in baseline characteristics, including age, gender, underlying diseases, APACHE II score, or SOFA score among the groups. However, levels of lactate, PCT, and IL-6 were significantly elevated in the SEP group compared to the NSEP group, with these differences being statistically significant ($P < 0.05$).

Table1 Baseline characteristics of patients in two groups			
	NSEP（n=30）	SEP（n=89）	*P*-value
Age(years)[a]	63.00 (55.00, 72.75)	69.00 (60.00, 80.00)	0.161
Male (n, %)[b]	12 (40.00)	51 (57.30)	0.101
aCCI[a]	5.00 (2.50, 7.75)	4.00 (3.00, 5.00)	0.087
APACHE II[a]	20.00 (14.25, 23.75)	18.00 (12.00, 25.00)	1.000
SOFA[a]	7.00 (5.00, 9.75)	9.00 (6.00, 10.00)	0.071
Shock(n,%)[b]	14 (46.67)	51 (57.30)	0.312
Mechanical ventilation(n,%)[b]	21 (70.00)	58 (65.17)	0.628
MAP(mmHg)[a]	89.00 (73.00, 99.50)	78.00 (60.00, 95.00)	0.157
Lac(mmol/L)[a]	3.15 (1.47, 4.72)	4.00 (2.80, 5.60)	0.031
PCT(ng/ml)[a]	0.82 (0.14, 1.07)	19.29 (2.63, 81.48)	<.001
IL-6(pg/ml)[a]	120.41 (51.22, 212.80)	431.44 (178.29, 1222.07)	<.001
28days death(n,%)[b]	7 (23.33)	31 (34.83)	0.243

aCCI,age-adjusted Charlson Comorbidity Index;APACHE II,acute physiology and chronic health evaluation II;SOFA, sequential organ failure assessment;MAP: mean arterial pressure;

aMann-Whitney test for comparison between two groups.bChi-square test for comparison between two groups.

3.2 Differential Metabolite Profiles Among Groups

In the context of clinical samples characterized by complex backgrounds, the utilization of supervised classification models becomes essential. Techniques such as PLS-DA have been employed to analyze the differences among two or more groups, thereby amplifying inter-group variations and efficiently extracting information pertaining to group-specific variability. The PLS-DA score plots illustrated the metabolic profile differences between the SEP group and the HC group, as well as between the SEP and NSEP groups (Figure 2, A and D). Additionally, distinctions were observed between the SS and NSS groups, as well as between SEPS and SEPNS groups (Figure S1).

We identified multiple metabolites with significantly altered abundances between the sepsis group and the control groups (VIP > 1, |FC| > 2, and P < 0.05). Volcano plots were utilized to visualize the relationship between the log2 fold change (x-axis) and the −log10 p-value (y-axis) for each metabolite in the group comparisons. Clustered heatmaps of the differential metabolites provide an intuitive display of the expression patterns of these metabolites across groups. The x-axis represents individual samples, while the y-axis lists the differential metabolites. The color in the heatmap indicates the relative abundance of each metabolite, with red signifying up-regulation and green indicating down-regulation in the respective group. Overall, the plots clearly demonstrate that metabolite profiles are similar within groups but significantly different between groups, further emphasizing the distinct metabolic signatures between sepsis patients and controls (Figure 2; B,E and C,F). Volcano plots and heatmaps for the comparisons between SS vs. NSS groups and SEPS vs. SEPNS groups are provided in the Supplementary Materials (Figure S1). The number of up-regulated and down-regulated differential metabolites for each comparison is detailed in Supplementary Table S4.

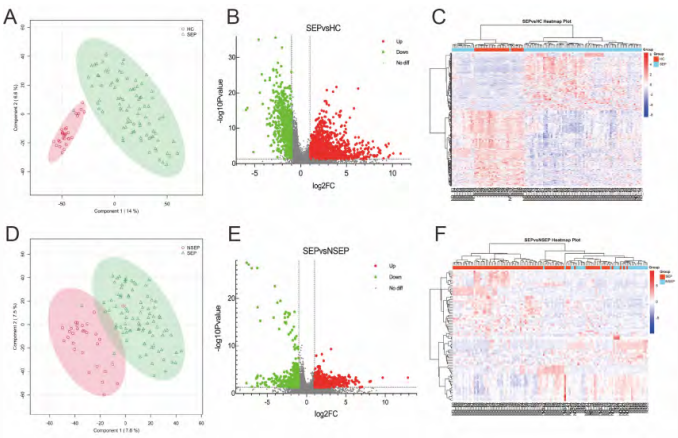


Figure 2. Metabolic profiling of sepsis patients and controls. (A) and (D) PLS-DA score plots for the SEP vs. HC and SEP vs. NSEP comparisons under positive ion mode, respectively. (B) and (E) Volcano plots for the SEP vs. HC and SEP vs. NSEP comparisons, respectively. (C) and (F) Heatmaps of differential metabolites for the SEP vs. HC and SEP vs. NSEP comparisons, respectively.

3.3 Differential Metabolites and Metabolic Pathways Enrichment Analysis

A total of 13,699 substances were detected in both positive and negative ion modes. The preliminary differential metabolites were compared and identified through secondary qualitative analysis by searching against spectral databases, including HMDB, LM, and KEGG.Between the SEP and HC group, 314 endogenous differential metabolites were identified, of which 136 were up-regulated and 178 were down-regulated. In the comparison between the SEP and NSEP groups, 83 endogenous differential metabolites were identified, with 45 being up-regulated and 38 down-regulated. Additionally, 120 endogenous differential metabolites were identified between the SEPS and SEPNS groups, while 133 were identified between the SS and NSS groups. Metabolic pathways enrichment analysis was conducted on the lists of differential metabolites using MetaboAnalyst. Pathways with significant impact ($P < 0.05$) were identified as relevant metabolic pathways.In the comparison between the SEP and HC groups, seven significantly altered metabolic pathways were identified, including Tryptophan metabolism, Tyrosine metabolism, Valine, leucine, and isoleucine biosynthesis, Pantothenate and CoA biosynthesis, and beta-Alanine metabolism (Figure 3A). In the comparison between SEP and NSEP groups, the analysis highlighted the Biosynthesis of unsaturated fatty acids and Histidine metabolism as the major affected pathways (Figure 3B).For the SS versus NSS groups, the significantly enriched pathways included Arginine biosynthesis, Arginine and proline metabolism, Alanine, aspartate and glutamate metabolism, Glyoxylate and dicarboxylate metabolism, Histidine metabolism, and Tryptophan metabolism. In the comparison of SEPNS versus SEPS groups, the major pathways involved were Tryptophan metabolism, Nicotinate and nicotinamide metabolism, Histidine metabolism, and Tyrosine metabolism (Figure S2).

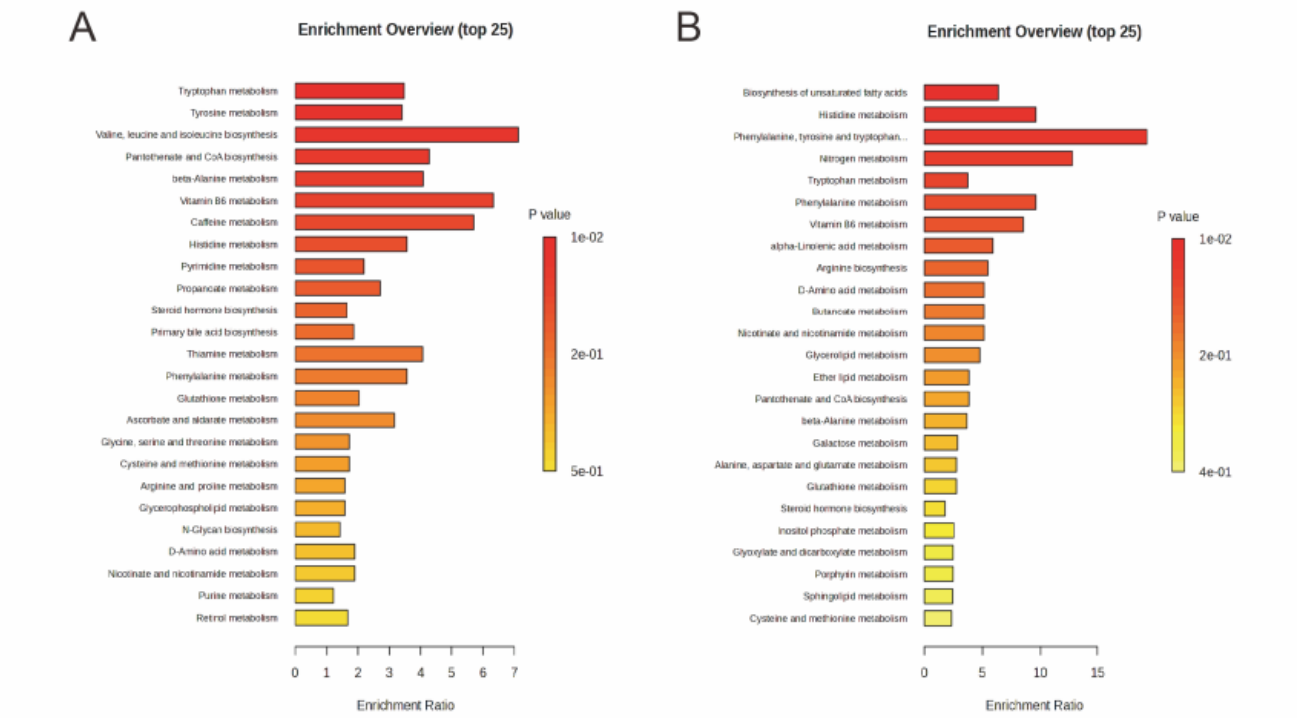


Figure 3, (A) and (B) show metabolic pathways enrichment analysis of differential metabolites between SEPvsHC group and NSEP vs SEP group.

3.4 Construction of a Sepsis Diagnostic Prediction Model Using Machine Learning

To better differentiate the metabolic features between sepsis patients and healthy controls, we investigated the association between metabolic characteristics and the disease using machine learning algorithms based on 43 common differential metabolites identified from both the SEP versus HC groups (314 endogenous differential metabolites) and the SEP versus NSEP groups (83 endogenous differential metabolites).Metabolite selection was performed using LASSO, RF-RFE, and SVM-RFE,

ultimately identifying six key metabolites (Figure 4) that are crucial for distinguishing sepsis from controls: N-Acetylasparagine, 20 beta-Dihydrocortisol, Cer(d18:0/33:0(33OH)), Isoxanthopterin, PC O-19:3, and PC O-34:9.To evaluate the predictive performance of these key metabolites, we constructed three prediction models—LR, FR, and SVM—utilizing 149 samples. All models were assessed through 5-fold cross-validation, with stratified sampling ensuring consistent case-control ratios across folds. The LR model exhibited the highest performance, achieving an AUC of 0.966 (95% CI: 0.938–0.993), and was selected as the metabolite combination scoring tool.

During the performance evaluation phase, the metabolite combination was systematically compared with the SOFA score, PCT, and IL-6. ROC curve analysis was employed to calculate the AUC values for each indicator and to assess the statistical significance of the differences between the curves. The results demonstrated that the diagnostic performance of the metabolite combination was significantly superior to that of the SOFA score, PCT, and IL-6 (Figure 5, Table 2). Furthermore, the IDI index was utilized to quantify the differences in mean predicted probabilities between the sepsis and non-sepsis groups, and the NRI index was employed to evaluate the proportion of correct reclassifications under three-category risk stratification. The results indicated that the metabolite combination exhibited a better discriminative ability for sepsis compared to traditional indicators (SOFA score, PCT, and IL-6) (Table 3).

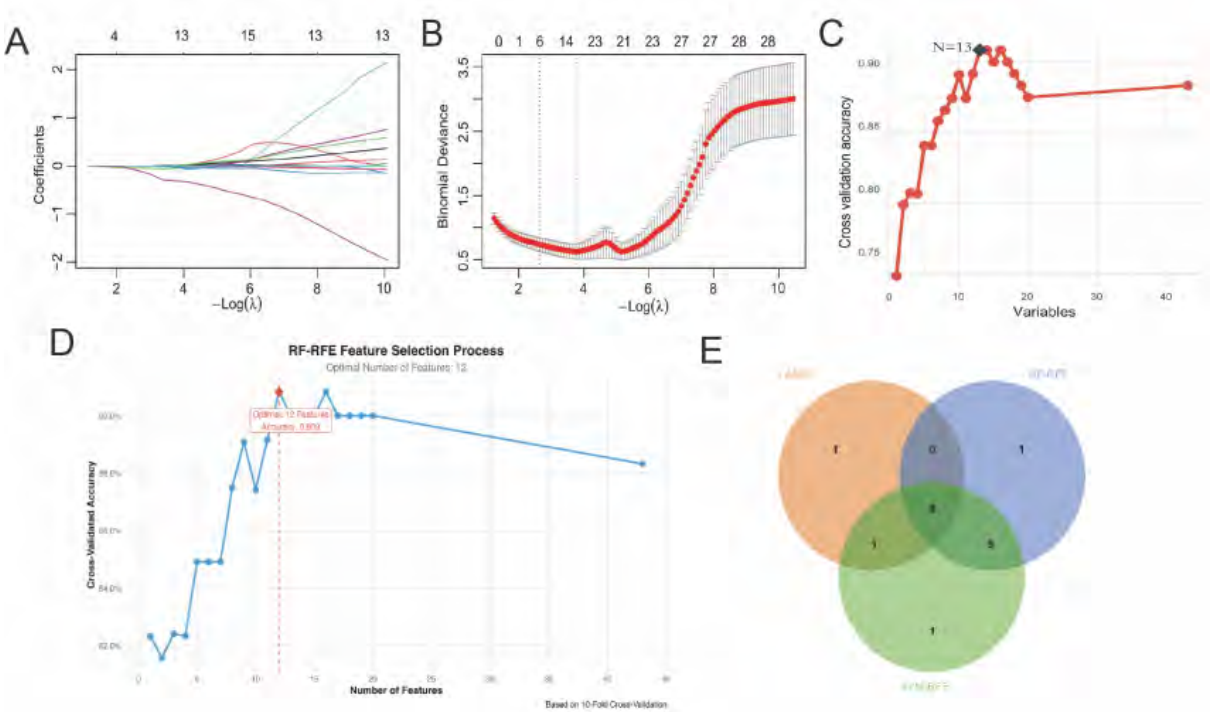


Figure 4, (A) shows the LASSO coefficient path. (B)displays the LASSO regression cross-validation curve. (C) presents the variable selection plot of the SVM-RFE algorithm. (D) shows the variable selection plot of the RF-RFE algorithm. (E) highlights the differential metabolites at the intersection of the LASSO regression, SVM-RFE, and RF-RFE algorithms.

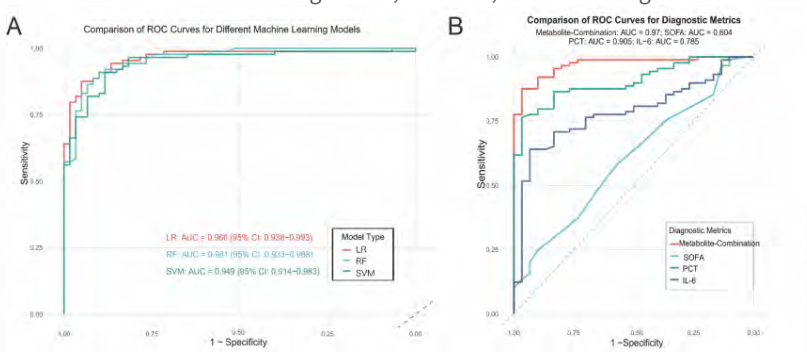


Figure 5, (A) displays the ROC curves and AUC values of the three prediction models: LR, RF, and SVM. (B) shows the comparison of ROC curves and AUC values between the metabolite combination and clinical indicators (SOFA score, PCT, and IL-6).

Table2, Diagnostic Performance Evaluation of Metabolite Combination and Clinical Indicators in SEP vs. NSEP groups.

	AUC	Sensitivity	Specificity	PPV	NPV	Accuracy
Metabolite Combination	0.97 (0.943- 0.997)	0.876 (0.802-0.944)	0.967 (0.889-1.000)	0.987 (0.960-1.000)	0.725 (0.579-0.861)	0.899 (0.840-0.950)
SOFA Score	0.61 (0.49 -0.73)	0.629 (0.532-0.728)	0.567 (0.391-0.741)	0.812 (0.716-0.896)	0.340 (0.208-0.475)	0.613 (0.529-0.697)
PCT	0.905 (0.853- 0.957)	0.764 (0.674-0.850)	0.967 (0.885-1.000)	0.986 (0.952-1.000)	0.580 (0.438-0.711)	0.815 (0.739-0.882)
IL-6	0.785 (0.698- 0.871)	0.640 (0.536-0.737)	0.933 (0.828-1.000)	0.966 (0.912-1.000)	0.467 (0.340-0.585)	0.714 (0.630-0.790)

PPV，Positive Predictive Value；NPV，Negative Predictive Value

Table3,IDI and NRI Analysis of Metabolite Combination for Sepsis Diagnosis

	NRI	NRI—95%CI	NRI *P*-value	IDI	IDI 95%CI	IDI *P*-value
Metabolite Combination vs. SOFA	1.2978	[1.0442, 1.5480]	<0.001	0.6104	[0.4714, 0.7373]	<0.001
Metabolite Combination vs. PCT	0.633	[0.4598, 0.8156]	<0.001	0.5333	[0.4170, 0.6424]	<0.001
Metabolite Combination vs. IL-6	0.6217	[0.4273, 0.7861]	<0.001	0.5821	[0.4683, 0.6810]	<0.001

IDI,Integrated Discrimination Improvement;NRI,Net Reclassification Improvement.

3.5 Construction of Sepsis Prognosis and Risk Stratification Prediction Models Using Machine Learning

To identify metabolites with predictive value for prognosis and risk stratification in sepsis patients, we developed prediction models based on endogenous differential metabolites from both the SEPNS versus SEPS groups (120 metabolites) and the SS versus NSS groups (133 metabolites) using machine learning algorithms.For the SEPNS versus SEPS groups, metabolite selection was performed using LASSO, RF-RFE, and SVM-RFE, ultimately identifying two key metabolites (Figure S3) for prognosis prediction: Butyrylcarnitine and Xanthurenic acid. To evaluate the predictive performance of these metabolites, we constructed three prediction models—LR, RF, and SVM—using 89 sepsis samples. All models were evaluated through 5-fold cross-validation with stratified sampling to maintain consistent case-control ratios across folds. The RF model demonstrated the highest performance, with an AUC of 0.742 (95% CI: 0.634–0.851), and was selected as the metabolite combination scoring tool.

During the performance evaluation, a composite prognostic model was developed utilizing metabolite combination, the SOFA score, the APACHE II score, and lactate levels. ROC curve analysis demonstrated that the composite prognostic model surpassed individual indicators, achieving an AUC of 0.859, with the difference being statistically significant ($P < 0.05$) (Figure 6, A).In the comparison between the SS group and the NSS group, the same methodology was employed, leading to the identification of seven key metabolites (Figure S4): Methylimidazoleacetic acid, Methionine sulfone, L-Arginine, L-2-Aminoadipate adenylate, Gluconic acid, Ascorbic acid, and Alanylisoleucine. The RF model yielded the highest AUC value of 0.868 (95% CI: 0.780–0.956) and was selected as the metabolite combination scoring tool. A composite risk stratification model was then constructed using the metabolite combination, SOFA score, APACHE II score, and lactate levels. ROC curve analysis indicated that the composite risk prediction model outperformed individual indicators, achieving an AUC of 0.878 (95%CI(0.808-0.947)); however, the difference was not statistically significant (Figure 6, B).

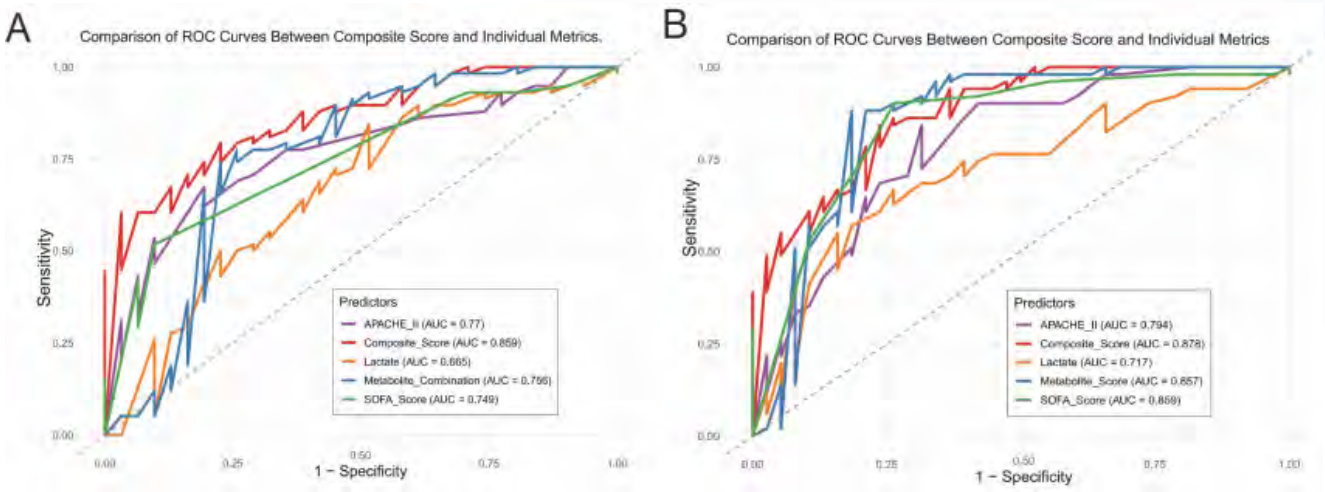


Figure 6, (A)Comparison of ROC Curves Between Composite Score and Individual Metrics in SEPS vs. SEPNS groups; (B) Comparison of ROC Curves Between Composite Score and Individual Metrics in SS vs. NSS groups.

Conclusion

This study employed metabolomics in conjunction with machine learning algorithms to identify differential metabolites, delineate the metabolic profile of sepsis patients, and construct models for sepsis diagnosis and prognosis assessment. Future multi-center studies with larger sample sizes are necessary to validate the current findings and to more comprehensively observe dynamic changes in serum metabolomics throughout the disease course. This approach holds promise for timely prognosis evaluation and guiding treatment strategies.

MRAB 协同恢复线粒体补充与自噬重建线粒体稳态改善脓毒症心肌功能障碍

姓名：宋瑞，段晨阳

单位：重庆医科大学附属第二医院

摘要

背景及目的：脓毒症心肌功能障碍（Sepsis-induced myocardial dysfunction，SIMD）是脓毒症患者死亡的重要原因，其核心病理基础为线粒体质量控制失衡。现有线粒体治疗策略主要依赖外源线粒体补充，但无法解决受损线粒体清除障碍。本研究拟构建一种兼具功能线粒体补充与线粒体自噬恢复能力的新型治疗平台，实现线粒体稳态重建，改善脓毒症心肌损伤。

方法：采用 LPS 处理 HL-1 心肌细胞及 CLP 小鼠模型以模拟脓毒症背景。构建由诱导多能干细胞来源富线粒体细胞外囊泡（MitoEVs）及靶向 STX17/VAMP7 的金纳米肽组成的线粒体补充 - 自噬桥接平台（mitochondrial replenishment and autophagy-bridge，MRAB），利用中性粒细胞作为递送载体实现炎症组织靶向运输。采用 SIM 超分辨显微镜、TEM、Western blot、Co-IP、Seahorse、Oroboros O2K 及超声心动图等技术评价 MRAB 对线粒体功能、自噬通量及心功能的影响。

结果：研究发现，脓毒症心肌细胞中 STX17-SNAP47-VAMP7 融合复合体功能受损，导致线粒体自噬通量阻断及受损线粒体异常积聚。MRAB 通过恢复 STX17-VAMP7 介导的自噬体 - 溶酶体融合，同时补充具有生物能活性的功能线粒体，实现线粒体质量控制重建。体外实验显示，MRAB 显著降低 ROS 水平，恢复线粒体膜电位，提高 ATP 生成、mtDNA 拷贝数及氧化磷酸化能力，并促进线粒体自噬恢复。CLP 模型中，MRAB 明显改善心功能，提高线粒体呼吸能力，减轻心肌炎症及多器官损伤，同时具有良好的体内安全性。

结论：MRAB 首次实现了“功能线粒体补充 + 线粒体自噬恢复”双重协同干预，通过重建线粒体稳态显著改善脓毒症心肌功能障碍，为脓毒症器官保护提供了一种具有临床转化潜力的新策略。

关键词：脓毒症、心脏功能障碍、线粒体自噬、纳米材料

研究内容

研究背景和现状：脓毒症是宿主对感染反应失调所导致的危及生命的多器官功能障碍综合征，其中心肌功能障碍（Sepsis-induced myocardial dysfunction，SIMD）发生率高达 40% ～ 50%，是导致患者死亡的重要原因之一。目前针对 SIMD 尚缺乏有效的靶向治疗策略。大量研究表明，线粒体功能障碍是 SIMD 发生发展的核心病理基础，表现为线粒体能量代谢障碍、氧化应激增加及线粒体质量控制（mitochondrial quality control，MQC）失衡。近年来，外源线粒体移植及线粒体递送等策略能够补充功能线粒体，在一定程度上改善心肌能量代谢，但持续积聚的受损线粒体无法被及时清除，仍不断释放 ROS 及炎症相关信号，限制了治疗效果。因此，如何同步恢复功能线粒体补充与受损线粒体清除，实现线粒体稳态重建，是目前线粒体治疗领域亟待解决的重要科学问题。

目的：本研究旨在解析脓毒症心肌线粒体自噬通量障碍的分子机制，构建一种兼具功能线粒体补充与受损线粒体清除能力的线粒体补充 - 自噬桥接平台（mitochondrial replenishment and autophagy-bridge，MRAB），实现线粒体稳态协同重建，系统评价其改善脓毒症心肌功能障碍及多器官损伤的治疗作用。

设计与方法：本研究首先采用 LPS 诱导 HL-1 心肌细胞及 CLP 诱导脓毒症小鼠模型，系统评价脓毒症过程中线粒体结构、能量代谢及线粒体自噬变化。随后结合免疫荧光、免疫共沉淀（Co-IP）、超分辨 SIM 成像、mt-Keima 示踪及透射电镜等技术，解析 STX17-SNAP47-VAMP7 介导的自噬体 - 溶酶体融合在脓毒症中的变化规律及其与线粒体自噬通量阻断之间的关系。在此基础上，构建 MRAB 平台。该平台利用诱导多能干细胞来源富线粒体细胞外囊泡（MitoEVs）补充具有完整生物能功能的健康线粒体，同时利用靶向 STX17 和 VAMP7 的金纳米肽重建 SNARE 融合复合体，并通过中性粒细胞天然炎症趋化能力实现炎症心肌精准递送。进一步采用 TEM、NTA、DLS 及荧光示踪等评价 MRAB 材料学特性及递送效率；采用 ROS 检测、JC-1、ATP、mtDNA 拷贝数、Seahorse、Oroboros O2K 等评价线粒体功能恢复情况；通过超声心动图、心肌应变分析、组织病理学及炎症因子检测系统评价 MRAB 改善心功能及器官损伤的效果，并对其体内生物安全性进行综合评估。

结果：

（1）脓毒症导致线粒体功能障碍及线粒体自噬通量阻断。 CLP 小鼠及 LPS 处理心肌细胞均出现明显心功能下降及线粒体损伤，表现为线粒体肿胀、嵴结构破坏、ROS 升高、膜电位下降等。同时，大量线粒体自噬体积聚，自噬体与溶酶体融合明显减少，提示线粒体自噬通量发生阻断（Figure 1）。

（2）首次发现 STX17-SNAP47-VAMP7 复合体功能障碍是脓毒症线粒体自噬阻断的重要机制。 虽然 STX17、SNAP47 及 VAMP7 蛋白表达水平无明显变化，但其膜共定位及相互结合能力明显下降，提示脓毒症主要破坏 SNARE 复合体功能性组装，而非影响蛋白表达，从而导致自噬体 - 溶酶体融合障碍及线粒体自噬通量受阻（Figure 2）。

（3）成功构建 MRAB 平台，实现功能线粒体补充与线粒体自噬恢复的协同调控。中性粒细胞可同时高效负载 MitoEVs 及金纳米肽，并实现炎症心肌靶向递送；外源线粒体能够成功进入受体心肌细胞并整合至宿主线粒体网络，同时 MRAB 显著促进 STX17 与 VAMP7 重新结合，恢复 SNARE 复合体功能（Figure 3）。

（4）MRAB 显著恢复心肌线粒体稳态及心脏功能。 与单独 MitoEVs 或自噬桥接模块相比，MRAB 显著降低细胞 ROS 水平，恢复线粒体膜电位及正常网络形态，提高 NDUFB8 表达等；同时明显促进自噬体与溶酶体融合，恢复线粒体自噬通量，实现功能线粒体补充与受损线粒体清除的双重协同。在 CLP 模型中，MRAB 明显改善左室射血分数及心肌应变，减轻心肌炎症及超微结构损伤（Figure 4）。

结论：本研究首次阐明了脓毒症通过破坏 STX17-SNAP47-VAMP7 复合体功能性组装导致自噬体 - 溶酶体融合障碍及线粒体自噬通量阻断的新机制，并创新性构建了中性粒细胞递送的 MRAB 平台，实现了功能线粒体补充与受损线粒体清除的双重协同，系统重建线粒体稳态，显著改善脓毒症心肌功能障碍及多器官损伤。本研究为脓毒症心肌损伤的线粒体精准治疗提供了新的理论依据和具有临床转化潜力的干预策略。

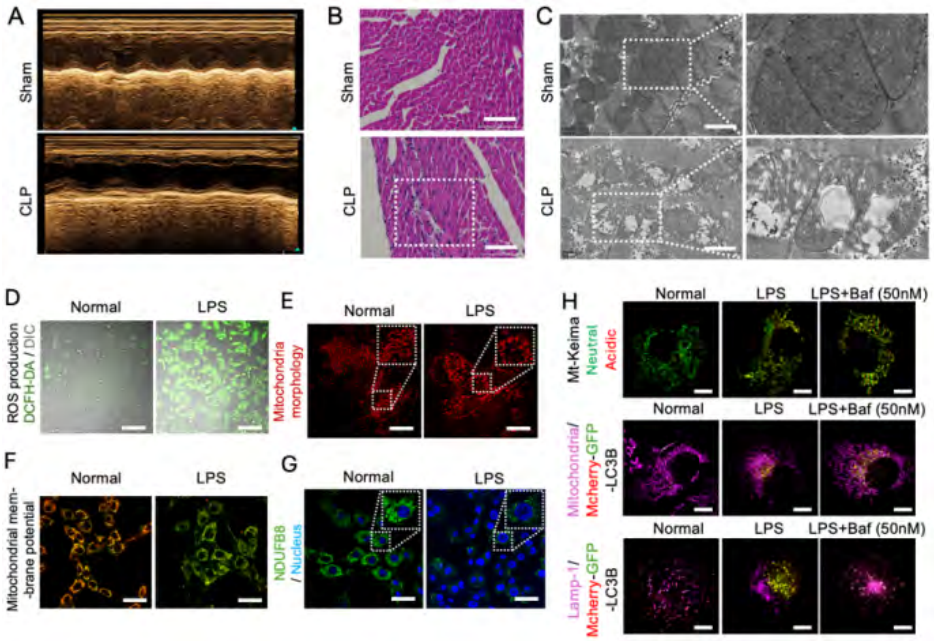


Figure 1. 脓毒症背景下，心肌细胞线粒体受损，心肌细胞功能障碍。A，心脏超声；B，心脏 HE 染色；C 心脏组织透射电镜；D，心肌细胞活性氧检测；E，心肌细胞线粒体形态观察；F，心肌细胞膜电位检测；G，心肌细胞 NDUFB8 含量检测；H，心肌细胞自噬水平检测。

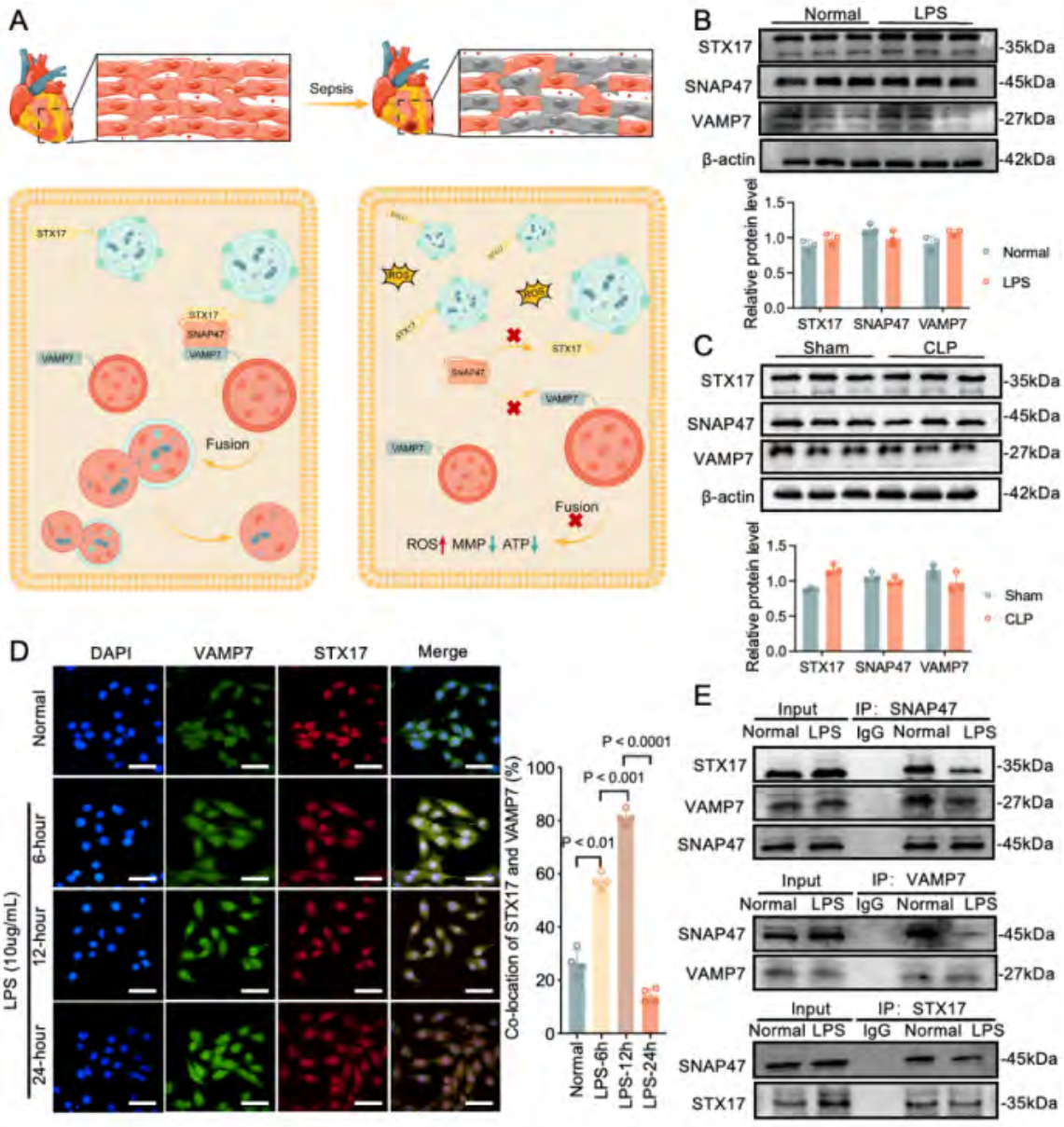


Figure 2. 脓毒症背景下，心肌细胞自噬小体与溶酶体融合障碍机制。A，STX17 与 VAMP7 结合机制示意图；B-C，STX17，VAM7 和 SNAP47 蛋白表达检测；D，心肌细胞 STX17 和 VAM7 荧光表达检测；E，心肌细胞内 STX17，VAM7 和 SNAP47 蛋白 CO-IP 检测。

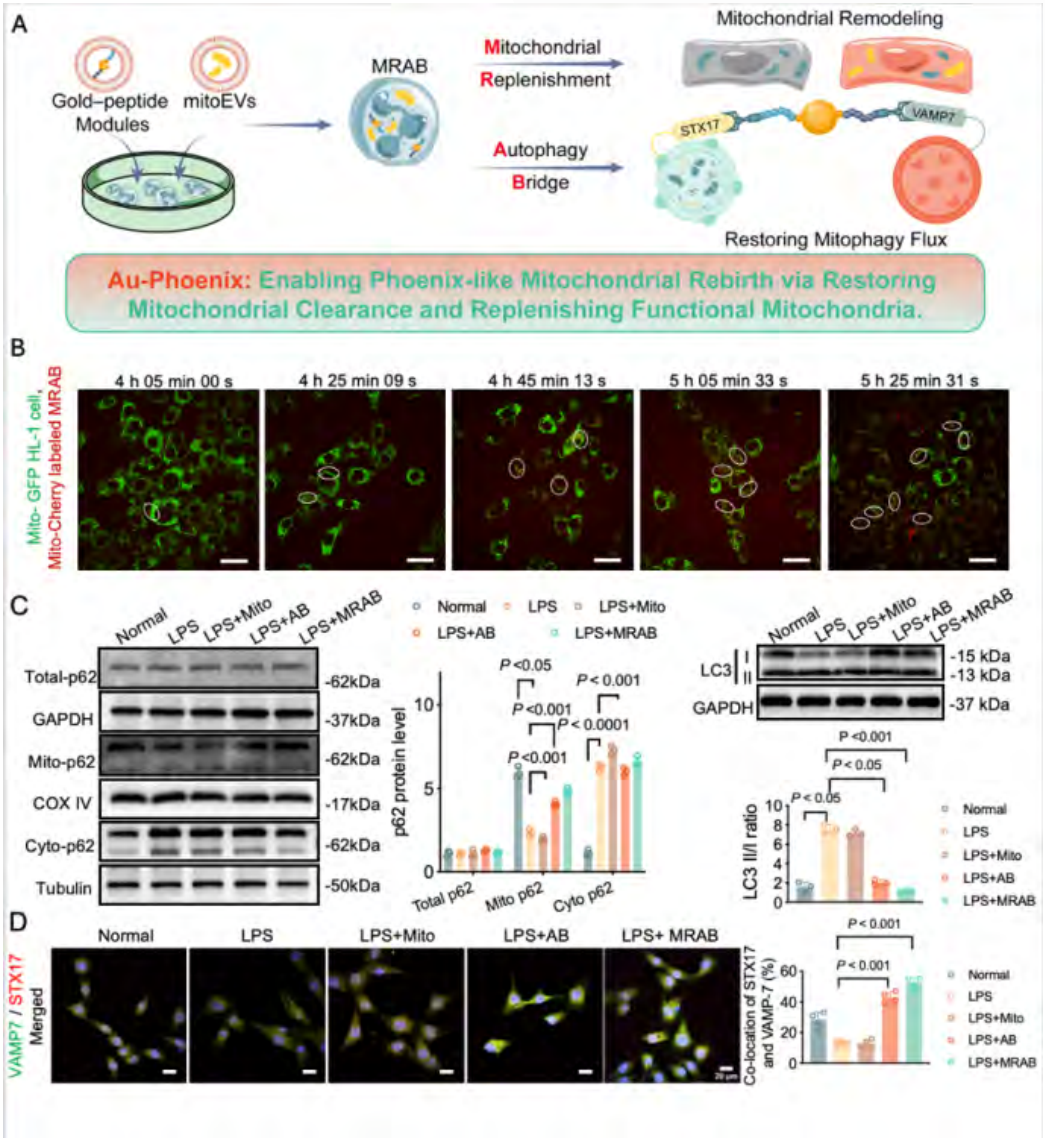


Figure 3. MRAB 构建及功能评估。A，MRAB 构建示意图；B，MRAB 递送 MitoEVs 效率评估；C- D，MRAB 改善心肌细胞 VAMP7-STX17 结合障碍。

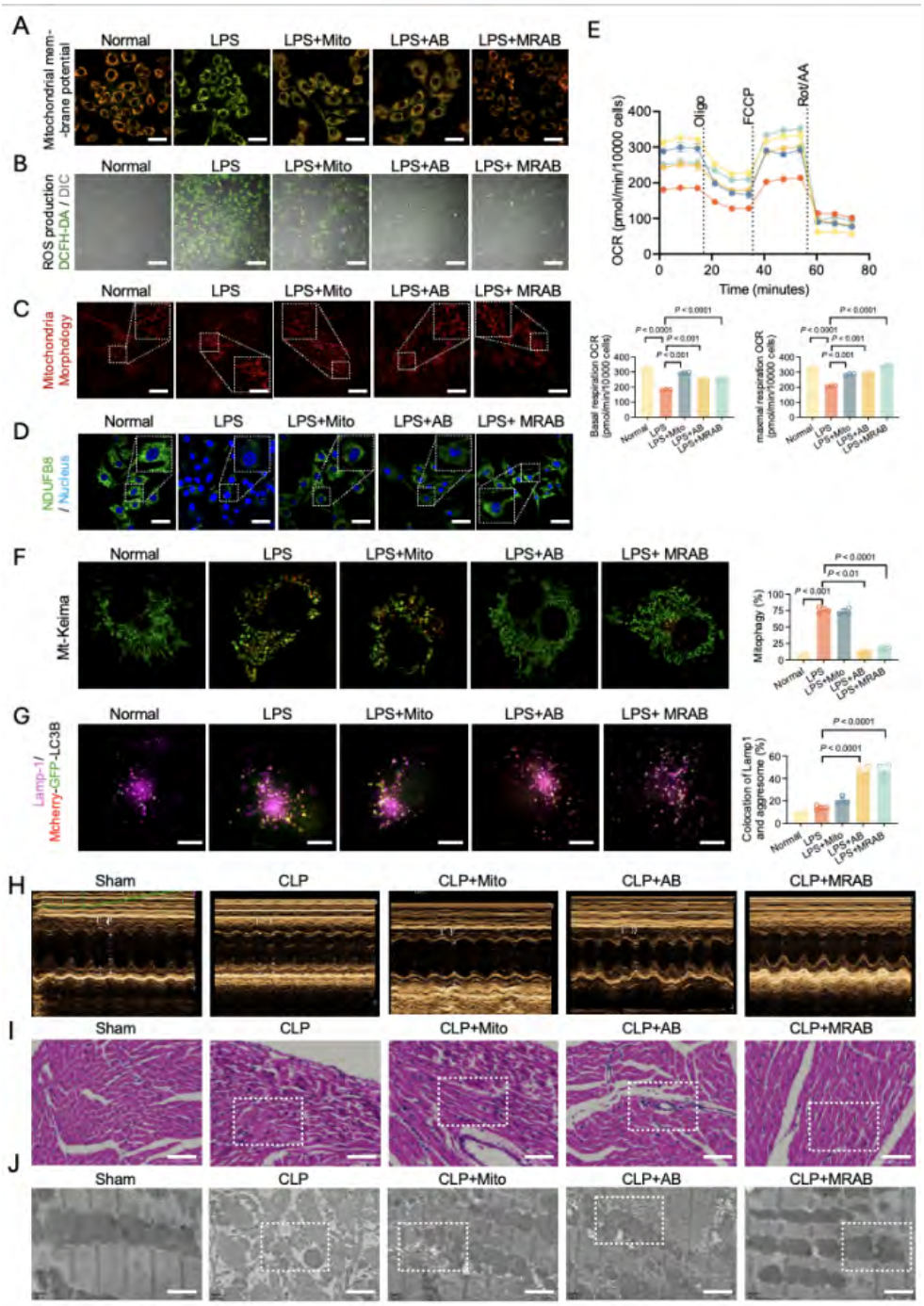


Figure 4，MRAB 及其组分改善心肌细胞线粒体功能障碍效果评估。A，线粒体膜电位检测；B，细胞活性氧检测；C，线粒体形态观察；D，线粒体 NDUFB8 表达检测；E，线粒体氧化呼吸能力检测；F- G，心肌细胞线粒体自噬通量检测；H，小鼠心脏超声检测；I，小鼠心脏组织 HE 染色；J，小鼠心脏组织透射电镜观察。CLP+Mito，即单纯只添加 MitoEVs，CLP+AB，即单纯只添加金颗粒肽段。

Neurogenic Pulmonary Edema in Acute Cerebral Infarction: A Case Report and Review of the Literature

姓名：张颖
单位：山东第一医科大学第一附属医院（山东省千佛山医院）

Abstract

Neurogenic pulmonary edema (NPE) is a life-threatening complication of acute central nervous system injury, characterized by acute respiratory distress and bilateral pulmonary infiltrates in the absence of a primary cardiogenic or infective etiology. Although well documented after subarachnoid hemorrhage and traumatic brain injury, NPE triggered by acute ischemic stroke is less frequently recognized and often misdiagnosed as severe pneumonia or cardiogenic edema. We report the case of a 59-year-old woman who presented with acute onset of coma and respiratory failure. Initial chest computed tomography revealed diffuse bilateral exudates, and she was erroneously treated for severe pneumonia with broad-spectrum antimicrobials without improvement. Subsequent neurological evaluation and brain imaging confirmed a large left hemispheric cerebral infarction. The integration of clinical, radiological, and hemodynamic findings led to the diagnosis of NPE. Discontinuation of antibiotics and institution of targeted neurocritical care, including ventilatory support and cerebral edema management, resulted in gradual pulmonary and neurological recovery. A comprehensive literature review on NPE in the setting of acute cerebral infarction is presented, emphasizing pathogenic mechanisms, diagnostic pitfalls, and management strategies. This case underscores the necessity of including NPE in the differential diagnosis of acute respiratory failure in patients with concomitant focal neurological deficits, and highlights the risks of anchoring bias towards infection.

Keywords: Neurogenic pulmonary edema; Cerebral infarction

1. Introduction

Neurogenic pulmonary edema (NPE) is an acute, protein-rich lung injury that develops rapidly after a significant insult to the central nervous system. It is classically associated with conditions that evoke a massive sympathetic discharge, such as aneurysmal subarachnoid hemorrhage, intracerebral hemorrhage, severe traumatic brain injury, and status epilepticus [1,2]. Acute ischemic stroke, particularly when it involves large territories or the insular cortex, is an underappreciated trigger for NPE. The clinical presentation—dyspnea, hypoxemia, and bilateral pulmonary infiltrates on imaging—can mimic cardiogenic pulmonary edema or severe community-acquired pneumonia, leading to diagnostic delays and potentially harmful therapeutic interventions [3].

We describe a patient with a large acute cerebral infarction secondary to atrial fibrillation, who presented with fulminant respiratory failure initially misdiagnosed as severe pneumonia. The correct identification of NPE fundamentally altered management and facilitated recovery. We further provide a narrative review of the literature to refine the understanding of NPE in acute cerebral infarction.

2. Case Presentation

A 59-year-old woman was transferred to our intensive care unit (ICU) with a diagnosis of “severe pneumonia” after experiencing abrupt loss of consciousness and respiratory distress.

Three days prior, she had developed rhinorrhea and an occasional dry cough without fever, chest pain, or significant dyspnea. No medication was taken. Twenty-nine hours before admission, while having dinner, she suddenly became unresponsive. There were no observed convulsions, vomiting, or gaze deviation. She exhibited labored breathing with audible gurgling. Her family immediately brought her to a local emergency department, where she underwent emergency endotracheal intubation and mechanical ventilation. An urgent non-contrast head computed tomography (CT) scan was interpreted as showing cortical atrophy and encephalomalacia. Chest CT demonstrated diffuse bilateral pulmonary exudative lesions. A preliminary diagnosis of “cerebral infarction? Severe pneumonia with respiratory failure” was made. She was administered a broad anti-infective regimen including oseltamivir, vidarabine, imipenem-cilastatin, teicoplanin, and voriconazole, alongside mannitol, circulatory

support, and neurotrophic agents. Despite this, her condition did not improve, and she was referred to our institution.Her medical history included atrial fibrillation of four years' duration, for which she intermittently took aspirin. Four years earlier, she had suffered an ischemic stroke that underwent hemorrhagic transformation, requiring burr-hole drainage of the hematoma; this left her with residual dysphagia and mild left-sided weakness. Notably, six months before this admission, she began experiencing dyspnea after walking a short distance (about ten meters), which subsided with rest. She had an untreated chronic hepatitis B infection for seven years. There was no history of tuberculosis, recent trauma, or drug allergy.

Upon ICU arrival, her temperature was 36.8° C, heart rate 136 beats per minute, respiratory rate 26 breaths per minute, and blood pressure 123/86 mmHg. She was in a stuporous state with passive positioning and could not cooperate with the examination. The right upper limb had an area of swelling measuring 22×5 cm, with erythema, local warmth, and non-blanching erythema. Cardiopulmonary examination revealed irregularly irregular heart rhythm with variable intensity of heart sounds, coarse breath sounds bilaterally, and diffuse crackles and rhonchi. The abdomen was distended but soft, with tympanic percussion. Neurologically, pupils were 2 mm bilaterally and sluggishly reactive. Painful stimulation elicited withdrawal of the left extremities, whereas the right limbs remained flaccid and immobile. The right Babinski sign was positive, and the left was negative.

A repeated brain CT, followed by diffusion-weighted magnetic resonance imaging, confirmed an extensive acute infarction in the territory of the left middle cerebral artery with prominent cytotoxic edema. Transthoracic echocardiography revealed a non-dilated left ventricle with preserved ejection fraction, moderate left atrial enlargement, and absence of regional wall motion abnormalities; the estimated pulmonary artery systolic pressure was mildly elevated. Serum procalcitonin was within normal limits, and serial sputum and blood cultures remained negative. A central venous catheter was placed; the central venous pressure was 8 mmHg. Based on the temporal association between the catastrophic neurological event and the acute onset of pulmonary edema, the exclusion of cardiogenic and infectious etiologies, and the inadequate response to broad-spectrum antimicrobials, a diagnosis of NPE secondary to massive acute cerebral infarction was established.

Antimicrobial therapy was discontinued. Management focused on lung-protective mechanical ventilation, intravenous mannitol, modest fluid restriction, and rate control for atrial fibrillation. Over the next five days, the pulmonary infiltrates resolved progressively, and oxygenation improved substantially, allowing extubation on day 7. Her neurological status gradually progressed from stupor to a minimally conscious state, with persistent dense right hemiplegia.

3. Discussion and Literature Review

The cardinal feature of NPE is the abrupt development of hypoxemic respiratory failure and diffuse alveolar edema following a central nervous system catastrophe, with no clinical evidence of left ventricular failure or volume overload [1]. The underlying pathophysiology is a massive, centrally mediated sympathetic surge that triggers transient systemic and pulmonary vasoconstriction. This catecholamine storm increases pulmonary capillary hydrostatic pressure and simultaneously disrupts the alveolar-capillary barrier through endothelial injury, leading to a high-permeability form of edema [2,4]. In ischemic stroke, particularly when the insular cortex, amygdala, or hypothalamus is involved, the inhibitory control over autonomic outflow is disrupted, unleashing this adrenergic discharge [5].

Our patient exhibited a classic sequence: a large left-hemispheric infarct, likely involving the insula, in the setting of atrial fibrillation, followed precipitously by acute pulmonary edema. The initial interpretation of her chest CT as "severe pneumonia" was understandable given the bilateral infiltrates and the background of mild viral prodrome. However, several clues argued against a purely infectious etiology: the suddenness of respiratory failure synchronous with a major neurological event, normothermia, negative microbiological studies, normal procalcitonin, and the complete lack of response to an exhaustive antimicrobial regimen. Moreover, the pre-existing exertional dyspnea suggested a baseline of compensated heart failure, but the acute echocardiogram excluded acute systolic dysfunction or severe diastolic abnormality to explain such florid edema. The swollen, erythematous right upper limb, possibly representing superficial thrombophlebitis or cellulitis, was a distracting extraneous finding that may have strengthened the initial suspicion of sepsis; yet it was anatomically limited and could not account for bilateral pulmonary infiltrates.Distinguishing NPE from cardiogenic edema and acute respiratory distress syndrome (ARDS) from other causes is crucial because treatment diverges. While supportive ventilatorycare is common, NPE mandates rigorous intracranial pressure control and avoidance of hypervolemia, which could exacerbate cerebral edema. Some expert opinions advocate for the judicious use of alpha-adrenergic blockers (e.g., phentolamine) or beta-agonists to attenuate the

sympathetic storm, though vidence is limited to experimental models and small series [4,6]. The pulmonary edema in NPE typically resolves rapidly—often within 72–96 hours—as the neurological insult is controlled, mirroring the transient nature of the sympathetic surge. This rapid reversibility was observed in our patient.

A literature review focusing on NPE precipitated by acute cerebral infarction reveals that it remains an underreported entity. Case series suggest that large hemispheric infarctions, particularly those with insular involvement and hemorrhagic transformation, carry the highest risk [5,7]. Diagnostic criteria proposed in the literature include the appearance of bilateral pulmonary infiltrates within hours of a documented acute brain injury, a normal cardiac silhouette and pulmonary artery wedge pressure, and absence of common ARDS risk factors such as aspiration or systemic infection [8]. Mortality is high when NPE goes unrecognized, largely because excessive fluid resuscitation and delayed neuroprotective measures aggravate brain injury. Our review of reports indexed in PubMed over the past two decades identified fewer than 50 well-documented cases of ischemic-stroke-induced NPE, indicating that the condition may be underdiagnosed rather than rare [7,9]. Misattribution to healthcare-associated pneumonia or aspiration pneumonitis is a recurring theme.

In the present case, the initial misdiagnosis led to the unnecessary exposure to multiple antimicrobials, with attendant risks of drug toxicity and selection pressure for resistant organisms. More importantly, the focus on a pulmonary infectious process likely delayed aggressive measures to control intracranial pressure. Once the diagnosis was corrected, targeted neurocritical care facilitated a favorable pulmonary outcome.

4. Conclusion

Neurogenic pulmonary edema must be considered in any patient who develops acute respiratory failure with bilateral pulmonary infiltrates in the immediate aftermath of an acute cerebral infarction, especially when the infarct is large and the neurological deficit is profound. Early distinction from pneumonia and cardiogenic shock is essential to avoid inappropriate therapies and to initiate both neuroprotective strategies and appropriate ventilatory support. Our case, in which NPE was initially mistaken for severe pneumonia, highlights the cognitive pitfalls that can arise when a systemic presentation coincides with a localized neurological event. Heightened clinical awareness, coupled with careful integration of neurological, cardiac, and infectious workups, can lead to timely diagnosis and improved outcomes.

References

[1] Davison DL, Terek M, Chawla LS. Neurogenic pulmonary edema. Crit Care. 2012;16(2):212.

[2] Busl KM, Bleck TP. Neurogenic pulmonary edema. Crit Care Med. 2015;43(8):1710-1715.

[3] Fontes RB, Aguiar PH, Zanetti MV, et al. Acute neurogenic pulmonary edema: case reports and literature review. J Neurosurg Anesthesiol. 2003;15(2):144-150.

[4] Šedý J, Zicha J, Kuneš J, et al. Mechanisms of neurogenic pulmonary edema development. Physiol Res. 2008;57(4):499-506.

[5] Wijdicks EFM, Le Roux PD. Neurogenic pulmonary edema in ischemic stroke: the central autonomic network at fault. Neurocrit Care. 2020;33(1):1-3.

[6] Inamasu J, Sugimoto K, Yamada Y, et al. The role of catecholamines in the pathogenesis of neurogenic pulmonary edema associated with subarachnoid hemorrhage. Acta Neurochir Suppl. 2012;113:33-37.

[7] Sawamura A, Gando S, Yagihashi T, et al. Neurogenic pulmonary edema after acute cerebral infarction: a report of two cases. J Stroke Cerebrovasc Dis. 2017;26(8):e160-e163.

[8] Mayer SA, Fink ME, Homma S, et al. Cardiac injury associated with neurogenic pulmonary edema following subarachnoid hemorrhage. Neurology. 1994;44(5):815-820.

[9] Zhao H, Lin G, Shi M, et al. Clinical characteristics and prognosis of neurogenic pulmonary edema after acute ischemic stroke. Am J Emerg Med. 2021;47:109-114.

Physiological comparison of high-flow oxygen via endotracheal tube and T-piece strategies during spontaneous breathing trials: a randomized crossover study

姓名：徐珊珊，张睿智，侯梦雪，安旭，苗明月，周建新

单位：首都医科大学附属北京世纪坛医院，首都医科大学肿瘤医学院，北京大学第九临床医学院

Background: The optimal spontaneous breathing trial (SBT) strategy remains uncertain. Pressure support ventilation (PSV) may reduce inspiratory effort, whereas T-piece trials more closely approximate unsupported breathing after extubation. Neither approach has shown clear superiority for extubation outcomes. High-flow oxygen (HFO) delivered via endotracheal tube has been proposed as an alternative SBT strategy, but the physiological effects remain insufficiently defined.

Methods: In a randomized crossover physiological study, patients receiving mechanical ventilation for at least 24 hours and deemed ready for weaning underwent five SBT conditions: T-piece and four HFO via endotracheal tube settings combining two interfaces with different expiratory port diameters (9.8 and 6.9 mm) and two flow rates (40 and 60 L/min). Airway and esophageal pressures, respiratory variables, and electrical impedance tomography parameters were measured during baseline mechanical ventilation and under each SBT condition. Esophageal pressure was also measured after extubation for comparison with post-extubation inspiratory effort (Figure 1).

Results: Twenty patients were analyzed. Compared with T-piece, HFO-6.9 at 60 L/min produced the largest increases in mean expiratory airway pressure (median paired difference, 7.0 cm H2O [95% CI, 6.7–7.4]) and PEEP (6.0 cm H2O [5.8–6.1]). HFO-6.9 at 60 L/min also attenuated global end-expiratory lung volume loss (321 mL [267–523]), increased the dependent fraction of ventilation, reduced dynamic transpulmonary driving pressure (3.3 cm H2O [1.8–4.1]), improved PaO2/FiO2 (28 mmHg [14–52]), and reduced respiratory rate (2 breaths/min [1–4]) compared with T-piece. Tidal swing of esophageal pressure during inspiration (ΔPes) did not differ across the five SBT conditions and post-extubation measurements (p = 0.24) (Figure 2 and Figure 3). Overall, tracheal HFO produced a flow- and expiratory port diameter-dependent physiological response. Improvements in ventilation homogeneity and oxygenation occurred mainly with the smaller expiratory port at higher flow, suggesting a pressure threshold effect.

Conclusions:

Tracheal HFO created an intermediate hybrid physiological condition between unsupported T-piece breathing and low-level positive-pressure support. Its flow- and expiratory port diameter-dependent airway pressure effect was associated with improved lung volume, ventilation distribution, oxygenation, dynamic transpulmonary driving pressure, and respiratory rate, whereas the absence of direct pressure support may explain why ΔPes remained comparable to T-piece and measured post-extubation values. These findings suggest that tracheal HFO is a physiologically distinct SBT strategy that may inform individualized SBT selection, although its relationship to clinical outcomes requires further evaluation.

Physiological effects of combining awake prone positioning with different oxygen therapies on regional ventilation assessed by electrical impedance tomography: a randomized crossover trial

姓名：Yuxian Wang[1#], Jie Li[2#*], Shengyu Hao[1#], QijingJiang[3], Yilin Wei[3], Zhanqi Zhao[4*], MingZhong[1,3*]

单位：1 Zhongshan Hospital, Fudan University，2 Rush University Medical Center

3 School of Public Health, Fudan University，4 Guangzhou Medical University

Conflict of interest:

Dr. Li discloses research funding from COPD Foundation, MEKICS Co. Ltd, Vincent Ltd, and American Association for Respiratory Care, and speaker fees from American Association for Respiratory Care, Aerogen Ltd, Vincent Ltd, and Fisher & Paykel Healthcare Ltd. Other authors do not have conflict of interest to disclose.

Short Running title:

Impact of APP on Lung ventilation during HFNC and CPAP

Keywords:

Acute hypoxemic respiratory failure; awake prone positioning; high-flow nasal cannula; continuous positive airway pressure; electrical impedance tomography

Funding Information:

This work was supported by the Shanghai Municipal Health Commission Fund(GWVI-11.1-14), the Open Project of State Key Laboratory of Respiratory Disease (SKLRD-OP-202321), the Shanghai Key Laboratory of Lung Inflammation and Injury, the Shanghai Health Commission Clinical Research Project (202240334), and the Youth Fund of Zhongshan Hospital, Fudan University (No.2024ZSQN48).

Abstract

Background: Awake prone positioning (APP) improves oxygenation and reduces intubation in COVID-19-related acute hypoxemic respiratory failure (AHRF). However, the physiological effects of combining APP with different non-invasive respiratory supports on regional ventilation remain unclear. Objectives: This study compared the physiological effects of APP combined with a high-flow oxygen mask (HFOM), high-flow nasal cannula (HFNC), or continuous positive airway pressure (CPAP) on ventilation distribution in spontaneously breathing patients with COVID-19-related AHRF.Methods: In a single-center, randomized crossover trial, 34 AHRF patients underwent 30-minute sessions of HFNC, HFOM, and CPAP in both supine and prone positions. Electrical impedance tomography (EIT)- derived indices (global inhomogeneity index [GI], center of ventilation [CoV], tidal impedance variation

[TIV], pendelluft), SpO2/FiO2 ratio, ROX index, and hemodynamics were measured. Results: APP significantly improved SpO2/FiO2 and ROX index, and reduced GI and pendelluft, irrespective of the respiratory support used. CPAP alone resulted in higher SpO2/FiO2 and ROX index values compared to HFOM and HFNC. However, CPAP also significantly increased TIV and GI. In the supine position, CoV was higher with CPAP than with HFOM or HFNC, but combining CPAP with APP significantly reduced CoV. Both APP and CPAP were associated with lower patient comfort levels compared to baseline. Conclusions: In patients with COVID-19-related AHRF, APP reduces ventilation inhomogeneity and pendelluft. While CPAP is effective for oxygenation, it increases ventilation inhomogeneity; however, this can be mitigated by combining it with APP. These findings highlight the potential for individualized

respiratory support strategies, combining APP with specific support modes to optimize outcomes. Trial registration: Clinicaltrials.gov, NCT05719103. Registered on February 7, 2023- retrospectively registered.

Introduction

Acute hypoxemic respiratory failure (AHRF) is a common indication for intensive care unit (ICU) admission and is associated with high mortality, particularly in severe pneumonia such as COVID-19. Although invasive mechanical ventilation can be lifesaving, it is also associated with ventilator-associated complications and prolonged ICU stay. Awake prone positioning (APP) has emerged as a simple, noninvasive adjunct that improves oxygenation and may reduce the need for intubation in spontaneously breathing patients [1-3]. In an individual participant data meta-analysis of adults with COVID-19-related AHRF, APP was associated with a higher likelihood of survival without intubation and lower risks of intubation and mortality, with the greatest benefit observed among patients receiving advanced respiratory support at enrollment [4]. Despite these clinical signals, the physiological mechanisms of APP—particularly its effects on regional ventilation distribution, ventilation homogeneity, alveolar recruitment, and intra-pulmonary gas redistribution (pendelluft)—remain incompletely understood [5, 6]. Moreover, most prior studies evaluated APP alone or combined with a single oxygen-delivery modality, leaving uncertainty regarding how APP interacts with different non-invasive respiratory support strategies that provide different levels of positive end-expiratory pressure (PEEP).High-flow nasal cannula (HFNC) may generate variable, generally low levels of PEEP, whereas continuous positive airway pressure (CPAP) delivers a fixed, set PEEP [7, 8]. Whether APP produces differential regional ventilation responses across these modalities—especially compared with oxygen therapy without PEEP—remains unclear. Therefore, we conducted a single-center, randomized crossover trial to compare the physiological effects of APP combined with high-flow oxygen mask (HFOM; high-flow oxygen without PEEP), HFNC, and CPAP on regional ventilation and recruitment assessed by electrical impedance tomography (EIT), including ventilation homogeneity quantified by the global inhomogeneity index (GI).We hypothesized that, compared with supine positioning, awake prone positioning would reduce EITderived ventilation heterogeneity and pendelluft, and that adding CPAP would produce the greatest improvements in oxygenation and global inhomogeneity index compared with HFNC or HFOM.

Methods

This single-center, randomized crossover trial was conducted in accordance with the Declaration of Helsinki and approved by the Institutional Ethics Committees of Zhongshan Hospital, Fudan University (No. B2022-359R) and Rush University Medical Center (No. 23042703). All participants or their legal representatives provided written informed consent. This study was registered at clinicaltrials.gov (NCT05719103).

Study protocol

Patient demographics and clinical characteristics were collected at enrollment. After written informed consent was obtained, the EIT belt was placed, and light sedation/analgesia was administered when necessary to improve comfort while maintaining spontaneous breathing. This was a randomized crossover study in which each patient underwent all six intervention conditions,

defined by three oxygen/ventilatory support modalities (HFOM, HFNC, and CPAP) combined with two 7 body positions (supine and awake prone positioning [APP]), yielding six support–position combinations. Each condition was maintained for 30 min (Table 1). Randomization applied to the order of the six conditions. An independent statistician generated a computer-based random permuted-block sequence (block size = 6) to assign, for each patient, the sequence in which the six conditions were delivered. Allocation was concealed using sealed, opaque envelopes, opened only after the baseline assessment at the start of the study session. A washout interval was implemented between consecutive conditions. During washout, patients were encouraged to sit upright, stand, walk briefly, or use the restroom, aiming to reduce potential carryover by allowing respiratory pattern and hemodynamics to return toward baseline before the next condition. The following data were collected at the end of each session: 1) Heart rate (HR) and noninvasive arterial pressure; 2) SpO2, respiratory rate (RR), the SpO2/FiO2 ratio, and ROX index (defined as[SpO2/FIO2]/RR); 3) Patient comfort scores, which was self-reported using a visual numerical scale with a score of 0 indicating the worst comfort and 10 indicating the best; 4) EIT data. EIT data were analyzed by investigators who were blinded to the intervention order, and comfort scores were self-reported by participants without influence from the staff. However, participant blinding was not feasible, which may have introduced potential bias in the assessment of comfort or respiratory effort.

Respiratory support modalities

High-flow nasal or mask oxygen was administered using the AIRVO2 device (Fisher and Paykel Healthcare, Auckland, New Zealand). Oxygen flow was set at 60 L/min or the maximum tolerated by the patient, and the humidification temperature was

adjusted to 37 °C , 34 °C , or 31°C based on patient comfort. Continuous positive airway pressure (CPAP) was delivered using the SV800 device (Mindray, Shenzhen, China) with a full-face mask at a pressure of 8-10 cmH2O. No humidification was applied during CPAP treatment. The fraction of inspired oxygen (FiO2) was adjusted to maintain an SpO2 range of 90-95% during all treatments.

EIT data

The EIT belt containing 16 electrodes was placed around the chest wall at the fourth or fifth intercostal space and connected to the EIT monitor (PulmoVista 500; Dräger Medical GmbH, Lübeck, Germany). Technical details of EIT have been previously described [9, 10]. The EIT signals were recorded at a frame rate of 50Hz. EIT ventilation maps were derived from offline analysis of tracings by calculating the average values over consecutive respiratory cycles lasting 40 seconds. The ventral and dorsal regions were definedas the upper and lower halves of an axis from the sternum to the vertebrae, respectively.

The following measurements were taken from the analysis of ventilation maps

1) TIV, computed as the difference between the end-expiratory and end-inspiratory impedance during the breathing cycle[10].

2) Four horizontal parallel regions of interest (ROIs) within the chest contour were selected: ROI 1 (ventral), ROI 2 (central ventral), ROI 3 (central dorsal), and ROI 4 (dorsal).

3) The ventral/ dorsal fraction of ventilation distribution[11].

4) The Global Inhomogeneity (GI) index [9], which quantifies the heterogeneity of ventilation distribution (11).

$$GI = \frac{\sum_{x,y\in lung} \left| DI_{xy} - Median\left(DI_{lung}\right) \right|}{\sum_{x,y\in lung} DI_{xy}}$$

where DI denotes the value of the differential impedance in the tidal images; DIxy is the pixel in the identified lung area; DIlung are all the pixels representing the lung area.

5) Center of ventilation (CoV), which refers to the weighted geometric center of the distribution of ventilation. When the tidal ventilation was predominantly located in the dependent lung region, the CoV value increased[12].

6) Pendelluft, which measures the asynchronous ventilation between different lung regions [13],

$$\text{Pendelluft} = \frac{1}{N}\sum_{n=1}^{N} (V_{R\_i,n} - V_{G\_i,n})/TV \times 100\%$$

VR_i is the pixel i in the regional ventilation image; VG_i is the pixel i in the global ventilation image; TV represents the global tidal variation.

Study endpoints

The primary endpoint was the change in dorsal ventilation percentage measured by EIT from supine to prone within each respiratory support modality. Secondary outcome included oxygenation (SpO2/FiO2 ratio, ROX index, GI, COV, TIV and pendelluft) and patient comfort.

Sample size calculation

This study used a one-group, pre–post crossover design. The sample size was calculated using crossover trial formulas incorporating the intra-class correlation coefficient (ρ). Assuming an expected mean difference of 10% in dorsal ventilation, a standard deviation of 15%, an intra-class correlation (ρ) of 0.3, a two-tailed α of 0.05, and a power (1 − β) of 80%, the required sample size per crossover arm was estimated to be 28 participants. To allow for potential dropouts, 34 participants were enrolled.

Statistics Analysis

The Kolmogorov-Smirnov test was used to assess the normality of continuous variables. Normally distributed data are presented as mean ± standard deviation, while non-normally distributed data are reported as median (interquartile range [IQR]). Depending on the distribution and number of groups, comparisons were made using Student' s t-test, the Mann-Whitney U test, or the Kruskal-Wallis test. Categorical variables are expressed as absolute counts and percentages and were analyzed using the chisquare or Fisher' s exact test. Differences across the six study settings, body positions, and types of respiratory support were examined using linear mixed-effects models, with age, BMI, APACHE II score, ROX index, and baseline dorsal ventilation as within-subject factors. Period was included as a fixed effect, and its interaction with treatment was tested. Sensitivity analyses were performed by excluding the first period, if necessary. The Bonferroni correction was applied to adjust for multiple comparisons across all primary and key secondary endpoints. To explore relationships between variables, Pearson correlation analysis was used for normally distributed data, while Spearman correlation was employed for non-linear or rank-based relationships. Latent profile analysis was conducted to identify potential underlying subgroups based on the variations in ROX. All tests were two-tailed, with statistical significance set at $P < 0.05$. Statistical analysis was conducted using IBM SPSS Statistics (Version 22.0, IBM Corp, Armonk, NY) and R (Version 4.2.2, R Foundation for Statistical Computing, Vienna, Austria; https://www.R-project.org/).

Results

Between January and March 2023, a total of 34 patients with COVID-19-related AHRF were enrolled in the intensive care unit of Zhongshan Hospital, Fudan University. All patients completed the six scheduled sessions, and no data imputation was required. The quality of EIT signals was deemed acceptable, with no data excluded. Baseline clinical characteristics and outcomes are summarized in Table S1. The cohort consisted of 24 males (71%), with a mean age of 73 ± 10 years and a mean body mass index (BMI) of 25.07 ± 3.36 kg/m^2. At study enrollment, the mean APACHE II score was 13 ± 4, the mean SpO_2/FiO_2 ratio was 165.78 ± 36.22, and the mean ROX index was 7.93 ± 2.30.

Gas Exchange, Vital Signs, and Self-reported Comfort

Across all respiratory support modalities, APP significantly improved both the SpO2/FiO2 ratio and ROX index but was associated with lower self-reported comfort compared to the supine position (all P<0.05) (Table 2, Figure 1). CPAP had higher oxygenation (SpO2/FiO2 ratio and ROX index) than HFOM and HFNC in both supine and prone positions (all P<0.05, Figure S1). Vital signs, including heart rates, respiratory rates, and mean arterial pressure, did not differ significantly across various respiratory support modes or positions (Table 2).

EIT-Derived Indices

Compared to supine position, APP significantly reduced the GI, CoV, and Pendelluft (main effect of position, all $P < .05$, Table 2). Ventral ventilation increased, while dorsal ventilation decreased in the prone position ($P = .017$ for both, Table 2). TIV did not differ significantly between positions ($P = .570$, Figure 2). In within-modality comparisons, pendelluft decreased with prone positioning for all supports, but the reduction in GI reached significance only during HFNC (0.43 ± 0.09 vs. 0.39 ± 0.06, $P < .05$, Figure 2) and CPAP (0.50 ± 0.09 vs. 0.45 ± 0.08, $P < .05$, Figure 2), not in HFOM; and CoV decreased with APP only during CPAP (53.44±8.08 vs 46.71±7.14, $P < .05$) (Table 2, Figure 2), with significantly decreased ROI3 and increased ROI1 (Table 2). Compared to HFOM and HFNC, CPAP resulted in significantly higher TIV and GI (main effect of respiratory supports, $P = .027$ and $P < .001$, respectively, Table 2). No significant differences were observed among respiratory supports in CoV or pendelluft. A significant interaction was noted for CoV ($P < .05$, Table 2), showing that the reduction in CoV with prone positioning was primarily driven by CPAP. No significant interactions were found for GI, TIV, or pendelluft, indicating that the effect of prone positioning on ventilation homogeneity was consistent across support modes.

Subgroup Analyses

In patients with BMI < 24 kg/m^2, APP decreased ROI 3 and increased ROI 1, with changes more pronounced when combined with HFNC or CPAP (Figure 3). Among patients with BMI > 24 kg/m^2, APP did not significantly alter ROI distribution across respiratory support modalities (Figure 3). In the higher BMI group, CoV was higher during PPHFNC and PPCPAP compared to the lower BMI group (49.79 ± 6.38 vs. 43.58 ± 5.28; 50.07 ± 7.49 vs. 43.36 ± 5.01, respectively, both $P < 0.05$) (Table S2).

Latent Profile Analysis

As shown in Table S3, the 3-profile model exhibited lower AIC, BIC, and aBIC values compared to the 1- and 2-profile models. Moreover, the significant p-value of the Bootstrapped Likelihood Ratio Test (pBLRT < .05) supported the 3-profile solution over the 2-profile solution. The entropy value of 0.91 indicates excellent classification certainty. Latent profile analysis (Table S4) identified three distinct classes of response to APP: class 1 (n = 17, 50%), class 2 (n = 8, 23%), and class 3 (n = 9, 27%). At baseline, class 1 patients had a lower ROX index (median 5.9 [IQR 4.4-6.9]), lower SpO2/FiO2 (151.8 ± 39.8), and higher respiratory rate (25.9 ± 6.7 breaths/min). In contrast, class 3 patients showed higher ROX index (9.3 [8.3-11.6]), higher SpO2/FiO2 (180.3 ± 32.1), and lower respiratory rate (18.4 ± 5.0 breaths/min), while class 2 patients demonstrated intermediate values.

As shown in Figure S3, class 2 patients exhibited the greatest improvement of ROX index during APP, particularly with CPAP ($p < 0.05$). Class 2 also showed stepwise increases in ROX with respiratory support escalation from HFOM to HFNC, and then to CPAP in both supine and prone positions. Class 1 patients showed minimal changes in ROX with HFNC but improved significantly upon escalation to CPAP in both positions. Conversely, class 3 patients demonstrated negligible changes in ROX with respiratory support escalation in supine position and a paradoxical decline in ROX during CPAP in the prone position (Figure S3). EIT-derived parameters revealed consistent interclass differences in ventilation distribution. At the supine position, dorsal ventilation in Class 1 and Class 2 remained balanced (~50–55%), while Class 3 exhibited markedly reduced dorsal contribution (33.4 ± 11.1%, $p = 0.006$). During prone CPAP (PPCPAP), dorsal ventilation decreased slightly in Classes 1 and 2 (~47–59%) but dropped further in Class 3 (29.3 ± 14.3%, $p = 0.005$). CoV values were comparable across groups in supine but were significantly lower in Class 3 during prone CPAP (40.8 ± 5.4%) than in Classes 1 and 2 (~50%, $p = 0.008$).

Correlation Analyses

As shown in Figure 4, greater TIV was correlated with higher ROX and lower respiratory rates ($p < 0.05$). However, no significant correlations were observed between GI or pendelluft and any clinical variables.

Discussion

In this randomized crossover trial, we employed EIT to explore the acute physiological effects of combining APP with three non-invasive respiratory supports in COVID-19-related AHRF. The main findings include: (1) APP improved oxygenation across all respiratory support modalities, with CPAP providing the greatest benefit; (2) APP did not alter global tidal volume but significantly improved ventilation homogeneity and reduced pendelluft, suggesting a redistribution of ventilation; and (3) CPAP increased ventilation inhomogeneity in the supine position, but the effects were attenuated when combined with APP.

Improvement of oxygenation

Consistent with prior studies and meta-analyses [5, 14, 15], APP significantly improved oxygenation in this cohort. The observed increase in SpO_2/FiO_2 and ROX index supports previous evidence that prone positioning enhances ventilation-perfusion matching by reducing dorsal shunt fraction [16]. Similarly, the superior oxygenation achieved with CPAP compared to HFNC and HFOM aligns with recent physiological studies by Menga et al. [8] and Grieco et al. [7], which emphasized the role of sustained positive airway pressure in alveolar recruitment. Notably, our study extends earlier work[5, 17-19] by demonstrating an interaction between position and support mode. The highest oxygenation levels were achieved during CPAP in the prone position, suggesting that combining APP with CPAP may provide additive physiological benefits. This supports a strategy of individualized respiratory support selection based on tolerance and oxygenation response, particularly in patients capable of maintaining spontaneous breathing.

Impact on TIV and pulmonary ventilation distribution

In this study, although APP did not change TIV, it did alter the regional distribution of ventilation. APP was associated with decreased dorsal (ROI 3) and increased ventral (ROI 1) ventilation. Several mechanisms have been proposed to explain positional changes in ventilation [2, 20], including gravitational redistribution, diaphragmatic mechanics, and changes in chest wall compliance. Some discrepancies exist in the literature regarding the direction and magnitude of these regional changes. Grieco et al. reported a shift in ventilation toward dependent lung regions during APP [21], whereas others observed no significant redistribution [5, 6]. Variability in trunk inclination, which can alter pleural pressure gradients and lung mechanics, may partly

account for these inconsistencies [22-24]. Sample size, disease severity, and differences in device settings may also contribute. Compared to HFNC and HFOM, CPAP resulted in greater TIV and COV, consistent with the generation of greater lung volumes and alveoli opening under higher positive pressure [25-27].

Impact on GI and Pendelluft

APP significantly reduced the global inhomogeneity index (GI) and pendelluft, indicating a more homogeneous and stable ventilation pattern. This finding aligns with Riera et al.[28], who observed improved ventilation uniformity during APP in 20 adult healthy subjects treated with HFNC, but contrasts with Brunelle et al.[29], who observed unchanged GI despite better oxygenation in COVID-19 patients with AHRF. The smaller sample size in Brunelle’ s study (n=10) and variable positioning protocols may explain these discrepancies [22-24]. In our study, the bed was raised 30 degrees in a semi-recumbent position for supine, and flat for prone, with cushions under the chest and hips, allowing the abdomen to rest lightly on the bed. While in Brunelle et al’ s study[29], they didn’ t mention the angle of the bed in the supine position and the prone position.

In our study, CPAP consistently increased GI compared to HFNC and HFOM in both supine and prone positions, suggesting greater ventilation inhomogeneity associated with higher airway pressures. However, when combined with APP, CPAP no longer increased inhomogeneity and was associated with reduced pendelluft. This is likely due to changes in the contraction pattern of the diaphragm and accessory muscle mechanics in the prone position, potentially stabilizing regional ventilation and reducing asynchronous inflation—a mechanism relevant to mitigating patient self-inflicted lung injury[30].

Clinical Implications and Personalized Strategy

The differential response to APP between BMI groups underscores the critical influence of body habitus on respiratory mechanics. In lower BMI patients (<24 kg/m^2), APP favorably redistributed ventilation from non-dependent (ROI 3) to dependent regions (ROI 1), an effect enhanced by HFNC or CPAP, likely by synergistically counteracting atelectasis through increased lung volume and modulated pleural pressures. Conversely, this redistributive effect was absent in higher BMI patients (>24 kg/m^2), suggesting that the substantial chest wall elastance and chronic lung compression in obesity may render APP ineffective against the dominant restrictive mechanics[31]. This interpretation is further supported by the significantly higher CoV observed in the high BMI group during PPHFNC and PPCPAP, indicating an underlying physiological state less amenable to external manipulation[32]. Consequently, while APP combined with positive pressure support appears beneficial for optimizing ventilation in non-obese individuals, its efficacy is limited in obese patients, necessitating future exploration of tailored therapeutic strategies for this population. Latent profile analysis based on the ROX index revealed three distinct physiological phenotypes. Patients in Class 1 (low ROX, high drive) showed marked oxygenation improvement with CPAP combined with awake prone positioning (APP), which stabilized dorsal ventilation. Class 2 (intermediate ROX) responded best to a stepwise escalation from HFNC to CPAP, with APP synergistically enhancing recruitment and homogeneity. In contrast, Class 3 (high ROX, low drive) exhibited a ventral-dominant ventilation pattern with limited recruitability, showing minimal benefit from CPAP and potentially facing overdistention risks, thus making HFNC ± APP a more suitable strategy. Integrating EIT with clinical phenotyping provides a framework for personalized respiratory support. Together, these observations emphasize that combining EIT-based assessment with clinical indices such as ROX may guide a phenotypedirected approach.

Limitations and future directions

Several limitations should be acknowledged. First, because this study was conducted exclusively in patients with COVID-19–related AHRF, generalizability to other etiologies of AHRF remains uncertain. Nevertheless, the physiological mechanisms observed—particularly improved ventilation homogeneity and reduced pendelluft with awake prone positioning—are likely not disease-specific and may extend to non– COVID-19 AHRF, although this extrapolation requires confirmation in dedicated cohorts. The single-center design and modest sample size may further limit external validity. The 30-minute intervention window captured only acute physiological responses and does not address sustainability. The absence of esophageal manometry restricted mechanistic interpretation, particularly regarding transpulmonary pressure and the work of breathing [7, 33]. In addition, absolute end-expiratory lung impedance was not analyzed because EIT measures have limited comparability across sessions [34]. Although statistical models adjusted for period effects, residual carryover cannot be fully excluded. Future multi-center studies with longer interventions and advanced respiratory mechanics monitoring are warranted.

Conclusions

In patients with COVID-19 associated AHRF, CPAP improved oxygenation more effectively than HFOM or HFNC but increased ventilation inhomogeneity. APP reduced global inhomogeneity and pendelluft, promoting more even ventilation. Combining APP with CPAP synergistically enhanced oxygenation while mitigating inhomogeneity. These findings clarify the interaction between posture and respiratory support, aiding the development of phenotype-based strategies for AHRF.

Abbreviations

AHRF: Acute Hypoxemic Respiratory Failure

APP: Awake Prone Positioning

CPAP: Continuous Positive Airway Pressure

EIT: Electrical Impedance Tomography

FiO2: Fraction of Inspired Oxygen

GI: Global Inhomogeneity

HFNC: High-Flow Nasal Cannula

HFOM: High Flow Oxygen Mask

NIV: Noninvasive Ventilation

PEEP: Positive End-Expiratory Pressure

PP: Prone Position

ROIs: Regions of Interest

RR: Respiratory Rate

S/F: SpO2/FiO2

SpO2: Peripheral Capillary Oxygen SaturationLimitations and future directions

Acknowledgements

The authors thank all the subjects for their participation in this study and thank Professor Oriol Roca for his assistance.

Ethical Statement

This study was conducted in accordance with the Declaration of Helsinki and approved by the Institutional Ethics Committees of Zhongshan Hospital, Fudan University (No. B2022-359R) and Rush University Medical Center (No. 23042703). Informed consent was obtained from all participants included in the study.

Author contributions:

JL, YXW and MZ designed the study. YXW, SYH, YLW and MZ conducted the study on the enrolled patients. YXW, QJJ, YLW and JL analyzed the data. All authors interpreted the data and wrote the first draft of the manuscript. JL and MZ revised the first draft of the manuscript. MZ organized the study as the overall supervisor. All the authors reviewed the final draft of the manuscript.

Availability of data and materials

The datasets used and/or analyzed during the current study are available from the corresponding author on reasonable request.

References

1. Ding L, Wang L, Ma W, He H: Efficacy and safety of early prone positioning combined with HFNC or NIV in moderate to severe ARDS: a multi-center prospective cohort study. Crit Care 2020, 24(1):28.

2. Pavlov I, He H, McNicholas B, Perez Y, Tavernier E, Trump MW, Jackson JA, Zhang W, Rubin DS, Spiegel T et al: Awake Prone Positioning in Non-Intubated Patients With Acute Hypoxemic Respiratory Failure Due to COVID-19. Respir Care 2022, 67(1):102-114.

3. McNicholas BA, Ibarra-Estrada M, Perez Y, Li J, Pavlov I, Kharat A, Vines DL, Roca O, Cosgrave D, Guerin C et al: Awake prone positioning in acute hypoxaemic respiratory failure. Eur Respir Rev 2023, 32(168).

4. Luo J, Pavlov I, Tavernier E, Perez Y, Kharat A, McNicholas B, Roca O, Vines DL, Ibarra-Estrada M, Alhazzani W et al: Awake Prone Positioning in Adults With COVID-19: An Individual Participant Data Meta-Analysis. JAMA Intern Med 2025.

5. Dos Santos Rocha A, Diaper J, Balogh AL, Marti C, Grosgurin O, Habre W, Peták F, Südy R: Effect of body position on the redistribution of regional lung aeration during invasive and non-invasive ventilation of COVID-19 patients. Sci Rep 2022, 12(1):11085.

6. Rosén J, Frykholm P, Jonsson Fagerlund M, Pellegrini M, Campoccia Jalde F, von Oelreich E, Fors D: Lung impedance changes during awake prone positioning in COVID-19. A non-randomized cross-over study. PLoS One 2024, 19(2):e0299199.

7. Grieco DL, Menga LS, Raggi V, Bongiovanni F, Anzellotti GM, Tanzarella ES, Bocci MG, Mercurio G, Dell'Anna AM, Eleuteri D et al: Physiological Comparison of High-Flow Nasal Cannula and Helmet Noninvasive Ventilation in Acute Hypoxemic Respiratory Failure. Am J Respir Crit Care Med 2020, 201(3):303-312.

8. Menga LS, Delle Cese L, Rosà T, Cesarano M, Scarascia R, Michi T, Biasucci DG, Ruggiero E, Dell'Anna AM, Cutuli SL et al: Respective Effects of Helmet Pressure Support, Continuous Positive Airway Pressure, and Nasal High-Flow in Hypoxemic Respiratory Failure: A Randomized Crossover Clinical Trial. Am J Respir Crit Care Med 2023, 207(10):1310-1323.

9. Zhao Z, Möller K, Steinmann D, Frerichs I, Guttmann J: Evaluation of an electrical impedance tomographybased Global Inhomogeneity Index for pulmonary ventilation distribution. Intensive Care Med 2009, 35(11):1900-1906.

10. Frerichs I, Amato MB, van Kaam AH, Tingay DG, Zhao Z, Grychtol B, Bodenstein M, Gagnon H, Böhm SH, Teschner E et al: Chest electrical impedance tomography examination, data analysis, terminology, clinical use and recommendations: consensus statement of the TRanslational EIT developmeNt stuDy group. Thorax 2017, 72(1):83-93.

11. Muders T, Luepschen H, Zinserling J, Greschus S, Fimmers R, Guenther U, Buchwald M, Grigutsch D, Leonhardt S, Putensen C et al: Tidal recruitment assessed by electrical impedance tomography and computed tomography in a porcine model of lung injury*. Crit Care Med 2012, 40(3):903-911.

12. Frerichs I, Zhao Z, Becher T: Simple Electrical Impedance Tomography Measures for the Assessment of Ventilation Distribution. Am J Respir Crit Care Med 2020, 201(3):386-388.

13. Sang L, Zhao Z, Yun PJ, Frerichs I, Möller K, Fu F, Liu X, Zhong N, Li Y: Qualitative and quantitative assessment of pendelluft: a simple method based on electrical impedance tomography. Ann Transl Med 2020, 8(19):1216.

14. Coppo A, Bellani G, Winterton D, Di Pierro M, Soria A, Faverio P, Cairo M, Mori S, Messinesi G, Contro E et al: Feasibility and physiological effects of prone positioning in non-intubated patients with acute respiratory failure due to COVID-19 (PRON-COVID): a prospective cohort study. Lancet Respir Med 2020, 8(8):765-774.

15. Ehrmann S, Li J, Ibarra-Estrada M, Perez Y, Pavlov I, McNicholas B, Roca O, Mirza S, Vines D, Garcia-Salcido R et al: Awake prone positioning for COVID-19 acute hypoxaemic respiratory failure: a randomised, controlled, multinational, open-label meta-trial. Lancet Respir Med 2021, 9(12):1387-1395.

16. Liu L, Xie J, Wang C, Zhao Z, Chong Y, Yuan X, Qiu H, Zhao M, Yang Y, Slutsky AS: Prone position improves lung ventilation-perfusion matching in non-intubated COVID-19 patients: a prospective physiologic study. Crit Care 2022, 26(1):193.

17. Cammarota G, Rossi E, Vitali L, Simonte R, Sannipoli T, Anniciello F, Vetrugno L, Bignami E, Becattini C, Tesoro S et al: Effect of awake prone position on diaphragmatic thickening fraction in patients assisted by noninvasive ventilation for hypoxemic acute respiratory failure related to novel coronavirus disease. Crit Care 2021, 25(1):305.

18. Lehingue S, Allardet-Servent J, Ferdani A, Hraeich S, Forel JM, Arnal JM, Prud'homme E, Penaranda G, Bourenne J, Monnet O et al: Physiologic Effects of the Awake Prone Position Combined With High-FlowNasal Oxygen on Gas Exchange and Work of Breathing in Patients With Severe COVID-19 Pneumonia: A Randomized Crossover Trial. Crit Care Explor 2022, 4(12):e0805.

19. Chiumello D, Chiodaroli E, Coppola S, Cappio Borlino S, Granata C, Pitimada M, Wendel Garcia PD: Awake prone position reduces work of breathing in patients with COVID-19 ARDS supported by CPAP. Ann Intensive Care 2021, 11(1):179.

20. Li J, Luo J, Pavlov I, Perez Y, Tan W, Roca O, Tavernier E, Kharat A, McNicholas B, Ibarra-Estrada M et al: Awake prone positioning for non-intubated patients with COVID-19-related acute hypoxaemic respiratory failure: a systematic review and meta-analysis. Lancet Respir Med 2022, 10(6):573-583.

21. Grieco DL, Delle Cese L, Menga LS, Rosà T, Michi T, Lombardi G, Cesarano M, Giammatteo V, Bello G, Carelli S et al: Physiological effects of awake prone position in acute hypoxemic respiratory failure. Crit Care 2023, 27(1):315.

22. Dellamonica J, Lerolle N, Sargentini C, Hubert S, Beduneau G, Di Marco F, Mercat A, Diehl JL, Richard JC, Bernardin G et al: Effect of different seated positions on lung volume and oxygenation in acute respiratory distress syndrome. Intensive Care Med 2013, 39(6):1121-1127.

23. Mezidi M, Guérin C: Effect of body position and inclination in supine and prone position on respiratory

mechanics in acute respiratory distress syndrome. Intensive Care Med 2019, 45(2):292-294.

24. Marrazzo F, Spina S, Forlini C, Guarnieri M, Giudici R, Bassi G, Bastia L, Bottiroli M, Fumagalli R, Langer T: Effects of Trunk Inclination on Respiratory Mechanics in Patients with COVID-19-associated Acute Respiratory Distress Syndrome: Let's Always Report the Angle! Am J Respir Crit Care Med 2022, 205(5):582- 584.

25. Pitre T, Zeraatkar D, Kachkovski GV, Leung G, Shligold E, Dowhanik S, Angriman F, Ferreyro BL, Scales DC, Rochwerg B: Noninvasive Oxygenation Strategies in Adult Patients With Acute Hypoxemic Respiratory Failure: A Systematic Review and Network Meta-Analysis. Chest 2023, 164(4):913-928.

26. Corley A, Rickard CM, Aitken LM, Johnston A, Barnett A, Fraser JF, Lewis SR, Smith AF: High-flow nasal cannulae for respiratory support in adult intensive care patients. Cochrane Database Syst Rev 2017, 5(5):Cd010172.

27. Hong H, Li XX, Li J, Zhang ZQ: High-flow nasal cannula versus nasal continuous positive airway pressure for respiratory support in preterm infants: a meta-analysis of randomized controlled trials. J Matern Fetal Neonatal Med 2021, 34(2):259-266.

28. Riera J, Pérez P, Cortés J, Roca O, Masclans JR, Rello J: Effect of high-flow nasal cannula and body position on end-expiratory lung volume: a cohort study using electrical impedance tomography. Respir Care 2013, 58(4):589-596.

29. Brunelle T, Prud'homme E, Alphonsine JE, Baumstarck K, Sanz C, Salmi S, Peres N, Forel JM, Papazian L, Hraiech S et al: Awake prone position in COVID-19 acute respiratory failure: a randomised crossover study using electrical impedance tomography. ERJ Open Res 2023, 9(2).

30. Grieco DL, Menga LS, Eleuteri D, Antonelli M: Patient self-inflicted lung injury: implications for acute hypoxemic respiratory failure and ARDS patients on non-invasive support. Minerva Anestesiol 2019, 85(9):1014-1023.

31. Jones RL, Nzekwu MM: The effects of body mass index on lung volumes. Chest 2006, 130(3):827-833.

32. Pelosi P, Croci M, Ravagnan I, Vicardi P, Gattinoni L: Total respiratory system, lung, and chest wall mechanics in sedated-paralyzed postoperative morbidly obese patients. Chest 1996, 109(1):144-151.

33. Morais CCA, Koyama Y, Yoshida T, Plens GM, Gomes S, Lima CAS, Ramos OPS, Pereira SM, Kawaguchi N, Yamamoto H et al: High Positive End-Expiratory Pressure Renders Spontaneous Effort Noninjurious. Am J Respir Crit Care Med 2018, 197(10):1285-1296.

34. Ling S, Zhao Z: End-Expiratory Lung Impedance Measured With Electrical Impedance Tomography at Different Days Are Not Comparable. Crit Care Med 2023, 51(2):e70-e72.

Figure legends

Figure 1. Comparison of SpO2/FiO2 (A), Respiratory Rate (RR) (B), ROX Index (C), and Comfort (D) across different treatment groups: SPOM, PPOM, SPHFNC, PPHFNC, SPCPAP, and PPCPAP. Statistical comparisons were performed using linear mixed-effects models, with post-hoc adjustments for multiple comparisons using the Bonferroni correction. *p < 0.05, #p < 0.001.

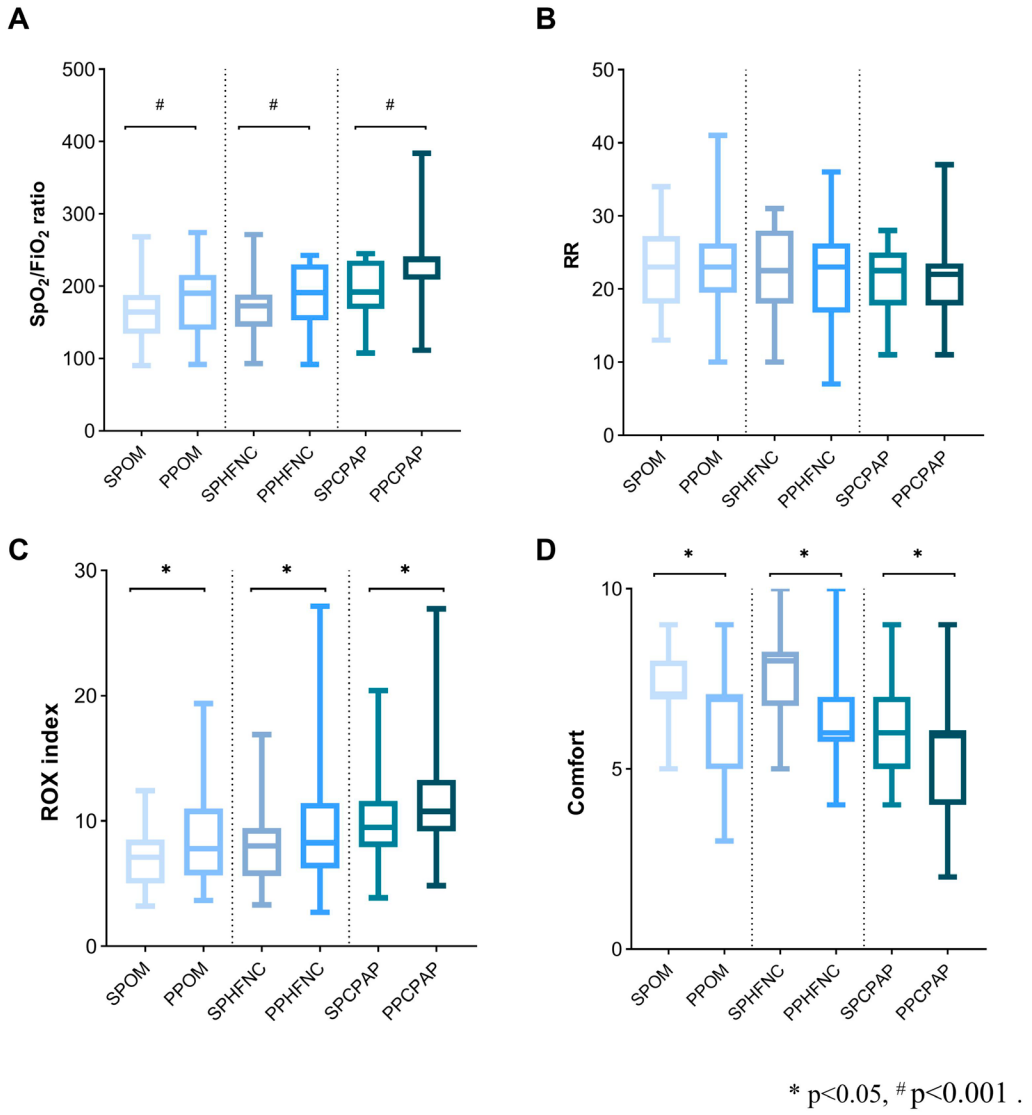


Figure 2. Comparison of Tidal impedance variation (TIV)(A), global inhomogeneity index (B), Center of ventilation (C), Pendelluft (D) across different treatment groups: SPOM, PPOM, SPHFNC, PPHFNC, SPCPAP, and PPCPAP. Statistical comparisons were performed using linear mixed-effects models, with post-hoc adjustments for multiple comparisons using the Bonferroni correction. *p < 0.05, #p < 0.001.

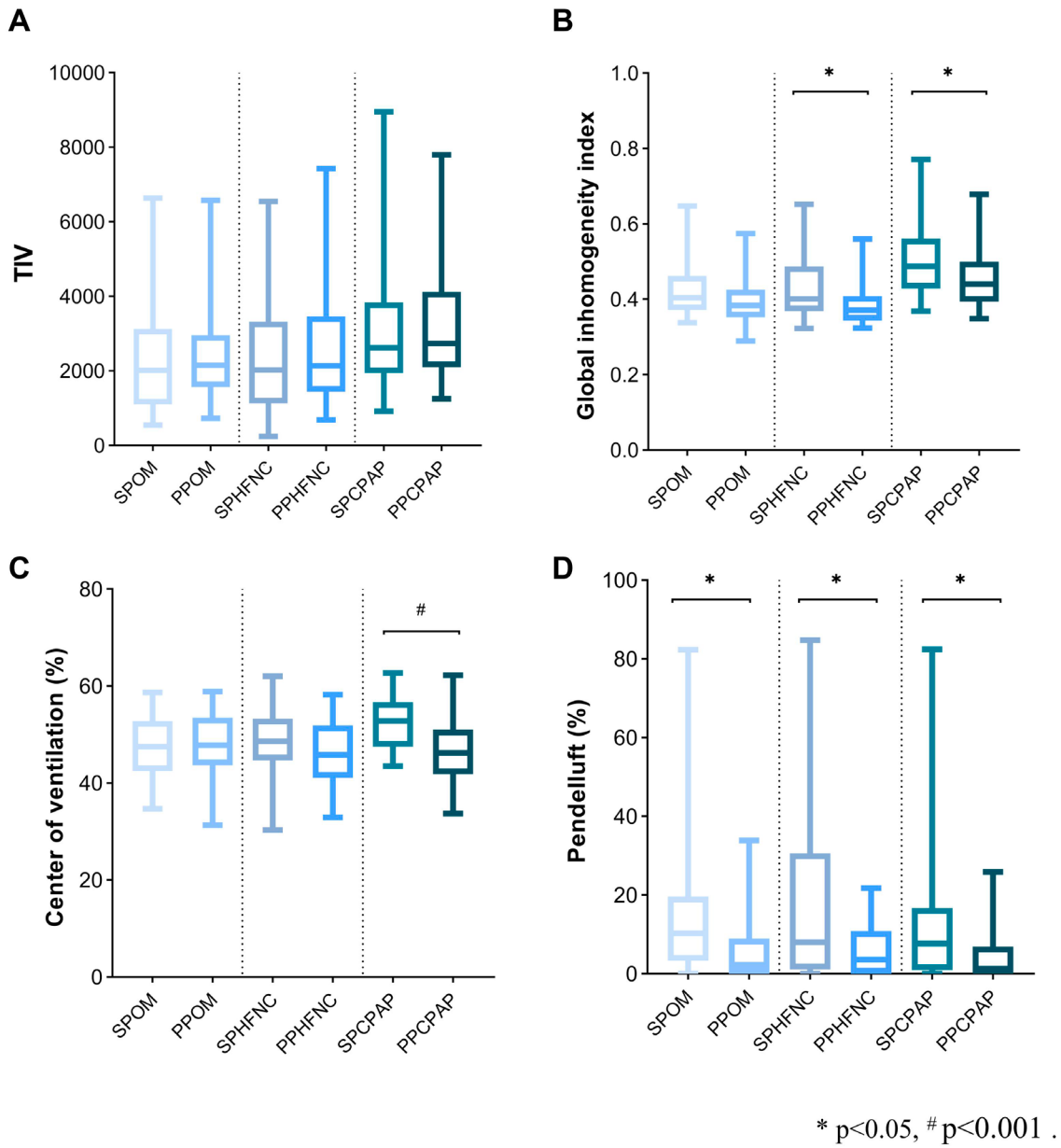


Figure 3. Ventilation distribution in different regions (RO1-RO4) under various treatment conditions. (A) HFOM, (B) HFNC, and (C) CPAP. The data represent the ventilation distribution (%) under the "Spine" (blue) and "Prone" (red) positions. Statistical comparisons were performed using paired t-test, with adjustments for multiple comparisons using the Bonferroni correction. *p < 0.05.

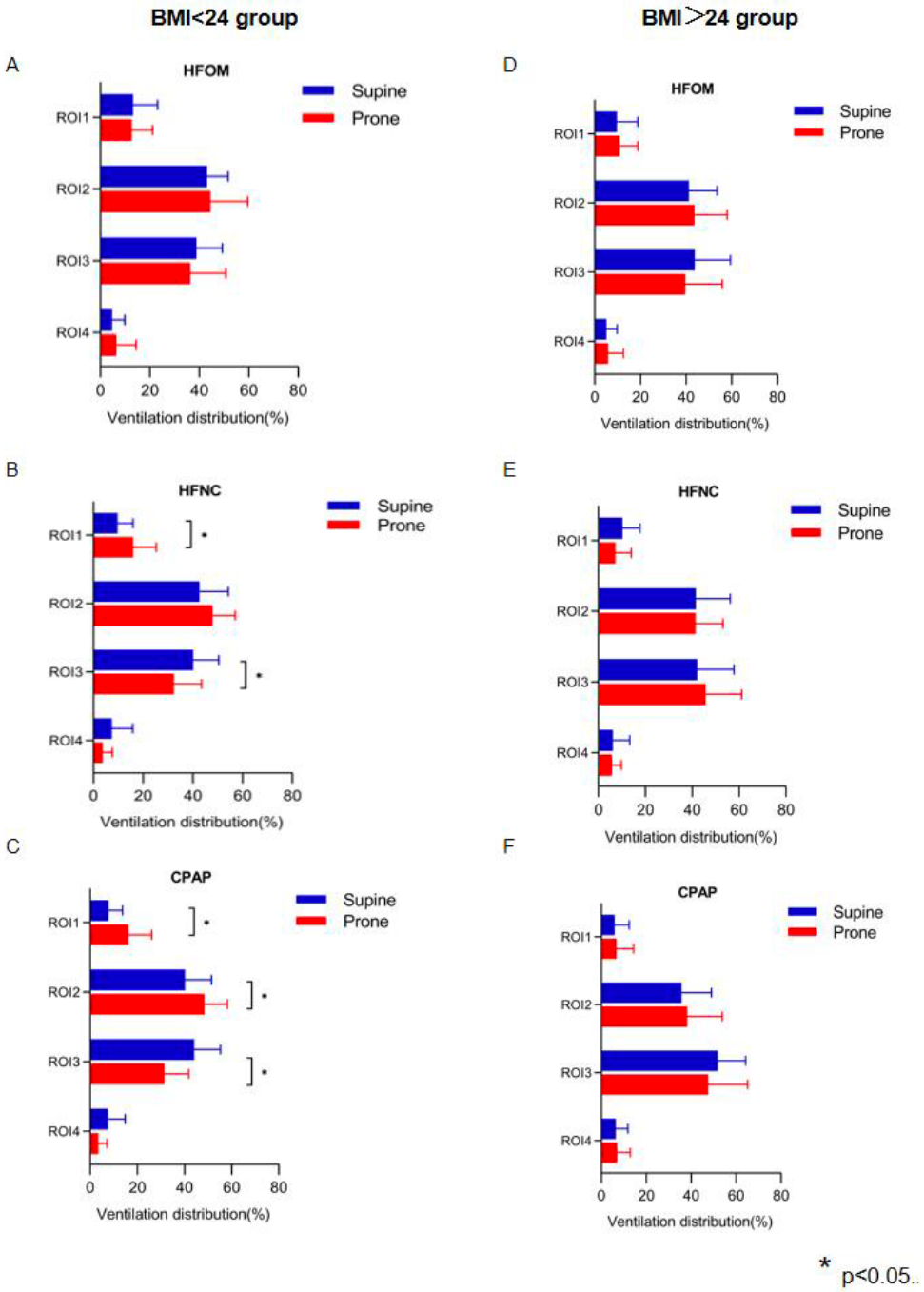


Figure 4. Correlation analyses between changes in TIV, GI, and Pendulant (%) with changes in SpO2/FiO2, RR, and ROX. Panels (A-C) show the relationship between ΔTIV and ΔSpO2/FiO2, ΔRR, and ΔROX, respectively. Panels (D-F) represent the relationship between ΔGI and ΔSpO2/FiO2, ΔRR, and ΔROX, respectively. Panels (G-I) display the relationship between ΔPendulant and ΔSpO2/FiO2, ΔRR, and ΔROX, respectively. Correlation analyses were performed using Pearson or Spearman tests as appropriate.

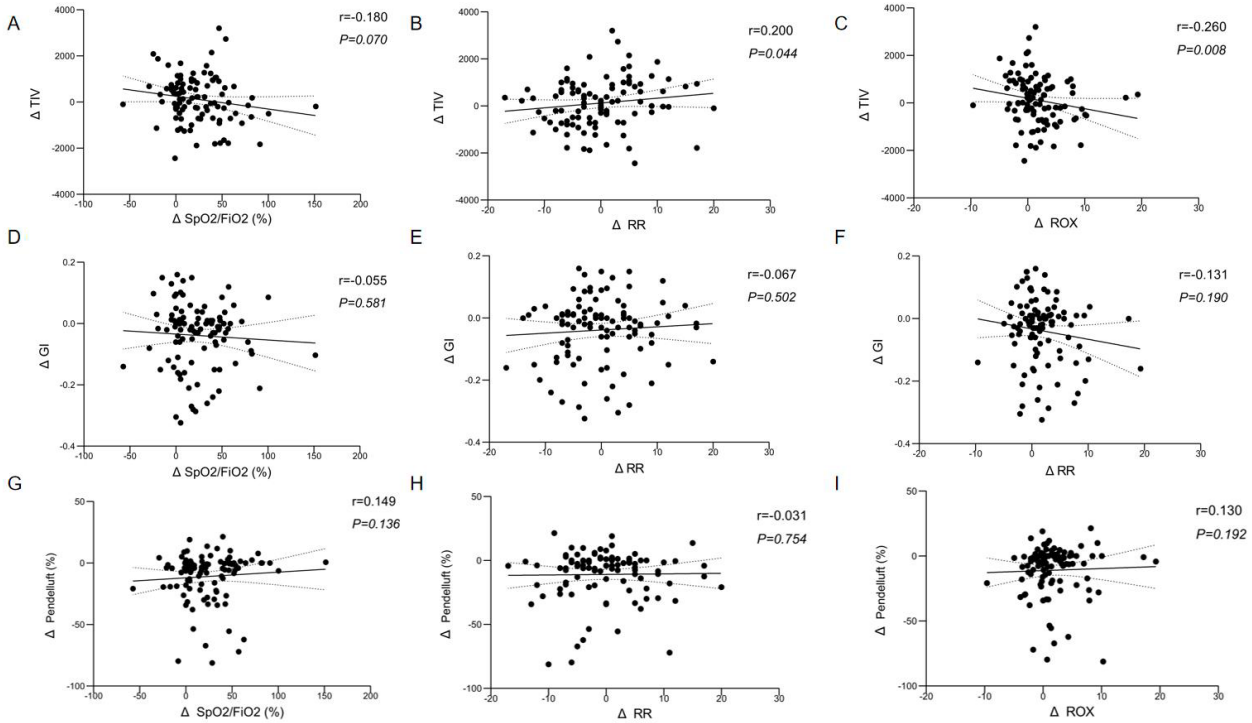


Table 1. Respiratory Support Methods and Abbreviations Based on Body Position

	Respiratory support	Body position	Character	Abbreviation
1	High flow oxygen mask	Supine	at 60 L/min or maximum tolerable flow	SPOM
2		Prone		PPOM
3	High-flow nasal cannula	Supine		SPHFNC
4		Prone		PPHFNC
5	Continuous positive airway pressure	Supine	full face mask at 8-10 cmH_2O	SPCPAP
6		Prone		PPCPAP

Table 2.Clinical variables and EIT-derived indices .

	MC		HFNC		CPAP		*P* values		
	Supine	Prone	Supine	Prone	Supine	Prone	Positioning effect	Respiratory support effect	Positioning and Respiratory support interaction
Hemodynamics									
HR	82.29±17.58	84.00±12.14	79.82±13.76	81.88±13.92	79.41±15.13	82.41±13.31*	0.265	0.572	0.964
MAP	88.92±11.62	89.03±14.41	88.33±12.03	88.22±14.19	89.17±11.23	91.40±14.54	0.686	0.662	0.846
Gas exchange									
RR	23.09±5.17	23.09±6.44	22.41±5.71	21.97±7.26	21.21±5.06	20.94±5.82	0.778	0.145	0.977
SpO_2	93.47+2.03	94.56+1.97*	94.15+1.42	95.18+1.66	95.21+1.18	95.97+1.29*	**<0.001**	**<0.001**	0.826
FiO_2	0.62±0.17	0.56±0.18*	0.60±0.16	0.50±0.16*	0.51±0.12	0.44±0.10*	**<0.001**	**<0.001**	0.612
S/F	161.84±40.68	186.52±62.63*	166.45±38.71	187.50±41.46*	196.31±38.31	226.94±44.72*	**<0.001**	**<0.001**	0.720
ROX	7.37±2.52	8.77±4.06*	7.97±2.89	10.18±5.86*	9.89±3.37	11.82±4.56*	**<0.005**	**<0.001**	0.737
Self-assessed symptoms									
Comfort	7.29±1.12	6.35±1.35*	7.47±1.40	6.44±1.42*	6.21±1.34	5.35±1.83*	**<0.001**	**<0.001**	0.937
EIT-derived indices									
TIV	2015.00[1101.75-3126.50]	2154.00[1570.00-2958.75]	2031.00[1125.25-3318.00]	2139.00[1446.25-3462.25]	2617.00[1945.00-3840.50]	2739.00[2100.75-4118.50]	0.570	**0.027**	0.942
GI	0.42+0.08	0.40+0.06	0.43+0.09	0.39+0.06*	0.50+0.09	0.45+0.08*	**<0.005**	**<0.001**	0.691
COV	47.76+5.96	47.54+6.93	48.13+7.22	46.69+6.57	53.44+8.08	46.71+7.14*	**<0.05**	0.131	**<0.05**
ROI1 layer	9.76+9.11	10.91+7.96	9.99+6.73	11.61+9.17	6.90+6.16	11.53+9.86*	**<0.05**	0.518	0.414
ROI2 layer	41.25+12.42	43.61+14.29	42.07+13.06	44.68+10.82	38.00+12.30	43.46+13.71	0.054	0.477	0.736
ROI3 layer	43.82+15.62	39.62+16.24	41.16+13.12	39.02+14.96	48.04+12.19	39.63+16.31*	**0.019**	0.338	0.455
ROI4 layer	5.14±4.74	5.88±6.66	6.77±7.74	4.69±4.05	7.06±6.28	5.35±5.13	0.221	0.783	0.320
Ventral ventilation	51.00±17.76	54.52±19.03	52.07±16.81	56.29±16.73	44.90±15.03	54.99±19.86*	**0.017**	0.363	0.490
Dorsal ventilation	48.96+17.76	45.50+19.03	47.93+16.81	43.71+16.72	55.09+15.03	44.97+19.85*	**0.017**	0.366	0.484
Pendelluft	10.27[3.27-19.61]	2.25[0-8.94]*	8.06[1.17-30.64]	3.62[0.05-10.85]*	7.65[0.99-16.73]	1.33[0-6.96]*	**<0.001**	0.278	0.670

SPOM: Supine Position with High Flow Oxygen Mask, SPHFNC: Supine Position with High-Flow Nasal Cannula, SPCPAP: Supine Position with Continuous Positive Airway Pressure, PPOM: Prone Position with High Flow Oxygen Mask, PPHFNC: Prone Position with High-Flow Nasal Cannula, PPCPAP: Prone Position with Continuous Positive Airway Pressure, TIV: Tidal impedance variation, GI: Global Inhomogeneity, COV: Center of Ventilation, ROI: Region of Interest, Ventral Ventilation: Ventilation in the Ventral (front) Region of the Lungs, Dorsal Ventilation: Ventilation in the Dorsal (back) Region of the Lungs, Pendelluft: Uneven Distribution of Air within the Lungs.

* Significant differences at each respiratory support strategy between supine and prone positioning.

Awake prone positioning with HFOM, HFNC, or CPAP in COVID-19-related acute hypoxemic respiratory failure: a randomized crossover EIT study

Yuxian Wang[1#], Jie Li[2#*], Shengyu Hao[1#], QijingJiang[3], Yilin Wei[3], Zhanqi Zhao[4*], Ming Zhong[1,3*]

[#]These authors contributed equally to the work.

Electronic supplementary material

TABLES

Table S1. Baseline characteristic..

NO.34	Mean ± SD or n (%)
Sex	24M/10F
Age	73±10
Height/m	1.65±0.07
Weight/kg	67.88±8.45
BMI Kg/m^2	25.07±3.36
Hypertension (%)	25(73.5%)
Diabetes mellitus (%)	12(35.3%)
SOFA	3.53±1.82
APACHEII	13±4
Days of hospitalization	9.50±6.78
Days of HFNC	3[1-8]
Days of COVID-19	19.79±6.06
History of COVID-19 vaccines	14Y/20N
HR	80.82±14.27
MAP	87.47±13.72
RR	22.82±6.51
SpO_2	94.82±2.19
FiO_2	60.29±14.75
SpO_2/ FiO_2	165.78±36.22
ROX	7.93±2.30
Outcomes	
Intubation	3
Do not intubate but died	6
Hospital length of stay	28[21-36]
Survival	25Y/9N

SD: Standard Deviation, BMI: Body Mass Index, SOFA: Sequential Organ Failure Assessment, APACHE II: Acute Physiology and Chronic Health Evaluation II, HFNC: High-Flow Nasal Cannula, HR: Heart Rate, MAP: Mean Arterial Pressure, RR: Respiratory Rate, SpO2: Peripheral Capillary Oxygen Saturation, FiO2: Fraction of Inspired Oxygen, SpO2/FiO2: Ratio of Peripheral Capillary Oxygen Saturation to Fraction of Inspired Oxygen, ROX: Ratio of SpO2/FiO2 to RR.

Table S2.Clinical variables and EIT-derived indices .

	MC		HFNC		CPAP		*P* values		
	Supine	**Prone**	**Supine**	**Prone**	**Supine**	**Prone**	**Positioning effect**	**Respiratory support effect**	**Positioning and Respiratory support interaction**
Hemodynamics									
HR	82.29±17.58	84.00±12.14	79.82±13.76	81.88±13.92	79.41±15.13	82.41±13.31*	0.265	0.572	0.964
MAP	88.92±11.62	89.03±14.41	88.33±12.03	88.22±14.19	89.17±11.23	91.40±14.54	0.686	0.662	0.846
Gas exchange									
RR	23.09±5.17	23.09±6.44	22.41±5.71	21.97±7.26	21.21±5.06	20.94±5.82	0.778	0.145	0.977
SpO2	93.47±2.03	94.56±1.97*	94.15±1.42	95.18±1.66	95.21±1.18	95.97±1.29*	**<0.001**	**<0.001**	0.826
FiO2	0.62±0.17	0.56±0.18*	0.60±0.16	0.50±0.16*	0.51±0.12	0.44±0.10*	**<0.001**	**<0.001**	0.612
S/F	161.84±40.68	186.52±62.63*	166.45±38.71	187.50±41.46*	196.31±38.31	226.94±44.72*	**<0.001**	**<0.001**	0.720
ROX	7.37+2.52	8.77+4.06*	7.97+2.89	10.18+5.86*	9.89+3.37	11.82+4.56*	**<0.005**	**<0.001**	0.737
Self-assessed symptoms									
Comfort	7.29±1.12	6.35±1.35*	7.47±1.40	6.44±1.42*	6.21±1.34	5.35±1.83*	**<0.001**	**<0.001**	0.937
EIT-derived indices									
TIV	2015.00[1101.75-3126.50]	2154.00[1570.00-2958.75]	2031.00[1125.25-3318.00]	2139.00[1446.25-3462.25]	2617.00[1945.00-3840.50]	2739.00[2100.75-4118.50]	0.570	**0.027**	0.942
GI	0.42±0.08	0.40±0.06	0.43±0.09	0.39±0.06*	0.50±0.09	0.45±0.08*	**<0.005**	**<0.001**	0.691
COV	47.76±5.96	47.54±6.93	48.13±7.22	46.69±6.57	53.44±8.08	46.71±7.14*	**<0.05**	0.131	**<0.05**
ROI1 layer	9.76±9.11	10.91±7.96	9.99±6.73	11.61±9.17	6.90±6.16	11.53±9.86*	**<0.05**	0.518	0.414
ROI2 layer	41.25+12.42	43.61+14.29	42.07+13.06	44.68+10.82	38.00+12.30	43.46+13.71	0.054	0.477	0.736
ROI3 layer	43.82±15.62	39.62±16.24	41.16±13.12	39.02±14.96	48.04±12.19	39.63±16.31*	**0.019**	0.338	0.455
ROI4 layer	5.14±4.74	5.88±6.66	6.77±7.74	4.69±4.05	7.06±6.28	5.35±5.13	0.221	0.783	0.320
Ventral ventilation	51.00±17.76	54.52±19.03	52.07±16.81	56.29±16.73	44.90±15.03	54.99±19.86*	**0.017**	0.363	0.490
Dorsal ventilation	48.96±17.76	45.50±19.03	47.93±16.81	43.71±16.72	55.09±15.03	44.97±19.85*	**0.017**	0.366	0.484
Pendelluft	10.27[3.27-19.61]	2.25[0-8.94]*	8.06[1.17-30.64]	3.62[0.05-10.85]*	7.65[0.99-16.73]	1.33[0-6.96]*	**<0.001**	0.278	0.670

SPOM: Supine Position with High Flow Oxygen Mask, SPHFNC: Supine Position with High-Flow Nasal Cannula, SPCPAP: Supine Position with Continuous Positive Airway Pressure, PPOM: Prone Position with High Flow Oxygen Mask, PPHFNC: Prone Position with High-Flow Nasal Cannula, PPCPAP: Prone Position with Continuous Positive Airway Pressure, TIV: Tidal impedance variation, GI: Global Inhomogeneity, COV: Center of Ventilation, ROI: Region of Interest, Ventral Ventilation: Ventilation in the Ventral (front) Region of the Lungs, Dorsal Ventilation: Ventilation in the Dorsal (back) Region of the Lungs, Pendelluft: Uneven Distribution of Air within the Lungs.

* Significant differences at each respiratory support strategy between supine and prone positioning

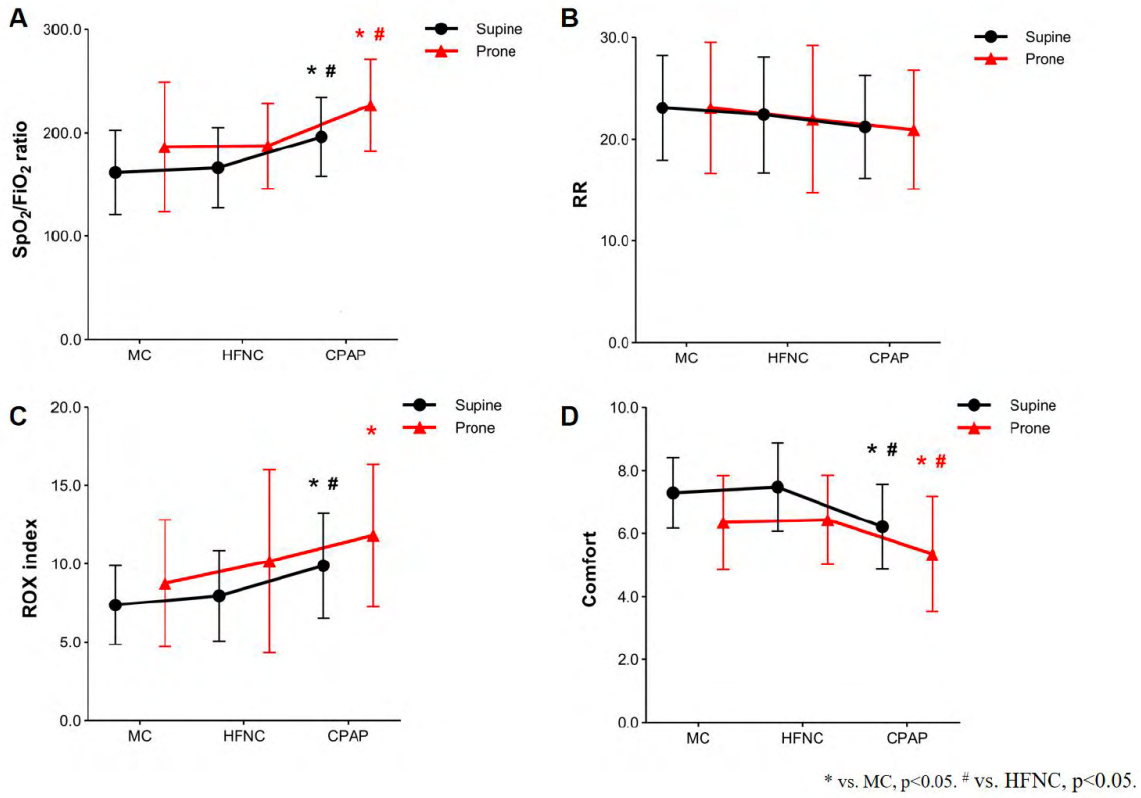


Figure S1. Evolution of SpO2/FiO2 (A), RR(B), ROX index(C) and Comfort(D) with MC, HFNC and CPAP in supine and prone position. * vs. MC, p<0.05, # vs. HFNC, p<0.05.

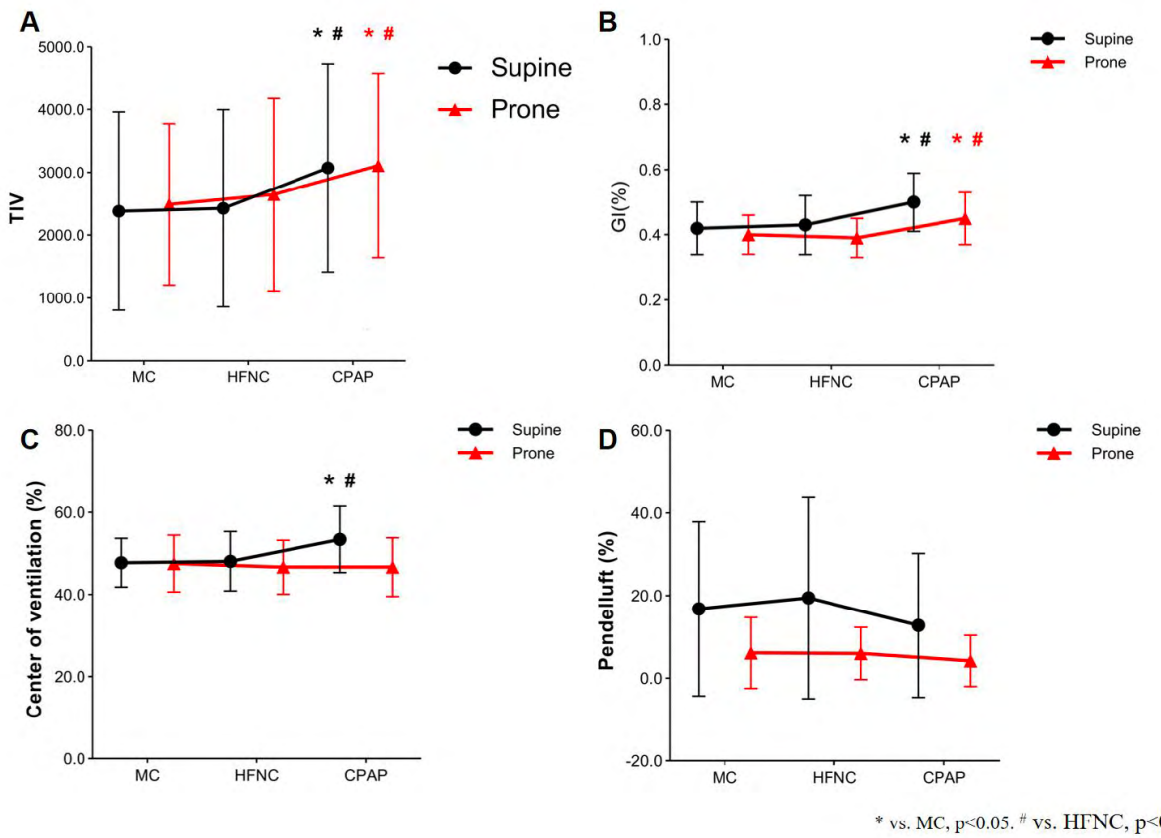


Figure S2. Evolution of Tidal impedance variation (TIV)(A), global inhomogeneity index (GI)(B), Center of ventilation (C), Pendelluft (D) with MC, HFNC and CPAP in supine and prone position. * vs. MC, p<0.05, # vs. HFNC, p<0.05.

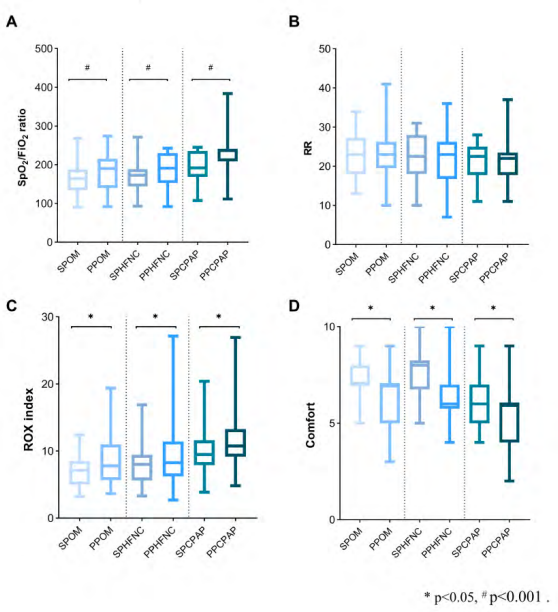


Figure S3. Comparison of SpO2/FiO2 (A), Respiratory Rate (RR) (B), ROX Index (C), and Comfort (D) across different treatment groups: SPOM, PPOM, SPHFNC, PPHFNC, SPCPAP, and PPCPAP. Statistical comparisons were performed using linear mixed-effects models, with post-hoc adjustments for multiple comparisons using the Bonferroni correction. *p < 0.05, #p < 0.001.

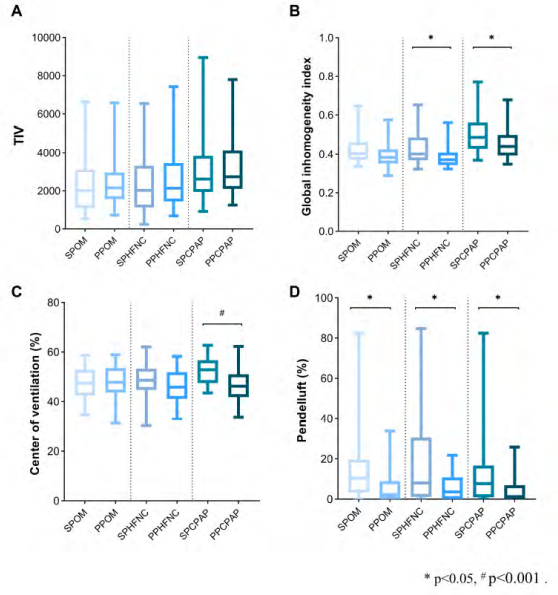


Figure S4. Comparison of Tidal impedance variation (TIV)(A), global inhomogeneity index (B), Center of ventilation (C), Pendelluft (D) across different treatment groups: SPOM, PPOM, SPHFNC, PPHFNC, SPCPAP, and PPCPAP. Statistical comparisons were performed using linear mixed-effects models, with post-hoc adjustments for multiple comparisons using the Bonferroni correction. *p < 0.05, #p < 0.001.

Predictive Value of the Murray Lung Injury Score for Ventilator-Associated Pneumonia and Mortality in Mechanically Ventilated ICU Patients: A Mediation Analysis

姓名：Sifeng Fu[1*], Zhenting Liang[1*],Ya Wang[1*], Yimin Li[1,2#], Yonghao Xu[1,2#]

单位：1 The First Affiliated Hospital of Guangzhou Medical University 2 Guangzhou National Laboratory

Abstract

Background: Mechanical ventilation is a major risk factor for ventilator-associated pneumonia (VAP) and mortality in critically ill patients. However, the predictive role of early lung injury severity and the mediating effect of VAP remain unclear.

Methods: We conducted a retrospective cohort study of 274 mechanically ventilated ICU patients. The Murray Lung Injury Score was assessed within 48 hours preceding pathogen identification. The primary outcome was hospital mortality, with VAP occurrence as a secondary outcome. Multivariable logistic regression and mediation analysis (bootstrap with 5000 resamples) were performed.

Results: Higher Murray scores were independently associated with increased risk of VAP (OR = 1.97, 95% CI: 1.28–3.04) and mortality (adjusted OR = 2.68, 95% CI: 1.70–4.37). Mediation analysis showed that VAP partially mediated the effect of lung injury severity on mortality (indirect OR = 1.11, 95% CI: 1.00–1.33; mediation proportion = 9.3%, 95% CI: 3.1–18.5%). The Murray score had moderate predictive accuracy for mortality (AUC = 0.697, 95% CI: 0.634–0.760).

Conclusion: Early assessment of lung injury severity using the Murray score can identify mechanically ventilated ICU patients at higher risk for VAP and mortality. VAP partially mediates this relationship, supporting the importance of early preventive strategies.

Keywords: Murray score, ventilator-associated pneumonia, acute lung injury, mortality, mediation analysis

Introduction

Ventilator-associated pneumonia (VAP) is a common and serious complication in critically ill patients undergoing mechanical ventilation, leading to increased morbidity, prolonged intensive care, and higher mortality [1,2]. Patients receiving mechanical ventilation have increased susceptibility due to compromised respiratory barrier function and dysregulated immune responses, which create a favorable environment for bacterial colonization and infection [3,4].

The Murray Lung Injury Score provides a quantitative assessment of lung injury severity by integrating radiographic infiltrates, hypoxemia (PaO_2/FiO_2 ratio), positive end-expiratory pressure (PEEP), and respiratory system compliance [5,6]. While originally developed to characterize ARDS, its utility in predicting secondary infections such as VAP and clinical outcomes in broader populations of mechanically ventilated patients remains underexplored [7-9].

Importantly, it remains uncertain to what extent VAP mediates the relationship between preceding lung injury severity and mortality [10,11]. Understanding whether and how much VAP explains or transmits the effect of lung injury on fatal outcomes is crucial for identifying high-risk patients and guiding early preventive strategies in the ICU setting [12-14].

Therefore, the primary objectives of this retrospective cohort study were: (1) to evaluate the predictive value of the Murray Lung Injury Score for VAP and hospital mortality in mechanically ventilated ICU patients; and (2) to quantify the mediating effect of VAP on the association between lung injury severity and mortality [15].

Methods

Study Design and Ethics

This retrospective cohort study was conducted at the First Affiliated Hospital of Guangzhou Medical University. The study protocol was approved by the Ethics Committee of Guangzhou Medical University’s First Affiliated Hospital (Approval No.: ES-2025-K265-01). Given the retrospective nature of the study, informed consent was waived, and all patient records were

anonymized preceding analysis. This study was designed and reported in accordance with the Strengthening the Reporting of Observational Studies in Epidemiology (STROBE) statement for cohort studies. All data were extracted from electronic medical records and de-identified prior to analysis to ensure patient confidentiality.

Patient selection

We screened all adult patients (age ⩾ 18 years) admitted to the ICU between January 1, 2020, and December 31, 2023, who received invasive mechanical ventilation for more than 48 hours. Patients were included if they met the following criteria: age ⩾ 18 years; invasive mechanical ventilation for ⩾ 48 hours; at least one respiratory pathogen detected from lower respiratory tract specimens (endotracheal aspirate or bronchoalveolar lavage fluid) during the ventilation period. Respiratory pathogen detection reflected microbiological identification and did not necessarily indicate clinical infection. Given the retrospective nature of the cohort, the distinction between airway colonization and true infection could not be fully ascertained and was therefore not used as an inclusion or exclusion criterion. Exclusion criteria were: active infection at extra-pulmonary sites at the time of respiratory sampling; incomplete clinical data (missing Murray score components or laboratory results); or do-not-resuscitate orders within 24 hours of ICU admission. A total of 274 patients meeting these criteria were enrolled consecutively and categorized based on hospital discharge status into survival (n = 166) and non-survival (n = 108) groups. The participant flow is shown in Figure 1.

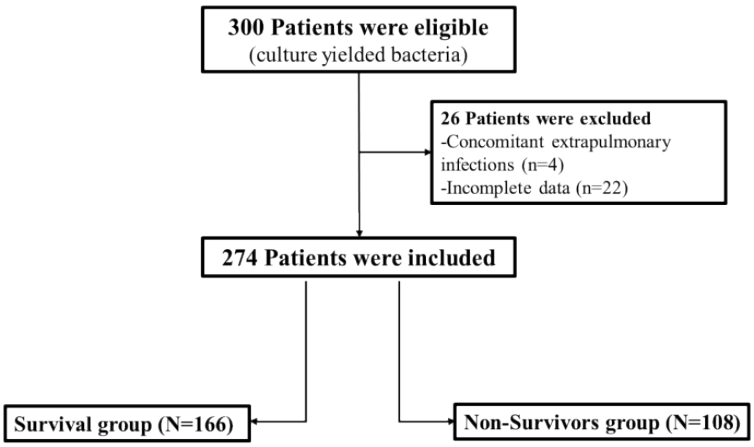


Figure 1. Flowchart of patient selection.

Data Collection

Demographic, clinical, and laboratory data were extracted from electronic medical records using standardized case report forms by trained research assistants. Collected data included:

Demographics: age, sex, body mass index (BMI); Severity scores: Acute Physiology and Chronic Health Evaluation II (APACHE II) score (assessed within 24 hours of ICU admission), Sequential Organ Failure Assessment (SOFA) score (on the first ICU day), and Murray Lung Injury Score (assessed 48 hours preceding pathogen identification). The Murray score was assessed 48 hours before the identification of pathogenic bacteria to ensure it reflected the severity of preceding lung injury antecedent to the development of ventilator-associated pneumonia (VAP), a prerequisite for valid mediation analysis; Laboratory indicators (within 24 hours of ICU admission): white blood cell count, lymphocyte count, serum lactate, aspartate aminotransferase (AST), alanine aminotransferase (ALT), and creatinine; Treatment information: continuous renal replacement therapy (CRRT) and extracorporeal membrane oxygenation (ECMO); Comorbidities: hypertension, coronary heart disease (CHD), chronic obstructive pulmonary disease (COPD), and immunosuppression (defined as active malignancy, long-term corticosteroid use equivalent to ⩾ 20 mg prednisone for ⩾ 14 days, immunosuppressive therapy, or solid organ transplantation); Microbiological data: pathogen species identified from lower respiratory tract specimens (endotracheal aspirate or bronchoalveolar lavage fluid). Only the first episode of a newly detected respiratory pathogen during the index mechanical ventilation period was included.

Murray Lung Injury Score Assessment

The Murray score was calculated based on four components: chest radiograph, PaO_2/FiO_2 ratio, PEEP, and respiratory system compliance. Each component was scored 0–4 and averaged to yield a final score ranging from 0 to 4, with higher scores indicating more severe lung injury. The score was assessed 48 hours preceding pathogen identification to ensure it reflected lung injury antecedent to VAP, which is essential for valid mediation analysis. Two independent investigators, blinded to outcomes, calculated the score. Inter-rater reliability was excellent (ICC = 0.94, 95% CI: 0.89–0.97).

Ventilator-Associated Pneumonia (VAP) Definition

VAP was defined using ATS/IDSA criteria: onset ⩾ 48 hours after intubation or within 48 hours post-extubation; new or progressive pulmonary infiltrates on chest imaging; at least two of the following (fever > 38.3 °C or hypothermia < 36.0 °C, leukocytosis > 12,000 cells/μL or leukopenia < 4,000 cells/μL, purulent secretions, worsening oxygenation with PaO_2/FiO_2 decrease ⩾ 25%); and microbiological confirmation (BAL ⩾ 10^4 CFU/mL or ETA ⩾ 10^5 CFU/mL). All VAP diagnoses were retrospectively reviewed by an independent adjudication committee blinded to Murray scores and outcomes.

Outcomes

The primary outcome was hospital mortality. Secondary outcomes included VAP occurrence, ICU length of stay, and duration of mechanical ventilation.

Statistical Analysis

Continuous variables are presented as medians (IQR) and categorical variables as frequencies (%). Group comparisons were performed using the Wilcoxon-Mann-Whitney test or chi-square/Fisher's exact test as appropriate. Univariate logistic regression was used to identify variables associated with mortality. Stepwise variable selection based on the Akaike Information Criterion (AIC) produced a parsimonious model. Multicollinearity was assessed using variance inflation factors (VIF < 5 considered acceptable). Mediation analysis used the product-of-coefficients approach on the log-odds scale to decompose total effects into direct and indirect effects of the Murray score on mortality via VAP. Mediation analysis was performed under the counterfactual framework, and indirect effects were estimated using nonparametric bootstrap resampling. Significance was assessed using bootstrap with 5,000 resamples and bias-corrected 95% confidence intervals. Predictive performance of the Murray score for mortality was evaluated using ROC curves and AUC with 95% CIs; the optimal cut-off was determined using the Youden index. Sensitivity analyses included: (1) excluding patients who died within 72 hours of ICU admission; (2) applying stricter VAP criteria (CPIS ⩾ 6); and (3) multiple imputation for missing data. All analyses were performed using R version 4.2.1 and GraphPad Prism 9.0. All tests were two-sided, and $P < 0.05$ was considered statistically significant.

Results

Population Characteristics

Baseline characteristics are summarized in Table 1. The two groups were comparable regarding sex, age, BMI, and comorbidities such as hypertension, coronary heart disease, and COPD ($P > 0.05$). However, non-survivors had significantly higher disease severity scores at admission, as indicated by higher APACHE II scores (24 [IQR: 18.62–29.38] vs. 22 [IQR: 17–27], $P < 0.05$) and worse pulmonary state indicated by higher Murray Scores (1.62 [IQR: 1.12–2.12] vs. 1.25 [IQR: 0.78–1.72], $P < 0.05$). Additionally, the prevalence of immunosuppression was greater in non-survivors (51.9% vs. 36.7%, $P < 0.05$). Regarding pathogen distribution, Klebsiella pneumoniae was more frequently isolated in the non-survivor group, whereas Pseudomonas aeruginosa was more common in survivors (Supplementary Table 1). Furthermore, A. baumannii was the most frequently isolated pathogen in both groups.

Table 1: Baseline characteristics of survivors and non-survivors.

Variable	Category	Survive	Non Survivors	*P-value*
Age, years		62(51.62-72.38)	66(58.38-73.62)	*0.132*
Sex, n (%)	Male	122 (73.5)	88 (81.5)	0.128
	Female	44 (26.5)	20 (18.5)	
BMI, kg/m2		22.82(20.09-25.55)	22.04(19.30-24.78)	*0.219*
APACHE II score		22(17-27)	24(18.62-29.38)	*0.002**
SOFA score		9(6.5-11.5)	10(8-12)	*0.148*
Hypertension, n (%)	**YES**	55 (33.1)	32 (29.6)	*0.543*
	NO	111 (66.9)	76 (70.4)	
Diabetes mellitus, n (%)	YES	28 (16.9)	20 (18.5)	*0.725*
	NO	138 (83.1)	88 (81.5)	
Coronary heart disease, n (%)	YES	26 (15.7)	15 (13.9)	*0.688*
	NO	140 (84.3)	93 (86.1)	
COPD, n (%)	YES	18 (10.8)	18 (16.7)	*0.166*
	NO	148 (89.2)	90 (83.3)	
Immunosuppression, n (%)	YES	61 (36.7)	56 (51.9)	*0.014**
	NO	105 (63.3)	52 (48.1)	
CRRT, n (%)	YES	38 (22.9)	49 (45.4)	*<0.001**

	NO	128 (77.1)	59 (54.6)	
ECMO, n (%)	YES	40 (24.1)	33 (30.6)	*0.238*
	NO	126 (75.9)	75 (69.4)	
Murray lung injury score		1.25(0.78-1.72)	1.62(1.12-2.12)	*<0.001**
PaO2/FiO2 ratio, n (%)	<300	86	72	*0.002**
	≥300	80	38	
		291(234-360.5)	250.5(177.5-337.8)	
Respiratory isolates	Acinetobacter baumannii	82 (49.3%)	54 (50%)	
	Klebsiella pneumoniae	18 (10.8%)	26(24.1%)	
	Pseudomonas aeruginosa	44 (26.5%)	19 (17.6%)	
	Staphylococcus aureus	7 (4.2%)	6 (5.6%)	
Lab Exam	White blood cell count, **10^9 /L**	10.14(6.53-13.75)	10.21(6.35-14.08)	*0.238*
	Lymphocyte count, 10^9 **/L**	0.7(0.35-1.05)	0.5(0.23-0.73)	*0.974*
	Lactate, **mmol/L**	1.6(1.18-2.02)	1.93(1.53-2.33)	*0.146*
	ALT, **U/L**	35.3(17.5-63)	30.1(15.1-50)	*0.586*
	AST, U/L		**38.7(28.18-73.15)**	
	Creatinine, μmol/L		**89.95(49.48-141.42)**	
VAP, n (%)	**YES**		**47 (28.3)**	
	NO		**119 (71.7)**	

Continuous variables are presented as median (interquartile range, IQR) and compared using the Mann–Whitney U test. Categorical variables are presented as n (%) and compared using the Chi-square test or Fisher' s exact test, as appropriate. *P < 0.05 was considered statistically significant.

Abbreviations: ALT, alanine aminotransferase; APACHE II, Acute Physiology and Chronic Health Evaluation II; AST, aspartate aminotransferase; BMI, body mass index; COPD, chronic obstructive pulmonary disease; CRRT, continuous renal replacement therapy; ECMO, extracorporeal membrane oxygenation; SOFA, Sequential Organ Failure Assessment; VAP, ventilator-associated pneumonia.

Risk factors for hospital mortality

Univariate logistic regression analysis identified several factors significantly associated with increased hospital mortality (Fig. 2). These included a higher APACHE II score (OR = 1.05, 95% CI: 1.02–1.09, P = 0.002), the presence of immunosuppression (OR = 1.85, 95% CI: 1.14–3.04, P = 0.014), the requirement for CRRT (OR = 2.80, 95% CI: 1.66–4.75, P < 0.001), and notably, a higher Murray Score (OR = 3.17, 95% CI: 2.11–4.90, P < 0.001). Additionally, VAP was associated with increased mortality risk (OR = 3.41, 95% CI: 2.06–5.71, P < 0.001). Variables such as age, sex, BMI, and comorbidities, including hypertension, coronary heart disease, COPD, and diabetes mellitus, did not show significant associations with mortality in the univariate analysis (all P > 0.05).

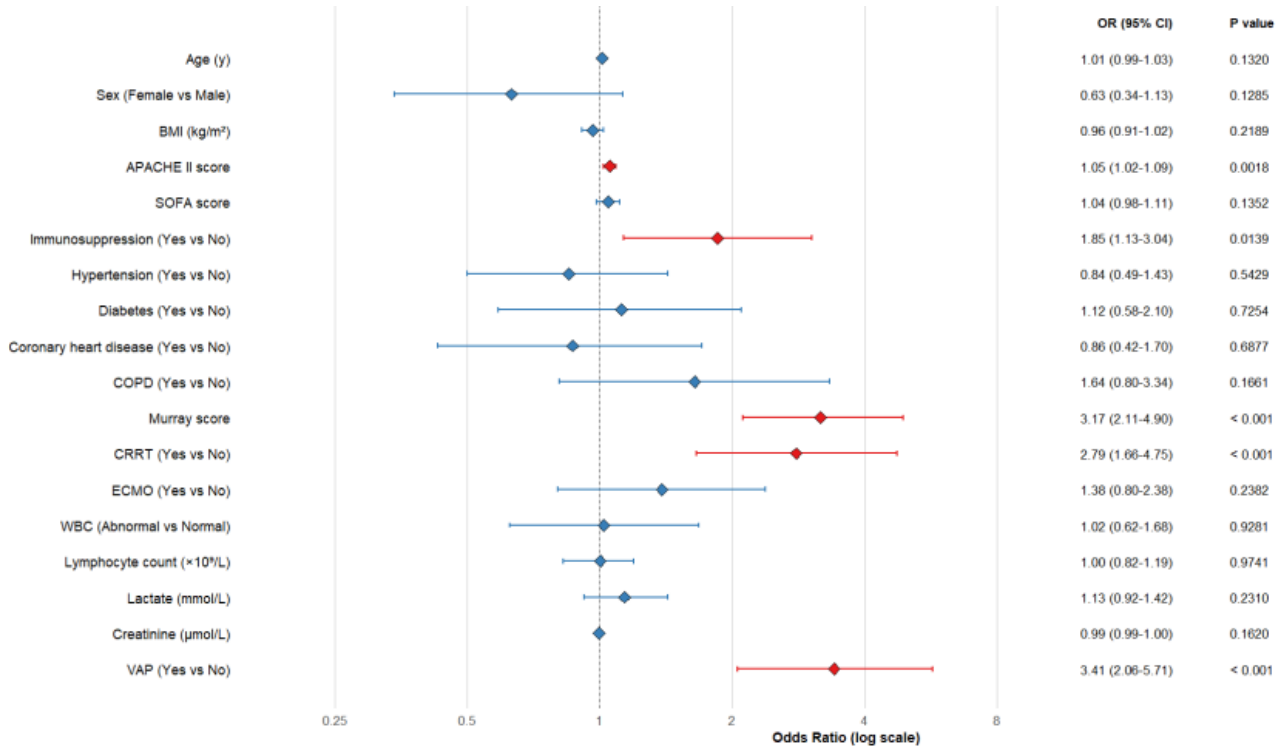


Figure 2. Univariable logistic regression analysis of factors associated with hospital mortality. Odds ratios (ORs) with 95% confidence intervals (CIs) are shown.

Association Between Murray Score and Mortality

Multicollinearity diagnostics (Table 2) revealed that all variance inflation factors (VIFs) were below 5, and tolerance values exceeded 0.2, indicating no substantial collinearity among the included variables.

Table 2: Multicollinearity diagnostics of covariates included in multivariable models

Variables	Collinearity Diagnostics	
	VIF	Tolerance
Age	1.14	0.88
Sex	1.17	0.86
BMI	1.13	0.88
APACHE II score	1.71	0.59
SOFA score	1.76	0.56
Murray lung injury score	1.08	0.92
Immunosuppression	1.12	0.89
CRRT	1.1	0.91
ECMO	1.08	0.92
VAP	1.15	0.87
White blood cell	1.13	0.88
Lactate	1.12	0.89

VIF < 5 was considered acceptable. Abbreviations: APACHE II, Acute Physiology and Chronic Health Evaluation II; BMI, body mass index; CRRT, continuous renal replacement therapy; ECMO, extracorporeal membrane oxygenation; SOFA, Sequential Organ Failure Assessment; VAP, ventilator-associated pneumonia.

To identify independent predictors of mortality while controlling for potential confounders, we constructed a series of multivariate logistic regression models (Table 3). In the unadjusted model (Model 1), the Murray score demonstrated a strong association with mortality (OR = 3.18, 95% CI: 2.12–4.90, P < 0.05). After sequentially adjusting for demographic factors (age, sex, BMI; Model 2: OR = 3.43, 95% CI: 2.26–5.39, P < 0.05), disease severity and immunosuppression (Model 3: OR = 3.16, 95% CI: 2.06–4.97, P < 0.05), and incorporating CRRT status (Model 4: OR = 3.2, 95% CI: 2.05–5.17, P < 0.05), the Murray score remained a robust and independent predictor of mortality (Model 5:OR = 2.68, 95% CI:1.70–4.37, P < 0.05). This persistence of significance across incrementally adjusted models underscores the substantial and independent contribution of preceding lung injury severity to mortality risk, beyond the effects of general illness severity, immune status, and critical organ support requirements.

Table 3: Multivariable logistic regression.

Model	**Murray Score**		
	OR	OR 95%CI	*P value*
Model 1	3.18	2.12-4.90	*<0.05*
Model 2	3.43	2.26-5.39	*<0.05*
Model 3	3.16	2.06-4.97	*<0.05*
Model 4	3.2	2.05-5.17	*<0.05*
Model 5	2.68	1.70-4.37	*<0.05*

Model 1: unadjusted. Model 2: adjusted for age, sex, and BMI. Model 3: additionally adjusted for APACHE II, SOFA, and immunosuppression. Model 4: additionally adjusted for CRRT. Model 5: fully adjusted, including all above, plus ECMO, White blood cell, and lactate.

VAP as a Mediator Between Lung Injury and Mortality

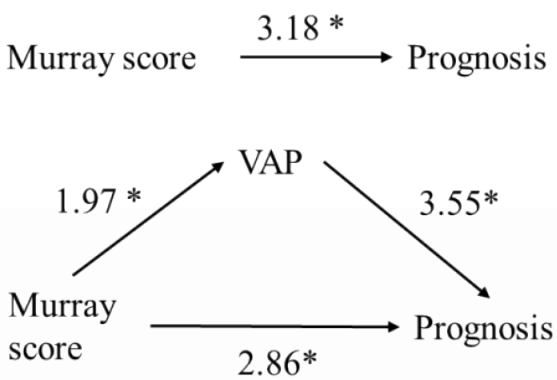
Given the established associations of the Murray score with both VAP and mortality, we employed mediation analysis to investigate whether VAP occurrence mediated the pathway from preceding lung injury to adverse outcomes (Table 4 and Fig. 3). The total effect of the Murray score on mortality was significant (OR = 3.18, 95% CI: 2.04–5.15, P < 0.001). This effect was decomposed into a direct effect (OR = 2.86, 95% CI: 1.79–4.73, P = 0.011) and an indirect effect mediated through VAP (OR = 1.11, 95% CI: 1.00–1.33, P = 0.006).

Table 4: Mediation analysis.

Variables	Prognosis _β	Prognosis__ OR (95CI%)	VAP_ β	VAP_OR (95CI %)	Prognosis _β	Prognosis__ OR (95CI%)
Murray lung injury score	1.158*	3.184 (2.035, 5.150)	0.680*	1.973 (1.323, 3.002)	1.050*	2.859 (1.791, 4.732)
Age	0.014	1.015 (0.993, 1.037)	0.005	1.005 (0.985, 1.025)	0.015	1.015 (0.992, 1.038)
Sex	-0.690.	0.501 (0.245, 0.993)	0.649*	1.913 (1.030, 3.585)	-0.978*	0.376 (0.175, 0.778)
BMI	-0.045	0.956 (0.895, 1.018)	0.008	1.008 (0.949, 1.070)	-0.053	0.948 (0.884, 1.014)
APACHE II score	0.033.	1.034 (0.996, 1.074)	0.006	1.006 (0.970, 1.043)	0.031	1.032 (0.992, 1.073)
Immunosuppression	0.677*	1.967 (1.106, 3.537)	-0.002	0.998 (0.578, 1.717)	0.720*	2.055 (1.134, 3.772)

CRRT	0.922*	2.515 (1.381, 4.636)	0.165	1.180 (0.665, 2.083)	0.926*	2.525 (1.355, 4.776)
ECMO	0.459	1.582 (0.845, 2.976)	0.291	1.338 (0.745, 2.395)	0.455	1.576 (0.822, 3.037)
VAP					1.267*	3.550 (1.940, 6.636)
White blood cell count	-0.078	0.925 (0.517, 1.651)	0.846*	2.331 (1.351, 4.086)	-0.344	0.709 (0.380, 1.309)
Lactate	0.148	1.159 (0.907, 1.541)	0.1	1.105 (0.879, 1.434)	0.13	1.139 (0.876, 1.510)

APACHE II, Acute Physiology and Chronic Health Evaluation II; BMI, body mass index; CRRT, continuous renal replacement therapy; ECMO, extracorporeal membrane oxygenation; VAP, ventilator-associated pneumonia. P < 0.05 was considered statistically



significan.

Figure 3: Mediation model examining the relationship between Murray score and hospital mortality mediated by VAP. Path coefficients are presented as odds ratios (ORs) with 95% confidence intervals. Indirect effects were estimated using bootstrap resampling (5,000 iterations). *P < 0.05 was considered statistically significant.

Bootstrap resampling (5000 iterations) confirmed the statistical robustness of both pathways. The proportion of the total effect mediated by VAP was calculated to be 9.3% (95% CI: 3.1%–18.5%). These findings indicated that while the Murray score exerted a substantial direct influence on mortality risk, a significant and measurable portion of its detrimental impact is attributable to an increased susceptibility to develop VAP (Table 5).

Table 5: Bootstrap estimation of direct, indirect, and total effects of Murray score on mortality.

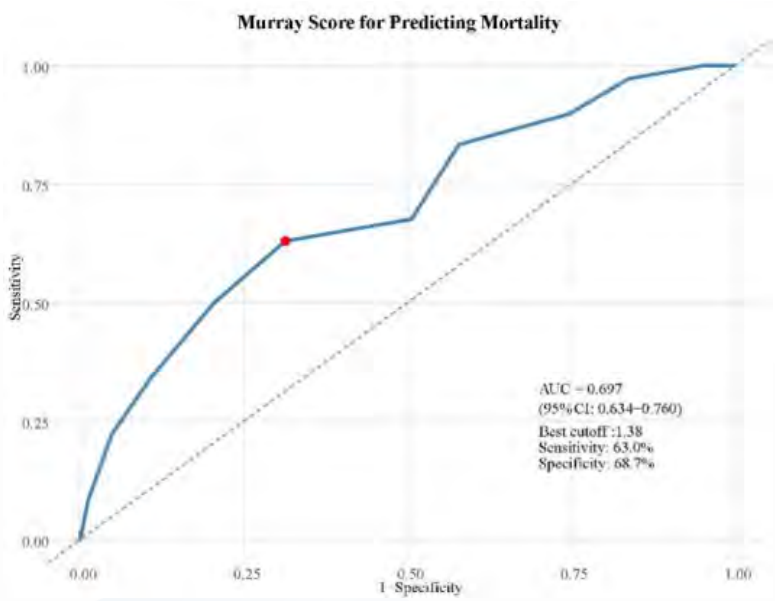
Paths	Observed Coefficient	Bootstrap test			
		Bootstrap Standard Error	*P*	LLCI	ULCI
Indirect effect	1.11	0.423	0.0004	1	1.33
Direct effect	2.86	0.286	0.00	1.79	4.73
Total effect	3.18	0.495	0.00	2.04	5.15

Bias-corrected bootstrap confidence intervals were calculated using 5,000 resamples.

Receiver Operating Characteristic (ROC) Analysis

To evaluate the discriminative ability of the Murray score, we performed ROC curve analysis (Fig. 4). For predicting hospital mortality, the AUC was 0.697 (95% CI: 0.634–0.760). The optimal cut-off value was >1.38, providing a sensitivity of 63.0% and a specificity of 68.7%. These results indicate a moderate but statistically significant predictive capacity of the Murray score for clinically relevant endpoints.

Notably, Spearman correlation analysis revealed no significant association between the Murray score and either ICU length of stay (β = 0.038, P = 0.912) or total duration of mechanical ventilation (β = 0.056, P = 0.365), suggesting its prognostic value is specific to mortality and infection risk rather than merely reflecting longer exposure time (Fig. S1 and S2).



Stratified Analysis by Murray Score

To investigate how this relationship varied across different levels of baseline lung injury severity, patients were divided into two groups: lower lung injury (Murray Score < 1.5, n=186) and higher lung injury (Murray Score ⩾ 1.5, n=88). As shown in Figure 5A, the incidence of VAP exhibited a disparity between groups: 34.4% in the lower injury group versus 51.1% in the higher injury group ($\chi^2 = 6.3$, $P < 0.05$). Mortality rates followed a similar pattern (Fig. 5B), with 29.0% and 61.4% in the lower and higher injury groups, respectively ($\chi^2 = 24.81$, $P < 0.05$). To further evaluate whether the association between VAP and mortality was modified by the severity of preceding lung injury, the interaction analysis was performed (Fig. 5C and D). When stratified by Murray score, VAP was associated with a relative risk (RR) for mortality of 2.38 (95 % CI: 1.53–3.71) in the lower injury group, whereas in the higher injury group, the RR was 1.39 (95 % CI: 0.98–1.97). However, the formal statistical test for the multiplicative interaction term between the Murray score group and VAP status was not statistically significant (interaction $P > 0.05$).

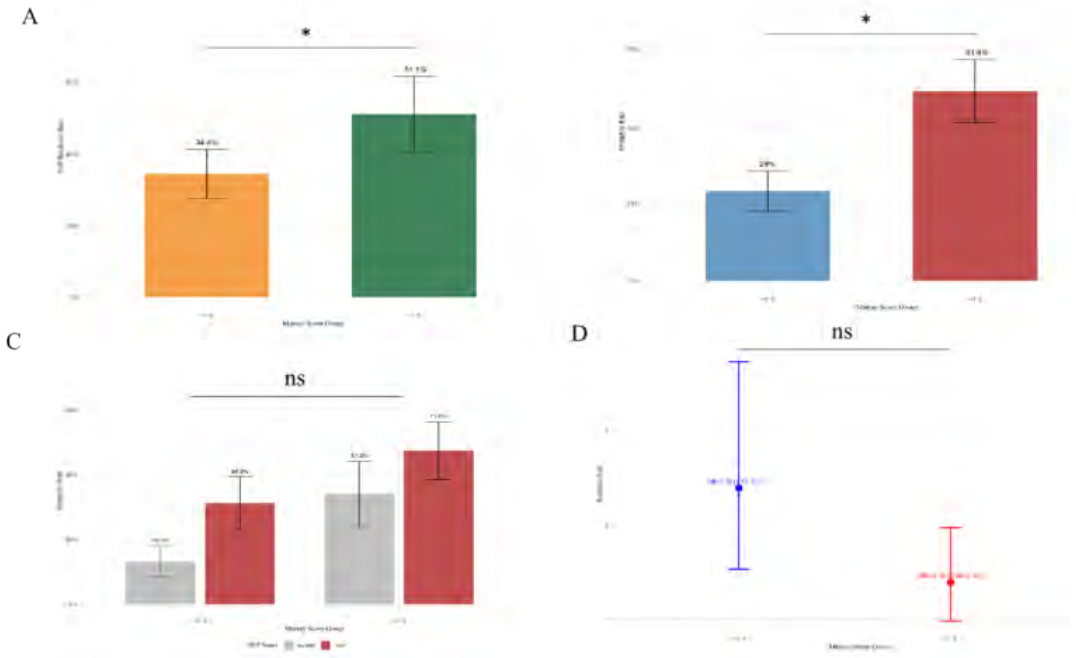


Figure 5: Stratified Analysis by Murray Score. (A) VAP Incidence between Murray score groups. (B) Mortality rate between Murray score groups. (C) Interaction between Murray score and VAP on mortality. (D) Relative risk of VAP between Murray score groups. *P < 0.05, ns means no significance.

Discussion

In this retrospective cohort study of mechanically ventilated ICU patients, we found that lung injury severity quantified by the Murray score was independently associated with increased hospital mortality. Importantly, VAP partially mediated this association, suggesting that lung injury predisposes patients to worse outcomes not only through direct physiological deterioration but also by increasing vulnerability to secondary nosocomial infection. To our knowledge, this is among the few studies to formally quantify the mediating role of VAP in the pathway from antecedent lung injury to mortality using bootstrap-validated mediation analysis.Our findings are consistent with existing evidence indicating that the severity of acute lung injury is a key determinant of both infection susceptibility and mortality in critically ill patients. The Murray score integrates oxygenation impairment, ventilatory support requirements, respiratory system compliance, and radiographic extent of lung involvement, thereby providing a lungspecific assessment of injury severity [16]. In a validation study of ARDS severity measures, the Murray Lung Injury Score demonstrated reasonable discrimination for pulmonaryspecific outcomes, although its performance for overall hospital mortality was more modest [17, 18]. In our cohort, patients with higher Murray scores (⩾ 1.5) exhibited significantly higher VAP incidence (51.1% vs. 34.4%) and markedly higher hospital mortality (61.4% vs. 29.0%), supporting the clinical relevance of this score for early risk stratification. The predictive value of the Murray score has also been evaluated in studies assessing 28-day mortality in ARDS patients, with oxygenation index (OI) and extravascular lung water index (EVLWI) showing stronger prognostic performance when measured serially over the first days after intubation [19]. Collectively, these observations reinforce the concept that progressive

lung injury establishes a vulnerable pulmonary state in which subsequent infectious complications may substantially worsen prognosis. Although the mediation proportion was modest (9.3%), this finding remains clinically meaningful. It indicates that a measurable fraction of mortality risk may be preventable through optimized VAP prevention strategies, while most mortality is likely attributable to the direct consequences of severe lung injury and multiorgan dysfunction.

The pathogenesis of VAP is multifactorial, involving impaired airway clearance, disruption of mucosal and epithelial barrier integrity, alterations in the pulmonary microenvironment, and dysregulated innate immune responses [20, 21]. Preclinical studies suggest that mechanical ventilation itself may enhance bacterialinduced lung injury. For example, Tsay et al. demonstrated that mechanical ventilation after Acinetobacter baumannii instillation increased neutrophil infiltration, interleukin6 expression, and impaired alveolar macrophage bactericidal activity through JNK signaling pathways [22]. Recent longitudinal cohort studies have shown that mechanical ventilation is associated with temporal changes in lung microbiome composition independent of VAP development, with VAP cases exhibiting higher TNF-α levels and metabolic profiles indicative of anaerobic adaptation [23]. These mechanistic findings align with our observation that greater lung injury severity (reflected by higher Murray scores) predisposes patients to VAP and worse outcomes. In this context, our mediation analysis provides quantitative evidence supporting the hypothesis that VAP represents an intermediate mechanism linking severe lung injury to mortality. Although the mediation proportion was modest, it was statistically robust and clinically meaningful, indicating that a measurable fraction of mortality risk may be attributable to infection occurring on the background of lung injury. These findings further imply that while the majority of mortality in severe lung injury may result from direct mechanisms such as refractory hypoxemia, ventilatorassociated lung injury, and multiorgan dysfunction, infectionrelated pathways contribute an additional and potentially modifiable component.

From a clinical perspective, the Murray score may serve as a simple bedside tool to identify patients at high risk of subsequent VAP and mortality, potentially supporting risk-stratified prevention bundle implementation. Patients with elevated scores may benefit from intensified monitoring and strict implementation of evidencebased VAP prevention measures, including headofbed elevation, structured oral hygiene protocols, subglottic secretion drainage when available, minimization of unnecessary sedation, and early spontaneous breathing trials to facilitate timely weaning [24, 25]. A systematic review of 38 studies demonstrated that multifaceted care bundles, particularly those combining headofbed elevation, oral hygiene, subglottic suctioning, and adequate endotracheal cuff pressure, can reduce VAP incidence by over 36%, with some studies reporting reductions exceeding 65% [26]. Similarly, in a tertiary care ICU setting, implementation of a comprehensive ventilator bundle was associated with a >70% reduction in VAP rates [27]. Meta-analyses have confirmed that care bundle implementation significantly reduces VAP incidence (RR = 0.52, 95% CI: 0.40-0.68) and mortality (RR = 0.53, 95% CI: 0.30-0.92) [28]. Current clinical practice guidelines recommend these preventive bundles for mechanically ventilated patients in general; however, they do not explicitly incorporate lung injury severity into stratified prevention algorithms. Our findings suggest that Murray scoreguided allocation of preventive resources may represent a more targeted approach, prioritizing higherintensity interventions for patients at greatest risk.

Clinical implications

The clinical implications of our findings are twofold. First, the Murray score may serve as a practical risk stratification tool that can be rapidly calculated using routinely available bedside parameters. In realworld ICU practice, such a tool may help clinicians identify a subgroup of patients in whom infection prevention efforts should be maximized early, before overt clinical deterioration occurs. Second, the observed mediation effect supports the hypothesis that a portion of mortality risk associated with severe lung injury may be indirectly driven by preventable infectious complications. Although causality cannot be established in a retrospective design, these results provide a rationale for future interventional studies testing whether intensified VAP prevention bundles or earlier diagnostic vigilance in high Murray score patients can reduce infection burden and improve survival.

Notably, the relative risk of mortality associated with VAP was numerically higher in patients with lower baseline lung injury severity than in those with more severe injury (RR = 2.38 vs. 1.39), although the interaction test was not statistically significant. This observation should be considered hypothesisgenerating. One plausible explanation is that in patients with profound lung injury, mortality may be primarily driven by refractory respiratory failure and systemic organ dysfunction, potentially diminishing the incremental contribution of VAP. In contrast, among patients with less severe baseline lung injury, VAP may represent a more distinct “second-hit” event capable of substantially altering the clinical trajectory. Larger prospective cohorts will be required to validate this pattern and clarify whether the mortality impact of VAP differs across lung injury severity strata.

This study has several strengths. First, we addressed an underexplored clinical question by applying formal mediation analysis to delineate the pathway from lung injury severity to mortality through VAP. Unlike conventional regression models that estimate adjusted associations, mediation analysis provides additional insight into indirect effects and potential mechanistic pathways [29]. Second, the Murray score provides a lungspecific evaluation of injury severity compared with global illness scores such as APACHE II and SOFA, which reflect systemic dysfunction but are less specific to pulmonary injury [17]. Third, rigorous multivariable adjustment for clinically relevant confounders and bootstrap validation enhanced the robustness of our findings. Finally, the predefined time window for Murray score assessment (48 hours preceding pathogen detection) strengthened the temporal plausibility of the mediation framework.

Several limitations should be acknowledged. The singlecenter retrospective design may limit external generalizability, and independent validation is warranted. Residual confounding cannot be fully excluded despite adjustment for major variables, including APACHE II score, immunosuppression, and CRRT. In addition, the Murray score was assessed at a single predefined time point and does not capture the dynamic evolution of lung injury over time, which may influence both VAP risk and mortality. Although microbiological confirmation was incorporated into the VAP definition, differentiating colonization from true infection remains challenging in retrospective studies and may introduce misclassification bias [30, 31]. Studies have shown that healthcare providers frequently order respiratory cultures based on non-specific clinical signs, and positive culture results can bias clinicians toward initiating unnecessary antibiotic therapy even in patients with low clinical probability of VAP [32]. Furthermore, key ICU factors such as prior antibiotic exposure, sedation strategy, ventilator settings, and adherence to prevention bundles could not be fully captured and may have influenced both VAP development and outcomes. Finally, we focused primarily on bacterial pathogens and did not evaluate viral or fungal pulmonary infections, which may have led to underestimation of the overall mediating contribution of nosocomial respiratory infections [33].

Future research should validate these findings in multicenter prospective cohorts and explore whether serial assessment of lung injury severity improves prediction accuracy. Integration of the Murray score with additional clinical markers, inflammatory biomarkers, or radiographic quantitative indices may further refine risk stratification. The lung microbiome and metabolomic profiles have emerged as promising areas for understanding VAP pathogenesis, with studies revealing shifts in the pentose phosphate and citric acid cycle pathways associated with anaerobic adaptation in VAP patients [23]. Importantly, randomized or pragmatic interventional studies are needed to determine whether Murray scoreguided implementation of intensified VAP prevention bundles can reduce infection burden and improve survival in highrisk mechanically ventilated patients.

Conclusion

In mechanically ventilated ICU patients, a higher Murray Lung Injury Score was independently associated with increased hospital mortality. Ventilator-associated pneumonia partially mediated this association, suggesting that secondary infection contributes to adverse outcomes in patients with pre-existing lung injury. These findings support the Murray score as a practical tool for early risk stratification and highlight the potential value of intensified VAP prevention strategies. Further multicenter prospective studies are needed to validate these results.

Abbreviations

ALI	Acute lung injury
ALT	Alanine aminotransferase
APACHE II	Acute Physiology and Chronic Health Evaluation II
ARDS	Acute respiratory distress syndrome
AST	Aspartate aminotransferase
AUC	Area under the curve
BAL	Bronchoalveolar lavage
BMI	Body mass index
CFU	Colony-forming units
CHD	Coronary heart disease
CI	Confidence interval
COPD	Chronic obstructive pulmonary disease
CPIS	Clinical Pulmonary Infection Score
CRRT	Continuous renal replacement therapy
ECMO	Extracorporeal membrane oxygenation
ETA	Endotracheal aspirate

ICU	Intensive care unit
IDSA	Infectious Diseases Society of America
IQR	Interquartile range
MV	Mechanical ventilation
OR	Odds ratio
PaO_2 /FiO_2	Ratio of arterial oxygen partial pressure to fractional inspired oxygen
PEEP	Positive end-expiratory pressure
ROC	Receiver operating characteristic
SOFA	Sequential Organ Failure Assessment
STROBE	Strengthening the Reporting of Observational Studies in Epidemiology
VAP	Ventilator-associated pneumonia
VIF	Variance inflation factor
WBC	White blood cell count

Declarations

Ethics approval and consent to participate

The study protocol was approved by the Ethics Committee of the First Affiliated Hospital of Guangzhou Medical University (Approval No.: ES-2025-K265-01). The requirement for informed consent was waived due to the retrospective nature of the study. All patient data were anonymized prior to analysis.

Consent for publication

Not applicable.

Data availability

The datasets used and/or analyzed during the current study are available from the corresponding author on reasonable request.

Competing interests

The authors declare no competing interests.

Funding

This work was funded with support from the Major Project of Guangzhou National Laboratory Grant (GZNL2023A01003), National Natural Science Foundation of China (82270085, 82570112), Science and Technology Program of Guangzhou (2023B01J1002), and Open Project of State Key Laboratory of Respiratory Disease (SKLRD-OP-202314).

Authors' contributions

Yimin Li and Yonghao Xu conceived and designed the study. Zhenting Liang and Ya Wang collected the data. Sifeng Fu performed the statistical analysis. Sifeng Fu drafted the manuscript. Yonghao Xu critically revised the manuscript for important intellectual content. All authors read and approved the final manuscript.

Acknowledgements

The authors would like to thank the medical staff of the intensive care unit at the First Affiliated Hospital of Guangzhou Medical University for their support in data acquisition.

References

[1] Mumtaz H, Saqib M, Khan W, et al. Ventilator associated pneumonia in intensive care unit patients: a systematic review. Ann Med Surg (Lond). 2023;85(6):2932-2939.

[2] Le Pape M, Besnard C, Acatrinei C, et al. Clinical impact of ventilator-associated pneumonia in patients with the acute respiratory distress syndrome: a retrospective cohort study. Ann Intensive Care. 2022;12(1):24.

[3] Wong IG, Paschini M, Stark J, et al. Airway injury induces alveolar epithelial responses mediated by macrophages. Cell Rep. 2026;45(2):116881.

[4] Tsay TB, Jiang YZ, Hsu CM, et al. Mechanical ventilation enhances Acinetobacter baumannii-induced lung injury through JNK pathways. Respir Res. 2021;22(1):159.

[5] Fan W, Gui B, Zhou X, Li L, et al. A narrative review on lung injury: mechanisms, biomarkers, and monitoring. Crit Care. 2024;28(1):352.

[6] Sedhai YR, Yuan M, Ketcham SW, et al. Validating Measures of Disease Severity in Acute Respiratory Distress Syndrome. Ann Am Thorac Soc. 2021;18(7):1211-1218.

[7] Shah CV, Lanken PN, Localio AR, et al. Development and validation of severe hypoxemia associated risk prediction model in 1,000 mechanically ventilated patients. Crit Care Med. 2014;42(1):45-54. PMID: 25318386

[8] Frenzel J, Paßvogel L, Schmitz J, et al. Outcome prediction in pneumonia induced ALI/ARDS by clinical features and peptide patterns of BALF. PLoS One. 2011;6(10):e25544.

[9] Klompas M, Speck K, Howell MD, et al. Reappraisal of routine oral care with chlorhexidine gluconate for patients receiving mechanical ventilation: systematic review and meta-analysis. JAMA Intern Med. 2014;174(5):751-761.

[10] Garnier M, Constantin JM, Heming N, et al. Epidemiology, risk factors and prognosis of ventilator-associated pneumonia during severe COVID-19: Multicenter observational study across 149 European Intensive Care Units. Anaesth Crit Care Pain Med. 2023;42(1):101184.

[11] Hu GN, Liu WL, Chang CH, et al. Microbial dynamics, risk factors and outcomes of secondary pneumonia in critically ill patients with COVID-19: A multicenter retrospective cohort study. J Formos Med Assoc. 2024;123(11):1186-1193.

[12] Gosens R, Hiemstra PS, Adcock IM, et al. Host-microbe cross-talk in the lung microenvironment: implications for understanding and treating chronic lung disease. Eur Respir J. 2020;56(2):1902320.

[13] Wu D, Wu C, Zhang S, et al. Risk Factors of Ventilator-Associated Pneumonia in Critically Ill Patients. Front Pharmacol.

2019;10:482.

[14] Rosenthal VD, Maki DG, Salomao R, et al. International Nosocomial Infection Control Consortium. Device-associated nosocomial infections in 55 intensive care units of 8 developing countries. Ann Intern Med. 2006;145(8):582-591.

[15] Huang B, Sivaganesan S, Succop P, et al. Statistical assessment of mediational effects for logistic mediational models. Stat Med. 2004;23(17):2713-2728.

[16] Murray JF, Matthay MA, Luce JM, et al. An expanded definition of the adult respiratory distress syndrome. Am Rev Respir Dis. 1988;138(3):720-723.

[17] Melsen WG, Rovers MM, Groenwold RH, et al. Attributable mortality of ventilator-associated pneumonia: a meta-analysis of individual patient data from randomised prevention studies. Lancet Infect Dis. 2013;13(8):665-671.

[18] Villar J, Blanco J, del Campo R, et al. Assessment of the lung injury score in the clinical evaluation of ARDS patients. Intensive Care Med. 2011;37(5):782-788.

[19] Huber W, Findeisen M, Lahmer T, et al. Prediction of outcome in patients with ARDS: A prospective cohort study comparing ARDS-definitions and other ARDS-associated parameters, ratios and scores at intubation and over time. PLoS One. 2020;15(5):e0232720.

[20] Dickson RP, Erb-Downward JR, Huffnagle GB. The role of the bacterial microbiome in lung disease. Expert Rev Respir Med. 2013;7(3):245-257.

[21] Papazian L, Klompas M, Luyt CE. Ventilator-associated pneumonia in adults: a narrative review. Intensive Care Med. 2020;46(5):888-906.

[22] Chastre J, Fagon JY. Ventilator-associated pneumonia. Am J Respir Crit Care Med. 2002;165(7):867-903.

[23] Kalil AC, Metersky ML, Klompas M, et al. Management of Adults With Hospital-acquired and Ventilator-associated Pneumonia: 2016 Clinical Practice Guidelines by the Infectious Diseases Society of America and the American Thoracic Society. Clin Infect Dis. 2016;63(5):e61-e111.

[24] Klompas M, Branson R, Cawcutt K, et al. Strategies to prevent ventilator-associated pneumonia in acute care hospitals: 2022 Update. Infect Control Hosp Epidemiol. 2022;43(6):687-713.

[25] La Combe B, Mahérault AC, Messika J, et al. Oropharyngeal Bacterial Colonization after Chlorhexidine Mouthwash in Mechanically Ventilated Critically Ill Patients. Anesthesiology. 2018;129(6):1140-1148.

[26] Mastrogianni M, Katsoulas T, Galanis P, et al. The Impact of Care Bundles on Ventilator-Associated Pneumonia (VAP) Prevention in Adult ICUs: A Systematic Review. Antibiotics (Basel). 2023;12(2):227.

[27] Singh C, Abdullah R. Impact of Ventilator-Associated Pneumonia Preventative Measures and Ventilator Bundle Care in a Tertiary Care Hospital's Adult Intensive Care Unit. Cureus. 2024;16(5):e59877.

[28] Lim S, Chae SM, Woo M, et al. Prevention effects of care bundles on the incidence of ventilator-associated pneumonia in neonatal intensive care units: A systematic review and meta-analysis. Intensive Crit Care Nurs. 2026;92:103976.

[29] VanderWeele TJ. Mediation analysis: a practitioner's guide. Annu Rev Public Health. 2016;37:17-32.

[30] Nussenblatt V, Avdic E, Beri A, et al. Potential role of report nudging on diagnosis and treatment of ventilator-associated pneumonia: a quantitative survey. Antimicrob Steward Healthc Epidemiol. 2025;5(1):e55.

[31] Torres A, Niederman MS, Chastre J, et al. International ERS/ESICM/ESCMID/ALAT guidelines for the management of hospital-acquired pneumonia and ventilator-associated pneumonia. Eur Respir J. 2017;50(3):1700582.

[32] Klein Klouwenberg PM, Ong DS, Bos LD, et al. Interobserver agreement of Centers for Disease Control and Prevention criteria

for classifying ventilator-associated pneumonia. Crit Care Med. 2016;44(1):112-119.

[33] Zhou F, Liu YM, Xie J, et al. Ventilator-associated pneumonia in critically ill patients with COVID-19: A multicenter cohort study. Crit Care. 2021;25(1):300.

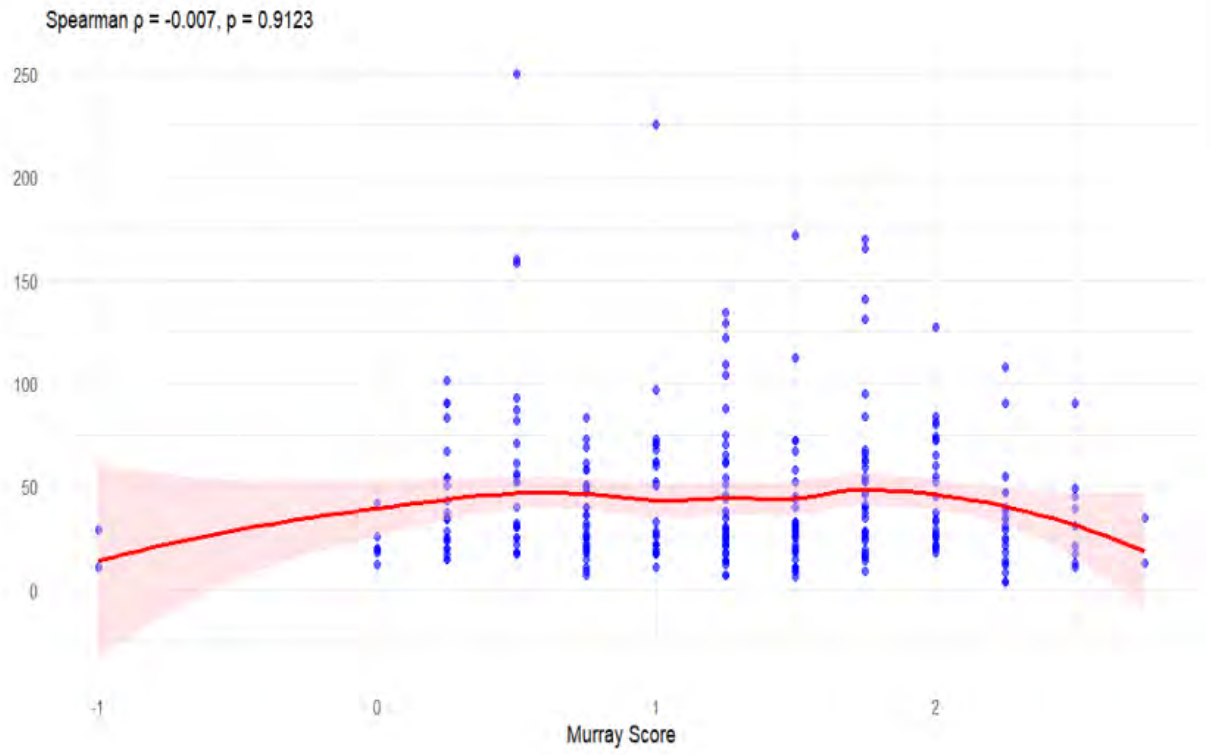


Figure S1. Correlation between Murray score and ICU length of stay.

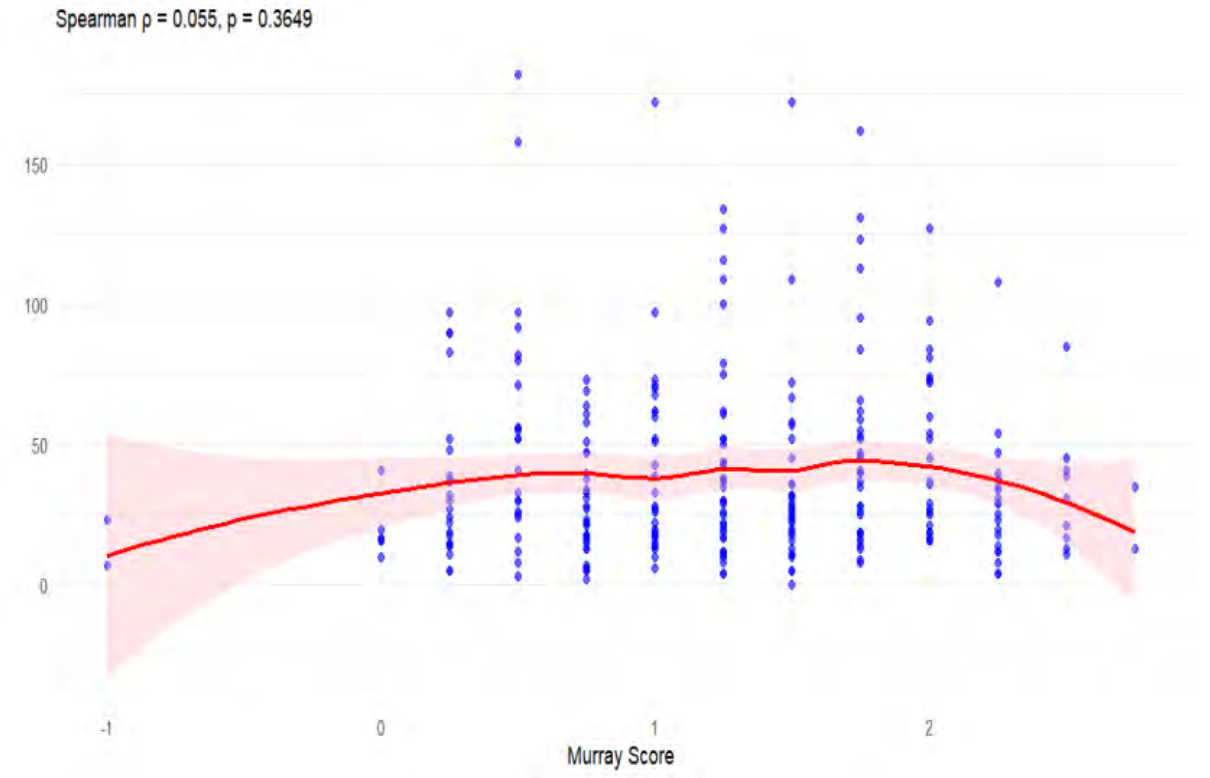


Figure S2. Correlation between Murray score and duration of mechanical ventilation.

Urinary [TIMP-2]×[IGFBP7] for biomarker-enhanced AKI staging and short-term prognosis in ICU patients

姓名：许萌，马文良，贾会苗，钱本淑，程丽，王静怡，李鑫成，郭方兴，田鹏超，黄立峰，郑悦，崔娜，李文雄
单位：首都医科大学附属北京朝阳医院，首都医科大学附属北京潞河医院

Abstract

Background: The 23rd Acute Disease Quality Initiative (ADQI-23) consensus recommends integrating biomarkers into acute kidney injury (AKI) classification, but optimal biomarkers and cutoffs remain undefined. We tested whether serum NGAL, urinary [TIMP-2]×[IGFBP7], DKK3, and CCL14 can predict 7-day renal non-recovery and differentiate 30-day survival.

Methods: This prospective study enrolled 300 AKI patients (derivation cohort, October 2020–October 2022) and 100 patients (validation cohort, January–June 2023) across two ICUs. Biomarkers were measured at AKI diagnosis; optimal cutoffs were determined by the Youden index. KDIGO stages 1–3 were subdivided into six categories (1A–3B) per the ADQI-23 framework for 30-day survival comparison.

Results: Urinary [TIMP-2]×[IGFBP7] showed the highest accuracy for predicting 7-day renal non-recovery (cutoff: 1.08 [ng/mL]^2/1000). Stages 1B and 2B had significantly lower 30-day survival than 1A and 2A, whereas stages 3A and 3B did not differ. In validation, survival discrimination was confirmed only in stage 2.

Conclusion: Urinary [TIMP-2]×[IGFBP7] outperformed NGAL, DKK3, and CCL14 in predicting 7-day renal non-recovery and improved 30-day risk stratification in KDIGO stage 2, supporting its potential for refining AKI classification. Generalizability to patients with CKD, ESKD, or kidney transplantation requires further study.

Keywords: Acute kidney injury, Biomarkers, [TIMP-2] × [IGFBP7], Survival

Introduction

Acute kidney injury (AKI) affects 10% - 15% of hospitalized patients and over 50% of intensive care unit (ICU) patients [1]. Its global mortality burden far exceeds that of breast cancer, heart failure, or diabetes, with reported 10 million AKI deaths [1]. Therefore, predicting patient outcomes and implementing early interventions are crucial strategies for improving prognosis. Previously, the Kidney Disease: Improving Global Outcomes (KDIGO) [2] criteria were employed to diagnose and stage AKI, which relies on urine output and serum creatinine (SCr) levels, that reflect only renal function and exhibits low sensitivity [3]. Notably, AKI biomarkers have enhanced our understanding of AKI pathophysiology [4]. The product of urinary tissue inhibitor of metalloproteinase-2 (TIMP-2) and insulin-like growth factor binding protein 7 (IGFBP7) ([TIMP-2] × [IGFBP7]) and urinary Dickkopf-3 (DKK3) reflects tubular stress, while neutrophil gelatinase-associated lipocalin (NGAL) and urinary C-C motif chemokine ligand 14 (CCL14) indicates tubular injury [5].

In 2020, the ADQI-23 working group proposed an updated AKI staging framework [6], in which KDIGO stages 1-3 were subdivided into six categories: 1A, 1B, 2A, 2B, 3A, and 3B. Here, "A" denotes a negative biomarker status and "B" indicates a positive status. Furthermore, ADQI-23 also proposed a special category-1S, which stands for “subclinical” AKI.

Previous studies have confirmed that certain biomarkers such as urinary [TIMP-2]×[IGFBP7] and CCL14 can effectively predict the lack of renal function recovery within seven days [7, 8]. And another retrospective study [9] reported that a positive urinary [TIMP-2] × [IGFBP7] correlated with a higher mortality and lower 30-day survival based on the ADQI-23 staging framework. However, whether these biomarkers can simultaneously predict both short-term renal prognosis and 30-day mortality within a unified staging framework remains insufficiently validated. So this prospective study had two objectives: (1) to compare the performance of four biomarkers in predicting non-recovery of renal function within seven days; and (2) to evaluate the ability of these biomarkers to discriminate 30-day survival within the updated ADQI-23 staging framework.

Methods

This cohort study was approved by the Human Ethics Committee of Beijing Chaoyang Hospital, Capital Medical University (Beijing,

China) (ethics number 2017-Ke-234), Beijing Luhe Hospital, Capital Medical University (Beijing, China) (ethics number 2019-KY-024). The registration number was ChiCTR1800015500. Written informed consent was obtained from patients or their immediate family members. The study adhered to the STROBE guidelines, STARD guidelines and Declaration of Helsinki declarations.

Study Setting and Population

This study was a prospective multicenter cohort study. The present study comprised two cohorts, stratified by time of enrollment. The derivation cohort was 300 patients consecutively enrolled from Beijing Chaoyang Hospital and Beijing Luhe Hospital between October 1, 2020, to October 31, 2022. The validation cohort was 100 patients from the same hospitals between January 1, 2023, to June 30, 2023. During phase 1, 2166 critically ill patients were screened; 385 (17.8%) developed AKI, and a total of 300 Asian patients with new-onset AKI were finally enrolled after excluding 85 patients. During phase 2, 550 patients were screened, 120 (21.8%) developed AKI, and finally 100 Asian patients with new-onset AKI were enrolled (Figure S1 in Supplement).

Patients who developed AKI following ICU admission were prospectively and consecutively enrolled. Patients were excluded, if they were: (1) age < 18 years, (2) expected ICU stay ⩽ 48 hours, (3) pre-existing AKI prior to ICU admission, (4) pre-existing kidney replacement therapy (KRT) prior to ICU admission, (5) pregnancy, (6) pre-existing chronic kidney disease (CKD), end-stage kidney disease (ESKD) or prior kidney transplantation, (7) recent immunosuppressive therapy, (8) human immunodeficiency virus infection, (9) anuric patients, (10) incomplete urine or blood sample collection. The management of all enrolled patients followed the Kidney Disease: Improving Global Outcomes (KDIGO) guideline [10].

Biomarker measurements

Following the diagnosis of AKI, blood and urine samples were promptly collected, with urine specimens obtained directly from the catheter bag. After standing for 30 min at room temperature, the samples were centrifuged at 4 °C and 3,000 rpm for 10 min, and the supernatant was stored at -80 °C until analysis. The biomarkers TIMP-2 and IGFBP7 were quantified using the NephroCheck ™ Test on the VITROS 5600 Integrated System (Astute Medical, San Diego, CA, USA). The system reports the product of the two urinary protein concentrations ([TIMP-2] × [IGFBP7]) in units of (ng/mL)2/1,000. Urinary DKK3, urinary CCL14, and serum NGAL concentrations were measured using enzyme-linked immunosorbent assay (ELISA) kits (Abcam, UK). All procedures were performed by laboratory technicians who were blinded to the patients' clinical data.

Clinical Endpoints and definitions

The primary endpoint was 30-day survival after enrollment. Secondary endpoints were: (1) 30-day mortality; (2) persistent AKI; (3) length of stay (LOS) in hospital; (4) LOS in ICU.

Previous literature has reported that urine output has a lower sensitivity for diagnosing AKI compared to serum creatinine, and that the use of diuretics reduces its diagnostic accuracy [11]. Additionally, some patients had their urinary catheters removed after being transferred out of the ICU, we were unable to obtain the hourly urine output of these patients. Therefore, AKI was diagnosed based on 2012 KDIGO criteria using SCr in this study [12]. Baseline SCr was based on applied hierarchically: (1) If available, the mean SCr value measured between one year and seven days before hospital admission [13]; (2) The lowest SCr value recorded within seven days before admission; (3) For patients admitted via the emergency department with abnormal creatinine levels (and no history of CKD), or when baseline values were unavailable, baseline SCr was determined with the Modification of Diet in Renal Disease (MDRD) equation by setting estimated glomerular filtration rate (eGFR) to 75 mL/min/1.73 m^2 [14].

The AKI patients with non-recovery of renal function was defined as SCr ⩾ 1.5 times higher than baseline within seven days [15]. Patients who underwent KRT up to the 7th day post-AKI onset were considered as non-recovered cases. Persistent kidney injury was defined as AKI exceeding 72 hours [16].

Data collection

Clinical and demographic data were prospectively collected using standardized case report forms. Comorbidities such as hypertension, diabetes, chronic obstructive pulmonary disease, coronary heart disease, cerebral vascular disease, chronic liver disease, and malnutrition, as well as interventions including KRT and mechanical ventilation, were recorded. The collected data included the Acute Physiology and Chronic Health Evaluation II (APACHE II) and Sequential Organ Failure

Assessment (SOFA) scores, which were assessed on the day of AKI diagnosis. The SCr levels were measured and recorded at ICU admission and every 12 hours thereafter until the seventh day post-AKI onset. Additionally, ICU duration and hospital stays, and persistent AKI as well as mortality within 30 days after AKI onset were recorded.

The updated staging system of AKI

Urinary levels of [TIMP-2] × [IGFBP7], DKK3, CCL14 and serum NGAL measured at the time of AKI diagnosis were employed to predict non-recovery of renal function within seven days. Receiver operating characteristic (ROC) curves were generated to identify the optimal biomarker and we employed to test the Youden index and determine the optimal cutoff for each biomarker.

Results at or above the predefined cutoff were classified as biomarker-positive, and those below as biomarker-negative. AKI was then reclassified using the ADQI-23 staging system, which subdivides KDIGO stages 1–3 into six categories (1A–3B), where "A" indicates biomarker-negative status and "B" indicates biomarker-positive status. Since all the patients included in the study met the KDIGO diagnostic criteria for AKI, the subjects of this study did not include patients with the 1s stage patients.

Sample size calculation

The minimum sample size required for developing the prediction model was calculated by the pmsampsize package (version 1.1.3) in R. The pmsampsize package was based on the method proposed by Riley et al [17]. The statistical assumptions used for the calculation are based on the expected 30-day population mortality rate, literature indicates an incidence of 10.5% [18], with a total of 2 candidate predictor parameters (each biomarker and APACHE II) and an expected C-statistic (AUC) of 0.8. A shrinkage factor of 0.9 was also specified so as to avoid overfitting. A total of 90 patients were finally determined as the minimum sample size for eac h of the derivation and validation cohorts.

Statistical Analysis

Continuous variables were expressed as a mean ± standard deviation (SD) or a median (interquartile range) as appropriate. Categorical variables are presented as frequencies with percentages. The Student's t-test, Mann-Whitney U test, or the $\chi 2$ test are used for baseline comparisons, as appropriate. Receiver operating characteristic (ROC) curve analysis was performed to evaluate the discriminative ability of [TIMP-2] × [IGFBP7], NGAL, DKK3 and CCL14 in predicting non-recovery of renal function within seven days. The optimal cut-off value was determined by calculating the maximum Youden index. The incremental predictive value of the selected biomarker was assessed using discrimination, calibration, reclassification, and clinical usefulness. Specifically, multiple Cox regressions were performed, and the △ c-index was calculated to assess discrimination. We assessed the proportional hazards assumption for all Cox regressions using Schoenfeld residuals, when the assumption was violated, we employed restricted mean survival time (RMST) analysis. Brier scores, Akaike information criterion (AIC), Bayesian information criterion (BIC), and the calibration plot were applied for calibration evaluation. Reclassification was assessed via integrated discrimination improvement (IDI) and net reclassification improvement (NRI). Its clinical usefulness was assessed by the net benefit derived from the decision curve analysis (DCA). Kaplan–Meier curves and log-rank tests were used to compare biomarker-negative and biomarker-positive groups within the same KDIGO stage. Secondary outcomes were reported as relative risks (RRs) with 95% confidence intervals (CIs) for categorical variables and Hodges–Lehmann median differences with 95% CIs for continuous variables. Sensitivity analyses were performed according to age (⩾ 65 vs. < 65 years), hypertension, coronary heart disease, sepsis, research center, and method for determining baseline creatinine, as well as in the population after inverse probability of treatment weighting (IPTW). All statistical analyses were conducted by SPSS Statistics version 27.0 (IBM Corp, Armonk, NY, USA) and R version 4.5.1. A two-sided $p < 0.05$ was considered statistically significant.

Results

Baseline characteristics of the enrolled patients

Baseline characteristics in two cohorts are shown in Table S1. In derivation cohort including 300 AKI patients, the median age was 62 (49–75) years, and 63.7% were male. Patients with KDIGO stages 1, 2, and 3 were 44.0%, 36.7%, and 19.3%, respectively. Renal recovery within 7 days occurred in 59.0% of patients, the remaining 41.0% had non-recovery, and 22.3% died within 30 days. There were statistically significant differences in the levels of urinary [TIMP-2] × [IGFBP7], DKK3, CCL14, and serum NGAL between patients with and without renal recovery within 7 days ($p < 0.001$) (Table 1).

The validation cohort included 100 patients, the median age was 69 (55-76) years, and 58% were male, with a 30-day mortality rate of 17%. The baseline characteristics of the two cohort are roughly balanced (Table S1 in Supplement).

Comparison of four biomarkers for predicting non-recovery of renal function within seven days in AKI patients in the derivation cohort

The area under the ROC curve (AUC) for predicting non-recovery of renal function within seven days was of urinary [TIMP-2] × [IGFBP7], serum NGAL, urinary DKK3 and urinary CCL14 were 0.860 (95% CI: 0.818–0.901, p < 0.001), 0.805 (95% CI: 0.756–0.855, p < 0.001), 0.785 (95% CI: 0.732–0.838, p < 0.001) and 0.771 (95% CI: 0.711–0.830, p < 0.001), respectively. Their optimal cutoff values were 1.08 $(ng/mL)^2/1000$, 66.18 ng/mL, 1989.58 ng/mL, and 594.39 pg/mL (Fig. 1).

Among these biomarkers, [TIMP-2]×[IGFBP7] showed the optimal performance for predicting non-recovery of renal function, with the highest AUC and lowest Brier score (Table 2). And DeLong test showed significant differences between [TIMP-2]×[IGFBP7] and all other biomarkers (all P < 0.05; Table S2 in Supplement). In addition, we also plotted calibration curves and DCA curves (Figure S2 and S3 in Supplement), which indicate [TIMP-2]×[IGFBP7] is well calibrated and shows a positive net benefit.

To evaluate the impact of death on the prediction of non-recovery of renal function, we further employed a competing hazard model, using failure to recover renal function within 7 days as the target event and death as a competing hazard event. The results were consistent with the main analysis, the sub-distribution hazard ratio (sHR) was highest in the [TIMP-2]×[IGFBP7] positive group (sHR = 3.47, 95% CI: 2.61–4.62, P < 0.001) (Table S3 in Supplement).

The association between updated acute kidney injury staging and 30-day survival rate in the derivation cohort

A cutoff of 1.08 $(ng/mL)^2/1000$ for urinary [TIMP-2]×[IGFBP7] was applied to refine KDIGO staging. Among patients with AKI stages 1, 2, and 3, 37.7% (39/132), 32.7% (36/110), and 37.9% (22/58) were classified as stages 1B, 2B, and 3B, respectively. All biomarkers satisfy the proportional hazards assumption (global P > 0.05) (Table S9 in Supplement).

[TIMP-2]×[IGFBP7] could further discriminate 30-day survival across different groups (P < 0.001; Fig. 2A). Mortality increased progressively from stage 1A to 3B, with each stage increment associated with a 36% higher risk of death (HR = 1.36; 95% CI, 1.17–1.57; P for trend < 0.001; Table 3). After adjustment, survival was significantly lower in stage 1B than 1A (HR = 2.88; 95% CI, 1.17–7.13; P = 0.022; Fig. 2B) and in stage 2B than 2A (HR = 3.29; 95% CI, 1.44–7.49; P = 0.005; Fig. 2C). However, no difference was observed between stages 3A and 3B (Fig. 2D).

Similar associations were observed between the updated AKI staging system and 30-day mortality for serum NGAL, urinary DKK3, and urinary CCL14 (Table 3). In comparison within the same KDIGO stages, NGAL-based staging showed no survival differences within the same KDIGO stage. DKK3- and CCL14-based staging demonstrated significantly lower survival in stage 2B versus 2A after adjustment (DKK3: HR = 2.47, P = 0.036; CCL14: HR = 3.10, P = 0.011) (Figure S4-S9 in Supplement). Univariate Cox regression of four biomarkers is presented in Table S4-S7.

Besides, the [TIMP-2]×[IGFBP7]-based model outperformed the other three biomarkers across some performance metrics, including C-index, AIC, BIC, IDI, NRI (Table S8 in Supplement). Calibration (Figure S10 in Supplement) and decision-curve analysis (DCA) (Figure S11 in Supplement) are generally satisfactory.

The bootstrap validation showed that the average optimism of the primary model (APACHE II + [TIMP-2]×[IGFBP7]) was 0.001, indicating extremely low overfitting. Results for the other three biomarker models are summarized in Table S10.

The associations between updated acute kidney injury staging and secondary outcomes in the derivation cohort

Table S11 compares the associations between the [TIMP2] × [IGFBP7]-based KDIGO staging and secondary outcomes. Compared to stage 1A, stage 1B patients had a higher rate of persistent AKI (79.5% (95% CI: 66.2%-92.7%) vs. 29.0% (95% CI: 19.6%-38.4%); P <0.001), with an RR of 2.74 (95% CI: 1.92-3.91). And stage 2B had a higher rate of persistent AKI compared to stage 2A (97.2% (95% CI: 91.6%-100.0%) vs.52.7% (95% CI: 41.1%-64.3%); P <0.001), with an RR of 1.85 (95% CI: 1.48-2.31). The associations between updated acute kidney injury staging based on the other three biomarkers and secondary outcomes were shown in Table S12-S14.

Predictive accuracy of urinary [TIMP-2]×[IGFBP7] for predicting 30-day survival in validation cohort

In the validation cohort, urinary [TIMP-2] × [IGFBP7], demonstrated predictive value for 30-day mortality, with a C-index of 0.723, AIC of 146.59, BIC of 148.26, IDI of 0.121 (95% CI: 0.017-0.326, P<0.001) and NRI of 0.394 (95% CI: 0.031-0.646, P<0.02) (Table S15 in supplement). A significant difference in 30-day mortality was observed across the six AKI stages (1A, 1B, 2A, 2B, 3A, 3B) (Figure S12A in Supplement). While no significant difference in 30-day mortality was found between stages 1A and 1B or 3A and 3B (Figure S12B and 12D in Supplement), stage 2B patients had a significantly higher mortality than stage 2A patients (HR = 10.79, 95% CI: 1.13-103.09; P = 0.038 (Figure S12C in Supplement). The calibration curve and DCA curve are also generally satisfactory (Figure S13 and S14 in Supplement).

We compared the baseline characteristics of patients with the same KDIGO stage between the two cohorts and found that, among stage 1 patients, all baseline characteristics were balanced except for persistent AKI (Table S16-S18 in Supplement).

Conclusions

In the derivation cohort, urinary [TIMP-2]×[IGFBP7] demonstrated excellent predictive performance for the failure of renal function to recover within 7 days. However, this superiority was not validated in an external cohort, and staging refined by this biomarker did not improve risk stratification for patients with KDIGO stage 3 acute kidney injury (AKI). These results suggest a potential role for [TIMP-2]×[IGFBP7] in the risk stratification of creatinine-defined mild-to-moderate AKI, warranting further multicenter validation studies; however, its clinical implementation, management implications, cost-effectiveness, and applicability to populations with CKD, anuria, or transplants remain unproven.

Figure Legends

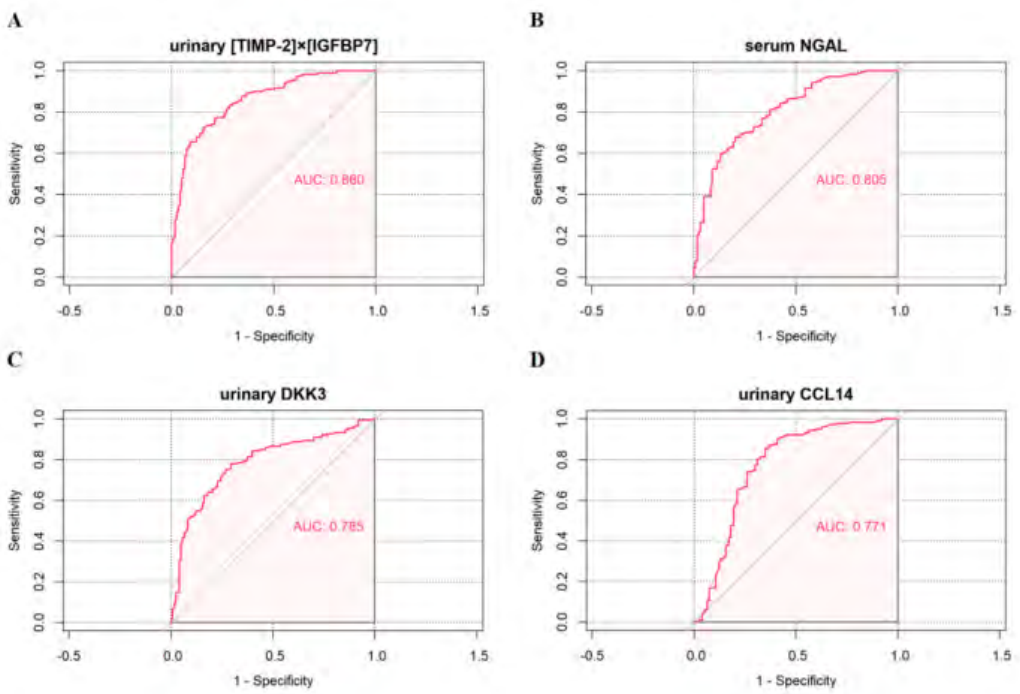


Fig. 1 Prediction of non-recovery of renal function from AKI within seven days using biomarkers. (A) urinary [TIMP-2] × [IGFBP7]. (B) serum NGAL. (C) urinary DKK3. (D) urinary CCL14. Abbreviations: AKI, acute kidney injury; AUC, area under the receiver operating characteristic curve; CCL14, C-C motif chemokine ligand 14; DKK3, Dickkopf-3; IGFBP7, insulin like growth factor binding protein 7; NGAL, neutrophil gelatinase-associated lipocalin; TIMP-2, tissue inhibitor of metalloproteinase 2.

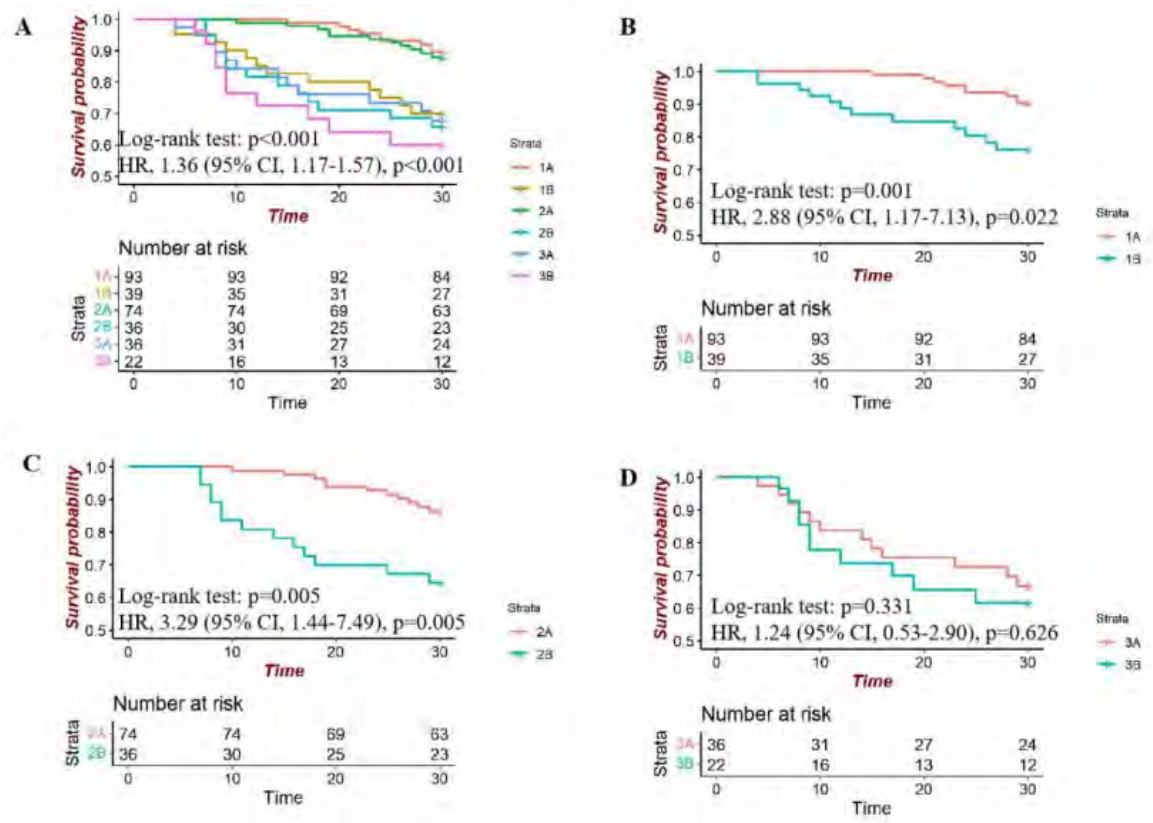


Fig. 2 Adjusted survival curves for the updated AKI staging based on urinary [TIMP-2] × [IGFBP7]. (A) all stages. (B) stage 1A vs 1B. (C) stage 2A vs 2B. (D) stage 3A vs 3B. Abbreviations: AKI, acute kidney injury; CI, confidence interval; HR, hazard ratio; IGFBP7, insulin like growth factor binding protein 7; TIMP-2, tissue inhibitor of metalloproteinase 2. Covariate used in the Cox proportional hazards regression models was APACHE II.

Table 1. The baseline characteristics of patients based on whether their renal function recovered within 7 days.

	Recovery (n=177)	Non-recovery (n=123)	P value [a]
Baseline characteristics			
Age	62 (48-75)	62 (51-74)	0.987
Male gender	113 (63.8%)	78 (63.4%)	0.940
Body weight, kg	68 (60-80)	75 (63-85)	0.010
SOFA score at enrollment, median (IQR)	7 (4-9)	8 (5-11)	<0.001
APACHE II score at enrollment, median (IQR)	17 (12-21)	21 (14-27)	<0.001
Comorbidities			
Hypertension	78 (44.1%)	68 (55.3%)	0.056

Diabetes	35 (19.8%)	35 (28.5%)	0.080
Chronic obstructive pulmonary disease	15 (8.5%)	18 (14.6%)	0.094
Coronary heart disease	41 (23.2%)	32 (26.0%)	0.571
Cerebral vascular disease	16 (9.0%)	19 (15.4%)	0.089
Chronic liver disease	36 (20.3%)	25 (20.3%)	0.998
Malnutrition	11 (6.2%)	4 (3.3%)	0.247
Mechanical ventilation	130 (73.4)	100 (81.3)	0.114
Kidney replacement therapy	19 (10.7)	43 (35.0)	<0.001
Shock	37 (20.9%)	36 (29.3%)	0.097
Sepsis	77 (43.5%)	45 (36.6%)	0.230
Baseline SCr, median (IQR), umol/L	69.8 (60-82)	70.5 (58.85-85.5)	0.779
AKI classification (KDIGO stage) at the day of AKI diagnosis			
Stage 1	96 (54.2%)	36 (29.3%)	<0.001
Stage 2	55 (31.1%)	55 (44.7%)	0.016
Stage 3	26 (14.7%)	32 (26.0%)	0.015
Serum NGAL, median (IQR), ng/ml	36.20 (23.51-74.25)	110.05 (61.98-197.13)	<0.001
Urinary [TIMP-2] × [IGFBP7], median (IQR), (ng/ml)2 /1000	0.14 (0.06-0.44)	1.53 (0.54-7.14)	<0.001
Urinary DKK3, median (IQR), ng/ml	322.06 (34.00-1760.26)	3147.93 (1481.30-5856.94)	<0.001
Urinary CCL14, median (IQR), pg/ml	221.24 (101.06-412.43)	846.2 (443.72-1512.79)	<0.001
Outcome			
Persistent AKI	83 (46.89%)	100 (81.30%)	0.055
LOS in hospital, median (IQR), d	23 (12-34.5)	22 (12-43)	0.244
LOS in ICU, median (IQR), d	6 (4-12)	8 (4-16)	0.016
Mortality at 30 d	32 (18.1%)	35 (28.5%)	0.034

Values are median (25th, 75th percentile interquartile range) or n (%).Abbreviations: AKI, acute kidney injury; APACHE, Acute Physiology and Chronic Health Evaluation; CCL14, C-C motif chemokine ligand 14; DKK3, Dickkopf-3; ICU, intensive care unit; IGFBP7, insulin like growth factor binding protein 7; KDIGO, Kidney Disease: Improving Global Outcomes; LOS, length of stay; NGAL, neutrophil gelatinase-associated lipocalin; SCr, serum creatinine; SOFA, Sequential Organ Failure Assessment; TIMP-2, tissue inhibitor of metalloproteinase 2.a.P-values are derived from the $\chi 2$ test or Mann-Whitney U test.

Table 2. The accuracy of four biomarkers for predicting non-recovery of renal function from acute kidney injury within seven days

	Cutoff value	Brier	Sensitivity	Specificity	PPV	NPV
[TIMP-2] × [IGFBP7], (ng/ml)²/1000	1.08	0.171	0.63 (0.54, 0.72)	0.89 (0.84, 0.93)	0.80 (0.71, 0.88)	0.78 (0.71, 0.83)
NGAL, ng/ml	66.18	0.178	0.71 (0.62, 0.79)	0.72 (0.65, 0.78)	0.64 (0.55, 0.72)	0.78 (0.71, 0.84)
DKK3, ng/ml	1989.58	0.198	0.71 (0.62, 0.79)	0.78 (0.71, 0.84)	0.69 (0.60, 0.77)	0.79 (0.73, 0.85)
CCL14, pg/ml	594.39	0.176	0.63 (0.54, 0.72)	0.87 (0.81, 0.92)	0.77 (0.68, 0.85)	0.77 (0.71, 0.83)
[TIMP-2] × [IGFBP7], (ng/ml)²/1000 in validation	1.08	0.223	0.73 (0.56, 0.86)	0.79 (0.67, 0.89)	0.68 (0.51, 0.81)	0.83 (0.71, 0.92)

Data presented as percentage (95% confidence interval).Abbreviations: CCL14, C-C motif chemokine ligand 14; DKK3, Dickkopf-3; IGFBP7, insulin like growth factor binding protein 7; NGAL, neutrophil gelatinase-associated lipocalin; NPV, negative predictive value; PPV ,positive predictive value; TIMP-2, tissue inhibitor of metalloproteinase 2.

Table 3: Trend test of four biomarkers for 30-day mortality rate in updated AKI staging

	[TIMP-2] × [IGFBP7]		NGAL		DKK3		CCL14	
Comparison	HR (95% CI)	P value	HR (95% CI)	P value	HR (95% CI)	P value	HR (95% CI)	P value
Stage 1A	-	-	-	-	-	-	-	-
Stage 1B vs Stage 1A	3.45 (1.45-8.20)	0.005	1.76 (0.75-4.14)	0.197	1.58 (0.67-3.72)	0.297	1.82 (0.73-4.52)	0.196
Stage 2A vs Stage 1A	1.17 (0.46-3.86)	0.743	0.90 (0.34-2.39)	0.828	1.02 (0.42-2.52)	0.960	0.86 (0.36-2.05)	0.730
Stage 2B vs Stage 1A	4.14 (1.76-9.70)	0.001	2.32 (1.04-5.18)	0.040	2.28 (0.98-5.3)	0.055	2.41 (1.13-5.16)	0.024
Stage 3A vs Stage 1A	3.80 (1.60-9.05)	0.003	2.20 (0.84-5.78)	0.110	2.22 (0.88-5.64)	0.093	2.19 (0.92-5.22)	0.078
Stage 3B vs Stage 1A	5.38 (2.17-13.33)	<0.001	4.46 (1.99-9.99)	<0.001	4.69 (2.07-10.61)	<0.001	4.34 (2.05-9.16)	<0.001
Trend test								
P for trend	1.36 (1.17-1.57)	<0.001	1.33 (1.15-1.54)	<0.001	1.33 (1.15-1.55)	<0.001	1.32 (1.14-1.52)	<0.001

Abbreviations: AKI, acute kidney injury; CCL14, C-C motif chemokine ligand 14; CI, confidence interval; DKK3, Dickkopf-3; HR, hazard ratio; IGFBP7, insulin like growth factor binding protein 7; NGAL, neutrophil gelatinase-associated lipocalin; TIMP-2, tissue inhibitor of metalloproteinases 2.

In trend tests, continuous variables across 6 groups were assigned values from 1 to 6. P-values and p for trend compared to stage 1A are based on Wald tests from Cox proportional hazards regression models.

改良时间加权平均动脉压对心脏术后患者急性肾损伤预测价值：一项前瞻性、观察性研究

姓名：毕铭泽 [1,2]，杨疏合 [1,2]，彭清云 [1,2]，仲世嘉 [1,2]，黄英姿 [1,2]（通讯）

单位：1. 东南大学附属中大医院 2. 江苏省重症医学重点实验室

目的

心脏手术相关急性肾损伤（Cardiac surgery-associated acute kidney injury，CSA-AKI）是心脏术后常见且严重的并发症，可显著增加患者病死率并影响短期及长期预后。术中低血压被认为是 CSA-AKI 的重要危险因素之一。目前关于体外循环（CPB）期间低血压持续时间与程度对 CSA-AKI 的的影响尚不明确。本研究旨在探讨时间加权平均动脉压（Time-weighted average mean arterial pressure，TWA-MAP）和基于患者基础血压控制情况定义的改良时间加权平均动脉压（mTWA-MAP）与对 CSA-AKI 及主要肾脏不良结局的预测价值，为术中个体化血压管理及肾脏预后风险评估提供临床依据。

方法

本研究为单中心、前瞻性、观察性研究。纳入 2024 年 10 月 1 日 -2026 年 1 月 31 日在东南大学附属中大医院心脏外科进行手术，且术后转入该院重症医学科的成年患者。收集人口学信息、围术期血流动力学数据、实验室检查及临床结局资料。主要研究终点为 CSA-AKI，次要终点包括术后 30 天内主要不良肾脏事件（MAKE30）和 28 天病死率。TWA-MAP 定义为 CPB 期间平均动脉压（MAP）低于 65mmHg 的曲线下面积除以 CPB 时间。mTWA-MAP 定义为（1）基础有高血压病史患者：CPB 期间 MAP 低于 80% 基线 MAP 的曲线下面积除以 CPB 时间；（2）非高血压患值与 TWA-MAP 一致。基线 MAP 定义为：手术前平静状态下连续测量三次血压的 MAP 平均值。比较不同肾脏预后组患者基线资料、围术期特征及血流动力学指标差异。并评估 TWA-MAP 与 mTWA-MAP 对心脏术后患者急性肾损伤的预测价值。

结果

共纳入 945 例患者，其中 227 例（24%）发生 CSA-AKI。与未发生 CSA-AKI 患者相比，CSA-AKI 患者年龄更大（72 vs 64 岁，$P < 0.001$），糖尿病、高血压、房颤、脑卒中等基础疾病发生率更高（$P < 0.05$）。此外，CSA-AKI 患者 CPB 时间、主动脉阻断时间及手术时长均显著延长（$P < 0.001$），APACHE II 评分及 SOFA 评分亦显著升高（$P < 0.001$）。多因素 logistic 回归分析显示，在校正年龄、糖尿病、CPB 时间等危险因素后，mTWA-MAP 是 CSA-AKI 的独立危险因素（OR=1.18，95%CI，$P < 0.001$），而 TWA-MAP 则与 CSA-AKI 无显著相关（OR=1.00，P=0.946）。此外，年龄（OR=1.07）、糖尿病（OR=2.04）及 CPB 时间（OR=1.01）亦是 CSA-AKI 的独立危险因素，而 LVEF（OR=0.98）为保护因素。ROC 曲线分析显示，mTWA-MAP 预测 CSA-AKI 的曲线下面积为 0.63，最佳截断值为 10.02，对应特异度为 0.91，敏感度为 0.30。

讨论

本研究发现，在进行 CPB 的心脏手术患者中，mTWA-MAP 与 CSA-AKI 发生显著相关，而 TWA-MAP 与 CSA-AKI 无显著相关性。该结果提示，对于基础存在高血压病史的患者，固定血压阈值（65mmHg）难以准确反映患者 CPB 期间低血压暴露风险，而基于基础血压控制情况的相对阈值指标能够更好地反映器官灌注不足程度。此外，年龄、糖尿病及 CPB 时间也是 CSA-AKI 的独立危险因素，与既往研究一致。ROC 分析显示 mTWA-MAP 对 CSA-AKI 具有一定预测能力。上述结果提示，在心脏手术围术期血压管理中，采用个体化血压目标可能有助于更准确识别 CSA-AKI 高风险患者，从而为优化血流动力学管理策略提供依据。

基于边际结构模型的充分营养干预生理阈值窗口识别及外部验证

姓名：范杰梅，邓宏彬

单位：中国人民解放军东部战区总医院（南京大学附属金陵医院）

摘要：

目的 为明确重症患者强化营养的获益生理窗口，为个体化动态营养策略制定提供循证依据。

方法 本研究以 MIMIC-IV 数据库 5370 例成年重症患者的纵向数据开展回顾性队列研究，构建逆概率加权的边际结构 Cox 模型，分析能量、蛋白达标喂养（80%–100% 静息能量消耗）与 28 天死亡风险的关联，并在 NEED 数据库 1322 例患者中完成外部支持性验证。

结果 总体人群中，能量、蛋白达标喂养均与 28 天死亡风险显著降低相关（能量 HR=0.610，蛋白 HR=0.513，均 P<0.001），但该获益存在明确生理阈值窗口：仅在等效去甲肾上腺素剂量 <0.3μg/kg/min、乳酸 <2mmol/L 时，能量与蛋白达标的保护效应显著，而蛋白达标在肌酐 <5mg/dL 时获益更稳定，上述高应激或器官功能严重受损亚组中，营养达标的生存获益减弱或无统计学意义。NEED 队列外部验证结果与研究队列一致，校正混杂因素后，对应生理阈值分层下的营养达标率仍与 28 天死亡风险显著负相关，超过阈值的分层中保护效应消失。

结论 本研究证实，重症患者充分营养干预的生存获益具有显著的生理窗口特征，基于循环（去甲肾上腺素、乳酸）和肾功能（肌酐）指标可识别营养干预的适宜人群，而血流动力学不稳定或器官功能严重受损时，需谨慎推进营养达标。

关键词：重症患者；营养支持；边际结构模型；生理阈值窗口；死亡风险；外部验证

1. 引言

营养支持是维持重症患者内环境稳定并改善预后的重要手段。通过维持肠道屏障完整性、减少炎症反应及缓解胰岛素抵抗，合理的营养支持可以帮助患者顺利度过应激期 [1]。ASPEN 和 ESPEN 等指南通常按体重估算患者的能量需求和蛋白需求，在无法实施间接量热测定时作为临床参考，其中推荐能量供给为 25–30 kcal/kg/d，蛋白质供给为 1.2–2.0 g/kg/d[2, 3]。上述指南倡导在患者入 ICU 后 48-72 小时内逐渐达到蛋白摄入目标量的 80% 以上。

值得注意的是，能量供给不足或过量均可能产生不良后果。能量摄入过低可增加感染发生率和器官功能障碍风险 [4, 5]；而能量供给过量则可能诱发高血糖、高甘油三酯血症、肝脂肪变性、氮质血症及二氧化碳潴留等并发症，并进一步增加患者死亡率 [6, 7]。研究发现，能量摄入与死亡风险之间呈“U 型”关系，即能量供给过低或过高均与较高死亡率相关，而当能量摄入维持在约 70% 预测需求水平时，患者死亡风险最低 [8]。

然而，近期多项 RCT 对“早期充分营养支持可改善预后”的传统观点提出了挑战。NUTRIREA-2 研究发现，在接受机械通气且合并休克的成人患者中，给予全量肠内营养（enteral nutrition，EN）并未带来预期的临床获益，反而与胃肠道不耐受症状增加相关，且少数患者出现急性肠系膜缺血及 Ogilvie 综合征等严重并发症 [9]。另另一项基于倾向得分匹配的研究也表明，早期实施全量营养支持，尤其是早期全量肠内营养，与 28 天死亡率升高相关；即使在 ICU 入住后 48 小时内蛋白质摄入量超过 0.3 g/kg/d，患者死亡风险仍呈剂量依赖性增加，进一步提示过早推进充足营养摄入可能带来潜在不利影响 [10]。NUTRIREA-3 研究进一步指出，在接受机械通气并使用血管活性药物的患者中，与第一周内实施全目标营养（能量 25 kcal/kg/d，蛋白质 1.0–1.3 g/kg/d）相比，适度限制营养供给（能量约 6 kcal/kg/d，蛋白质 0.2–0.4 g/kg/d）可显著缩短患者达到“出院准备状态”的时间，同时减少呕吐、腹泻及急性肠系膜缺血等并发症发生率 [11]。此外，高蛋白摄入（≥ 2.2g/kg/d）在某些存在急性肾损伤或重症程度更高的患者中可能有害。

上述研究提示，在 ICU 早期阶段，适度限制能量及蛋白质供给可能更有利于患者恢复。尤其在休克及血流动力学不稳定阶段，患者组织灌注和代谢利用能力明显受限，大量能量供给不仅难以被有效利用，反而可能加重机体代谢负担及器官功能损伤 [12, 13]。休克早期由于血流重新分布，可导致肠系膜灌注下降及氧供需失衡；同时，血管活性药物的应用可能进一步降低肠道血流灌注，诱发肠黏膜损伤 [14]。鉴于肠系膜缺血及非闭塞性肠坏死的潜在风险，多项指南及综述建议，在血流动力学尚未稳定时应暂缓肠内营养支持，待患者充分液体复苏并达到相对稳定状态后，再谨慎启动肠内喂养，并采用低剂量起始策略，如 10–20 kcal/h 或目标能量供给量的 20%–50%，随后逐步递增 [15]。这些策略说明在休克等严重应激状态下应根据患者生理耐受能力合理控制能量供给，而非单纯追求营养达标率。

综上所述，在 ICU 治疗过程中采用统一固定的能量及蛋白质供给标准，可能难以满足危重症患者复杂且动态变化的营养需求。因此，亟需进一步明确在不同病理状态及临床特征背景下，营养达标是否均能带来一致的临床获益，或是否存在显著的差异化治疗效果。本研究拟利用 ICU 患者临床队列数据，构建多状态 Cox 回归模型，将每日能量摄入是否达到推荐目标水平（80%–100%）作为主要暴露变量，系统评估不同临床分层人群中达标营养与生存结局之间的关联关系，以期为重症患者精准化、个体化营养支持策略的制定提供循证医学依据。

2. 材料和方法

2.1 研究设计与研究对象

本研究为一项基于 MIMIC-IV 数据库开展的回顾性队列研究。该数据库收录了 2008 年至 2019 年期间在 Beth Israel Deaconess Medical Center 接受重症监护治疗患者的临床数据，涵盖人口学特征、生命体征、实验室检查结果、用药记录及治疗过程等医疗信息。

2.1.1 入选标准

（1）年龄≥ 18 岁的成年患者；

（2）ICU 住院时间≥ 7 天；

（3）ICU 住院期间至少有一次肠内或肠外营养治疗记录；

2.1.2 排除标准

（1）存在多次 ICU 入科记录者；

（2）身高或体重缺失者；

（3）每日卡路里摄入量记录缺失率 <33% 者（在营养数据中，若某日饮食类型记录不属于 NPO、Sips、Tube Feeding、TPN、Enteral feeding、No Liquid、PPN，则该日热量记为空值）；

（4）ICU 住院期间无蛋白质摄入量记录者；

（5）ICU 住院期间缺失血气分析、血常规或生化检查数据者。

2.2 变量提取和数据收集

本研究提取患者的基线资料、每日观察数据、每日营养摄入数据及临床结局。基线资料包括年龄、性别、体重、种族、入院类型、合并症情况，以及 SOFA 评分及其各组成部分。每日观察数据涵盖生命体征（平均动脉压、心率、呼吸频率、体温、格拉斯哥昏迷评分）、实验室指标（血红蛋白、白细胞、血小板、电解质、肌酐、尿素氮、肝功能指标、乳酸、凝血功能及血气分析等）和支持治疗信息（去甲肾上腺素使用、肾脏替代治疗、机械通气情况）。若同一 ICU 日内某变量存在多次记录，则选择与病情最严重相关的数值。

每日营养数据包括肠内营养和 / 或肠外营养摄入的能量（kcal）和蛋白质量（g），并根据预测需求量计算实际摄入比例。当能量或蛋白质摄入达到推荐目标的 80%–100% 时，定义为“达标营养”。

主要结局为 28 天死亡率，次要结局包括 ICU 住院时间及机械通气持续时间。

对于缺失率低于 60% 的变量，采用于加权预测均值匹配（predictive mean matching, PMM）的多重插补方法进行补全。所有测量时间点及数值均直接来源于数据库提取。

2.3 主要暴露因素

根据既往临床研究及营养治疗实践标准，本研究将充足喂养定义为实际能量摄入达到静息能量消耗的 80%-100%，不足喂养定义为低于 REE 的 80%。

2.4 结局与随访

主要结局为 28 天全因死亡。随访自 ICU 入院日起算，以 24 小时为时间尺度构建时间依赖生存数据。患者在死亡、转出 ICU 或达到 28 天随访终点时停止观察。

2.5 协变量

为控制潜在混杂因素，模型纳入以下协变量：基线变量：性别、年龄、Charlson 合并症指数、入院体重、身高；随时间变化的临床变量：白细胞计数（WBC）、动脉二氧化碳分压（pCO_2）、乳酸、谷丙转氨酶（ALT）、肌酐、氧合指数（PaO_2/FiO_2）、平均动脉压（MAP）、每日尿量、机械通气（vent）、肾替代治疗（RT）、体温、白蛋白、血管活性药物剂量（vaso_dose）、格拉斯哥昏迷评分（GCS）及序贯器官衰竭评分（SOFA）。

2.6 逆概率权重的构建

为控制时间依赖性混杂因素，本研究采用逆概率加权方法估计患者每日处于不同喂养水平下的暴露概率，并构建稳定化权重。

权重的计算分为分子模型和分母模型：分子模型仅纳入基线人口学变量，包括性别、年龄、Charlson 合并症指数、体重及身高。分母模型在分子模型的基础上进一步纳入随时间变化的临床变量，包括 WBC、pCO_2、乳酸、ALT、肌酐、PaO_2/FiO_2、MAP、尿量、vent、RT、体温、albumin、vaso_dose、GCS、SOFA。

采用多项式 logistic 回归模型，以每日喂养暴露状态为因变量，估计个体在给定基线与动态临床状态条件下实际暴露的概率。患者 i 在时间 t 的稳定化权重定义为：

$$sw_{it}^{T} = \prod_{j=0}^{t} \frac{Pr\left(A_{ij} = a_{ij} | \bar{A}_{i(j-1)}, L_{i0}\right)}{Pr\left(A_{ij} = a_{ij} | \bar{A}_{i(j-1)}, L_{i0}, L_{ij}\right)}$$

其中 A_{ij} 表示第 i 个患者在第 j 日的 TCI 状态，$\bar{A}_{i(j-1)}$ 为前一天喂养状态，分别为基线与随时间变化的协变量。通过分子概率 / 分母概率实现稳定化，并对权重进行 1%-99% 分位数截尾以减少极端值对模型的不稳定影响。

2.7 统计学分析

在构建稳定化逆概率权重后，采用边际结构 Cox 模型评估不同喂养水平对 28 天死亡的影响。在加权样本中拟合 Cox 比例风险模型，以估计各喂养水平相对于参考组的风险比及其 95% 置信区间：

$$h(t|A) = h_0(t)\exp(\beta A)$$

其中 A 表示每日喂养水平（充足喂养 vs 未充足喂养），β 为暴露对死亡风险的对数风险比。模型中使用权重 sw_{it}^{T}，并在患者层面引入聚类稳健方差估计，以处理个体内多段区间的相关性。

连续变量根据分布情况以均值（标准差）或中位数 [四分位间距，IQR 表示，分类变量以频数（百分比）表示。组间比较中，分类变量采用卡方检验或 Fisher 精确检验，连续变量根据正态性检验结果采用 Student’s t 检验或 Mann–Whitney U 检验。对于亚组分析，通过在模型中引入交互项检验不同亚组间效应差异，并采用 Benjamini–Hochberg 方法控制多重比较的假发现率。所有统计分析均使用 R 软件（version 4.2.2）完成，双侧 P < 0.05 视为差异具有统计学意义。

2.8 外部验证队列分析方法

为验证基于 MIMIC 纵向数据中边际结构模型识别出的充分营养干预生理阈值窗口的稳定性与外部可推广性，本研究在独立的 NEED 数据集中构建外部验证队列。

从 NEED 研究数据库中筛选接受营养支持的重症患者组成验证队列。提取患者基线人口学特征、疾病严重程度指标、实验室指标及首周营养摄入数据。基于 MIMIC 队列中 MSCM 分析所得的生理阈值窗口，在 NEED 队列中采用基线时点对应变量进行分层分析。营养暴露定义为 ICU 入科后第 1 至第 7 天平均每日热量达标率（%TCI）及蛋白达标率（%TPI）。

在统计方法上，采用 Cox 比例风险回归模型评估首周平均营养达标率与 28 天死亡风险之间的关系。在总体人群及各阈值分层人群中分别建立模型，并对年龄、性别、CCI 评分及入 ICU 时 SOFA 评分等潜在混杂因素进行校正。通过比较不同生理状态分层下营养达标率与死亡风险之间的关联方向与显著性，验证 MIMIC 队列中识别的营养干预适用窗口是否在独立数据集中得到重复。

3. 结果

3.1 患者特征

基于 MIMIC-IV 成人 ICU 住院记录（N = 94458），首先排除重复 ICU 入住患者 9216 例，进一步排除 ICU 住院时长 < 7 天者 73764 例。随后按数据完整性标准依次排除：身高或体重数据缺失者 2706 例、每日热量摄入记录缺失率 > 33% 者 2457 例、缺失蛋白质摄入数据 850 例，以及关键实验室指标缺失 95 例。最终纳入 5370 例构成研究队列，用于后续时间依赖暴露与结局分析（图 1）。

在纳入的重症患者中，男性占 58.7%，机械通气率为 67.9%。总体人群的年龄中位数为 65.8 岁，BMI 中位数为 28.0 kg/m²，Charlson 合并症评分和 SOFA 评分的中位数分别为 5 分和 7 分。按 28 天死亡结局分组比较显示，死亡组患者年龄显著高于生存组（70.9 vs 63.7 岁，P<0.001），BMI 更低（27.1 vs 28.4 kg/m²，P<0.001），Charlson 评分及 SOFA 评分均更高（6 vs 5 分，P<0.001；7 vs 6 分，

P<0.001），GCS 分布亦较差（P=0.006）。死亡组去甲肾上腺素当量剂量更高 (0.08 vs 0.05 μg/kg/min，P=0.0004)。性别构成（男：57.8% vs 59.1%，P=0.396）与机械通气比例（66.0% vs 68.0%，P=0.091）在两组间差异均无统计学意义。

实验室指标方面，死亡组血小板计数更低（194 vs 213×109/L，P<0.001），乳酸水平更高（2.20 vs 1.90 mmol/L，P<0.001），肾功能受损更明显 (肌酐 1.40 vs 1.10 mg/dL，P<0.001；尿素氮 31.0 vs 23.0 mg/dL，P<0.001)；总胆红素略高（0.80 vs 0.70 mg/dL，P<0.001），白蛋白分布差异也具有统计学意义（P=0.010）。白细胞与血糖在两组间差异不显著（P=0.134；P=0.129）。

生命体征方面，死亡组的 PaO2/FiO2 比值更低（145.0 vs 156.7，P<0.001），体温略低（37.44 vs 37.67 °C，P<0.001），平均动脉压更低（57 vs 58 mmHg，P=0.002），呼吸频率更快（29 vs 28 次 / 分，P<0.001），而心率差异不显著（P=0.493）。

死亡组患者表现出年龄更高、基础疾病负担更重及器官功能障碍更为严重的特征， 并伴随血小板减少、肾功能损害及营养 / 炎症相关指标异常；而性别构成、白细胞计数、血糖水平、机械通气比例及心率在两组间未观察到显著差异（表 1）。

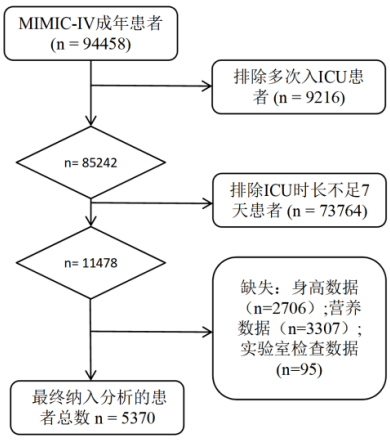


图 1. 研究对象的筛选流程

表 1：纳入患者的基线特征

变量	总人群	生存人群	死亡人群	P 值
年龄（岁）	65.80 [54.42, 75.98]	63.69 [52.41, 73.85]	70.92 [60.17, 80.13]	< 0.001
性别（男）	3154 (58.7%)	2344 (59.1%)	810 (57.8%)	0.3961
BMI(kg/m²)	28.03 [23.88, 33.41]	28.40 [24.14, 33.77]	27.10 [23.24, 32.26]	< 0.001
机械通气	3644 (67.9%)	2718 (68.5%)	926 (66.0%)	0.0914
察尔森共病评分	5.00 [3.00, 7.00]	5.00 [3.00, 7.00]	6.00 [4.00, 8.00]	< 0.001
SOFA score	7.00 [4.00, 10.00]	6.00 [4.00, 9.00]	7.00 [5.00, 10.00]	< 0.001
GCS	15.00 [13.00, 15.00]	15.00 [13.00, 15.00]	15.00 [13.00, 15.00]	0.006
等价去甲用量 (μg/kg/min)	0.05 [0.00, 0.25]	0.05 [0.00, 0.22]	0.08 [0.00, 0.28]	0.0004
白细胞(×10⁹ /L)	13.70 [9.90, 18.90]	13.60 [9.90, 18.70]	13.90 [10.10, 19.18]	0.1343
血小板(×10⁹ /L)	208.00 [147.00, 286.00]	213.00 [153.00, 290.00]	194.00 [130.00, 274.75]	< 0.001

乳酸(mmol/L)	2.00 [1.30, 3.60]	1.90 [1.20, 3.52]	2.20 [1.40, 3.90]	< 0.001
肌酐(mg/dL)	1.20 [0.80, 2.10]	1.10 [0.80, 2.00]	1.40 [0.90, 2.50]	< 0.001
尿素氮(mg/dL)	25.00 [16.00, 44.00]	23.00 [15.00, 40.00]	31.00 [19.00, 53.00]	< 0.001
胆红素(mg/dL)	0.70 [0.40, 1.40]	0.70 [0.40, 1.30]	0.80 [0.40, 1.80]	< 0.001
白蛋白(g/dL)	2.80 [2.40, 3.30]	2.80 [2.40, 3.40]	2.80 [2.30, 3.30]	0.0101
血糖(mg/dL)	160.00 [126.00, 212.00]	159.00 [126.00, 210.00]	162.00 [127.00, 218.75]	0.129
PaO_2/FiO_2	154.00 [85.00, 286.50]	156.67 [88.00, 292.00]	145.00 [77.50, 276.14]	< 0.001
体温(° C)	37.60 [37.11, 38.22]	37.67 [37.17, 38.33]	37.44 [37.00, 38.00]	< 0.001
心率(次/分)	108.00 [94.00, 124.00]	108.00 [94.00, 124.00]	109.00 [93.00, 124.00]	0.493
平均动脉压(mmHg)	57.00 [50.00, 64.00]	58.00 [51.00, 64.00]	57.00 [49.00, 64.00]	0.002
呼吸频率(次/分)	28.00 [24.00, 33.00]	28.00 [24.00, 33.00]	29.00 [25.00, 34.00]	< 0.001

在 MIMIC-IV 数据库 5370 例患者中，共有 440 例（8.2%）在 ICU 住院期间接受肠外营养支持，而其余 5370 例中的 91.8% 未使用肠外营养，进一步分析首周肠外营养使用情况，提示研究总体人群以肠内营养为主要营养支持方式。仅有 276 例（5.1%）在 ICU 入科首周接受肠外营养治疗，94.9% 的患者首周未使用肠外营养，表明早期营养策略以肠内营养为主，肠外营养应用比例较低（图 2）。

整体而言，该结果提示本研究队列中绝大多数患者接受的是纯肠内营养或以肠内营养为主的支持策略，肠外营养的使用比例相对有限，尤其在 ICU 治疗的早期阶段更为明显。



图 2. MIMIC-IV 数据库中接受重症营养治疗患者中肠外营养的使用情况

A 在全部 5370 例患者中，共有 440 例（8.2%）在 ICU 住院期间接受肠外营养支持。B. 在 5370 例患者中，仅有 276 例（5.1%）在 ICU 入科首周接受肠外营养治疗。

图 3A 展示了研究队列每日热卡达标率（TCI）与蛋白达标率（TPI）随时间变化的趋势。在整体人群中，两项达标率自 ICU 入院后均呈持续上升趋势。入 ICU 后前 5–7 天上升最为明显。日 TCI 由较低水平快速提升，一周后达到约 70%；日 TPI 也同步上升，但整体水平低于 TCI，一周后约为 60%。此后两者增幅逐渐减缓，呈平稳上升趋势，并于第 3 周后趋于平台期；至随访末期，TCI 接近 90%，TPI 约为 80%。图 3B 比较了生存组和死亡组患者每日热量和蛋白达标率随 ICU 住院时间的变化趋势。结果显示，在病程早中期，两组的每日热量和蛋白达标率相对接近，而病程后期死亡组未能维持达标率的持续上升趋势，整体水平逐渐低于生存组。

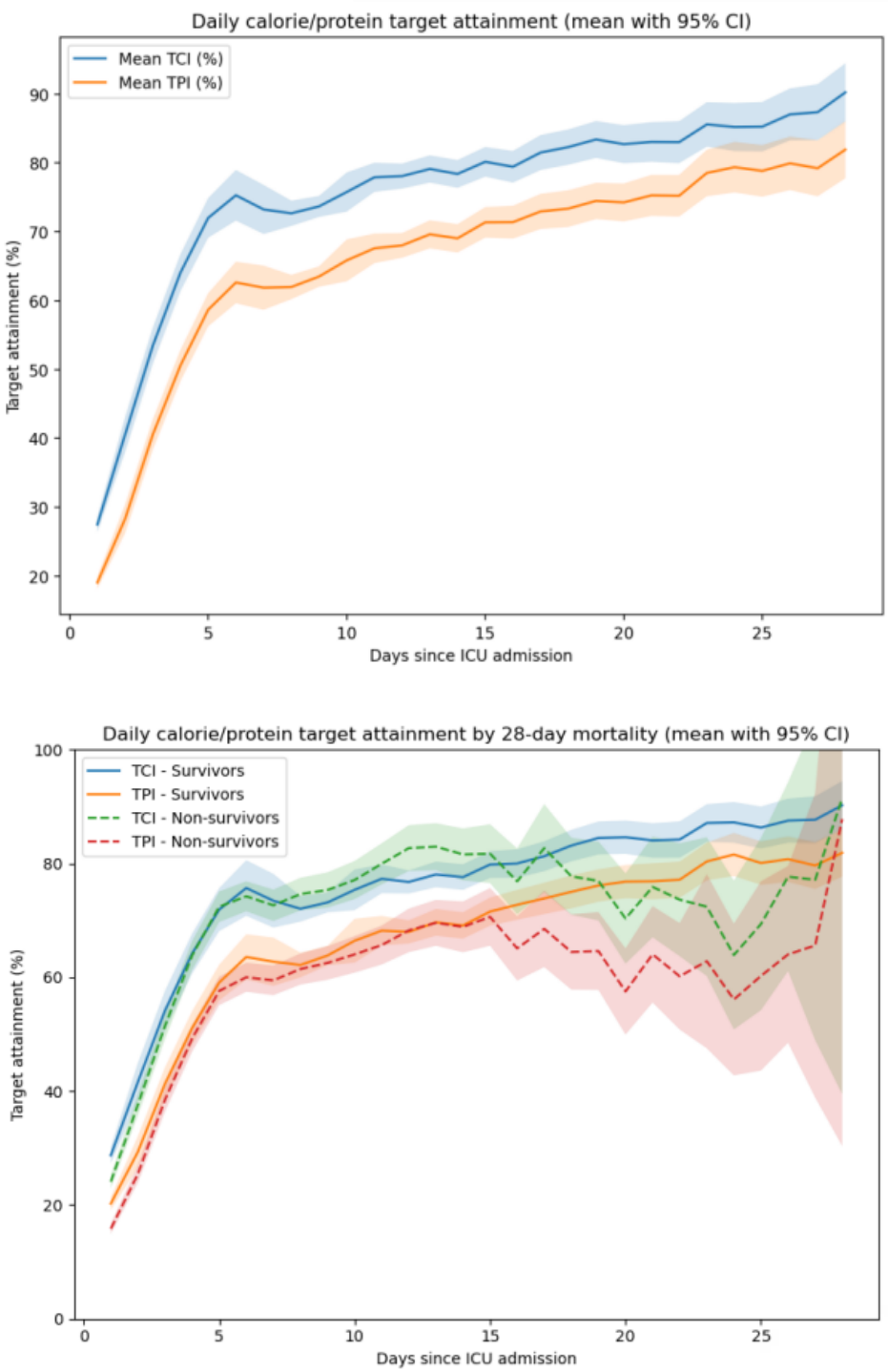


图 3：总体队列在入 ICU 后每日热量与蛋白目标达标率的时间趋势

A. 每日热卡达标率（TCI）与蛋白达标率（TPI）随时间变化的趋势。蓝线代表 TCI，黄线代表 TPI。B. 生存组和死亡组患者每日热量和蛋白达标率随 ICU 住院时间的变化趋势。蓝色实线代表生存组 TCI；黄色实线代表生存者 TPI; 绿色虚线代表死亡组 TCI；红色虚线代表死亡组 TPI。

3.2 热量达标喂养对 28 天死亡风险的影响

在逆概率加权的边际结构 Cox 模型中，以每日总热卡摄入达到 80%–100%REE 定义为热量达标，并以不足喂养（<80%）作为参照组进行比较。结果显示，在总体人群中，能量达标与 28 天死亡风险显著降低相关（HR = 0.610，95%CI = 0.500–0.740，P < 0.001）。

在 MIMIC-IV 数据库中，超过 90% 的患者接受纯肠内营养治疗。按等效去甲肾上腺素剂量分层分析显示，在低剂量血管活性药物支持人群中，热量达标与 28 天死亡风险显著降低相关（<0.2μg/kg/min：HR = 0.510，95%CI = 0.410–0.630，P < 0.001；0.2–<0.3μg/kg/min：HR = 0.230，95%CI = 0.070–0.740，P = 0.014），然而，当等效剂量≥ 0.3 μg/kg/min 时，热量达标与死亡风险之间的关联减弱且不再具有统计学显著性（0.3–<0.4 μg/kg/min：HR = 1.380，P = 0.521；≥ 0.4 μg/kg/min：HR = 1.010，P = 0.979）。

按乳酸水平分层分析显示，仅在乳酸 < 2 mmol/L 的患者中观察到热量达标与 28 天死亡风险显著降低相关（HR = 0.510，95%CI = 0.400–0.640，P < 0.001），而乳酸≥ 2 mmol/L 的各亚组中，该关联均未达到统计学显著性（表 2）。

表 2 不同临床分层下能量达标喂养与 28 天死亡风险的逆概率加权边际结构 Cox 回归分析结果

		HR	95%CI	P
总人群		0.61	0.502, 0.742	<0.001
等效去甲使用量				
	<0.2	0.506	0.406, 0.632	<0.001
	≥0.2 且 <0.3	0.225	0.068, 0.743	0.014
	≥0.3 且 <0.4	1.377	0.518, 3.659	0.521
	≥0.4	1.007	0.622, 1.628	0.979
乳酸				
	<2	0.508	0.400, 0.644	<0.001
	≥2 且 <3	0.777	0.490, 1.232	0.283
	≥3 且 <4	0.667	0.296, 1.504	0.329
	≥4	0.619	0.348, 1.100	0.102

3.3 蛋白达标喂养对 28 天死亡风险的影响

在总体人群中，能量达标与 28 天死亡风险显著降低相关（HR = 0.513，95%CI = 0.421–0.616，P < 0.001）。

分层分析显示，在分别以等效去甲肾上腺素剂量 < 0.3 μg/kg/min（<0.2 μg/kg/min：HR = 0.460，95%CI = 0.369–0.574，P < 0.001；0.2–<0.3 μg/kg/min：HR = 0.134, 95%CI = 0.029–0.612，P = 0.009）、乳酸 < 2 mmol/L（HR = 0.375，95%CI =0.291–0.485，P < 0.001） 及肌酐 < 5 mg/dL （<1.3 mg/dL：HR = 0.521，P < 0.001；1.3–<2 mg/dL：HR = 0.454，P = 0.003；2–<5 mg/dL：HR = 0.538，P = 0.001）为界进行亚组划分时，各亚组内达到充足蛋白供给水平均与 28 天死亡风险下降显著相关（表 3）。总体而言，蛋白达标在总体人群中与 28 天死亡风险降低显著相关，其潜在获益主要集中于组织供养相对较好、循环状态稳定及肾功能尚可的患者亚组。

表 3 不同临床分层下蛋白达标喂养与 28 天死亡风险的逆概率加权边际结构 Cox 回归分析结果

		HR	95%CI	P
总人群		0.513	0.421, 0.626	<0.001
等效去甲使用量				
	<0.2	0.460	0.369, 0.574	<0.001
	≥0.2 且 <0.3	0.134	0.029, 0.612	0.009
	≥0.3 且 <0.4	0.698	0.265, 1.841	0.467
	≥0.4	0.981	0.578, 1.664	0.943
乳酸				
	<2	0.375	0.291, 0.485	<0.001
	≥2 且 <3	0.683	0.435, 1.071	0.097
	≥3 且 <4	0.577	0.279, 1.191	0.137
	≥4	0.884	0.500, 1.564	0.672
尿素氮				
	>=7 且 <20	0.473	0.277, 0.806	0.006
	>=20 且 <40	0.483	0.339, 0.687	<0.001
	>=40 且 <100	0.547	0.404, 0.740	<0.001
	>=100	0.526	0.277, 1.001	0.051
肌酐				
	<1.3	0.521	0.391, 0.693	<0.001
	>=1.3 且 <2	0.454	0.271, 0.759	0.003
	>=2 且 <5	0.538	0.372, 0.779	0.001
	>=5	0.875	0.437, 1.755	0.707

3.4 NEED 队列中营养干预生理阈值的外部验证结果

外部验证 Cox 回归分析队列的初始筛查人群为 NEED 试验中所有 2772 例入组患者。排除 ICU 住院时间少于 7 天者 212 例、首周接受口服饮食者 235 例、营养数据缺失者 35 例以及首周接受肠外营养者 965 例后，共 1325 例患者符合纳入标准。进一步排除 28 天死亡结局缺失者 3 例，最终纳入 1322 例纯肠内营养患者用于外部验证分析。

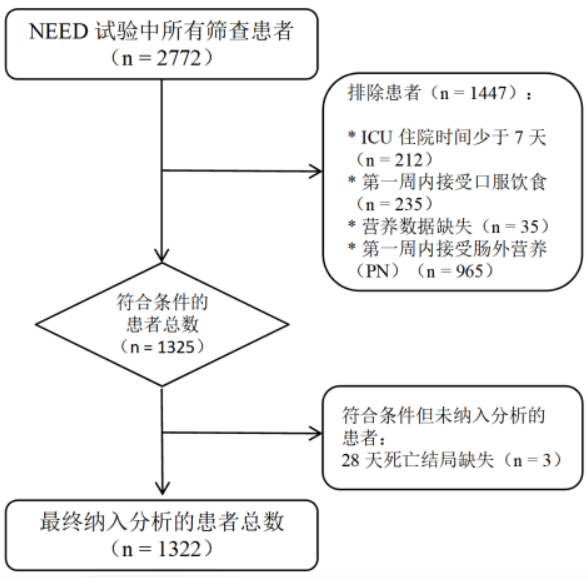


图 4. NEED 队列用于外部验证的患者筛选流程

表 4 展示了用于外部验证分析的 NEED 队列患者基线临床特征。共纳入 1322 例纯肠内营养患者，年龄中位数为 64 岁，男性占 66%。整体疾病严重程度中等偏重，APACHE II 评分中位数为 18，SOFA 评分为 7，mNUTRIC 评分为 4。乳酸水平中位数为 1.8 mmol/L，提示多数患者入科时血流动力学状态相对稳定。ICU 入科类型以综合 ICU 为主（86.5%），62.2% 患者属于积极喂养指导组。入组时 63.8% 接受机械通气，30.1% 使用血管活性药物，10.7% 接受 CRRT 支持。28 天死亡率为 13.2%，28 天内 ICU 自由天数中位数为 6 天。

表 4. NEED 外部验证队列的基线临床特征

	总人群 n=1322
年龄，岁	64（49 - 76）
BMI，kg/m2	22.5（20.8 - 24.5）
性别，男	873（66%）
APACHE II	18（14 - 23）
SOFA 评分	7（5 - 10）
mNUTRIC 评分	4（3 - 6）
合并症数	2（1—3）
乳酸，mmol/L	1.8（1.2 - 3）
ICU 入科类型	
综合	1143（86.5%）
急诊	105（7.9%）
外科	53（4%）
内科	21（1.6%）
积极喂养指南组(NEED 干预)	822（62.2%）
入组时器官支撑	
CRRT	141（10.7%）
机械通气	844（63.8%）
血管活性药物	398（30.1%）
临床结局	
28 天死亡率	175（13.2%）
28 天内 ICU 自由天数	6（0 - 18）

表 5 总结了 NEED 外部验证队列在 ICU 入科后首周的营养治疗实施过程及实际能量与蛋白供给情况。总体来看，患者开始肠内营养的时间中位数为 2 天，75.9% 的患者在入科 48 小时内启动肠内营养，提示多数患者接受了相对早期的营养支持。21.1% 的患者使用促胃肠动力药物。肠内营养途径以胃内喂养为主（91.6%），幽门后喂养占 8.4%。在首周营养供给方面，患者平均每日能量供给量为 928.6 kcal，折算为 14.6 kcal/kg·d，能量达标率中位数为 58.5%。蛋白质供给量为 36.7 g/d，相当于 0.6 g/kg·d，蛋白达标率为 44%。

表 5. NEED 外部验证队列入组后首周营养治疗过程及能量与蛋白供给情况

	总人群 n=1322
入组后第一周的营养治疗过程	
开始肠内营养（EN）的时间（天）	2（1－2）
ICU 入科后 48 小时内开始肠内营养的患者	1004（75.9）
使用促胃肠动力药物的患者	279（21.1）
肠内营养起始途径	
胃内喂养	1211（91.6）
幽门后喂养	111（8.4）
入组后第一周的平均能量和蛋白质供给量	
能量供给量（kcal/天）	928.6（654.3－1214.3）
单位体重能量供给量（kcal/kg · 天）	14.6（10.3－19.6）
能量供给达标率（%）	58.5（41.3－78.3）
蛋白质供给量（g/天）	36.7（25.7－48）
单位体重蛋白质供给量（g/kg · 天）	0.6（0.4－0.8）
蛋白质供给达标率（%）	44（31.2－59）

表 6 展示了在 NEED 外部验证队列中，根据 MIMIC-IV 队列边际结构模型（MSCM）识别出的生理阈值（乳酸 2 mmol/L、去甲肾上腺素 0.3 μg/kg/min、肌酐 5 mg/dL）进行分层后，首周平均热量达标率与蛋白达标率（每提高 10%）与 28 天死亡风险之间的 Cox 回归分析结果。

在总体人群中，热量与蛋白达标率均与 28 天死亡风险显著负相关，且在调整年龄、性别、疾病严重程度等混杂因素后仍保持统计学意义。分层分析显示，当乳酸 <2 mmol/L 或去甲肾上腺素 <0.3 μg/kg/min 时，充分达标的热量与蛋白供给与死亡风险下降显著相关；而在乳酸 ⩾ 2 mmol/L 或去甲肾上腺素 ⩾ 0.3 μg/kg/min 的患者中，该保护效应不再显著。同样，在肌酐 <5 mg/dL 的患者中，蛋白达标率与死亡风险降低显著相关，而在肌酐 ⩾ 5 mg/dL 人群中未观察到统计学意义。表 6 基于 MIMIC-IV 队列识别的生理阈值窗口在 NEED 队列中的分层 Cox 回归分析结果

	未校正协变量			校正协变量		
	HR	95% CI	P	HR	95% CI	P
总人群（n=1322）						
热量达标率（per 10%）	0.918	0.868-0.970	0.002	0.930	0.877-0.987	0.017
蛋白达标率（per 10%）	0.899	0.836-0.967	0.004	0.912	0.843-0.986	0.021
亚组分析						
乳酸浓度<2mmol/L(n=729)						
热量达标率（per 10%）	0.891	0.821-0.967	0.006	0.887	0.811-0.970	0.009
蛋白达标率（per 10%）	0.865	0.777-0.964	0.008	0.855	0.760-0.962	0.010
乳酸浓度≥2mmol/L(n=593)						
热量达标率（per 10%）	0.956	0.887-1.031	0.245	0.969	0.895-1.049	0.434
蛋白达标率（per 10%）	0.949	0.859-1.047	0.296	0.964	0.868-1.071	0.494
等价去甲<0.3μg/kg/min(n=1138)						
热量达标率（per 10%）	0.911	0.854-0.971	0.004	0.911	0.851-0.976	0.008
蛋白达标率（per 10%）	0.889	0.817-0.968	0.007	0.885	0.809-0.969	0.008
等价去甲≥0.3μg/kg/min(n=184)						
热量达标率（per 10%）	1.009	0.901-1.130	0.876	0.999	0.883-1.130	0.985
蛋白达标率（per 10%）	1.025	0.881-1.192	0.747	1.021	0.865-1.206	0.804
肌酐浓度<5mg/dL(n=1275)						
蛋白达标率（per 10%）	0.896	0.832-0.966	0.004	0.906	0.836-0.982	0.016
肌酐浓度≥5mg/dL(n=47)						
蛋白达标率（per 10%）	1.053	0.764-1.452	0.754	1.026	0.702-1.501	0.893

4. 讨论

本章在前述亚型分析基础上，进一步从动态生理状态角度出发，探讨在真实 ICU 场景中是否存在可重复、可推广的营养获益窗口。基于 MIMIC 纵向数据，在控制时间依赖性混杂因素的前提下，我们采用边缘结构模型系统评估持续维持较高营养达标率对 28 天死亡风险的影响。结果显示，在总体人群中，充分达标的能量与蛋白摄入均与死亡风险显著下降相关。然而，这种生存获益并非在所有生理状态下均保持稳定。分层分析进一步揭示，营养获益具有明确的窗口特征：当等价去甲肾上腺素使用量 <0.3μg/kg/min，乳酸 <2 mmol/L 时，充分能量与蛋白达标所带来的死亡风险降低效应得以保留；而在循环灌注不足或组织缺氧明显的高应激状态下，该获益减弱甚至消失。对于蛋白摄入而言，在肾功能严重受损（肌酐≥ 5 mg/dL）时，提高蛋白达标率的生存优势不再显著，提示代谢耐受性可能是蛋白强化策略安全性的关键前提。尽管 NEED 队列的数据结构与 MIMIC-IV 存在一定差异，其中 NEED 队列主要基于基线临床特征并采用 Cox 比例风险模型进行分析，而 MIMIC-IV 则利用纵向数据并通过边际结构模型控制时间依赖性混杂因素，但两种分析策略所得结果在方向上保持一致，均提示在循环灌注相对稳定的患者中，充分营养摄入与更低的死亡风险相关。

NUTRIREA-2 等大型 RCT 指出，在血流动力学不稳定或需较高剂量血管活性药物支持的患者中，积极推进至全量喂养并未优于保守策略，且更易发生胃肠道不耐受及相关并发症 [5, 10]。这与本研究在高去甲肾上腺素剂量亚组中未观察到显著收益的结果相一致。本研究观察到的异质性可能反映了组织灌注与肾功能状态对营养干预效果的调节作用。循环状态是营养耐受性的关键因素，低剂量去甲肾上腺素支持提示组织灌注尚可，肠道吸收与利用能力相对保留。但当血管活性药物剂量升高时，提示存在显著循环功能障碍及肠系膜缺血风险，外源性营养难以被充分吸收，甚至可能加重肠道负担和代谢紊乱，此时推进达标喂养可能难以转化为实际生理收益 [11, 12]。蛋白摄入在血肌酐 <5mg/dL 时对生存获益更为稳定，可能与肾功能状态对氮代谢负荷的调控能力密切相关。在肾功能相对保留的情况下，机体能够有效清除蛋白代谢产生的含氮废物，维持内环境稳定，从而使充足蛋白供给更有利于抑制分解代谢、促进肌肉蛋白合成与组织修复，并改善免疫功能与整体恢复能力。相反，在肌酐显著升高提示肾功能严重受损时，氮代谢产物清除能力下降，过量蛋白摄入可能加重尿素氮蓄积、酸碱失衡及代谢负担，甚至增加肾替代治疗需求，从而削弱甚至抵消其潜在获益。

然而，本研究仍存在若干局限。首先，MIMIC-IV 数据主要来源于单中心回顾性数据库，其营养实践模式可能受到当地临床习惯的影响；而 NEED 队列虽然提供了外部验证，但由于缺乏完整的纵向喂养数据，无法完全复现 MSCM 分析框架，因此两队列之间的方法学差异可能影响结果的直接可比性。此外，本研究所识别的阈值主要基于观察性数据推断，尚不能完全等同于因果性的临床干预阈值，未来仍需通过前瞻性研究或随机对照试验进一步验证。

5. 结论

本章基于 MIMIC 纵向数据，采用边缘结构模型控制时间依赖性混杂因素，评估了热量与蛋白达标率对 28 天死亡风险的影响。结果显示，充分达标与死亡风险下降显著相关，但其获益呈现明确的生理窗口特征：当去甲肾上腺素使用量 <0.3 μg/kg/min、乳酸 <2 mmol/L 时，热量与蛋白达标带来的生存获益得以保留；其中，蛋白摄入在肌酐 <5 mg/dL 时表现出更为稳定的获益。上述结果在 NEED 队列中得到一致验证，提示在临床实践中可基于循环与代谢相关指标识别相对安全且具有潜在生存优势的营养干预窗口，为后续构建动态个体化决策模型提供重要的阈值依据。

参考文献

[1] NDAHIMANA D, KIM E K. Energy Requirements in Critically Ill Patients [J]. 2018, 7(2): 81-90.

[2] MCCLAVE S A, TAYLOR B E, MARTINDALE R G, et al. Guidelines for the provision and assessment of nutrition support therapy in the adult critically ill patient: Society of Critical Care Medicine (SCCM) and American Society for Parenteral and Enteral Nutrition (ASPEN) [J]. JPEN Journal of parenteral and enteral nutrition, 2016, 40(2): 159-211.

[3] SINGER P, BLASER A R, BERGER M M, et al. ESPEN guideline on clinical nutrition in the intensive care unit [J]. Clinical nutrition (Edinburgh, Scotland), 2019, 38(1): 48-79.

[4] FAISY C, LEROLLE N, DACHRAOUI F, et al. Impact of energy deficit calculated by a predictive method on outcome in medical patients requiring prolonged acute mechanical ventilation [J]. British journal of nutrition, 2008, 101(7): 1079-87.

[5] GINER M, LAVIANO A, MEGUID M M, et al. In 1995 a correlation between malnutrition and poor outcome in critically ill patients still exists [J]. Nutrition, 1996, 12(1): 23-9.

[6] WEIJS P J, LOOIJAARD W G, BEISHUIZEN A, et al. Early high protein intake is associated with low mortality and energy overfeeding with high mortality in non-septic mechanically ventilated critically ill patients [J]. Critical care, 2014, 18(6): 701.

[7] KLEIN C J, STANEK G S, WILES III C E. Overfeeding macronutrients to critically ill adults: metabolic complications [J]. Journal of the American Dietetic Association, 1998, 98(7): 795-806.

[8] YATABE T. Strategies for optimal calorie administration in critically ill patients [J]. Journal of Intensive Care, 2019, 7(1): 15.

[9] REIGNIER J, BOISRAM -HELMS J, BRISARD L, et al. Enteral versus parenteral early nutrition in ventilated adults with shock: a randomised, controlled, multicentre, open-label, parallel-group study (NUTRIREA-2) [J]. The Lancet, 2018, 391(10116): 133-43.

[10] PARDO E, LESCOT T, PREISER J-C, et al. Association between early nutrition support and 28-day mortality in critically ill patients: the FRANS prospective nutrition cohort study [J]. Critical Care, 2023, 27(1): 7.

[11] REIGNIER J, PLANTEF VE G, MIRA J-P, et al. Low versus standard calorie and protein feeding in ventilated adults with shock: a randomised, controlled, multicentre, open-label, parallel-group trial (NUTRIREA-3) [J]. The Lancet Respiratory Medicine, 2023, 11(7): 602-12.

[12] BENDAVID I, SINGER P. Nutrition During Prolonged Hemodynamic Instability [M]. Critical Care Nutrition Therapy for Non-nutritionists. Springer. 2017: 15-28.

[13] LIM H S, GONZ LEZ-COSTELLO J, BELOHLAVEK J, et al. Hemodynamic management of cardiogenic shock in the intensive care unit [J]. The Journal of Heart and Lung Transplantation, 2024, 43(7): 1059-73.

[14] AL-DIERY H, PHILLIPS A, EVENNETT N, et al. The pathogenesis of nonocclusive mesenteric ischemia: implications for research and clinical practice [J]. Journal of intensive care medicine, 2019, 34(10): 771-81.

[15] YANG S, WU X, YU W, et al. Early enteral nutrition in critically ill patients with hemodynamic instability: an evidence - based review and practical advice [J]. Nutrition in Clinical Practice, 2014, 29(1): 90-6.

[16] ZUSMAN O, THEILLA M, COHEN J, et al. Resting energy expenditure, calorie and protein consumption in critically ill patients: a retrospective cohort study [J]. Critical care, 2016, 20(1): 367.

[17] SINGER P, BLASER A R, BERGER M M, et al. ESPEN guideline on clinical nutrition in the intensive care unit [J]. Clinical nutrition, 2019, 38(1): 48-79.

类别 :// 基础研究：涉及重症相关问题的基础研究

基于单细胞转录组学细胞间通讯分析机械通气相关肺纤维化中成纤维细胞与肺泡上皮细胞的时空交互

姓名：黄晰，冯金华，杨辛夷，梅舒雅，皋源，何征宇

单位：上海交通大学医学院附属仁济医院

机械通气（mechanical ventilation, MV）是急性呼吸窘迫综合征及呼吸衰竭患者的重要生命支持手段。然而，长期或不恰当的机械通气可诱发肺纤维化进程，导致机械通气相关肺纤维化（mechanical ventilation-induced pulmonary fibrosis, MVPF）的发生与发展。目前，MVPF 的细胞与分子机制尚未完全阐明。肺纤维化的发生主要涉及肺泡上皮细胞反复微损伤所引发的异常修复反应及上皮功能障碍，同时伴随成纤维细胞 / 肌成纤维细胞的异常活化、增殖与分化，最终导致细胞外基质（extracellular matrix, ECM）过度沉积。其中，肺成纤维细胞的异常激活被认为是肺纤维化发生与进展的核心病理事件。因此，明确病理性成纤维细胞的来源及其调控机制，对于揭示 MVPF 的分子基础并开发潜在干预策略具有重要意义。

1. 采用高潮气量机械通气建立小鼠 MVPF 模型：MV 组小鼠接受机械通气 2 小时（潮气量 20 ml/kg，呼吸频率 70 次 / 分钟），对照组仅行气管插管处理。2. 收集对照组与 MV 组小鼠肺组织进行单细胞转录组测序：基于 10x Genomics 平台开展单细胞 RNA 测序，以表征细胞异质性及谱系动态变化；进一步结合轨迹推断和 CellChat 细胞间通讯分析等计算方法，解析肺泡上皮细胞与成纤维细胞之间的时空互作关系。通过上述分析筛选出关键的信号通路及配体 – 受体相互作用，并结合实验验证对其进行进一步整合分析。

1. 单细胞转录组揭示机械通气诱导的 ECM 重塑增强：我们首先通过单细胞 RNA 测序分析机械通气条件下肺组织的细胞组成。UMAP 降维结果显示，对照组与 MV 组中均可鉴定出多种细胞类型，包括肺泡上皮细胞（AT1、AT2）、成纤维细胞、内皮细胞及多种免疫细胞等（图 1A–B）。我们进一步通过经典 marker 基因表达验证了细胞注释的准确性（图 1C）。随后我们利用通过细胞外基质重塑评分（ECM remodeling score）评估了各细胞类型的纤维化相关功能状态；结果显示成纤维细胞具有最高的 ECM 重塑活性，同时部分上皮细胞也表现出明显的 ECM 相关基因表达（图 1D–E）。与对照组相比，MV 组整体 ECM remodeling score 显著升高（图 1F）。在细胞类型水平分析中发现，该升高不仅存在于成纤维细胞中，在肺泡上皮细胞等多种细胞类型中亦显著增强（图 1G）。上述结果提示，机械通气可诱导多细胞参与的 ECM 重塑过程，以及上皮 - 间质的相互作用在 MVPF 发生发展中发挥了重要作用。

2. 机械通气重塑细胞间通讯并促进上皮 - 成纤维细胞促纤维化信号传递：通过 CellChat 分析发现，与对照组相比，MV 组细胞间相互作用的数量及强度均显著增加，提示机械通气显著增强肺组织内的细胞通讯网络（图 2A）。信号通路分析显示，多种与纤维化相关的通路（如 COLLAGEN、FN1、TGFb 等 ECM 相关通路）在 MV 组显著增强，表明 MV 后肺组织微环境向促纤维化状态转变（图 2B）。我们随后选择了 COLLAGEN 相关的细胞间通讯通路来进一步阐明 MVPF 过程中的 ECM 重塑。我们通过分析细胞通讯角色发现，成纤维细胞、间皮细胞和上皮干细胞是胶原蛋白的主要细胞信号来源，而肺泡上皮细胞（AECs，包括 AT1 和 AT2）也参与了 COLLAGEN 信号网络（图 2C-D）。此外，肺泡上皮细胞和成纤维细胞均在 COLLAGEN 信号网络中具有很强的自分泌信号（图 2E）。我们还分析了该通路中不同细胞类型中配体和受体的相对表达水平（图 2F），并展示了不同细胞类型中贡献最大的配体 - 受体（Col1a1 - Itga1 + Itgb1）的相互作用（图 2G）。最后我们利用散点图全面说明了 MV 组肺组织中不同细胞类型间 ECM 相关通路输入和输出的相互作用强度；我们发现成纤维细胞表现出最高水平的输入和输出相互作用强度，表明它们在纤维化网络中充当中心枢纽的重要作用。AECs（尤其是 AT2）也表现出显著的相互作用强度，进一步提示了肺泡上皮细胞在 MVPF 期间 ECM 重塑和上皮 - 间质相互作用中的积极作用。综上，机械通气通过重塑细胞间通讯网络，促进肺泡上皮细胞与成纤维细胞的信号传递，从而推动了 MVPF 的进展。

3. 拟时序轨迹分析揭示 MVPF 进程中上皮细胞与成纤维细胞的动态转变：为进一步阐明纤维化进展过程中上皮细胞与成纤维细胞之间的动态关系，我们采用 Monocle2 算法对单细胞转录组数据中的上皮与间质区室进行了拟时序轨迹分析。结果显示，存在一条清晰的拟时序演变轨迹，其起始于 AT2 细胞，并逐步向成纤维细胞群体过渡（图 3A）。在该过程中，伴随着上皮 – 间质转化（epithelial–mesenchymal transition, EMT）相关标志基因（如 Vim、Fn1）的逐渐上调，提示上皮细胞在纤维化进展中向间质表型转变的趋势（图 3B-C）。值得注意的是，这一动态变化与前述细胞间通讯分析中观察到的 AT2 细胞与成纤维细胞之间增强的细胞外基质（extracellular matrix, ECM）相关信号通路相一致。综上，该结果从轨迹动态角度支持了 MVPF 过程中肺泡上皮细胞与成纤维细胞之间存在连续且协调的相互作用过程。

4. 单细胞分析揭示成纤维细胞的异质性及其促纤维化亚群特征：为明确特定成纤维细胞亚群在 MVPF 中的作用，我们对单细胞转录组数据中的成纤维细胞群体进行了再分群分析。结果显示，成纤维细胞可划分为多个具有差异性转录特征的亚群（图 4A），提示其存在显著的细胞异质性。基于 marker 基因表达分析，不同亚群呈现出差异化的功能特征，包括基质生成相关亚群及增殖相关亚群等。其中，部分亚群高表达细胞外基质 ECM 相关基因，提示其可能在纤维化过程中发挥关键作用（图 4B）。进一步分析发现，$Pdgfra^+$ 和 $Col14a1^+$ 成纤维细胞在 ECM 重塑相关通路中呈现显著激活状态（图 4C），提示其可能是驱动纤维化进程的重要效应细胞群体。功能评分结果进一步表明，与对照组相比，MV 组中多种成纤维细胞亚群在纤维化相关通路（包括 TGF-β 信号通路、上皮 – 间质转化及炎症反应）上的活性显著增强

（图 4D）。值得注意的是，Pdgfra^{+} 和 Col14a1^{+} 成纤维细胞在 EMT 相关过程中亦表现出更高的活化水平，提示其在成纤维细胞 - 上皮通讯以及纤维化进展中可能发挥重要的调控作用。综上所述，成纤维细胞在 MVPF 中呈现出显著的异质性，其中以 Pdgfra^{+} 和 Col14a1^{+} 成纤维细胞为代表的促纤维化亚群的扩增及功能激活，可能是驱动 MVPF 进展的重要机制。

本研究基于单细胞转录组学系统解析了机械通气相关肺纤维化的细胞图谱及其动态变化。结果表明，机械通气通过增强细胞外基质重塑及上皮细胞向成纤维细胞的信号传递，促进肺组织纤维化进展。拟时序分析提示上皮细胞在成纤维细胞活化过程中具有持续贡献，而成纤维细胞亚群分析进一步揭示其显著异质性，并鉴定出以 Pdgfra^{+} 和 Col14a1^{+} 为代表的促纤维化关键效应细胞群体。这些亚群在 ECM 重塑及纤维化相关通路中表现出显著活化状态。综上，本研究揭示了上皮 – 成纤维细胞相互作用及成纤维细胞异质性在机械通气相关肺纤维化中的关键作用，为靶向特定成纤维细胞亚群及其上游调控信号提供了潜在干预策略。

类别 :// 临床研究：设计规范的各类临床研究及研究方案报告

脓毒症患者淋巴细胞数目与出院后健康相关生活质量相关：一项多中心研究

姓名：廖梓怀，刘巧焓，顾彬，管向东，吴健锋，裴飞

单位：中山大学附属第一医院

随着脓毒症院内死亡率下降，脓毒症患者出院后的健康相关生活质量（health-related quality of life, HRQOL）受损日益受到关注。2026 年拯救脓毒症运动指南已将改善脓毒症出院后 HRQOL 作为脓毒症全程管理的重要目标。脓毒症诱导的免疫功能障碍不仅与短期死亡相关，还可能通过持续炎症、继发感染易感性增加及恢复迟缓等途径影响远期功能恢复。然而，常用免疫功能与脓毒症出院患者 HRQOL 之间的关系缺乏直接证据，最佳评估时间点尚不明确。

本研究基于一项全国多中心 RCT 研究（TESTS 试验）的二次分析，排除住院期间死亡、90 天时仍住院、90 天 SF-36 缺失及可能影响生活质量评估的患者后，共纳入 661 例脓毒症出院患者。采集研究入组的基线、第 7 天和第 14 天检测淋巴细胞数目（ALC）、单核细胞 HLA-DR（mHLA-DR）和中性粒细胞 / 淋巴细胞比值（NLR），并于第 90 天采用 SF-36 评估 HRQOL，包括躯体健康总分（PCS）和心理健康总分（MCS）。采用相关性分析比较不同时间点免疫指标与 HRQOL 的关系，采用广义线性模型评估第 7 天免疫指标与 90 天 HRQOL 的独立关联，并通过 Logistic 回归、有序 Logistic、交互作用分析及亚组分析验证结果稳健性。

90 天生存组与死亡组的 ALC、mHLA-DR 和 NLR 动态变化存在显著差异。基线时，仅部分免疫指标与 90 天 HRQOL 相关。第 7 天和第 14 天，ALC、mHLA-DR 和 NLR 均与 90 天 HRQOL 显著相关（$P < 0.05$）。鉴于第 7 天已呈现与第 14 天相似的结果，且时间上更早，因此后续分析聚焦第 7 天。在 90 天存活患者中，第 7 天 ALC 与 PCS 独立正相关（RR=1.031，95%CI 1.000–1.063，P=0.047），年龄和第 7 天 SOFA 评分也与 PCS 独立相关；mHLA-DR 和 NLR 与 PCS 无显著关联。MCS 模型中，仅第 7 天 SOFA 评分与 MCS 独立相关。敏感性分析显示，第 7 天 ALC 与较低的 90 天躯体健康受损风险相关（OR=0.465，95%CI 0.215–0.920，P=0.042）。将 90 天前死亡作为竞争事件后，该关联仍显著（SHR=0.548，95%CI 0.330–0.910，P=0.020）。未观察到年龄或第 7 天 SOFA 评分对 ALC 与 PCS 关联的显著修饰作用，P for interaction 分别为 0.709 和 0.521，亚组分析结果总体一致。

在脓毒症出院患者中，脓毒症第 7 天淋巴细胞数目与远期躯体健康相关生活质量独立相关。第 7 天可能是评估免疫状态与远期 HRQOL 关系的合适时间点。这一发现为脓毒症出院患者的长期管理提供理论依据。

类别 :// 临床研究：设计规范的各类临床研究及研究方案报告

脓毒症患者入 ICU 24 h 内的糖皮质激素使用与 28 d 死亡率的队列研究

姓名：徐继前、王维、姚璐、 陈湘、尚游 *

单位：华中科技大学同济医学院附属协和医院

摘要

目的 探讨脓毒症患者入住 ICU 后 24 h 内糖皮质激素（glucocorticoids，GC）累积剂量与 28 d 全因死亡率之间的关系，为脓毒症患者 GC 治疗剂量优化提供临床依据。

方法 基于重症监护医学信息数据库IV（Medical Information Mart for Intensive Care IV，MIMIC-IV）开展回顾性队列研究。纳入符合 Sepsis-3 诊断标准且年龄≥ 18 岁的脓毒症患者，根据入 ICU 后 24 h 内 GC 累积剂量（氢化可的松当量）分为未使用 GC 组、0 ～ 300 mg 组、300 ～ 800 mg 组、800 ～ 1200 mg 组及＞ 1200 mg 组。采用限制性立方样条（restricted cubic spline，RCS）分析 GC 剂量与 28 d 死亡风险之间的非线性关系，并采用多因素 Logistic 回归、倾向评分匹配（propensity score matching，PSM）及逆概率加权（inverse probability of treatment weighting，IPTW）进行敏感性分析。

结果 共纳入 20 672 例脓毒症患者，其中 2 548 例接受 GC 治疗。RCS 分析显示，GC 累积剂量与 28 d 死亡率呈显著非线性关系（P ＜ 0.001）。多因素 Logistic 回归分析显示，与未使用 GC 相比，800 ～ 1200 mg 组 28 d 死亡风险最低（OR ＝ 0.55，95%CI：0.35 ～ 0.82，P ＝ 0.005）。PSM 及 IPTW 分析结果与主分析一致。亚组分析提示，该关联在年龄＜ 65 岁、SOFA 评分＞ 10 分、合并肝脏疾病及未使用血管活性药物患者中更为明显。

结论 脓毒症患者早期 GC 累积剂量与 28 d 死亡率呈非线性关系。氢化可的松当量 800 ～ 1200 mg 可能与较低死亡风险相关，为优化脓毒症 GC 个体化治疗策略提供了参考依据。

1 引言

脓毒症是感染诱导的宿主反应失调导致的危及生命的器官功能障碍，也是 ICU 患者死亡的重要原因之一 [1-3]。糖皮质激素（glucocorticoids，GC）具有抗炎、免疫调节及维持血流动力学稳定等作用，是脓毒性休克的重要辅助治疗药物。目前国际指南推荐，对于持续需要血管活性药物支持的脓毒性休克患者，可给予氢化可的松 200 mg/d[4, 5]。然而，多项随机对照研究对于 GC 能否改善患者长期预后仍存在争议。APROCCHSS[6] 研究显示，氢化可的松联合氟氢可的松能够降低 90 d 死亡率，而 ADRENAL[7] 及 CORTICUS[8] 研究虽然证实 GC 可加快休克逆转，却未观察到明显的长期生存获益。这些争议可能源于不同研究之间 GC 制剂种类、给药时机、治疗持续时间及患者疾病严重程度存在显著差异。

近年来研究发现，GC 疗效可能具有明显的剂量依赖性。低剂量 GC 可能不足以抑制过度炎症反应，而过高剂量则可能增加感染、代谢紊乱及免疫抑制等风险 [9, 10]。早期 GC 剂量与患者预后之间是否存在最佳剂量区间，仍缺乏充分证据。目前多数研究主要比较是否应用 GC，而较少关注不同累积剂量对临床结局的影响。

本研究基于 MIMIC-IV 数据库，分析脓毒症患者入住 ICU 后 24 h 内 GC 累积剂量与 28 d 死亡率之间的关系，并结合限制性立方样条、多因素 Logistic 回归及倾向评分分析评价不同剂量 GC 对患者预后的影响，以期为脓毒症患者 GC 个体化治疗提供循证依据。

2 资料与方法

2.1 研究对象

本研究为回顾性队列研究，数据来源于 MIMIC-IV 3.0 数据库。纳入 2008—2019 年首次入住 ICU、年龄≥ 18 岁且符合 Sepsis-3 诊断标准的脓毒症患者。排除 ICU 住院时间＜ 24 h、长期接受系统性糖皮质激素治疗以及临床资料缺失严重者。最终共纳入 20672 例患者，其中 2548 例于入住 ICU 后 24 h 内接受 GC 治疗。

2.2 资料收集

提取患者人口学资料、生命体征、实验室检查结果、SOFA 评分、器官支持治疗情况及基础疾病等临床信息。所有生命体征和实验室指标均采用入住 ICU 后 24 h 内最异常值进行分析。不同种类 GC 统一换算为氢化可的松当量，并计算入住 ICU 后 24 h 内累积剂量。

2.3 统计学分析

采用限制性立方样条分析 GC 累积剂量与 28 d 死亡率之间的剂量 - 反应关系，根据拟合曲线将 GC 剂量划分为未使用 GC、0 ～ 300 mg、300 ～ 800 mg、800 ～ 1200 mg 及＞ 1200 mg 五组。采用多因素 Logistic 回归分析不同剂量 GC 与 28 d 死亡率之间的关系，并依次建立未调整模型及多因素调整模型。进一步采用 PSM 及 IPTW 进行敏感性分析，以验证研究结果的稳健性。所有统计分析均采用 R 4.4.1 软件完成，以 P ＜ 0.05 为差异具有统计学意义。

3 结果

3.1 研究对象及基线特征

共纳入 20 672 例脓毒症患者，中位年龄为 66 岁〔四分位数间距（interquartile range，IQR）：55 ～ 77 岁〕，其中女性 8 186 例（39.6%），SOFA 评分中位数为 6 分（IQR：4 ～ 9 分）。总体而言，共有 3 189 例患者（15.4%）于入住 ICU 后 28 d 内死亡（表 S3）。

入住 ICU 后 24 h 内，共有 2 548 例患者接受了全身 GC 治疗。与未接受 GC 治疗患者相比，GC 治疗患者疾病严重程度更高，基础合并症及器官支持治疗情况亦存在明显差异。此外，GC 治疗组 28 d 病死率显著高于未治疗组（24.5% vs. 14.2%，P<0.001）（表 S3）。

3.2 糖皮质激素剂量与 28 d 死亡率之间的非线性关联

限制性立方样条（restricted cubic spline，RCS）分析显示，入住 ICU 后 24 h 内 GC 累积剂量（以氢化可的松当量计）与 28 d 死亡率之间呈显著 U 型非线性关系（非线性检验 P<0.001，图 1）。

模型拟合结果显示，死亡风险最低点对应的氢化可的松当量约为 1 088.2 mg，但该数值来源于模型拟合结果，并非预先设定的治疗阈值。为了进一步描述这一非线性剂量 - 反应关系，根据 GC 累积剂量将患者分为 5 组：未使用 GC 组（n=18 124）、0 ～ 300 mg 组（n=1 416）、300 ～ 800 mg 组（n=592）、800 ～ 1 200 mg 组（n=279）以及 >1 200 mg 组（n=261）。各组 28 d 病死率分别为 14.2%、28.6%、16.2%、11.1% 和 31.5%（表 1）。

Kaplan–Meier 生存分析显示，五组患者 28 d 累积生存曲线存在显著差异（总体 Log-rank 检验 P<0.0001）。其中，800 ～ 1 200 mg 组具有最佳生存曲线。然而，与未接受 GC 治疗组进行两两比较时，两组间生存差异未达到统计学意义（Log-rank P=0.276）（图 2）。

3.3 多因素分析

在未调整模型中，0 ～ 300 mg 组和 >1 200 mg 组患者死亡风险均高于未接受 GC 治疗组，而 300 ～ 800 mg 组和 800 ～ 1 200 mg 组与未治疗组相比差异无统计学意义。

在进一步调整人口学特征、疾病严重程度、实验室指标、器官支持治疗及基础疾病等混杂因素后，各剂量组效应发生变化。在完全调整模型中，800 ～ 1 200 mg 组 28 d 死亡风险显著降低（OR=0.55，95%CI：0.35 ～ 0.82，P=0.005）。

相比之下，0 ～ 300 mg 组（OR=1.50，95%CI：1.29 ～ 1.74，P<0.001） 及 >1 200 mg 组（OR=3.03，95%CI：2.24 ～ 4.09，P<0.001）死亡风险仍显著高于未接受 GC 治疗组，而 300 ～ 800 mg 组未观察到统计学显著关联（OR=1.17，95%CI：0.89 ～ 1.51，P=0.248）（表 2）。

3.4 交互作用及亚组分析

共进行了 21 项交互作用检验，其中 9 项交互作用的名义 P 值 <0.05。交互作用最明显的因素包括肝脏疾病、慢性肺部疾病、血管活性药物使用情况及 SOFA 评分分层（交互作用检验均 P<0.001）。此外，年龄、性别、脑血管疾病、社区获得性肺炎及充血性心力衰竭等因素亦观察到显著交互作用（图 S2）。

探索性亚组分析进一步显示，与未接受 GC 治疗相比，800 ～ 1 200 mg 组在以下患者中均表现出更低的 28 d 死亡风险：年龄 <65 岁患者（OR=0.32，95%CI：0.16 ～ 0.58，P<0.001）、男性患者（OR=0.30，95%CI：0.16 ～ 0.55，P<0.001）、合并肝脏疾病患者（OR=0.16，95%CI：0.07 ～ 0.32，P<0.001）、SOFA 评分 >10 分患者（OR=0.20，95%CI：0.09 ～ 0.38，P<0.001）和未使用血管活性药物患者（OR=0.42，95%CI：0.22 ～ 0.73，P<0.001）（图 3 及图 S3）。

3.5 倾向评分敏感性分析

倾向评分匹配（propensity score matching，PSM）及逆概率加权（inverse probability of treatment weighting，IPTW）分析结果与主分析一致（表 S4 ～ S7）。

在 PSM 队列中，800 ～ 1 200 mg 组仍与较低 28 d 死亡风险显著相关（OR=0.51，95%CI：0.28 ～ 0.92，P=0.027；表 S8）；IPTW 分析亦获得一致结果（OR=0.48，95%CI：0.26 ～ 0.89，P=0.021；表 S9）。

此外，0 ～ 300 mg 组及 >1 200 mg 组在两种敏感性分析中仍表现为较高死亡风险，而 300 ～ 800 mg 组仍未观察到稳定的统计学关联（表 S8、表 S9）。

4 结论

脓毒症患者入住 ICU 后 24 h 内 GC 累积剂量与 28 d 死亡率呈显著非线性关系，其中氢化可的松当量 800 ～ 1200 mg 与较低死亡风险相关。研究结果提示，GC 治疗可能存在最佳剂量窗口，合理优化早期给药剂量有望改善患者预后。未来仍需高质量前瞻性研究进一步验证最佳剂量范围及适用人群，为脓毒症 GC 精准治疗提供更充分的循证医学证据。

Table 2. Association between early cumulative glucocorticoid dose and 28-day mortality

Dose group	Model 1		Model 2		Model 3	
	OR (95%CI)	*P* value	OR (95%CI)	*P* value	OR (95%CI)	*P* value
0-300 mg	2.43 (2.15-2.75)	<0.001	1.51 (1.309-1.74)	<0.001	1.50 (1.29-1.74)	<0.001
300-800 mg	1.17 (0.94-1.46)	0.158	1.31 (1.00-1.69)	0.043	1.17 (0.89-1.51)	0.248
800-1200 mg	0.76 (0.51-1.09)	0.149	0.53 (0.34-0.78)	0.002	0.55 (0.35-0.82)	0.005
>1200 mg	3.30 (2.54-4.26)	<0.001	3.14 (2.33-4.21)	<0.001	3.03 (2.24-4.09)	<0.001

Abbreviations: CI=confidence interval; OR=odds ratio.

The no-GC group was the reference. Model 1 was unadjusted. Model 2 adjusted for demographics, severity scores, laboratory measurements, and organ-support therapies. Model 3 additionally adjusted for comorbidities.

Model 1: steroid;

Model 2: Model 1+age+gender+SOFA score+SAPS II score+APS III score+LODS score+OASIS score+SIRS score+Mechanical ventilation+Vasopressor+CRRT+Creatinine+WBC+lactate+HB+BUN+PT+APTT+INR;

Model 3: Model 2+metastatic solid tumor+cerebrovascular disease+congestive heart failure+renal disease+chronic pulmonary disease+liver disease+myocardial infarct+diabetes.

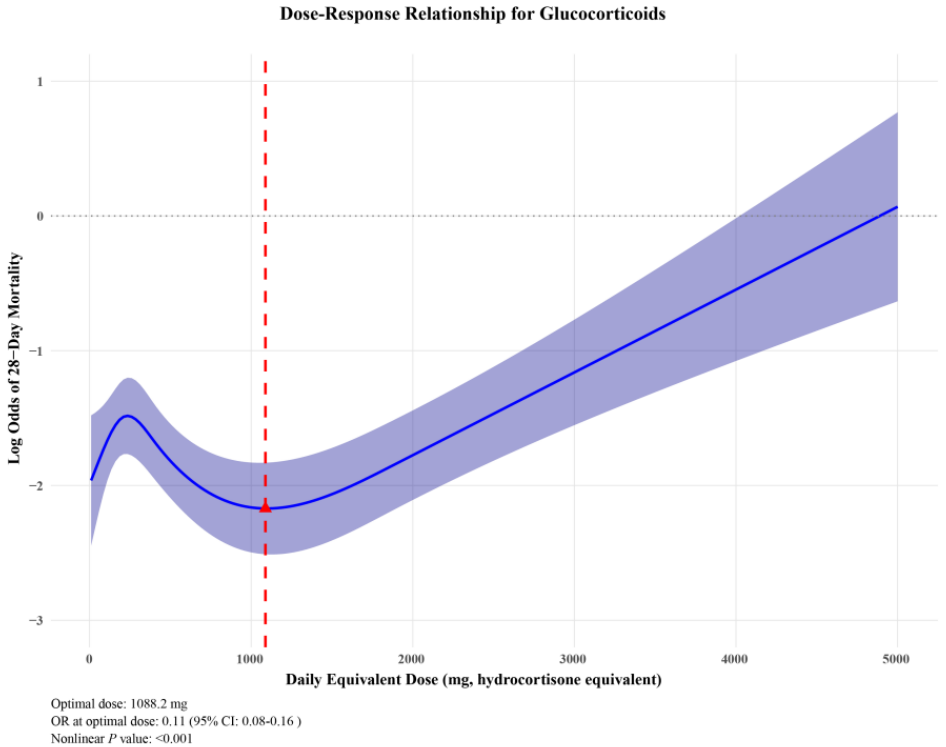


Figure 1. Dose-response curve for early glucocorticoid dose and 28-day mortality. Adjusted for demographics, severity scores, laboratory measurements, organ-support therapies, and comorbidities. Shaded area represents 95% CI.

脓毒症凝血动态轨迹识别及基于组学的分子内型特征研究

姓名：曹媛，王敏，王承瑾，康红军

单位：中国人民解放军总医院第一医学中心

摘要

背景：脓毒症诱导性凝血病（sepsis-induced coagulopathy，SIC）是脓毒症患者器官功能障碍与不良预后的重要环节。当前 SIC/DIC 评分体系以血小板计数、国际标准化比率（INR）与序贯器官功能衰竭评估（SOFA）评分在单一时间点的组合赋分实现二分类判别，本质上是横断面的，难以刻画凝血功能在 ICU 早期数日内的演变方向；同时，脓毒症人群在凝血反应上具有显著异质性，基于横断面定义的分层方式可能掩盖了不同凝血演变模式所对应的分子机制差异。

目的：本研究旨在基于入 ICU 早期多项凝血指标的纵向轨迹识别脓毒症患者的凝血轨迹亚表型。进一步利用全血转录组与血浆蛋白质组层面刻画 SIC 状态及各凝血轨迹亚表型的分子内型特征，最终从差异蛋白中筛选具有临床转化潜力的 SIC 候选生物标志物。

方法：开发队列来源于中国多中心脓毒症多组学数据库（The Chinese Multi-omics Advances In Sepsis，CMAISE）的脓毒症患者 1327 例；验证队列来源于 ZiGong 数据库的 2790 例危重症感染患者。提取入 ICU 后第 1—5 天的血小板计数、INR、活化部分凝血活酶时间（APTT）、凝血酶时间（TT）及 D- 二聚体，经 Z 分数标准化后，构建组基多轨迹模型（GBMTM），采用共识聚类及 AIC、BIC、SABIC、熵值与对数似然确定最佳亚表型数，并在验证队列中进行外部验证。采用 XGBoost 建立基于基线特征的亚表型预测模型并以 SHAP 值评估特征重要性，以 Kaplan-Meier 曲线比较 30 天预后。组学分析中，全血转录组采用 dream 线性混合效应模型进行差异分析；血浆蛋白质组基于 Olink 邻位延伸分析（PEA）平台，经 OlinkAnalyze 质控后以线性混合效应模型分析。功能富集采用 GO、KEGG、Reactome 过表达分析及基因集富集分析（GSEA）；采用 STRING 构建蛋白质相互作用（PPI）网络，以 Boruta 算法筛选特征并以 ROC 曲线下面积（AUC）评估单变量预测效能。

结果：开发队列最终纳入 971 例患者（2698 患者日），验证队列纳入 555 例。共识聚类与模型拟合指标一致支持亚表型数 K=4；K=4 时各亚表型的平均后验概率均高于 0.94，以 prob>0.7 为标准的分类占比均超过 90%。四个亚表型分别为：Class 1（n=54，5.6%）以严重血小板减少与 APTT 显著延长为特征；Class 2（n=122，12.6%）以高 D- 二聚体与高 INR 为特征，提示持续性凝血 - 纤溶失衡；Class 3（n=380，39.1%）与 Class 4（n=415，42.7%）凝血功能相对稳定。四个亚表型的 ICU 期间 SIC 发生率（75.9%、90.2%、71.3%、32.0%）与住院死亡率（29.6%、27.0%、15.3%、5.1%）差异均有统计学意义（均 P<0.001），开发队列与验证队列的 30 天生存曲线趋势一致（P<0.0001）。组学子队列中转录组匹配 730 例（1891 样本），蛋白质组匹配 136 例（364 样本）。转录组共检出 77 个 SIC 相关差异表达基因，上调基因包括 CD177、MMP8、ADAMTS3 与 TIMP4 等；GSEA 提示染色体分离及有丝分裂相关通路在 SIC 中激活，而 T 细胞受体信号、抗原加工与呈递、血小板活化及内皮细胞迁移通路受抑。蛋白质组显示 SIC 中 IL-6、IL-10、CXCL8、CSF3、SIGLEC10 及 PLAUR（uPAR）等显著上调，EGF、PDGFB、ANGPT1、HGF 及 MPIG6B 等显著下调；Reactome 富集分别指向白介素信号与纤维蛋白凝块溶解通路，以及血小板活化、信号转导与聚集和止血通路。跨组学配对分析显示蛋白与 mRNA 变化量呈显著正相关（$r = 0.417$，$P = 1.16 \times 10^{-5}$），总体方向一致率为 67%，其中 PLAUR 呈现蛋白显著升高而 mRNA 基本不变的解耦模式。各亚表型与 Class 4 比较的差异蛋白数量随凝血损伤程度递增，PLAUR 在所有涉及 Class 4 的比较中均为关键差异蛋白。Boruta 算法确认 CXCL8、PLAUR、FCAR、FSTL3 等为重要特征，8 个代表性候选标志物的 AUC 均超过 0.69，其中 PLAUR 的 AUC 为 0.739。

结论：基于五项凝血指标纵向轨迹构建的 GBMTM 可将脓毒症患者稳定划分为四个凝血轨迹亚表型，该分型在独立队列中得到外部验证，并与 ICU 期间 SIC 发生率及 30 天预后显著相关。转录组与蛋白质组分析显示，SIC 状态及凝血损伤较重的亚表型共同表现为固有免疫过度激活、适应性免疫受抑与血小板 - 内皮信号耗竭；PLAUR（suPAR）在蛋白与 mRNA 层面呈现解耦特征，且与凝血轨迹分型稳定关联，是本研究中最具临床转化潜力的候选生物标志物。

关键词：脓毒症；脓毒症诱导性凝血病；轨迹分析；亚表型；转录组学；蛋白质组学；可溶性尿激酶型纤溶酶原激活物受体

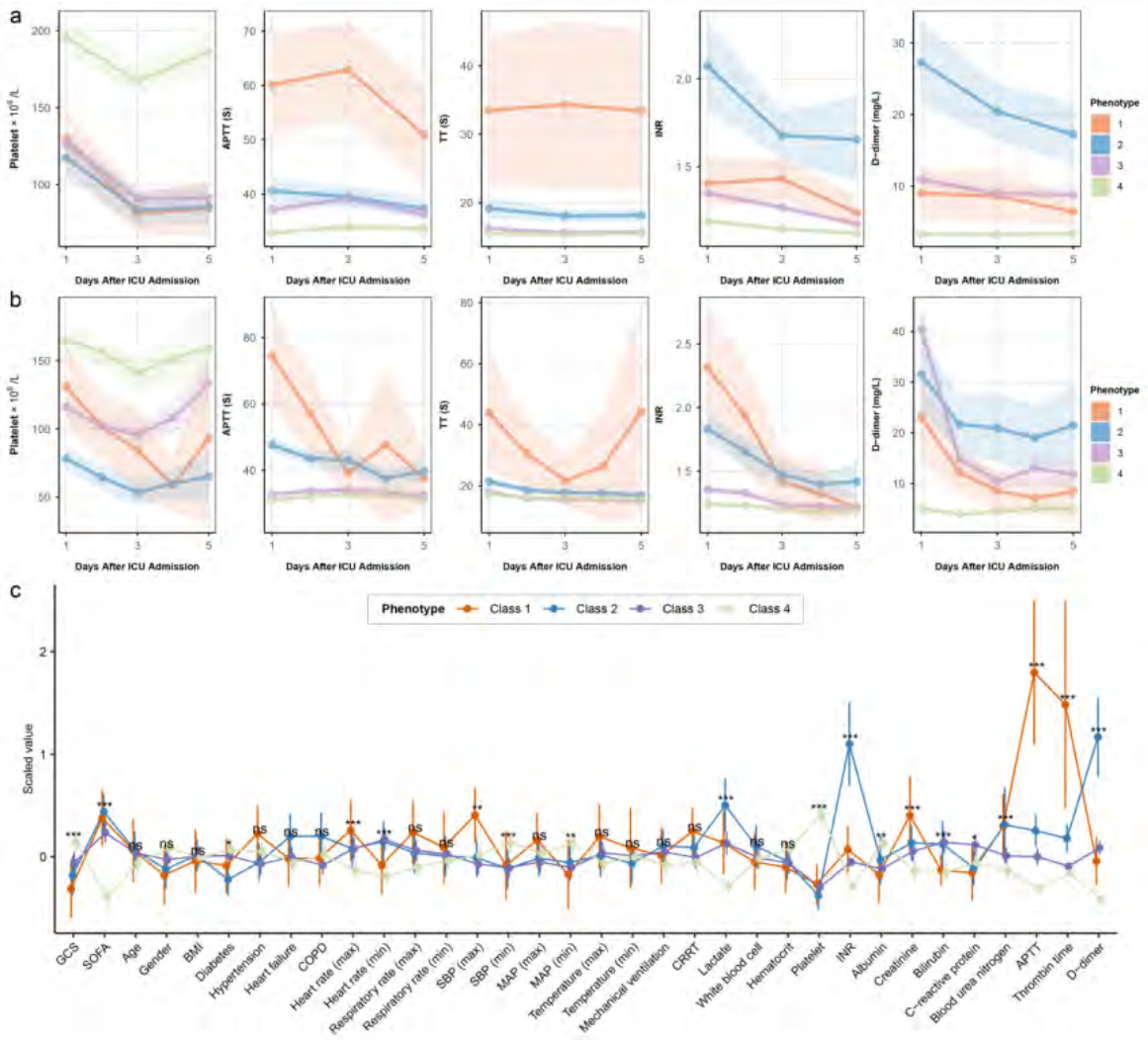


图 1 凝血轨迹亚型图及其基线特征图。a，开发队列中凝血指标轨迹图；b，验证队列中凝血指标轨迹图；c，开发队列中不同亚型的基线特征图。ns，无显著性；*，P<0.05；**，P<0.01；***，P<0.001。缩写：APTT，活化部分凝血活酶时间；TT，凝血酶时间；INR，国际标准化比率；GCS，Glasgow 昏迷评分；SOFA，序贯器官功能衰竭评估；COPD，慢性阻塞性肺疾病；SBP，收缩压；MAP，平均动脉压。

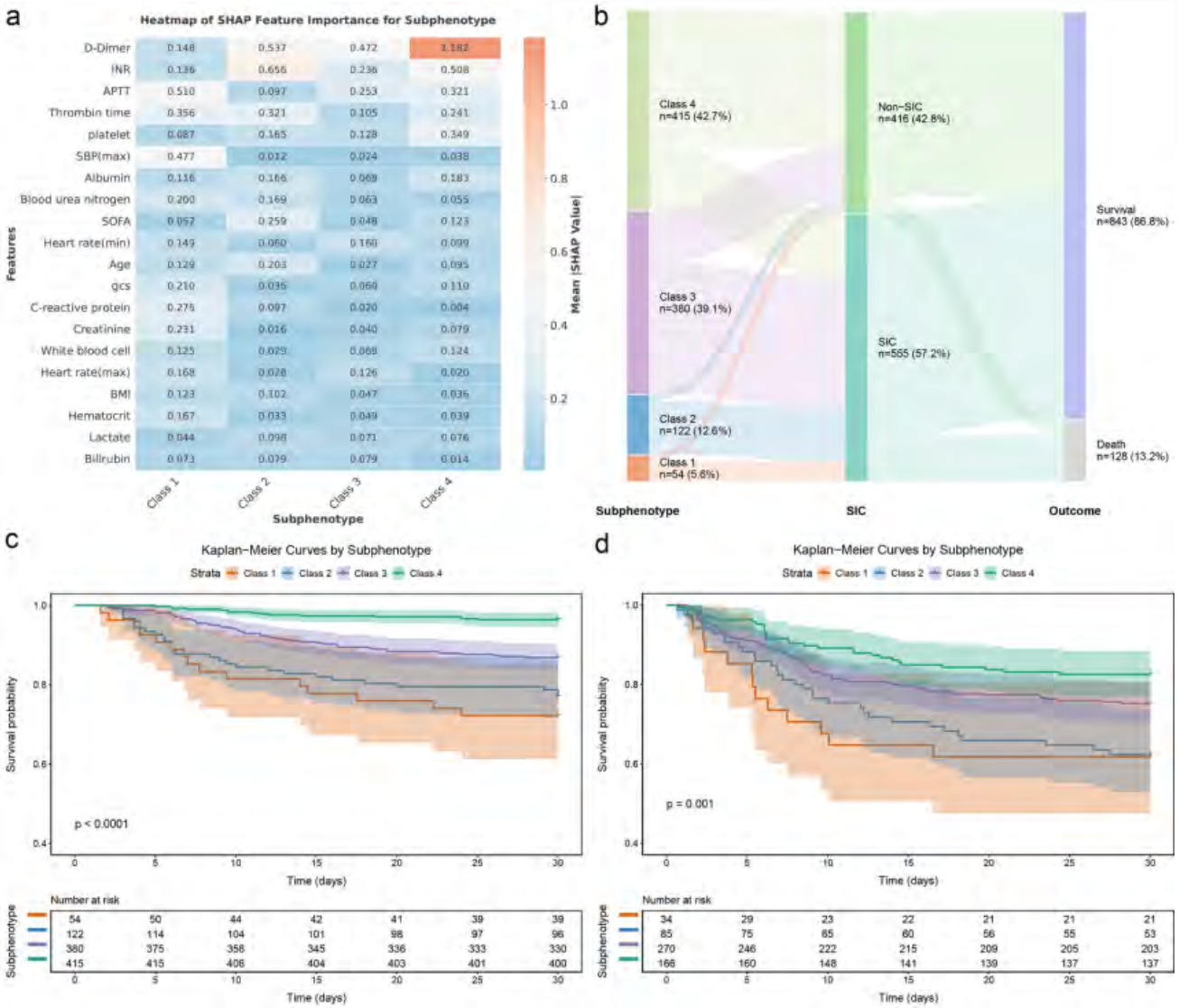


图 2 不同亚表型的临床特征重要性及结局转归图。a，不同亚表型基于 SHAP 的特征重要性热图，展示 XGBoost 模型在开发队列中基线特征对亚表型的贡献强度（mean(|SHAP interaction|)）；b，桑基图，展示不同亚表型住 ICU 期间 SIC 发生及死亡事件的转归；c，开发队列 30 天 Kaplan-Meier 生存曲线；d，验证队列 30 天 Kaplan-Meier 生存曲线。缩写同图 3

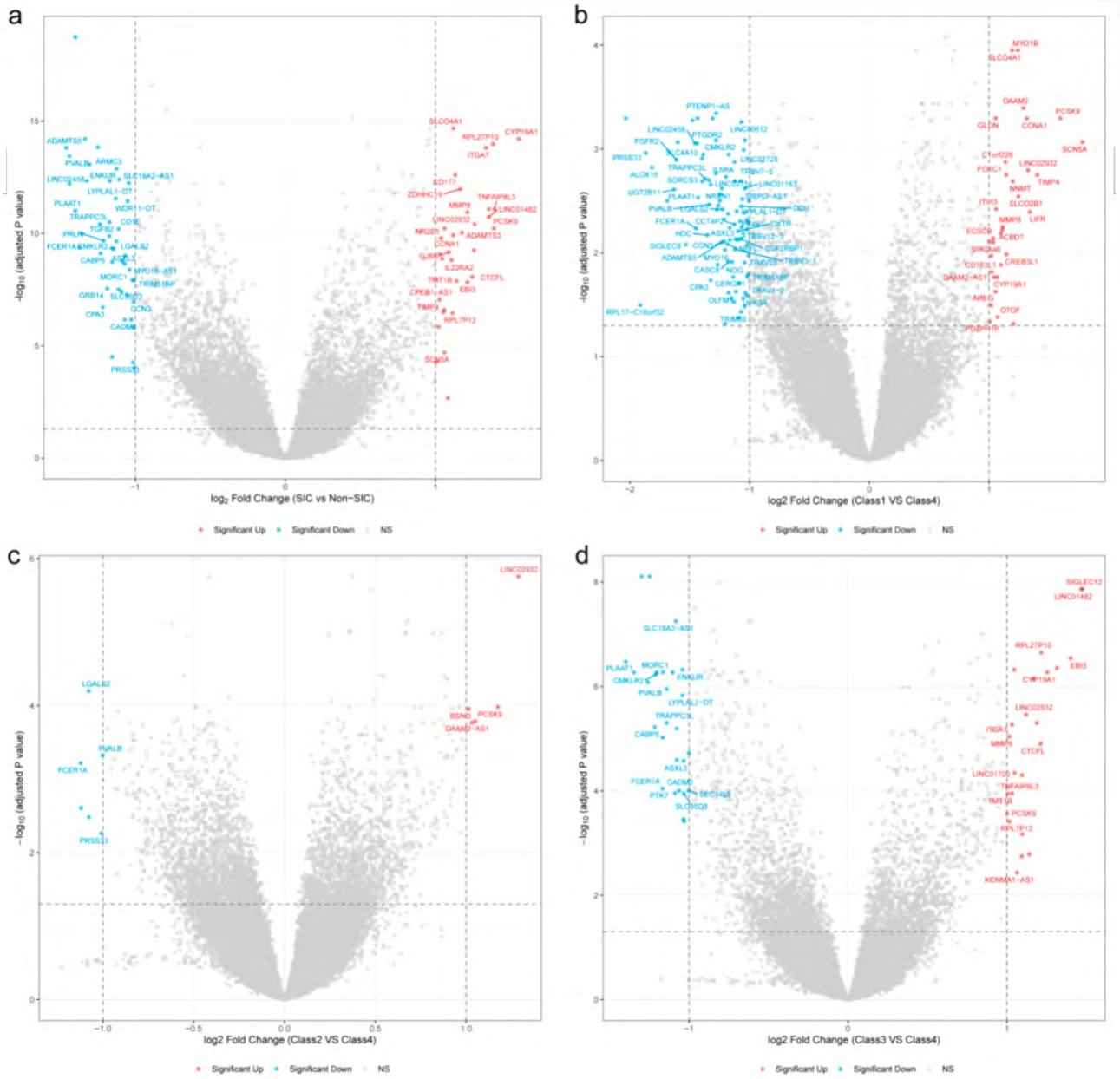


图 3 脓毒症全血转录组学差异表达火山图。a，SIC 组与 Non-SIC 组间差异表达基因火山图，横轴为 log_2 Fold Change（SIC vs Non-SIC），纵轴为－ log_{10}（校正 P 值）；红色点表示在 SIC 组中显著上调的基因（$|log_2FC| \geqslant 1$，adj.P<0.05），蓝色点表示显著下调的基因，灰色点表示无统计学差异的基因（NS）。b，Class 1 与 Class 4 间差异表达基因火山图。c，Class 2 与 Class 4 间差异表达基因火山图。d，Class 3 与 Class 4 间差异表达基因火山图。各图中标注的基因符号为校正 P 值最小的代表性差异基因。

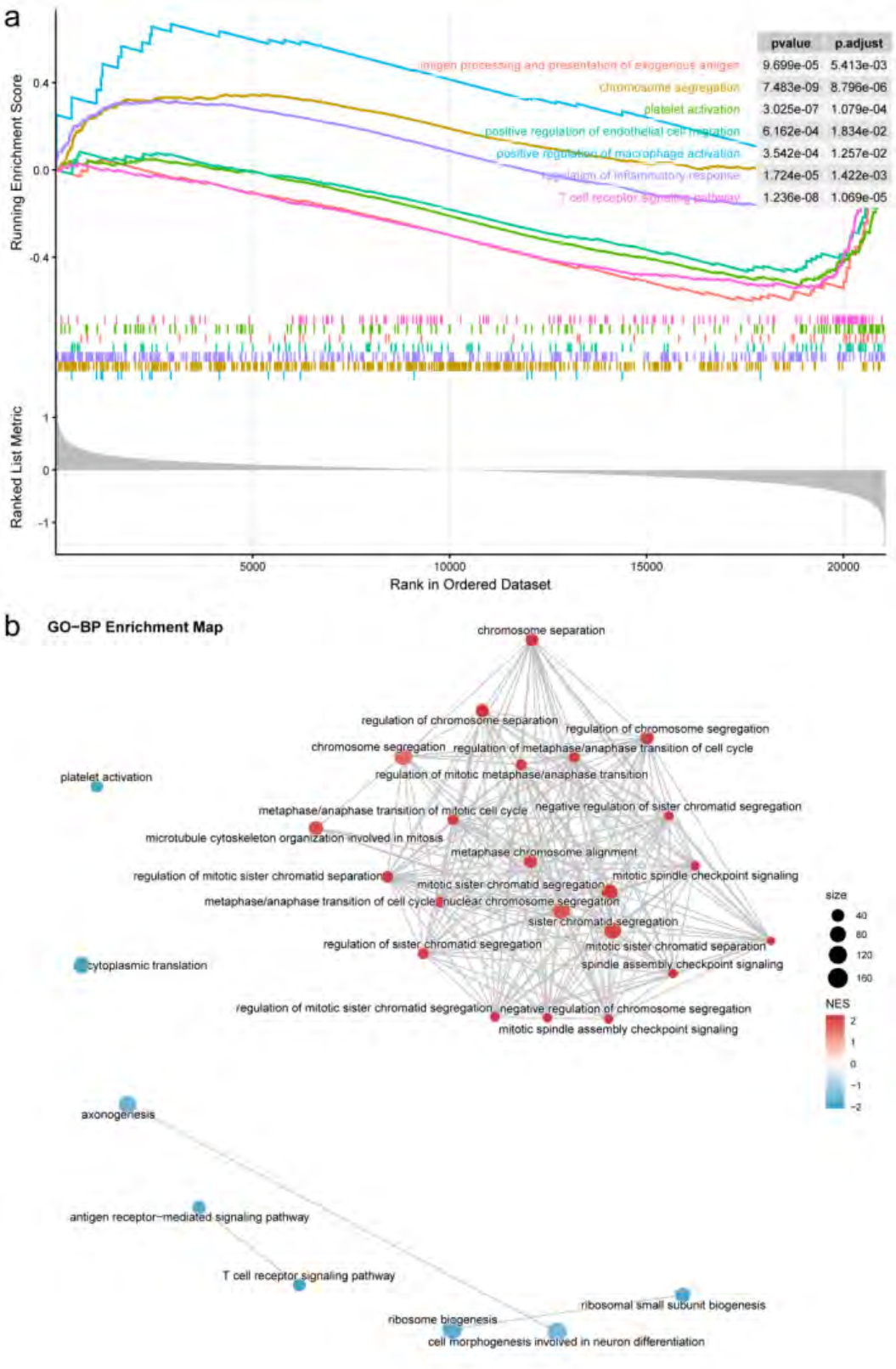


图 4 转录组基因集富集分析及 GO 生物过程富集网络图。a，基于 dream 线性混合效应模型全基因组 log_2FC 排序列表的 GSEA 富集得分图，展示 7 条代表 SIC 核心病理特征的 GO 生物过程通路。b，GO 生物过程显著富集通路的富集网络图；节点代表达到统计学显著性的 GO-BP 通路（adj.P<0.05），节点颜色表示标准化富集分数（红色表示 SIC 中激活，蓝色表示 SIC 中抑制），节点大小反映基因集规模，连线表示两通路间共享基因。

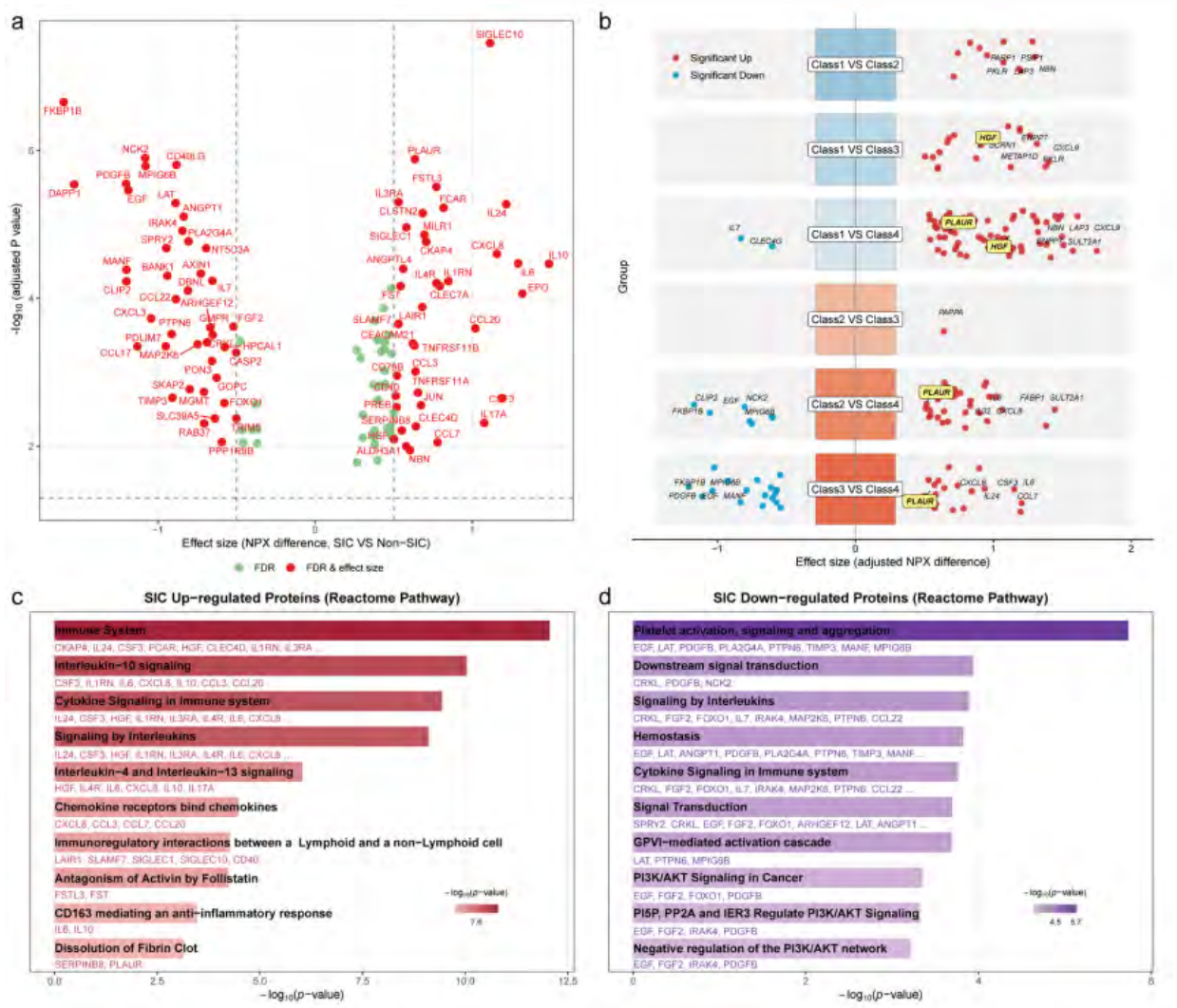


图 5 脓毒症患者血浆蛋白质组学差异表达分析及通路富集结果。a，SIC 组与 Non-SIC 组间差异蛋白火山图；横轴为效应量（NPX 差值，SIC vs Non-SIC），正值表示 SIC 中蛋白水平更高，纵轴为 $-\log_{10}$（校正 P 值）；红色点表示同时满足效应量（|NPX 差值 | ≥ 0.5）与统计学显著性（adj.P<0.05）阈值的差异蛋白，绿色点表示仅满足统计学显著性阈值的蛋白。b，不同凝血轨迹亚表型（Class 1—4）间蛋白质组学两两比较效应量图；横轴为各对比组中前一亚表型相对后一亚表型的调整后 NPX 差值。c，SIC 组相较于 Non-SIC 组显著上调蛋白的 Reactome 通路富集分析结果。d，SIC 组相较于 Non-SIC 组显著下调蛋白的 Reactome 通路富集分析结果。

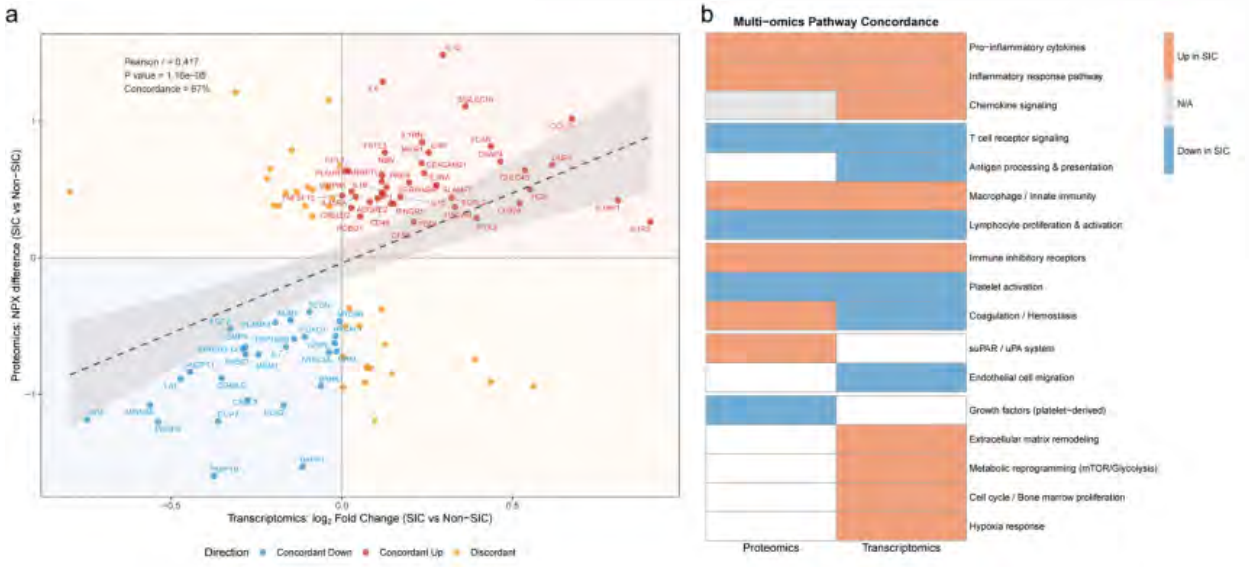


图 6 SIC 患者转录组学与蛋白质组学的交叉整合分析。a，基因 / 蛋白水平的转录组 - 蛋白质组定量一致性散点图；横轴为转录组差异分析的 log_2 Fold Change（SIC vs Non-SIC），纵轴为蛋白质组学差异分析的 NPX 差值（SIC vs Non-SIC），正值均代表 SIC 中高表达；点颜色表示两个组学中变化方向的一致性（红色为方向一致升高，蓝色为方向一致降低，橙色为方向不一致）；虚线为线性回归拟合线，灰色区域为 95% 置信区间；左上角标注 Pearson 相关系数、P 值及总体方向一致率。b，基于 16 个生物学主题的多组学通路层面一致性图；每个主题对应两列，左列为蛋白质组学证据，右列为转录组学证据；颜色表示通路激活方向。

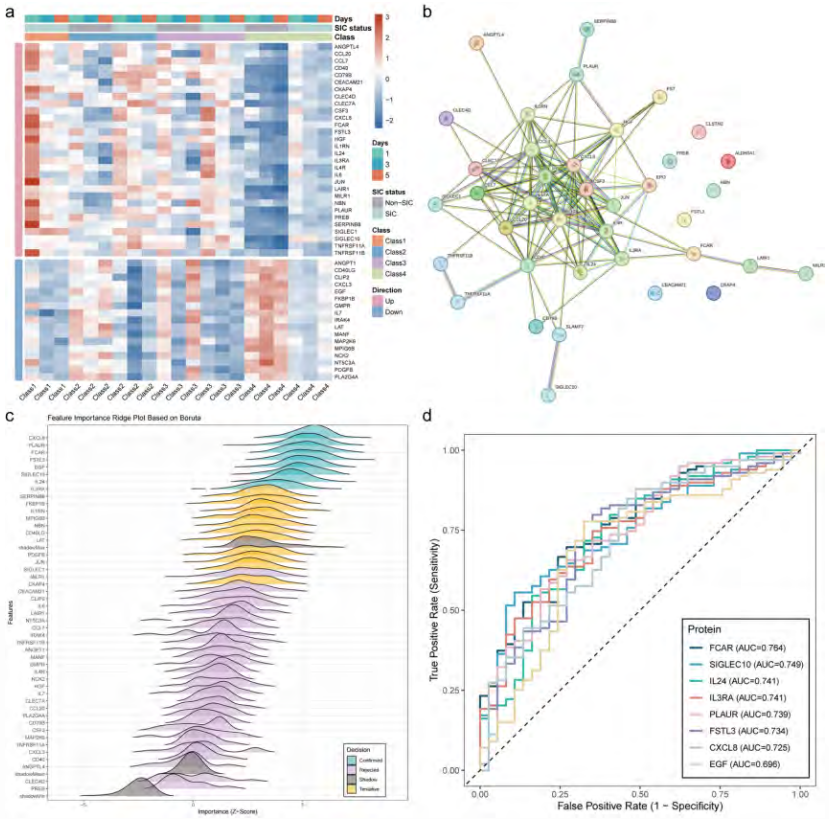


图 6 SIC 相关差异蛋白的表达模式、蛋白互作网络及 SIC 诊断生物标志物筛选。a，SIC 差异蛋白（同时满足 |NPX 差值 | ≥ 0.5 且 adj. P<0.05）在不同凝血轨迹亚表型及 ICU 第 1、3、5 天样本中的表达热图。b，SIC 组相较 Non-SIC 组上调差异蛋白的 STRING 蛋白质 - 蛋白质相互作用网络图。c，基于 Boruta 算法的 SIC 相关蛋白特征重要性山脊图；横轴为随机森林 Z-score，纵轴为各候选特征蛋白。d，Boruta 算法筛选的代表性候选生物标志物预测 SIC 的单变量 ROC 曲线及 AUC 值。

下呼吸道感染中抗菌药物耐药性的全球负担：基于 2021 年全球疾病负担研究的系统分析

姓名：秦伟栋 #，王昊 #，吕琨鹏，刘飒，马腾之，桑少伟 *，陈玉国 *

单位：山东大学齐鲁医院

论文摘要

题目：下呼吸道感染中抗菌药物耐药性的全球负担：基于 2021 年全球疾病负担研究的系统分析

目的（Objective）

全面评估 1990—2021 年全球及各地区下呼吸道感染（LRI）中，与抗菌药物耐药（AMR）相关及由其直接导致的疾病负担。

方法（Methods）

利用 2021 年全球疾病负担（GBD）研究数据，分析 1990—2021 年全球及地区 LRI 的 AMR 相关死亡与 AMR 归因死亡负担，分析覆盖多种病原体 – 药物组合。采用年度变化百分比（EAPC）量化年龄标化死亡率（ASMR）的变化趋势。

结果（Results）

2021 年，全球因 LRI 且与 AMR 相关的死亡为 164 万例（95% 不确定区间 UI：144 万～ 184 万），直接归因于 AMR 的死亡为 40 万例（34 万～ 46 万）。1990—2021 年，年龄标化死亡率显著下降（AMR 相关 EAPC：－ 2.31；AMR 归因 EAPC：－ 2.05），但疾病负担在年龄分布上发生明显转移：5 岁以下儿童死亡大幅减少，而 60 岁及以上成人死亡数上升。全球男性死亡负担高于女性，差异幅度与统计学意义随年龄组变化。撒哈拉以南非洲地区负担最高。6 种病原体占总死亡的 92.1%：肺炎链球菌、金黄色葡萄球菌、肺炎克雷伯菌、铜绿假单胞菌、鲍曼不动杆菌、大肠埃希菌。全球范围内，肺炎链球菌对复方新诺明和大环内酯类耐药导致的 AMR 相关死亡最多；而 β 内酰胺类耐药成为 AMR 归因死亡的首要原因，主要来自肺炎链球菌及鲍曼不动杆菌、肺炎克雷伯菌、铜绿假单胞菌等关键革兰阴性菌。

结论（Conclusion）

本研究表明，1990—2021 年，全球 LRI 的 AMR 年龄标化死亡率下降，但绝对负担持续向老年人群转移，伴随成年男性更高死亡与革兰阴性菌耐药贡献上升。儿童 AMR 相关死亡率显著下降，但革兰阴性菌耐药防控、老年人群负担加重、地区不平等问题仍亟待解决。

研究内容

1 研究背景：脓毒症是感染引发宿主反应失调，进而导致危及生命的器官功能障碍。在所有可引发脓毒症的感染来源中，肺部感染最为常见，占脓毒症病例的 40%~60%。抗菌药物耐药（AMR）的日益流行降低了抗菌治疗效果，增加进展为重症脓毒症及死亡的风险。

2019 年一项里程碑研究估算，当年约 770 万死亡与细菌感染相关，其中 495 万与 AMR 相关，127 万直接归因于 AMR。更近的 2021 年数据显示，约 471 万死亡与细菌 AMR 相关，其中 114 万直接归因于耐药感染。

本研究首次全面评估 1990—2021 年全球及地区 LRI 的 AMR 相关死亡负担，覆盖 16 种关键病原体与 13 类抗菌药物，旨在填补证据空白，为公共卫生策略、抗菌药物管理、新型治疗药物与疫苗研发提供依据。

2 研究方法

2.1 数据来源

LRI 的 AMR 负担估计来自 2021 年全球疾病负担（GBD）研究。

方法学框架详见已发表文献。分析采用多步骤方法：首先基于 1.39 亿条死亡原因记录、1010 万次出院及死亡 – 医院关联数据，采用混合效应逻辑回归模型拟合脓毒症死亡；随后将脓毒症死亡分层至特定感染综合征，利用 142 个国家的 2400 万株菌株数据（在 RegMod 回归环境中调整医疗可及性与质量指数及多种偏倚校正协变量），估算病原体特异性病死率与病原体分布；对每种病原体 – 药物组合采用 “集成堆叠回归 + 高斯过程平滑” 两阶段时空模型拟合耐药流行率；采用贝叶斯正则化方法对 2.96 亿样本进行 meta 回归分析，获得耐药 vs 敏感感染的相对死亡风险。最终负担估计同时包含归因与相关指标。

2.2 统计分析

为量化 ASMR（AMR 相关与归因）的时间趋势，采用对数线性回归模型计算 1990—2021 年 EAPC。

采用 Spearman 秩相关分析 ASMR（AMR 相关与归因）与社会人口学指数（SDI）的关系。所有统计分析采用 R 软件（4.0.2 版）。

3 研究结果

3.1 1990—2021 年全球 AMR 负担趋势

1990 年，全球 LRI 中 AMR 相关死亡 211 万例（95% UI：172 万～ 250 万），归因死亡 47 万例（36 万～ 58 万）。到 2021 年，分别降至 164 万例（144 万～ 184 万）与 40 万例（34 万～ 46 万）。

全球 AMR 相关 ASMR 从 1990 年 45.08/10 万（37.08~53.08）降至 2021 年 20.89/10 万（18.27~23.50），EAPC 为－ 2.31（95% CI：－ 2.47~ － 2.15）；AMR 归因 ASMR 从 10.27/10 万（7.95~12.58）降至 5.05/10 万（4.29~5.81），EAPC 为－ 2.05（－ 2.20~ － 1.90）。

各 GBD 超级地区的 AMR 相关与归因 ASMR 均显著下降，东南亚、东亚及大洋洲降幅最快（相关 EAPC：－ 3.32，－ 3.51~ － 3.13；归因 EAPC：－ 3.21，－ 3.42~ － 2.99）。但绝对死亡数趋势不均，拉丁美洲与加勒比等地区出现上升。

3.2 AMR 负担的年龄与性别分层

1990—2021 年，AMR 相关死亡的年龄分布发生显著转移：负担从低龄儿童转向老年人群。5 岁以下儿童死亡大幅下降（如 1~5 月龄：相关死亡从 336421 降至 77661；归因死亡从 70125 降至 17232）；而 60 岁及以上人群死亡数上升（如 80~84 岁：相关死亡从 128721 升至 199198；归因死亡从 30923 升至 49123）。全球及各地区所有年龄组的年龄别死亡率整体呈下降趋势，5 岁以下儿童降幅最陡（各亚组 EAPC< － 3）。

全球点估计显示，研究期间男性 AMR 相关与归因死亡绝对数始终高于女性。

1990—2021 年全球年龄标化点估计显示，男性下降速率慢于女性，但 95% CI 重叠提示总体差异无统计学意义（相关：－ 2.20 vs － 2.47；归因：－ 1.97 vs － 2.18）。然而，年龄分层 EAPC 分析揭示特定年龄组存在统计学显著的性别差异：2~4 岁男童、25~39 岁男性下降显著更慢；70~79 岁女性下降更慢。

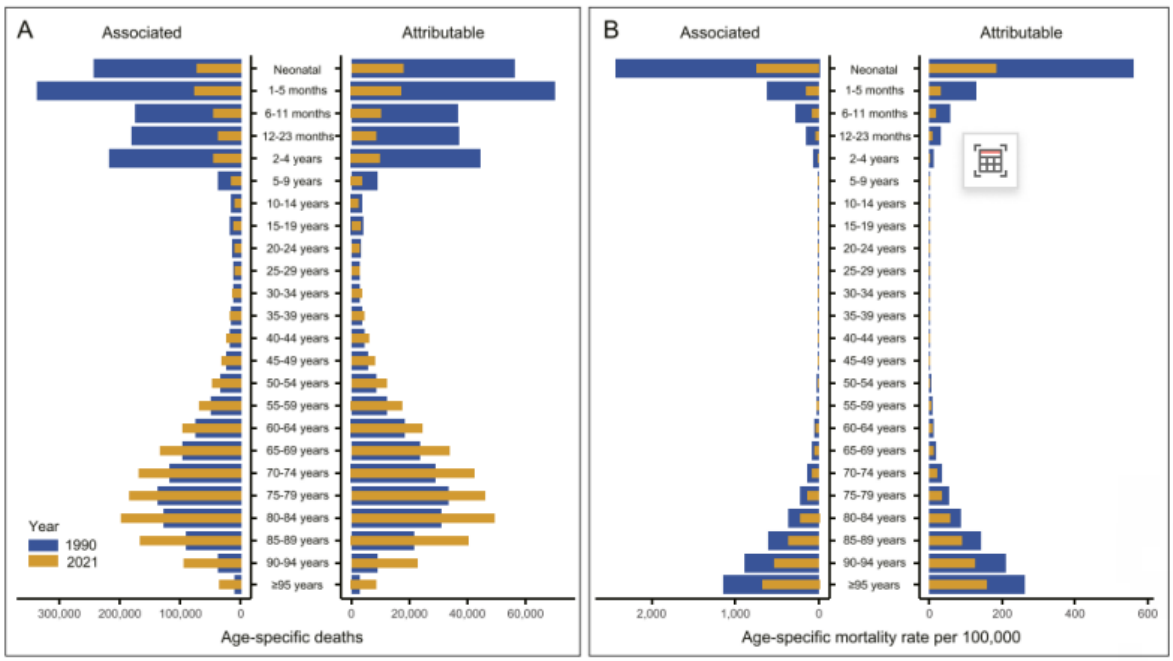


Fig. 1. Age-stratified AMR-associated and AMR-attributable burden in 1990 and 2021, globally. A, Age-specific number of deaths. B, Age-specific mortality rate per 100 000. AMR: antimicrobial resistance.

3.3 2021 年全球、地区及病原体特异性 AMR 负担

2021 年，6 种细菌占全球 LRI 中 AMR 相关死亡的绝大多数：

1. 肺炎链球菌：相关 56 万例（48 万～ 64 万），归因 11 万例（9 万～ 14 万）

2. 金黄色葡萄球菌：相关 27 万例（24 万～ 30 万），归因 7 万例（6 万～ 7 万）

3. 肺炎克雷伯菌：相关 24 万例（21 万～ 27 万），归因 7 万例（6 万～ 8 万）

4. 铜绿假单胞菌：相关 17 万例（15 万～ 19 万），归因 4 万例（4 万～ 5 万）

5. 鲍曼不动杆菌：相关 14 万例（13 万～ 16 万），归因 6 万例（5 万～ 6 万）

6. 大肠埃希菌：相关 13 万例（11 万～ 14 万），归因 3 万例（2 万～ 3 万）

以上 6 种病原体合计占 AMR 相关死亡的 92.1%、归因死亡的 94.3%。

地区层面，肺炎链球菌在多数 GBD 超级地区为优势病原体，相关与归因死亡率均最高。撒哈拉以南非洲的肺炎链球菌负担居全球首位（相关 19.31/10 万，15.90~22.73；归因 3.86/10 万，2.80~4.92），且金黄色葡萄球菌、肺炎克雷伯菌、铜绿假单胞菌、鲍曼不动杆菌、大肠埃希菌的死亡率也均为全球最高。与之相对，高收入地区的首位死因是金黄色葡萄球菌（相关 2.15/10 万，1.91~2.38；归因 0.55/10 万，0.49~0.62）。

6 种主要细菌中，金黄色葡萄球菌在多个地区 ASMR 呈上升趋势，拉丁美洲与加勒比升速最快（相关 EAPC：1.59，1.30~1.87；归因 EAPC：2.02，1.67~2.37）。与之相反，4 种病原体全球持续下降：高收入地区肺炎链球菌、鲍曼不动杆菌降幅最陡；肺炎克雷伯菌、铜绿假单胞菌在所有地区呈中度但持续的下降。



Fig. 2. AMR-associated and AMR-attributable burden stratified by pathogen and GBD super-region. A, Number of deaths in 2021. B, ASMR in 2021. Others include *Citrobac-*

3.4 病原体 – 年龄 – 性别分层的 AMR 负担

2021 年全球数据显示，6 种主要细菌均呈现男性、儿童与老年人死亡负担更高的一致格局。除新生儿外，肺炎链球菌在所有年龄组均为相关死亡首位病因；新生儿以肺炎克雷伯菌为主，死亡数与死亡率均最高（男性 12855 例，9910~15800；女性 9390 例，7445~11336；死亡率男性 255.24/10 万，196.77~313.72；女性 199.42/10 万，158.10~240.74）。

1990—2021 年，所有年龄组 AMR 相关死亡率均下降，5 岁以下儿童最快。成人进展较慢，特定年龄 – 性别亚组的金黄色葡萄球菌、大肠埃希菌呈上升趋势。多数病原体中，女性 AMR 死亡率下降普遍快于男性。

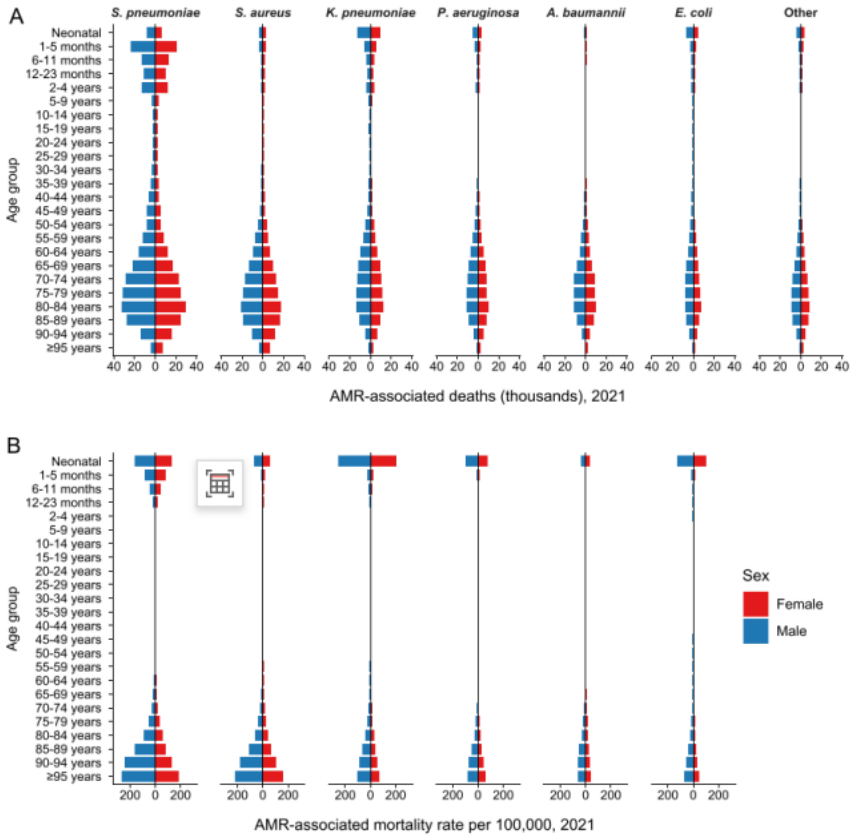


Fig. 3. Global AMR-associated burden, by pathogen, age group and sex. A, AMR-associated number of deaths, 2021. B, AMR-associated mortality rate per 100 000, 2021. Others include *Citrobacter* spp, *Enterobacter* spp, *Enterococcus faecalis*, *Enterococcus faecium*, *Haemophilus influenzae*, *Morganella* spp, *Proteus* spp, *Serratia* spp, group A *Streptococcus* and group B *Streptococcus*. AMR: antimicrobial resistance.

3.5 病原体 – 药物组合的 AMR 负担

GBD 数据集评估 16 种细菌、13 类抗菌药物的 74 种病原体 – 耐药组合。2021 年全球有 6 类抗菌药物各自相关死亡超 50 万例：氟喹诺酮类（795388）、复方新诺明（744933）、三代头孢（627372）、大环内酯类（576382）、碳青霉烯类（541393）、β 内酰胺 /β 内酰胺酶抑制剂（524907）。值得注意的是，碳青霉烯类耐药导致的 AMR 归因死亡最多（124036 例）。

具体病原体 – 药物组合中，全球 AMR 相关死亡主要来自肺炎链球菌对复方新诺明（392808 例）、大环内酯类（364098 例）、青霉素（216726 例）耐药。在 7 个 GBD 超级地区中，有 6 个地区的首位相关死亡均为肺炎链球菌对复方新诺明或大环内酯类耐药。高收入地区出现明显差异：甲氧西林耐药金黄色葡萄球菌（MRSA）为相关死亡首位。

AMR 归因死亡全球排名首位为肺炎链球菌合并 β 内酰胺耐药（聚合青霉素、头孢、碳青霉烯耐药）。

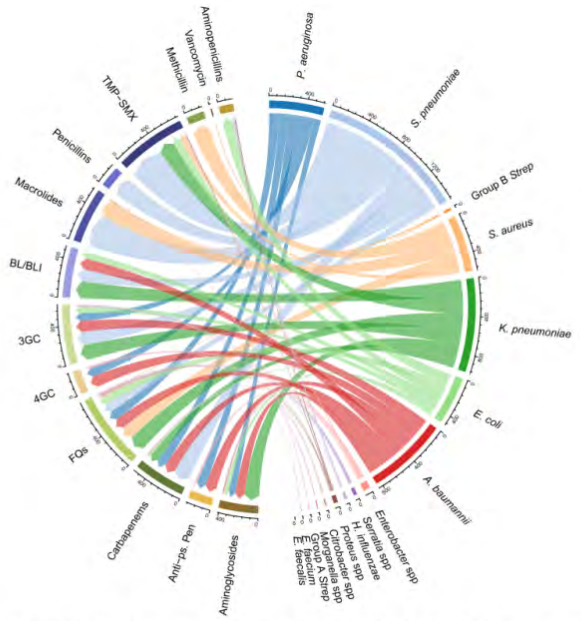


Fig. 4. Global burden of AMR-associated pathogen-drug combinations, 2021. The chord diagram visualises the relationships between antimicrobial classes (left arc) and bacterial pathogens (right arc) for AMR-associated deaths. Chord width corresponds to the number of deaths in thousands. Note: For *S. pneumoniae*, the prominent connection to 'Carbapenems' reflects the GBD hierarchical classification rule. Isolates resistant to multiple β-lactams (e.g., penicillins and cephalosporins) are categorised under carbapenem resistance, serving as a proxy for broad β-lactam non-susceptibility rather than specific carbapenemase production. 3GC: third-generation cephalosporins; 4GC: fourth-generation cephalosporins; Anti-ps. pen: anti-pseudomonal penicillins; BL/BLI: β-lactam/β-lactamase inhibitors; TMP-SMX: trimethoprim-sulfamethoxazole; AMR: antimicrobial resistance.

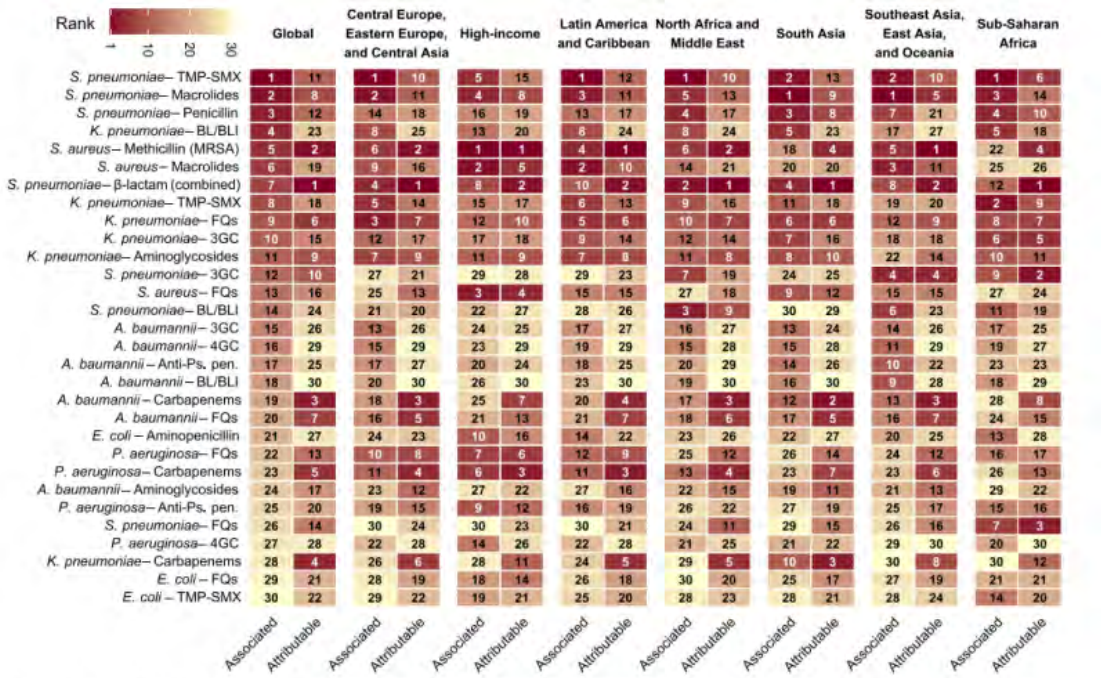


Fig. 5. Heatmap ranking of the top 30 pathogen-drug combinations by the number of AMR deaths globally and in seven GBD super-regions, 2021. Pathogen-drug combinations on the y-axis are ordered descending by the global number of AMR-associated deaths. The heatmap displays paired columns for associated and attributable burdens within each region. Note: A rank of 1 (dark red) indicates the highest mortality burden, while a rank of 30 (light yellow) indicates a relatively lower burden among the top 30. "*S. pneumoniae*–β-lactam (combined)" aggregates resistance to penicillin, cephalosporins and carbapenems to reflect the broader burden of β-lactam resistance. 3GC: third-generation cephalosporins. 4GC: fourth-generation cephalosporins. Anti-Ps. pen.: anti-pseudomonal penicillins. BL/BLI: β-lactam/β-lactamase inhibitors. FQs: fluoroquinolones. MRSA: methicillin-resistant *S. aureus*. TMP-SMX: trimethoprim-sulfamethoxazole. AMR: antimicrobial resistance.

3.6 AMR 负担与 SDI 的关联

基于 1990—2021 年 7 个 GBD 超级地区及全球的纵向数据，采用平滑曲线拟合分析 ASMR（相关与归因）与 SDI 的关系。结果显示强负相关（Spearman ρ= — 0.97，P<0.0001），即 SDI 越低（发展水平越落后）的地区，AMR 相关死亡率越高。

4 讨论

下呼吸道感染（LRI）仍是全球主要死亡原因，而 AMR 显著增加治疗难度并恶化临床结局。本研究首次全面评估 1990—2021 年细菌性

LRI 中 AMR 相关与归因死亡，揭示 4 个关键流行病学特征：

1. 年龄分布显著转移：5 岁以下儿童死亡下降，60 岁及以上成人负担上升；

2. 持续性别差异：全球男性 AMRLRI 死亡率高于女性，且下降更慢；

3. 显著地区不平等：撒哈拉以南非洲负担最高，高收入地区耐药问题持续加剧；

4. 病原体特异性威胁凸显，需因地制宜开展干预。

本研究核心发现为 AMRLRI 负担的年龄两极分化。5 岁以下儿童年龄别死亡数与死亡率降幅超 70%， 与之相反，尽管 60 岁及以上成人年龄别死亡率下降，但绝对死亡数上升。

本研究发现持续的性别差异：男性全球死亡点估计更高，多个成年年龄组差异具统计学意义。

地理层面，高收入地区与撒哈拉以南非洲 ASMR 相差 8 倍，凸显疫苗可及、诊断能力、抗菌药物监管的结构性不平等。东南亚、东亚及大洋洲 ASMR 降幅最快。撒哈拉以南非洲进展缓慢。

病原体格局凸显因地制宜策略的必要性。全球多数地区肺炎链球菌为首位死因，但高收入地区以金黄色葡萄球菌（主要为 MRSA）为主。

2021 年，6 种细菌占全球 LRI 中 AMR 相关死亡的 92.1%，与 WHO 2024 年细菌优先病原体清单高度吻合：碳青霉烯耐药鲍曼不动杆菌、耐三代头孢 / 碳青霉烯肠杆菌目为临界优先级；碳青霉烯耐药铜绿假单胞菌、MRSA 为高优先级；大环内酯耐药肺炎链球菌为中等优先级。

药物类别分析揭示关键区别：氟喹诺酮类、复方新诺明耐药导致的相关死亡最多，而碳青霉烯类耐药导致的归因死亡最多。对鲍曼不动杆菌、肺炎克雷伯菌等革兰阴性菌而言，碳青霉烯耐药后几乎无替代药物。

各地区主导耐药药物类别存在明显异质性：多数地区以氟喹诺酮耐药为主；东南亚、东亚及大洋洲以大环内酯耐药为主；撒哈拉以南非洲以复方新诺明耐药为主（尤其 5 岁以下儿童）。高收入地区氟喹诺酮耐药与 MRSA 占比高。南亚与撒哈拉以南非洲集中大量碳青霉烯与广谱 β 内酰胺耐药。

将流行病学结果转化为实践需解决全球关键缺口：儿童 AMRLRI 死亡下降证实预防干预成功，但 2019 年全球 PCV 与 b 型流感嗜血杆菌（Hib）疫苗覆盖率仅 47.9% 与 70.6%，远低于全球疫苗行动计划 90% 的目标，加速疫苗公平可及至关重要。革兰阴性菌耐药威胁加剧，需持续投入新型抗菌药物与快速诊断。针对碳青霉烯耐药肠杆菌目的亚胺培南 / 西司他丁 / 瑞来巴坦、针对鲍曼不动杆菌的舒巴坦 / 杜洛巴坦等新药是重要治疗进展，但其长期疗效依赖全球公平可及与严格抗菌药物管理。

高收入地区金黄色葡萄球菌死亡上升，需优先强化医疗相关感染防控与 MRSA 去定植；中低收入地区面临革兰阴性菌高传播与治疗选择有限的双重压力，需优先医疗机构感染防控、普及 WASH、保障儿童高疫苗覆盖率。

组织灌注压与心脏手术相关急性肾损伤发生的相关性研究

姓名：金楷，陈辉，刘松桥，邱海波，杨毅（通讯）

单位：东南大学附属中大医院，江苏省重症医学重点实验室

目的

心脏手术相关急性肾损伤（CSA-AKI）的发生显著增加患者不良肾脏结局及死亡风险。维持肾脏灌注是预防 CSA-AKI 的关键。然而，传统的平均动脉压（MAP）或平均灌注压（MPP）忽略了血管的可塌陷性。基于“血管瀑布”理论，临界闭合压（Pcc）是限制血流进入微循环的有效背压。因此，大循环向微循环的灌注需要足够的压力梯度，即组织灌注压 TPP = MAP - Pcc，而微循环的畅通则依赖于 Pcc 的维持，即血管瀑布效应的存在。本研究利用高频波形分析，评估 TPP 与 CSA-AKI 的相关性，并探讨 Pcc 与 TPP 的交互作用。

方法

回顾性分析 MIMIC-III 数据库中接受体外循环心脏手术并转入 ICU 的成年患者。排除术前维持性透析及肾移植患者。提取术后 24 小时高频动脉血压波形，利用自动化算法估算 Pcc 及 TPP，计算 24 小时时间加权平均值。

主要结局为术后 48 小时内严重 AKI（KDIGO 2-3 期）。统计方法：(1) 比较 AKI 与非 AKI 组的传统指标差异；(2) 构建多因素 Logistic 回归评估 TPP 的独立预测价值；(3) 构建“Pcc-TPP”四象限分型（双低、高流量低闭合压、低流量高闭合压、双高组），评估不同血管瀑布状态与灌注压组合对预后的影响。

结果

最终纳入 660 例拥有高质量波形数据的患者。

1. 传统指标：严重 AKI 组 MPP 显著低于非 AKI 组（62.4 vs 65.0 mmHg, P<0.001）。多因素回归显示 MPP 是严重 AKI 的独立保护因素（OR 0.68, P=0.001）。

2. TPP 分析：单因素分析显示，高 TPP 组严重 AKI 发生率低于低 TPP 组（44.5% vs 52.4%, P=0.043）。但在校正混杂因素后，TPP 分组并非独立预测因子（OR 0.78, P=0.141）。RCS 分析未显示显著非线性关系。

3. 四象限分析：基于 Pcc 和 TPP 的交互分析差异显著。以“双低组”（低灌注伴血管瀑布效应丧失）为参照，其严重 AKI 发生率最高（59.2%）；“双高组”（灌注充足且血管瀑布存在）发生率最低（38.8%），组间 Log-rank 检验趋势显著（P=0.037）。回归证实，仅“双高组”是严重 AKI 的独立保护因素（OR 0.44, 95% CI: 0.24-0.83, P=0.011）。

讨论

本研究发现，尽管传统 MPP 指标具有预测价值，但在引入 Pcc 概念后，我们揭示了更深层的血流动力学机制。单纯依赖 TPP 这一指标不足以准确预测严重 CSA-AKI，原因在于 TPP 的计算掩盖了 Pcc 的变化：部分 TPP 较高的患者实际上处于 Pcc 极低的状态。Pcc 的降低意味着血管瀑布效应的丧失，即失去了维持微循环开放的有效下游压力，导致微循环发生了塌陷。

四象限分析证实，Pcc 与 TPP 的交互作用是决定肾脏预后的关键。只有当患者同时具有充足组织灌注压与血管瀑布时，才能显著降低 AKI 发生的风险。这提示临床在围术期管理中，应从单一追求压力达标转向“压力 - 瀑布效应”双重优化的精准策略。